



Understanding the Role of Bcl-3 in Triple-Negative Breast Cancer

William W. Yang

Thesis submitted for the award of Doctor of Philosophy (PhD),
European Cancer Stem Cell Research Institute, Cardiff University,
September 2018





Declaration

This work has not been submitted in substance for any other degree or award at this or any other university or place of learning, nor is being submitted concurrently in candidature for any degree or other award.

Signed (candidate) Date

STATEMENT 1

This thesis is being submitted in partial fulfilment of the requirements for the degree of PhD.

Signed (candidate) Date

STATEMENT 2

This thesis is the result of my own independent work/investigation, except where otherwise stated, and the thesis has not been edited by a third party beyond what is permitted by Cardiff University's Policy on the Use of Third Party Editors by Research Degree Students. Other sources are acknowledged by explicit references. The views expressed are my own.

Signed (candidate) Date

STATEMENT 3

I hereby give consent for my thesis, if accepted, to be available online in the University's Open Access repository and for inter-library loan, and for the title and summary to be made available to outside organisations.

Signed (candidate) Date

STATEMENT 4: PREVIOUSLY APPROVED BAR ON ACCESS

I hereby give consent for my thesis, if accepted, to be available online in the University's Open Access repository and for inter-library loans **after expiry of a bar on access previously approved by the Academic Standards & Quality Committee.**

Signed (candidate) Date

Abstract

Triple-negative breast cancer (TNBC) represents an aggressive subtype associated with progression to metastasis and poor prognosis. The NFkB co-factor B-cell lymphoma 3 (Bcl-3) is a proto-oncogene commonly dysregulated in a range of cancers and has been shown to be up-regulated in metastatic breast cancer lesions. In this study we investigated the therapeutic potential of targeting Bcl-3 in TNBCs.

Knockdown of Bcl-3 with siRNA in a panel of TNBC cell lines resulted in reduced cellular proliferation, collective migration, single-cell motility, NFkB-targeted transcriptional activity and increased apoptosis-mediated cell death. Ectopic overexpression of wild type (WT) Bcl-3 protein in TNBC cells resulted in increased proliferation, single cell motility, and NF-kB activity; however, substantially increased apoptosis-mediated cell death was also observed, resulting in an overall reduced cell turnover. Affymetrix gene expression profiling of MDA-MB-231-Luc cells treated with Bcl-3 siRNA revealed enrichment of up-regulated genes associated with BCL2-mediated apoptosis regulators (MCL1, TP53, BAX, BAK1, BCL2); as well as enrichment of down-regulated genes associated with migration including Rho GTPase signalling (CDC42, RHOB, CFL2, ROCK1, PAK1, PFN2).

In a murine *in vivo* xenograft metastasis model, MDA-MB-231 cells treated with Bcl-3 siRNA were injected via the tail vein, resulting in significantly fewer pulmonary metastatic lesions at experimental endpoint when compared with controls. Tail vein injection of MDA-MB-231 cells overexpressing WT Bcl-3 resulted in significantly increased pulmonary and hepatic metastatic lesions when compared with controls, as well as colonisation at novel distal organs including the heart, mammary gland and bone marrow (femur).

Pharmacological inhibition of Bcl-3 with novel small molecule inhibitors, JS6 and CB1, were able to recapitulate Bcl3 siRNA responses in functional assays. Affymetrix gene expression profiling of MDA-MB-231-Luc cells treated with CB1 revealed a significant proportion of the genes that responded to siRNA treatment also responded to this pharmacological inhibitor (including TFGB1, INPP4B, IL1B, IL24), highlighting mechanistic similarities. In a murine *in vivo* xenograft tail vein metastasis model, daily treatment of CB1 significantly inhibited early metastatic seeding events and reduced

average metastatic burden, as well increased the proportion of disease free animals at experimental endpoint when compared to controls.

The findings from this study highlighted Bcl-3 as a promising therapeutic target in TNBCs and we were able to demonstrate that the novel Bcl-3 inhibitor, CB1 functioned as an effective anti-metastatic agent in murine models of advanced TNBC.

Contents

Declaration	2
Abstract	3
Contents	5
List of figures	12
List of tables	14
1 General Introduction	16
1.1 Hallmarks of cancer	16
1.2 Breast cancer	17
1.2.1 Triple-negative breast cancer	17
1.2.2 Sub-typing within TNBC	18
1.2.3 Genetic markers in TNBC and targeted therapies	19
1.2.3.1 TP53	20
1.2.3.2 BRCA1/2	20
1.2.3.3 PI3K pathway	21
1.2.3.4 Tyrosine kinase receptors	22
1.2.3.5 Androgen receptors	23
1.2.3.6 BCL2	23
1.2.4 Immunotherapy in TNBC	23
1.2.5 TNBC metastatic progression	24
1.2.5.1 Local invasion and intravasation	25
1.2.5.2 Survival in circulation	26
1.2.5.3 Extravasation	26
1.2.5.4 Metastatic colonisation	26
1.3 Apoptosis pathways	27
1.3.1 Intrinsic mitochondria-mediated pathway	27
1.3.2 Extrinsic receptor-mediated pathway	28
1.3.3 BCL2 protein family	29
1.3.4 Inhibitor of apoptosis proteins	30
1.4 Rho family of small GTPases in actin regulation and motility	31
1.4.1 Rho GTPases and upstream regulation	31
1.4.2 Rho GTPase downstream targets	32
1.5 The NFkB signalling pathway	34
1.5.1 NFkB subunits	34
1.5.2 Mechanisms activating NFkB signalling pathways	35

1.5.3 NFkB in cancer	37
1.6 B-cell lymphoma 3 (Bcl-3)	39
1.6.1 Bcl-3 interactions	39
1.6.2 Bcl-3 related malignancies	41
1.6.3 Bcl-3 in breast cancer	42
1.6.4 Bcl-3 as a therapeutic target for metastasis	43
1.6.5 Development of a small molecule inhibitor of Bcl-3	44
1.7 Project Aims	45
2 Materials and Methods	47
2.1 Cell culture	47
2.1.1 Experimental cell lines	47
2.1.2 Maintenance of cell lines	48
2.1.3 Cell counting and seeding	49
2.1.4 Long term frozen storage of cell lines	49
2.1.5 Raising cells lines from frozen storage	49
2.2 Transfection and drug treatment of cell lines	50
2.2.1 Single siRNA transfection	50
2.2.2 Bcl-3 plasmid constructs	51
2.2.3 Tranfection of NFkB reporter and Bcl-3 plasmids	51
2.2.4 Generation of stable overexpression clones	51
2.2.5 Drug treatments	52
2.3 Cell based functional assays	52
2.3.1 Migration assays	52
2.3.1.1 Wound-healing assay	52
2.3.1.2 Fluoroblok migration assay	53
2.3.1.3 Single cell migration assay	53
2.3.2 Colony formation assay	54
2.3.3 CellTiter-Blue assay	54
2.3.4 Realtime-glo assay	54
2.3.5 NFkB luciferase reporter assay	55
2.3.6 DAPI cell cycle assay via flow cytometry	55
2.3.7 Caspase-glo -3/-7 assay	56
2.3.8 Mammosphere assay	56
2.4 Protein analysis	56
2.4.1 Protein extraction from cells	56
2.4.2 Nuclear and cytoplasmic protein extraction	57

2.4.3 Quantification of protein	57
2.4.4 Coimmunoprecipitation	58
2.4.5 Western Blotting	58
2.4.5.1 Protein sample preparation	58
2.4.5.2 Gel electrophoresis	58
2.4.5.3 Membrane transfer	59
2.4.5.4 Blocking and primary antibody incubation	59
2.4.5.5 Detection and quantification	60
2.4.6 Immunofluorescence	60
2.5 RNA analysis	61
2.5.1 RNA extraction	61
2.5.2 cDNA synthesis	61
2.5.3 Quantitative-real time-polymerase chain reaction (qRT-PCR)	61
2.5.3.1 Primer acquisition	61
2.5.3.2 qRT-PCR reaction	62
2.5.3.3 qRT-PCR data analysis	63
2.6 Animal experiments	63
2.6.1 Licensing	63
2.6.2 Animals	64
2.6.3 Experimental models	64
2.6.3.1 Subcutaneous orthotopic xenograft tumour model	64
2.6.3.2 Tail vein xenograft tumour model	64
2.6.4 In vivo treatment of mice	64
2.6.5 Tumour monitoring and measurements	65
2.6.6 Imaging of luciferase expressing tumour metastasis model	65
2.7 Affymetrix DNA Microarray GeneChip array analysis	66
2.7.1 Gene function analysis with the PANTHER classification system	66
2.8 Statistical analysis	66
Chapter 3: Results	67
3.1 Introduction	68
3.2 Bcl-3 expression in breast cancer cell lines	69
3.3 Bcl-3 siRNA knockdown had no observable effects on bulk cellular monolayer morphology and knockdown was stable up to 96h	70
3.4 Bcl-3 siRNA knockdown significantly reduced cell population growth in TNBC cell lines but not in the non-malignant MCF10a cell line	75
3.5 Bcl-3 siRNA knockdown significantly reduced Ki67 expression in TNBC cell lines but not in the non-malignant MCF10a cell line	77

3.6 Bcl-3 siRNA knockdown significantly reduced phosph-Histone H3 (ser10) expression in TNBC cell lines but not in the non-malignant MCF10a cell line	80
3.7 Effects of Bcl-3 siRNA knockdown on the cell cycle	83
3.8 Bcl-3 siRNA knockdown significantly increased caspase-3/-7 activity in TNBC cell lines but not in the non-malignant MCF10a cell line	90
3.9 Bcl-3 siRNA knockdown did not affect mammosphere numbers but significantly reduced mammosphere size in TNBC cell lines	92
3.10 Bcl-3 siRNA knockdown significantly impaired clonogenic survival in TNBC cell lines but not the non-malignant MCF10a cell line	95
3.11 Effects of Bcl-3 siRNA knockdown on cellular migration	97
3.11.1 Bcl-3 siRNA knockdown significantly inhibited collective migration in wound-healing assay in TNBC cell lines but not the non-malignant MCF10a cell line	97
3.11.2 Bcl-3 siRNA knockdown significantly inhibited amoeboid-like single cell migration in TNBC cell lines but not the non-malignant MCF10a cell line	103
3.11.3 Bcl-3 siRNA knockdown significantly inhibited mesenchymal-like single cell migration in TNBC cell lines but not the non-malignant MCF10a cell line	104
3.12 Bcl-3 siRNA knockdown significantly inhibited NFkB activity	109
3.13 Bcl-3 knockdown reduced metastatic occurrence in a murine tail vein xenograft metastasis model	110
3.14 Affymetrix DNA microarray analysis of Bcl-3 siRNA knockdown	113
3.14.1 Gene function analysis of significantly up/down-regulated genes following Bcl-3 siRNA knockdown using the PANTHER classification system	113
3.14.1 PANTHER statistical overrepresentation analysis	120
3.14.2 PANTHER statistical enrichment analysis	120
3.15 Discussion	123
3.15.1 Bcl-3 regulated cellular proliferation through modulation of the cell cycle	123
3.15.2 Bcl-3 regulated apoptosis signalling pathways	125
3.15.2.1 Bcl-3 protected against intrinsic mitochondria-mediated apoptosis	125
3.15.2.2 Bcl-3 protected against stress induced apoptosis	127
3.15.2.3 Bcl-3 and the extrinsic receptor-mediated apoptosis pathways	127
3.15.3 Bcl-3 implicated in NFkB signalling	129
3.15.4 Bcl-3 did not regulate cancer cell stemness but affected clonogenic survival	130
3.15.5 Bcl-3 regulated various modes of migration potentially through Rho GTPases	131
3.15.6 Bcl-3 knockdown reduced metastatic occurrence in a murine tail vein xenograft metastasis model	137
3.15.7 Bcl-3 knockdown and other downstream implications	138
3.15.8 Concluding remarks	139
Chapter 4: Results	140

4.1 Introduction	141
4.2 Generation of TNBC cell lines overexpressing ectopic Bcl-3	142
4.3 Ectopic WT Bcl-3 overexpression reduced cell population growth	145
4.4 Ectopic WT Bcl-3 overexpression increased Ki67 expression in -231-luc cells	146
4.5 Ectopic WT Bcl-3 overexpression increased pHH3 expression	146
4.6 Effect of ectopic WT Bcl-3 overexpression on the cell cycle	149
4.6.1 Ectopic WT Bcl-3 overexpression in MDA-MB-436 increased the subG1 population and decreased the G0/G1 population	149
4.6.2 Ectopic WT Bcl-3 overexpression in MDA-MB-231-Luc increased the subG1 population and decreased the G0/G1 population	149
4.7 Ectopic Bcl-3 overexpression increased caspase-3/7 activity	152
4.8 Ectopic Bcl-3 overexpression did not affect total mammosphere numbers but significantly reduced mammosphere size	153
4.9 Ectopic Bcl-3 overexpression significantly impaired clonogenic survival	153
4.10 Effect of ectopic Bcl-3 overexpression on cellular migration	157
4.10.1 Ectopic Bcl-3 overexpression significantly inhibited collective migration	157
4.10.1.1 Ectopic Bcl-3 overexpression significantly inhibited collective migration in MDA-MB-436	157
4.10.1.2 Ectopic Bcl-3 overexpression significantly inhibited collective migration in MDA-MB-231-Luc	157
4.10.2 Ectopic WT Bcl-3 overexpression increased amoeboid-like single cell migration	160
4.10.3 Ectopic Bcl-3 overexpression significantly increased mesenchymal-like single cell migration in the -231-Luc cell line	161
4.11 Ectopic overexpression of WT Bcl-3 increased NFkB activity	166
4.12 Effect of ectopic Bcl-3 overexpression in murine xenograft metastasis models	167
4.12.1 Ectopic overexpression of Bcl-3 exhibited a trend of reduced growth rates at the orthotopic site	167
4.12.2 Ectopic overexpression of WT Bcl-3 increased metastases to distal organs but significantly reduced average tumour size	168
4.13 Discussion	171
4.13.1 Overexpression of WT Bcl-3 reduced cell turnover	171
4.13.2 Overexpression of WT Bcl-3 did not affect mammosphere numbers but impaired clonogenicity	172
4.13.3 Overexpression of WT Bcl-3 enhanced metastatic capacity	173
4.13.4 Overexpression of WT Bcl-3 increased NFkB activity	173
4.13.5 Overexpression of WT Bcl-3 increased in vivo metastatic seeding but tumours had reduced growth rates	174

4.13.6 Overexpression of Bcl-3 ANK mutant in TNBC cell lines mimicked Bcl-3 suppression with siRNA	174
4.13.7 Concluding remarks	175
Chapter 5: Results	176
5.1 Introduction	177
5.2 JS6 and CB1 disrupted Bcl-3-p50 protein-protein binding	178
5.3 48h JS6 and CB1 treatment reduced cell viability at higher drug concentrations	179
5.4 48h CB1 treatment did not affect mammosphere numbers but significantly reduced mammosphere size	182
5.3 48h JS6 and CB1 impaired clonogenic survival at 100µM concentration	183
5.4 48h JS6 and CB1 treatment did not affect NFκB activity	185
5.5 Affymetrix DNA microarray analysis following 48h CB1 treatment	186
5.5.1 PANTHER functional classification analysis	186
5.5.2 PANTHER statistical overrepresentation analysis	187
5.5.3 PANTHER statistical enrichment analysis	187
5.5.4 Overlapping gene changes between CB1 treatment and Bcl-3 siRNA knockdown	190
5.6 Relative expression of a Bcl-3 responsive gene panel following siRNA knockdown, JS6 or CB1 treatment	192
5.7 Daily refresh of JS6 and CB1 more effectively impaired clonogenic survival	196
5.8 In vivo xenograft modelling	199
5.8.1 Xenograft model one: The effects of Bcl-3 inhibitors on metastatic seeding capabilities of MDA-MB-231-Luc cells	199
5.8.1.1 Anti-metastatic efficacy of JS6 and 15F in xenograft model one	201
5.8.1.2 Anti-metastatic efficacy of CB1 in xenograft model one	203
5.8.1.3 JS6 and CB1 significantly reduced metastatic burden in xenograft model one	206
5.8.2 Anti-metastatic efficacy of CB1 was maintained in xenograft model one when administered via oral gavage	207
5.8.3 Xenograft model two: The effects of Bcl-3 inhibitors on metastatic colonisation and expansion capabilities of MDA-MB-231-Luc cells	209
5.8.3.1 JS6 and CB1 did not significantly inhibit metastatic colonisation and expansion	209
5.8.3.2 Daily JS6 and CB1 treatment did not significantly cause adverse toxicity	212
5.8.4 Xenograft model three: The effects of CB1 on TNBC orthotopic tumour growth	213
5.8.4.1 CB1 significantly reduced orthotopic tumour growth	213
5.9 Discussion	215

5.9.1 JS6 and CB1 disrupted Bcl-3-p50 protein-protein binding	215
5.9.2 JS6 and CB1 demonstrated in vitro efficacy	216
5.9.3 Global gene expression profiling following 48 hour CB1 treatment	216
5.9.3.1 Overlapping genes in similar directions following CB1 and siRNA	217
5.9.3.2 Overlapping genes in opposing directions following CB1 and siRNA	220
5.9.3.3 Gene changes seen only following CB1 treatment	221
5.9.4 CB1 found to most effectively confer transcriptional changes between the 8 and 24 hour time points	222
5.9.5 Daily JS6 and CB1 treatment improved drug efficacy	223
5.9.6 Bcl-3 inhibitors demonstrated in vivo efficacy	223
5.9.7 Concluding remarks	226
Chapter 6:	227
6.1 General Discussion	228
Chapter 7:	233
7 References	234

List of figures

Fig. 1.1 The ten hallmarks of cancer

Fig. 1.2 Processes involved in metastatic progression of the primary tumour

Fig. 1.3 Apoptosis pathways

Fig. 1.4 Fluorescent biosensor data showing activation patterns of RhoA at the leading edge

Fig. 1.5 Downstream effector targets of Rho family of GTPases

Fig. 1.6 The five subunits of the mammalian NFkB family.

Fig. 1.7 The canonical, non-canonical and the atypical NFkB signalling pathways

Fig. 1.8 Model of Bcl-3 activation.

Fig. 1.9 Bcl-3 small molecule binding sites.

Fig. 3.1 Relative Bcl-3 protein and RNA expression in breast cancer cell lines.

Fig. 3.2 Bcl-3 siRNA knockdown had no effects on bulk monolayer morphology and knockdown was stable up to 96h

Fig. 3.3 Bcl-3 siRNA knockdown reduced cell population growth

Fig. 3.4 Bcl-3 siRNA knockdown reduced Ki67 expression

Fig. 3.5 Bcl-3 siRNA knockdown reduced phospho-Histone H3 (ser10) expression

Fig. 3.6 Bcl-3 siRNA knockdown in MDA-MB-436 increased the subG1 population while decreasing the G0/G1, S, and G2/M populations

Fig. 3.7 Bcl-3 siRNA knockdown in MDA-MB-231-Luc decreased the G2/M population

Fig. 3.8 Bcl-3 siRNA knockdown in MDA-MB-231 increased the G0/G1 and decreased the G2/M populations

Fig. 3.9 Bcl-3 siRNA knockdown in SUM149 increased the G0/G1 and decreased the S, and G2/M populations

Fig. 3.10 Bcl-3 siRNA knockdown in MCF10a did not affect the cell cycle

Fig. 3.11 Bcl-3 siRNA knockdown increased caspase-3/7 activity in TNBC cell lines

Fig. 3.12 Bcl-3 siRNA knockdown did not affect mammosphere numbers but significantly reduced mammosphere size

Fig. 3.13 Bcl-3 siRNA knockdown significantly impaired clonogenic survival

Fig. 3.14 Bcl-3 siRNA knockdown significantly inhibited collective migration in MDA-MB-436

Fig. 3.15 Bcl-3 siRNA knockdown significantly inhibited collective migration in MDA-MB-231-Luc

Fig. 3.16 Bcl-3 siRNA knockdown significantly inhibited collective migration in MDA-MB-231

Fig. 3.17 Bcl-3 siRNA knockdown significantly inhibited collective migration in SUM149

Fig. 3.18 Bcl-3 siRNA knockdown did not affect collective migration in MCF10a

Fig. 3.19 Bcl-3 siRNA knockdown significantly inhibited amoeboid-like single cell migration in TNBC cell lines

Fig. 3.20 Bcl-3 siRNA knockdown significantly inhibited mesenchymal-like single cell migration in TNBC cell lines

Fig. 3.21 Bcl-3 siRNA knockdown significantly inhibited NFkB activity

Fig. 3.22 Bcl-3 knockdown reduced metastatic occurrence in a murine tail vein xenograft metastasis model

Fig. 3.23 PANTHER Functional Classification Tool for Bcl-3 siRNA knockdown

Fig. 3.24 Bcl-3 regulates Rho GTPases signalling pathways which potentially impacts on migration

Fig. 4.1 Bcl-3 constructs

Fig. 4.2 Relative Bcl-3 protein RNA expression and cellular localisation in breast cancer cell lines.

Fig. 4.3 Ectopic overexpression of Bcl-3 constructs reduced cell population growth

Fig. 4.4 Ectopic WT Bcl-3 overexpression increased Ki67 expression in -231-luc

Fig. 4.5 Ectopic WT Bcl-3 overexpression increased pHH3 expression

Fig. 4.6 Ectopic WT Bcl-3 overexpression in MDA-MB-436 increased the subG1 population and decreased the G0/G1 population

Fig. 4.7 Ectopic WT Bcl-3 overexpression in MDA-MB-231-Luc increased the subG1 and G2/M populations and decreased the G0/G1 population

Fig. 4.8 Ectopic Bcl-3 overexpression increased caspase-3/7 activity

Fig. 4.9 Ectopic Bcl-3 overexpression did not affect total mammosphere numbers but significantly reduced mammosphere size

Fig. 4.10 Ectopic Bcl-3 overexpression significantly impaired clonogenic survival

Fig. 4.11 Ectopic Bcl-3 overexpression significantly inhibited collective migration in MDA-MB-436

Fig. 4.12 Ectopic Bcl-3 overexpression significantly inhibited collective migration in MDA-MB-231-Luc

Fig. 4.13 Ectopic WT Bcl-3 overexpression increased amoeboid-like single cell migration

Fig. 4.14 Ectopic Bcl-3 overexpression significantly increased mesenchymal-like single cell migration in the -231-Luc cell line

Fig. 4.15 Ectopic overexpression of WT Bcl-3 increased NFkB activity

Fig. 4.16 Ectopic overexpression of Bcl-3 reduced growth rates at the orthotopic site

Fig. 4.17 Ectopic overexpression of WT Bcl-3 increased metastases to distal organs

Fig. 5.1 JS6 and CB1 disrupted Bcl-3-p50 protein-protein binding

Fig. 5.2 48h JS6 and CB1 treatment reduced cell viability at higher drug concentrations

Fig. 5.3 48h CB1 treatment did not affect mammosphere numbers but significantly reduced mammosphere size

Fig. 5.4 48h JS6 and CB1 treatment impaired clonogenic survival at 100µM concentration

Fig. 5.5 48h JS6 and CB1 treatment did not affect NFkB activity

Fig. 5.6 PANTHER Functional Classification Tool for 48h 100µM CB1 treatment

Fig. 5.7 Relative expression a Bcl-3 responsive gene panel following siRNA knockdown, JS6 or CB1 treatment.

Fig. 5.8 Daily refresh of JS6 and CB1 more effectively impaired clonogenic survival

Fig. 5.9 Daily refresh of JS6 and CB1 more effectively impaired clonogenic survival

Fig. 5.10 Quantification of metastatic progression through *in vivo* luminescence imaging

Fig. 5.11 Anti-metastatic efficacy of JS6 and 15F in xenograft model one

Fig. 5.12 Anti-metastatic efficacy of CB1 in xenograft model one

Fig. 5.13 CB1 and JS6 significantly reduced metastatic burden in xenograft model one

Fig. 5.14 Anti-metastatic efficacy of CB1 was maintained in xenograft model one when administered via oral gavage

Fig. 5.15 JS6 and CB1 did not significantly inhibit metastatic colonisation and expansion

Fig. 5.16 Daily JS6 and CB1 treatment did not significantly cause adverse toxicity

Fig. 5.17 CB1 significantly reduced orthotopic tumour growth in xenograft model three

List of tables

Table 1.1 Bcl-2 protein family members and their function

Table 2.1 Transfection concentration for siRNA

Table 2.2 Sequences of siRNA

Table 2.3 NFkB luciferase reporter assay transfection volumes

Table 2.4 List of novel Bcl-3 inhibitors

Table 2.5 Primary antibodies used in western blotting

Table 2.6 List of antibodies used for immunofluorescence

Table 2.7 cDNA synthesis master mix reagents

Table 2.8 Taqman gene expression assay probes

Table 2.9 qRT-PCR reaction component mix

Table 2.10 Injected drug volume based on animal weight for 3.5mg/kg

Tab. 3.1 PANTHER Statistical Overrepresentation Test for Bcl-3 siRNA knockdown

Tab. 3.2 PANTHER Statistical Enrichment Test for Bcl-3 siRNA knockdown

Chapter 1:

General Introduction

1 General Introduction

1.1 Hallmarks of cancer

The hallmarks of cancer first proposed by Hanahan and Weinberg, comprised of a number of common biological capabilities acquired during the complex multistep processes of human tumourigenesis. Outlining these hallmarks provides us with an organised approach for rationalising the complexities of this neoplastic disease. They include ‘sustaining proliferative signalling’, ‘evading growth suppressors’, ‘resisting cell death’, ‘enabling replicative immortality’, ‘inducing angiogenesis’, ‘activating invasion and metastasis’, ‘genome instability’, ‘inflammation’, ‘reprogramming of energy metabolism’ and ‘evading immune destruction’. Furthermore, cancer cells exhibit another dimension of complexity as they contain a repertoire of recruited, ostensibly normal cells that continue to contribute towards the acquisition of hallmark traits and creates what we know as the tumour microenvironment. Recognition and understanding these concepts will help us develop new means to combat human cancers (Hanahan and Weinberg, 2011).

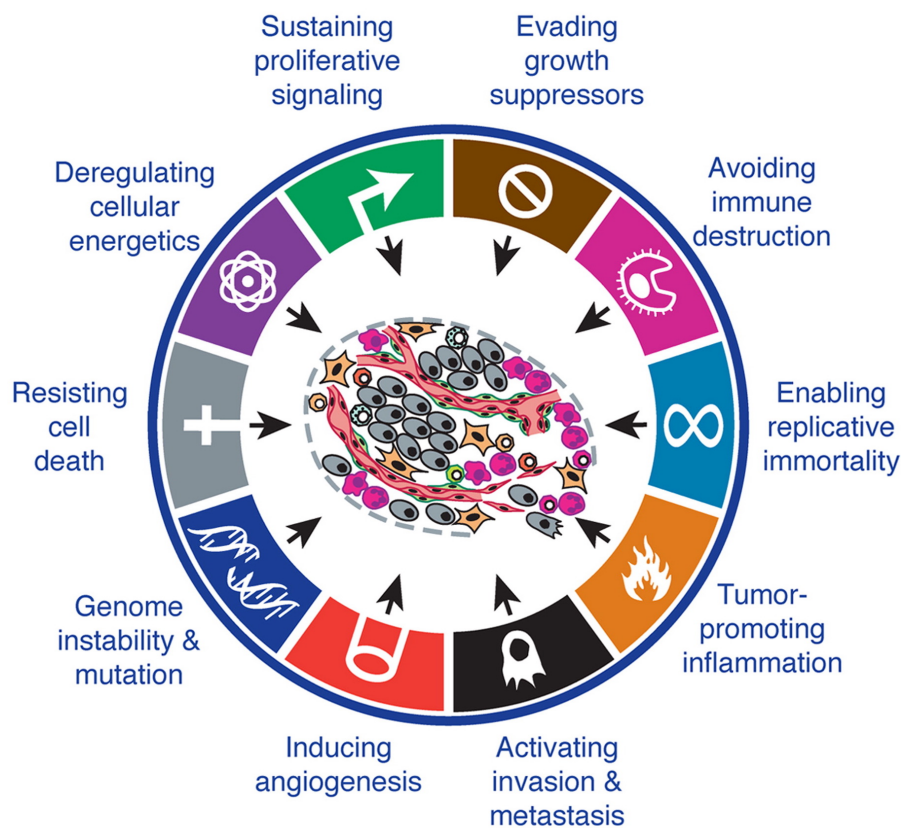


FIG. 1.1 THE TEN HALLMARKS OF CANCER

Figure adapted from Hanahan and Weinberg, 2011.

1.2 Breast cancer

Breast cancer remains one of the leading causes of cancer related deaths in women worldwide and is the most common form of cancer in the United Kingdom, with a steadily increasing incidence rate in recent years (Torre et al., 2016).

1.2.1 Triple-negative breast cancer

Triple-negative breast cancer (TNBC) accounts for 15-20% of all diagnosed breast tumours (Torre et al., 2016). Molecularly, TNBC is defined by the absence of oestrogen (ER), progesterone (PR) receptors and the lack of any overexpressed human epidermal growth factor receptor 2 (HER2 or ERBB2) proteins. Despite these common identifying features, TNBC is in fact a highly heterogeneous disease that can be further classified according to clinical, histopathologic, and molecular profiles.

Patients with TNBC are often young (<40 years), African American and have worse prognoses compared with other breast cancer subtypes; as well as a high prevalence of highly proliferating grade 3 tumours at diagnosis (Heitz et al., 2009). They feature earlier relapse after standard anthracycline and/or taxane-based chemotherapy treatments, typically 1-3 years after diagnosis and TNBC patients often develop visceral metastases. TNBCs typically have better pathologic complete response (pCR) rates following neoadjuvant chemotherapy compared with non-TNBCs, and patients who experience pCR have great long-term clinical outcomes. However, conversely TNBC patients with residual disease after neoadjuvant chemotherapy have extremely poor prognoses (Lin et al., 2012). Therefore, despite their high sensitivity to chemotherapy, the median survival of patients with metastatic disease very rarely exceeds 12 months, exemplifying a 'triple-negative paradox' (Bulut et al., 2008).

Patients with TNBC do not benefit from traditional hormonal or trastuzumab-based therapies due to loss of receptors. Hence, standard of care for patients with early or advanced TNBC remains surgery and chemotherapy, yet few effective novel drugs have been introduced in the last few decades. Many studies have been done to determine whether TNBC patients were more likely to undergo mastectomy or lumpectomy. Though the results show that despite the fact that TNBC tend to be more aggressive, surgical decision making tend to rest more on traditional clinicopathological variables and patient

preferences (Ajay and Radhakrishnan, 2017). The local recurrence rate following breast conservative surgery is not as high in TNBC compared to other subtypes of BC, so this remains yet an appropriate candidate for breast conservation (Freedman et al., 2009). Traditionally, radiotherapy is given following surgery, however there is still controversy surrounding this practice (Dawood, 2010).

Typical current therapeutic TNBC management strategies include targeting DNA repair complexes (platinum compounds or taxanes) or cell proliferation (anthracyclines) (Berrada et al., 2010). While the most effective specific adjuvant regimes for TNBC therapy remains incompletely defined for both early or advanced stages of the disease, third-generation chemotherapy regimens using dose dense or metronomic polychemotherapies are among the most effective tools available (Cardoso et al., 2010). Ultimately due to the a lack of predictors of therapy response in TNBC, there is also an ever increasing need for specific targetable markers for personalised therapies. For these reasons, identification of molecular targets and development of new therapeutic options remains critical for these patients.

1.2.2 Sub-typing within TNBC

Breast cancer in general is comprised of a large group of heterogeneous diseases that can be classified by gene expression profiling into luminal A, luminal B, basal-like, normal-like and HER2-enriched subgroups (Perou et al., 2000). Although both terms like 'basal-like' and 'triple-negative' are often used synonymously, it is important to highlight that not all TNBC are identified as basal-like by gene expression profiling, and immunohistochemical assays show that not all basal-like tumours are TNBC. There are about a 70-80% concordance between the terms (Lehmann and Pietsenpol, 2014). A recent landmark publication by Lehmann et al. categorised TNBC into six different subtypes following gene expression profiling: basal-like 1 and 2 (BL1 & BL2), immunomodulatory (IM), mesenchymal-like (M), mesenchymal stem-like (MSL) and luminal androgen receptor (LAR) (Lehmann et al., 2011).

The BL1 subtype exhibits high rates of cellular proliferation and Ki67 levels, due to being heavily enriched in cell cycle-related genes and pathways involving DNA repair. The BL2 subtype expresses high levels of glycolysis and gluconeogenesis pathways, as well as tyrosine kinase receptor signalling. The IM subtype is enriched for genes involved in

immune processes such as B, NK and T cell, cytokine signalling, chemokine receptor/ligand activity, complement cascades and antigen presentation. This subgroup has also been correlated with the highest levels of tumour-infiltrating lymphocytes (TILs) and has an expression profile that overlaps with medullary breast cancer (Bertucci et al., 2006). The M and MSL subtypes show gene signatures overlapping with chemo-resistant metaplastic breast cancer and have up-regulated genes associated with cell motility, epithelial-mesenchymal transition (EMT), differentiation and extracellular matrix remodelling. More specifically, the M subtype displays overexpression of proliferation genes, while the MSL subtype is more enriched in mesenchymal stem-cell associated genes, as well as angiogenesis and growth factor pathways. The MSL subtype overlaps with the previously defined 'claudin-low' subtype (Prat et al., 2010). Finally, the LAR subtype expresses androgen receptors (AR) and features hormonally regulated pathways leading to increased steroid metabolism and synthesis (Ring et al., 2016). Patients with the LAR subtype have the shortest relapse-free survival and this subtype overlaps with the previously described 'apocrine' subtype (Farmer et al., 2005).

1.2.3 Genetic markers in TNBC and targeted therapies

The molecular and genetic profiles of TNBC can be complex and diverse and studies have focused on identifying markers that influence prognosis and/or predict response to therapy. One unfortunate nature of TNBC is the tendency to develop multidrug resistance to conventional therapies and often progresses rapidly despite an often good initial response. For this reason, many recent targeted therapies have focused on the identification of either biologic or immunologic agents. The genomic profile of tumours has been shown to frequently change during chemotherapy, and these potentially explain mechanisms for acquired resistances (Balko et al., 2014). Therefore molecular analysis of post-treatment biopsy samples is crucial for patients who do not experience pCR after neoadjuvant chemotherapy to help identify new druggable targets and improve TNBC outcomes.

It is worth noting, to date, stratifying TNBC into additional subtypes by gene expression analysis is not a routinely performed clinical practice. However by doing so, it may offer novel therapeutic approaches and many studies have investigated different strategies targeting specific TNBC subtypes. For example, BL1 and BL2 subtypes may respond preferentially to anti-mitotic and DNA-damaging agents either alone or in

combination with platinum or taxane-based chemotherapy or poly-ADP ribose polymerase (PARP) inhibitors. On the other hand, the M and MSL subtypes might better respond to PI3K, c-MET, VEGFR2 or mammalian target of rapamycin (mTOR) inhibitors. The LAR subtype could demonstrate sensitivity to the AR antagonist bicalutamide (Gucalp et al., 2013), enzalutamide (Caiazza et al., 2016) and PI3K inhibitors (Lehmann et al., 2014).

Recent studies on primary TNBC patient samples, analysing genomic DNA copy numbers, methylation, exome-sequencing, mRNA arrays, microRNA sequencing and reverse-phase protein arrays have consistently observed genes with frequent somatic mutations and copy number aberrations (Cancer Genome Atlas Network, 2012). We will outline and discuss the significance of some of these important markers below.

1.2.3.1 TP53

TP53 is one of the most important genes involved in the maintenance of genomic integrity throughout cell-cycle arrest, DNA repair and apoptosis. Aberrant p53 expression has been described in all breast cancer subtypes (Hussain and Harris, 2006). In TNBC, TP53 is the most frequently mutated gene and in one recent study, the rate of mutation in basal-like tumours was 62% and in non-basal TNBCs it was 43% (Shah et al., 2012). These mutations result in increased genetic instability and a range of cytogenetic changes. Recent findings have linked decreased p53 functions with worse overall survival and increased metastatic risk in TNBC patients (Powell et al., 2016). Other studies found TP53 mutations to be a predictor of chemoresistance (Aas et al., 1996). Taken together, this gene is mutated in a majority of TNBCs and therefore presents an attractive candidate for anti-tumour therapies. Such therapies include inhibition of Chk1 in p53-deficient TNBC tumours, leading to sensitisation to DNA damaging agents (Bryant et al., 2014); or the emerging approach of inhibiting a downstream Chk1 target, WEE1 resulting in decreased toxicity and enhanced tumour growth suppression when combined with cisplatin (Zheng et al., 2017).

1.2.3.2 BRCA1/2

Breast-related cancer antigen 1 (BRCA-1) and BRCA-2 tumour suppressor genes plays an essential role in DNA double-strand break repairs through homologous

recombination (HR) pathways. About 15-20% of TNBC patients carry germline mutations of these two genes (Turner et al., 2004). Over 2000 different mutations have been identified with BRCA1 and BRCA2 and the most common are deletions or insertions, as well as single-nucleotide substitutions in either coding and/or non-coding sequences, resulting in protein dysfunction (Lips et al., 2013). Benefits from neoadjuvant chemotherapies such as PARP inhibitors were found to be higher in TNBC patient with germline BRCA1/2 mutations (von Minckwitz et al., 2014).

Poly ADP ribose polymerase (PARP) is a family of proteins involved in the DNA base excision repair pathway and PARP inhibition leads to the persistence of single-strand DNA breaks that collapse replication forks resulting in double-strand breaks. These lesions are typically repaired by the high-fidelity HR system that requires functional BRCA genes. Subsequently, in BRCA-deficient cells, double-strand breaks are repaired by the alternative error-prone non-homologous repair processes, resulting in chromosomal instability, cell cycle arrest and apoptosis. This is a model of synthetic lethality where the combination of two mutations in two or more genes results in cell death, whereas a mutation in only one of these genes has no effect (Robson et al., 2017).

Combination of a PARP inhibitor (olaparib/AZD2281) and cisplatin or carboplatin prolonged overall survival of mice implanted with BL breast cancer mouse tumours (Rottenberg et al., 2008). Olaparib has also been tested in clinical trials and high doses showed better objective responses with acceptable toxicity, although resistance has been observed in patients (Tutt et al., 2010).

1.2.3.3 PI3K pathway

Increased PI3K/Akt/mTOR signalling is frequently observed in TNBCs and causes changes in cells survival, differentiation, proliferation and the stability of double-strand DNA breaks through the HR complex (Gonzalez-Angulo et al., 2009). In basal-like tumours, PTEN and INPP4B alterations are more common than PIK3CA mutations as this is more typically associated with ER positivity. PTEN is an important negative regulator of the PI3K pathway and its loss contributes to both rapid tumour proliferation as well as poor prognosis in TNBC (Beg et al., 2015). The INPP4B phosphatase is another negative regulator of PI3K and is associated with high clinical grade, increase tumour size, loss of hormone receptors and aggressive basal-like breast cancers (Fedele et al., 2010).

Furthermore, mutations of PIK3CA, which encodes a catalytic subunit of PI3K, occurs in about 10% of TNBCs and can further activate PI3K signalling. Among the TNBC subtypes, LAR features the highest PIK3CA mutation prevalence, so combined therapeutic targeting of AR and PIK3CA could prove beneficial (Lehmann et al., 2014). Preclinical data have shown that TNBC tumours are more sensitive to combination therapy. PI3K inhibition has been shown to disrupt HR of DNA in TNBCs by down-regulating BRCA1/2 and sensitising BRCA-proficient tumours to PARP inhibitors (Ibrahim et al., 2012).

The PI3K/mTOR inhibitor, BEZ235 enhanced the tumour suppressive effects of chemotherapy agents carboplatin and docetaxel in an orthotopic MDA-MB-231 murine model as a proof of concept experiment (Montero et al., 2014). In addition, many clinical trials have evaluated the clinical benefits of combining PI3K or mTOR inhibitors with chemotherapy in TNBC. A phase II showed that 36% of metastatic TNBC patients benefited from the combination of everolimus and carboplatin. However another phase II trial of a PI3K inhibitor, GDC-0941, plus cisplatin in TNBC was terminated (Singh et al., 2014). All in all, recent studies generally suggest further analysis is required for determining the effectiveness of these combinatory chemotherapies and which TNBC subpopulation will benefit most from PI3K/mTOR inhibitors.

1.2.3.4 Tyrosine kinase receptors

Tyrosine kinase receptors from the EGFR, FGFR and VEGFR families have all been reported to have clinical relevance in TNBCs (Cheng et al., 2015). EGFR (HER1) mediates proliferation, angiogenesis, metastasis, inhibition of apoptosis and is overexpressed in about 60% of TNBCs. Results from trials testing EGFR tyrosine kinase inhibitors as well as anti-EGFR monoclonal antibodies either alone or in combination have thus far been disappointing (Nakai et al., 2016) Addition of the anti-EGFR antibody, cetuximab to cisplatin significantly increased the response rate in TNBC patients (Baselga et al., 2013). However, another phase I trial of erlotinib plus the nitrogen mustard derivative alkylating agent, bendamustine, in TNBC patients resulted in severe lymphopenia and only 1 out of 11 patients had partial responses (Layman et al., 2013). FGFR mediates proliferation, survival, migration and differentiation. Alterations in FGFR genes occur in about 10% of TNBCs and tumours with constitutively activation of this receptor is sensitive to the FGFR ATP-competitive inhibitor brivanib (Shiang et al., 2010). Preliminary studies with the FGFR

inhibitor, PD173074, inhibited the growth of BL breast cancer cell line xenografts (Sharpe et al., 2011). The VEGFR family plays an important role in angiogenesis, which in turn affects cancer development and the addition of bevacizumab to chemotherapy has improved pCR rates in a number of TNBC patients (von Minckwitz et al., 2012).

1.2.3.5 Androgen receptors

Along with ER and PR, AR belongs to the nuclear steroid hormone receptor family and plays an important role in cell signalling through the Wnt pathway. It is able to regulate genes involved in metastasis, PTEN, p53, along with other cell-cycle regulators, as well as the PI3K/Akt/mTOR pathways (Peters et al., 2009). In TNBC, AR positivity is found in 13-37% of cases and associates with the LAR subtype. It typically has a lower Ki67 index when compared with AR-negative TNBCs and is therefore less sensitive to chemotherapy (Barton et al., 2015). AR presents an easily detectable marker that can identify a subgroup of TNBCs that could benefit from targeted AR antagonist therapy. A phase II clinical trial of bicalutamide resulted in 19% of patients showing a therapeutic response to this agent for at least 6 months and the treatment toxicity was moderate (Gucalp et al., 2013).

1.2.3.6 BCL2

BCL2 is an anti-apoptotic mitochondrial protein with oncogenic effects. The role of BCL2 in TNBC is not well established, but its absence in pre-chemotherapy samples correlate with high probability of pCR to neoadjuvant doxorubicin-based chemotherapy (Pusztai et al., 2004). Similarly in the adjuvant setting, low BCL2 expression was associated with better TNBC outcome when treated with anthracycline-based chemotherapy (Bouchalova et al., 2015). Adding BCL2 to the clinical screening panel would be easy and could provide useful prognostic predictive information pertaining to TNBC patients.

1.2.4 Immunotherapy in TNBC

Despite evidence that breast cancer in general is not considered an immunogenic cancer, TNBC has been shown to be a lymphocyte-predominant breast cancer, with high stromal TIL percentages of 50-60% (Coates et al., 2015). Clinical studies have

demonstrated that tumour infiltration of certain immune cell types (CD8+, CD4+ TH1 T cells, NK cells and M1 macrophages) correlated with more favourable prognoses. Presence of lymphocytes in the tumour proximity have served as a surrogate marker for the immune response against tumour antigens and acts as an independent prognostic marker. Both high levels of intra-tumoural and stromal TILs have been associated with better disease outcome and various trials have demonstrated for every 10% increase in stromal TILs, there is a 15-20% reduction in recurrence and mortality (Loi et al., 2013). Conversely, higher intra-tumoural presence of tumour-associated macrophages (TAM), myeloid-derived suppressor cells (MDSC), CD4+ Treg and TH2 cells, as well as their associated cytokines (IL6, TNF, IL10, IL23 and TGF- β) have been associated with a worsening prognosis.

TNBCs often exhibit genomic instabilities causing greater immunogenicity and neoantigen production, complementing higher expressions of PDL1. Clinical trials investigating the roles of PD1 and PDL1 inhibition in the adjuvant, neoadjuvant and metastatic settings are ongoing (Mittendorf et al., 2014). The high TIL levels within TNBCs are possibility due to various mutations resulting in the creation of new epitopes that are better able to elicit an immune-mediated anti-tumour response. The presence of a lymphocytic infiltrate has also been associated with better responses to neoadjuvant chemotherapy and can better predict pCR, especially in TNBCs over other breast cancer subtypes (Mao et al., 2014).

1.2.5 TNBC metastatic progression

Metastatic disease remains incurable and the eventual dissemination of breast cancer cells to distal organs such as the bone, lungs and brain represents a significant clinical challenge. Metastatic progression is a complex process that is poorly understood and is the primary cause of death for the vast majority of TNBC patients. There are several steps involved, including the acquisition of invasive properties through genetic and epigenetic alternations, angiogenesis, tumour-stromal interactions, intravasation through the basement membrane, survival in the circulation and extravasation of cancer cells to distal tissues (**Fig 1.2**) (Nguyen and Massagué, 2007). However, disseminated cells that complete this process often remain quiescent in the secondary organs undergoing long periods of latency known as the dormancy period (Giancotti, 2013). It has been well established that the expansion of metastatic cells in a foreign tissue

microenvironment is a highly inefficient process and is considered as the rate-limiting step for breast cancer metastasis. Though during this stage, the disease is difficult to detect and exhibits resistance to chemotherapy due to their low proliferating nature. This highlights the current clinical problems pertaining to patients who respond well to initial therapy, but can often develop metastatic disease years later.

Disseminated tumour cells (DTC) can achieve a state of indefinite dormancy by balancing the proliferative cycle with apoptosis. Successful emergence from this state is a result of further molecular evolution possibly acquired through interactions with the tumour microenvironment. While significant progress has been made to understand specific processes required for breast cancer initiation, it is important to shift our efforts towards elucidating the underlying mechanisms and signalling pathways involved in the fatal late stages of metastatic dissemination. Development of effective treatments against the metastasis of TNBC cells therefore remains of the utmost importance (Neophytou et al., 2018).

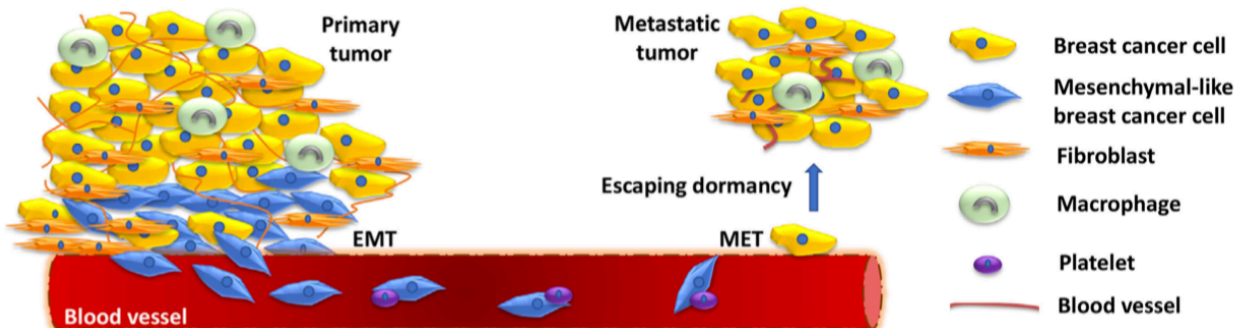


FIG. 1.2 PROCESSES INVOLVED IN METASTATIC PROGRESSION OF THE PRIMARY TUMOUR
Figure adapted from Neophytou et al., 2018.

1.2.5.1 Local invasion and intravasation

Following tumour initiation, TNBC cells in the primary tumour must acquire properties such as self-renewal, migration and the ability to invade surrounding normal tissue. During local invasion, cancer cells undergo epithelial-to-mesenchymal transition (EMT), a highly orchestrated transcriptional program associated with embryonic development in the normal context. This involves the remodelling of cytoskeleton, loss of apico-basolateral polarity, dissolution of cell-cell junctions along with down-regulation of

epithelial markers and up-regulation of mesenchymal genes (De Craene and Berx, 2013). This process is controlled by EMT-master regulatory genes such as Slug, Snail and Twist to promote TNBC migration and intravasation into the circulation. The TGFB signalling pathways plays a prominent role in regulating this early metastatic event and it is able to promote the expression of many of the EMT-regulators listed above as well as silencing epithelial genes, like CDH1 (Papageorgis et al., 2010).

1.2.5.2 Survival in circulation

Following entry into the blood vessels, circulating tumour cells express anti-apoptotic and pro-survival proteins which also allow them to attach and infiltrate specific secondary sites. Neurotrophic tyrosine kinase receptor (TRKB) has been shown to inhibit anoikis, a form of cell death caused by the lack of adhesion via the PI3K/Akt signalling pathway (Douma et al., 2004). The ability to bind platelets has also been shown to be essential for the survival of circulating TNBC cells and have been shown to be involved in their survival and evasion of pro-apoptotic signals (Wenzel et al., 2010).

1.2.5.3 Extravasation

Many common genetic aberrations associated with intravasation are also implicated in extravasation since these two processes are considered 'mirrored' to each other. The TGFB/Smad pathways are able to assemble a mutant-p53/Smad complex that inhibits the function of the metastasis suppressor TP63 (Adorno et al., 2009). TGFB also induces angiopoietin-like 4 (ANGPTL4) expression, enhancing the retention of cancer cells in the lungs through disruption of vascular endothelial cell-cell junctions (Padua et al., 2008).

1.2.5.4 Metastatic colonisation

Once extravasation and infiltration has taken place, EMT plasticity and the reversal to a MET phenotype has been shown to be important factors for colonisation (Gunasinghe et al., 2012). During this process, the epithelial phenotype is re-established through miR-200-mediated down-regulation of genes such as ZEB1 (Gregory et al., 2008). Various chemokines and inflammatory microenvironment signals have been implicated in the promotion of colonisation and escape from dormancy (Dongre et al.,

2017). It is also important to note that cellular and genetic context is critical in determining whether a protein acts as a tumour suppressor or metastatic promoter. One controversial example is LOXL4, which has been shown to facilitate colonisation of TNBC in the lungs via a HIF1a-dependent mechanism (Wong et al., 2011). However another study showed that knockdown of LOXL4 expression in TNBC cells promoted primary tumour growth and further lung metastasis due to associations with thickening collagen bundles and remodelling of the extracellular matrix within tumours (Choi et al., 2017).

1.3 Apoptosis pathways

Underneath the intricacy of every cancer lies different and mysterious events that impel tumour cells into abnormal growth and tissue invasion. Oncogenic mutations such as those resulting in elevated Bcl-3 disturb normal regulatory circuits and permit tumour cells to endure deregulated proliferation, invade and erode normal tissues and above all escape apoptosis.

Apoptosis or otherwise known as programmed cell death is a physiological process that is responsible for elimination of unwanted, damaged, mutated and/or aged cells that might pose robust threats. Cell death is essential for life and must balance cell proliferation in the living body (Czabotar et al., 2014). The principle of apoptosis is the dismissal of damaged cells in a fashion that causes the least damage and inflammation. The primary morphological feature of apoptosis is shrinkage of nuclei, nuclear chromatin condensation, cytoplasmic shrinkage, dilated endoplasmic reticulum and membrane blebbing. The contents of the cell are then wrapped in apoptotic bodies which are recognised and engulfed by phagocytic cells and digested in lysosomes (Hotchkiss et al., 2009). Apoptotic mechanisms are typically interlinked with other prominent pathways such as cell cycle, metabolism and receptor transduction pathways. Dysregulation of this pathway, either excessive or recessive is central to many diseases, cancer being one of them (Walsh, 2014).

1.3.1 Intrinsic mitochondria-mediated pathway

Apoptosis is triggered by activation of caspase families via two distinct but congregating pathways known as the intrinsic and extrinsic pathways. The intrinsic or otherwise known as the stress or mitochondrial pathway is dominantly controlled by the

BCL2 family of proteins. This mitochondria-controlled cell death is firstly triggered by an increase in mitochondrial permeability, resulting in release of apoptogenic factors BAX and BAK through the outer membrane, disturbing the electrochemical gradient of the inner membrane. This change is detected by a multiprotein mitochondrial permeability transition complex that resides at the junction of inner and outer mitochondrial membranes. Secondly this mitochondrial dysfunction results in either the disturbance of plasma membrane integrity leading to necrosis and/or the activation of specific caspases by the mitochondrial protein cytochrome c leaking into the cytosol. Cytochrome c forms an apoptosome complex and one of its key constituents, apoptotic protease activating factor 1 (APAF-1) binds procaspase 9, activates effector caspases and induces apoptosis. The released protein second mitochondria-derived activator of caspases (SMAC) blocks the caspase inhibitor called X-linked inhibitor of apoptosis protein (XIAP). The intrinsic pathway could also be engaged and magnified when certain death receptor ligands in the extrinsic pathway, such as FAS and TNF signalling activate caspase-8 and generate tBID via FADD and TRADD. These two pathways subsequently congregate at the effector caspases-3, -6 and -7 (Zamzami and Kroemer, 2001).

1.3.2 Extrinsic receptor-mediated pathway

Alternatively, activation of caspases is also brought about through death receptor (DR) signalling initiated at the cellular surface. This pathway is referred to as extrinsic or death receptor pathway. All DRs expressed on the cell membrane are characterised by the presence of a death domain (DD) that play a crucial role in the apoptotic signal transduction. So far, six members of the DR family have been recognised: TNF-R1, CD95 (APO1/FAS), DR3, TRAIL-R1, TRAIL-R2 and DR6. The DRs are triggered following activation by death ligands, resulting in the formation of a death-inducing signalling complex (DISC). This DISC is comprised of oligomerised receptors: Fas-associated death domain, procaspase-8 (FLICE), procaspase-10 and the cellular FLICE inhibitory proteins (c-FLIP). Formation of DISC activates procaspase-8/-10 and initiates the proapoptotic cascade of caspases (Ashkenazi, 2002).

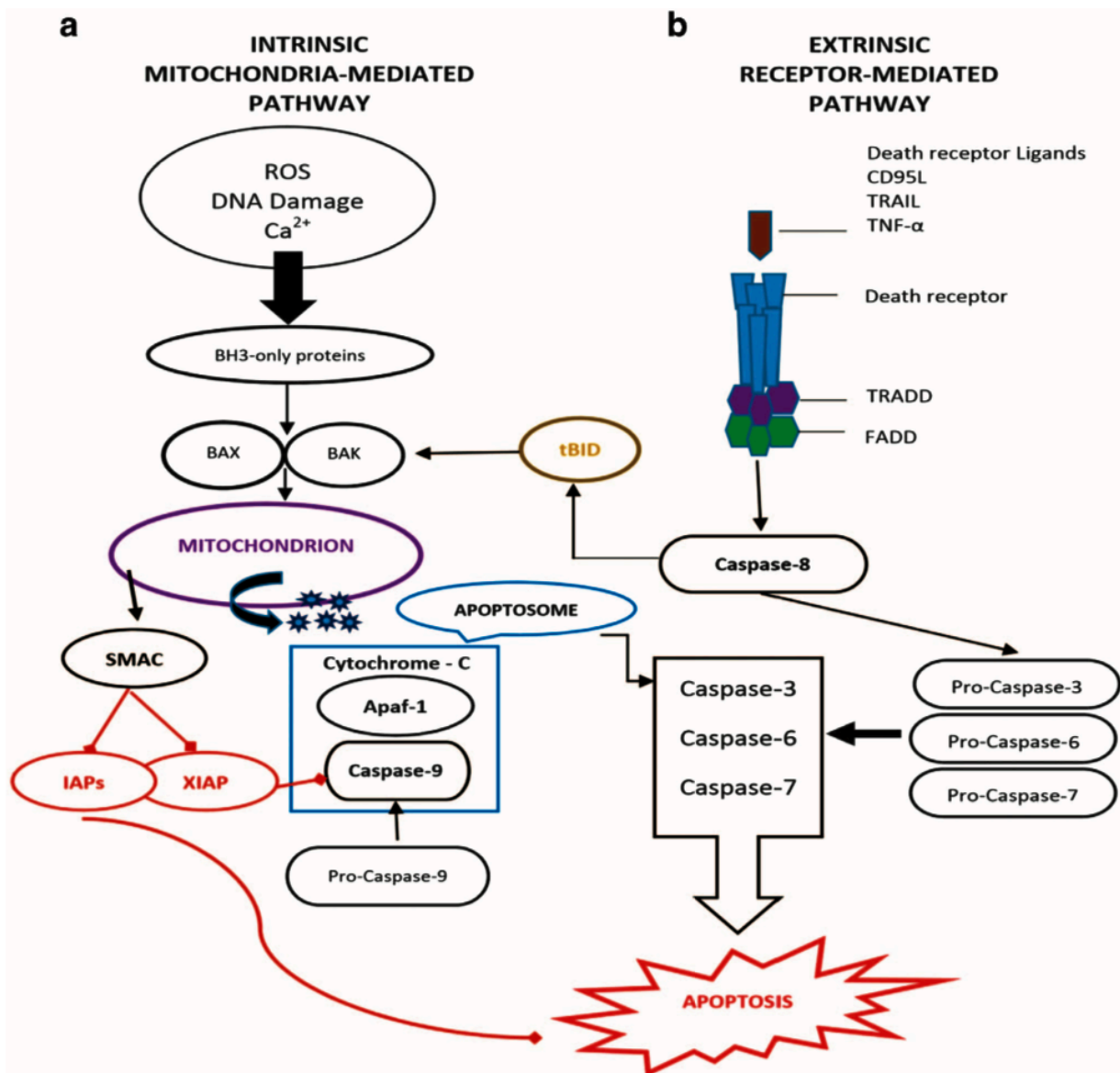


FIG. 1.3 APOPTOSIS PATHWAYS

a. The mitochondria-mediated intrinsic and **b.** death receptor-mediated extrinsic pathway. Adapted from Baig et al., 2016.

1.3.3 BCL2 protein family

There are a total of 25 known genes of the BCL2 protein family and members are characterised by four conserved amphipathic α -helical regions designated BCL2 homology (BH) 1-4 domains. Based on these domains, members could be broadly categorised into three subgroups: [1] pro-apoptotic multi-domain proteins BAX and BAK, [2] anti-apoptotic multi-domain proteins BCL2, BCLXL, BCLW, BFL1 and MCL1, and [3]

pro-apoptotic single domain BH3-only proteins BID, BIM, BAD, p53 unregulated controller of apoptosis (PUMA) and NOXA (Danial and Korsmeyer, 2004).

Bcl-2 family member	BH domain	Proapoptotic	Antiapoptotic	Proapoptotic function
BCL	BH 1-4	-	Y	-
BCLXL	BH 1-4	-	Y	-
BCLW	BH 1-4	-	Y	-
MCL1	BH 1-4	-	Y	-
BAX	BH 1-3	Y	-	Effector
BAK	BH 1-3	Y	-	Effector
BIM	BH3-only	Y	-	Activator
BID	BH3-only	Y	-	Activator
BAD	BH3-only	Y	-	Sensitiser
BIK	BH3-only	Y	-	Sensitiser
NOXA	BH3-only	Y	-	Sensitiser
PUMA	BH3-only	Y	-	Sensitiser

TABLE 1.1 BCL-2 PROTEIN FAMILY MEMBERS AND THEIR FUNCTION

1.3.4 Inhibitor of apoptosis proteins

Inhibitor of apoptosis proteins (IAPs) are a family of proteins that serve as endogenous inhibitors of apoptosis and all have a common domain of 70 amino-acid baculo-virus repeats (BIR) that suppress caspase function by facilitating protein-protein interactions. XIAP prevents caspase-3 processing in response to caspase-8 activation, inhibiting the extrinsic apoptotic signalling. The human IAP family consists of eight members: NAIP, XIAP, cIAP1, cIAP2, ILP2, survivin, livin and BRUCE (Lemke et al., 2014).

1.4 Rho family of small GTPases in actin regulation and motility

1.4.1 Rho GTPases and upstream regulation

The Rho-family of p21 small GTPases are critical to the regulation of actin cytoskeleton and cell motility. Rho GTPases function as molecular switches and can interact with downstream effector molecules to propagate signal transduction when in their GTP-loaded “on” state (Bourne et al., 1991). Intrinsic phosphatase activity can hydrolyses the GTP to GDP, turning the Rho GTPase “off”. This process is accelerated by interactions with GTPase activating proteins (GAPs). The relative affinity difference for effector molecules from the GTP “on” versus GDP-loaded “off” states of the Rho GTPase can be as much as 100-fold, resulting in a highly specific signalling processes only in the GTP-bound activated state. Interaction with guanine-nucleotide exchange factors (GEFs) facilitates the exchange of GDP back to GTP (Rossman et al., 2005).

Binding of GAP or GEF interactions take place directly at the same effector binding interface of the Rho GTPase. The binding of GAP confers slight structural changes that act to insert a water molecule into the catalytic pocket of the Rho GTPase to facilitate the hydrolysis of GTP into GDP by a factor of almost 4000-fold greater than the rate of intrinsic phosphates. The binding of GEF displaces the Mg⁺² and releases the bound GDP in exchange for GTP (Moon and Zheng, 2003). There exists mutant versions of Rho GTPase, either dominant negative or constitutively active and they can sequester upstream GAPs and GEFs.

Guanine-nucleotide dissociation inhibitors (GDIs) are another class of molecules that interact with Rho GTPases as they bind and inhibit the dissociation of the guanine nucleotide, preventing the activation of Rho GTPases. The N-terminal regulatory portion of GDI also interacts with the effector binding interface of the Rho GTPases, preventing binding with any of its effectors. Binding of GDI to Rho GTPases at the plasma membrane causes the bound complex to be pulled into the cytoplasm. The shuttling of the active fraction of Rho GTPase between membranes and the inactive fraction in the cytoplasm constitutes one of the major regulatory dynamics of Rho GTPases (DerMardirossian and Bokoch, 2005). Various upstream kinases target GDI and Rho GTPases including Src, PKC, PKA and specifically modulate the affinity of GDI towards members of the Rho GTPase family.

Traditionally, the Rho family of GTPases, RhoA, Rac1 and Cdc42 have been primarily associated with cytoskeleton rearrangements. Microinjections of the activated mutants of Rho GTPases into starved and quiescent Swiss3T3 cells induced dramatic actin cytoskeletal rearrangements where RhoA caused stress fibre and adhesion formation, Rac1 induced sheet-like lamellipodial protrusions and Cdc42 produced filopodial protrusions (Bishop and Hall, 2000).

While it is easy to conclude that any one of the GTPases could have distinct and isolated effects on cell motility, it appears more likely these Rho GTPases exist in complex activation cascades. An example of this effect is the antagonism between Rac1 and RhoA and it has been observed that the protrusive phenotype driven by Rac1 must prevail at the leading edge and the contractile phenotype by RhoA primarily drives the tail retraction in locomoting cells (Rottner et al., 1999).

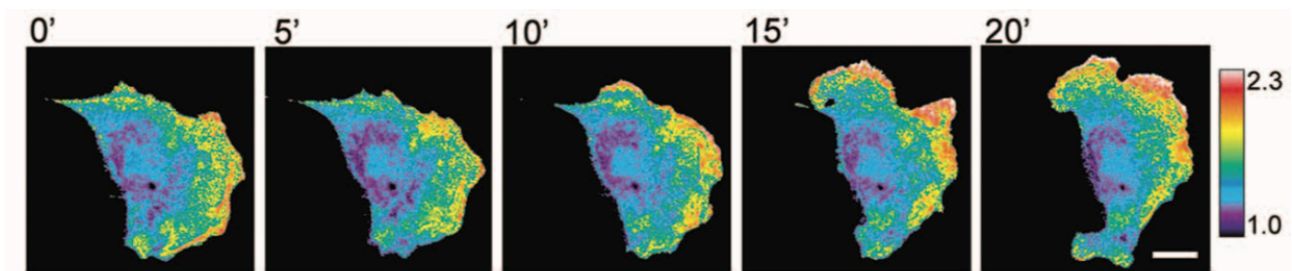


FIG. 1.4 FLUORESCENT BIOSENSOR DATA SHOWING ACTIVATION PATTERNS OF RHOA AT THE LEADING EDGE

Figure adapted from Pertz et al., 2006.

1.4.2 Rho GTPase downstream targets

The downstream Rho targets are well described and include kinases, formins, WASp proteins, and other scaffolding molecules. Of these major subclasses, the p21-activated kinase (PAK), mammalian Diaphanous formin (mDia) and proteins of the WASp family including WASp, N-WASp and WAVE, all have direct effects on actin cytoskeleton rearrangements crucial to motility. RhoA, B and C activate the immediate downstream kinase target ROCK, which phosphorylate a number of actin cytoskeleton regulators including myosin light chain phosphatase and LIM kinase (LIMK). (Narumiya et al., 2009) Direct phosphorylation of myosin light chain or of myosin light chain phosphatase impacts on the level of phosphorylated myosin light chain, which contributes to contractility. Activation of LIMK by ROCK phospho-regulates ADF/cofilin, which is one of

the key regulators of actin severing, nucleation and capping within the protrusive machinery. Feeding directly into this pathway, Rac1 and Cdc42 activates p21-activated kinase1 (PAK1), which also activates LIMK (DesMarais et al., 2005). The Slingshot and Chronophin family of phosphatases activated by Rac1 can also dephosphorylate cofilin to activate it.

Another critical downstream effector of RhoA, B and C is the Formin family of proteins. Formins produce straight, unbranched actin fibres through the formin homology domain 2 (FH2). FH2 is associated with the tip of the growing actin filament and accelerates the incorporation of actin monomers. Formin homology 1 (FH1) delivers profilin-bound actin monomers to FH2. These actin fibres are typically evident in actin stress fibres, filopodia, actin cables and cytokinesis actin rings. Formins are typically activated by Rho GTPases which displaces the auto-inhibitory domain, relaxing the closed conformation, allowing for FH1/FH2 to process actin polymerisation (Goode and Eck, 2007).

Rac1 and Cdc42 activate Wiskott-Aldrich Syndrome family of proteins including, WASp, N-WASp and WAVE1/2. These molecules exist in an auto-inhibited, closed conformation where the C-terminal VCA motif binds to the GTPase binding domain (GBD). Activated Cdc42 or Rac 1 competes against this auto-inhibition, releasing the VCA from the GBD, which allows binding of Arp2/3 complex and subsequent activation of the Arp2/3 complex. Unlike WASp, WAVE proteins do not have a GBD domain and their activation requires binding of Rac1 to the adapter molecule IRSp53, followed by binding of this complex to the WAVE protein (LeClaire et al., 2008).

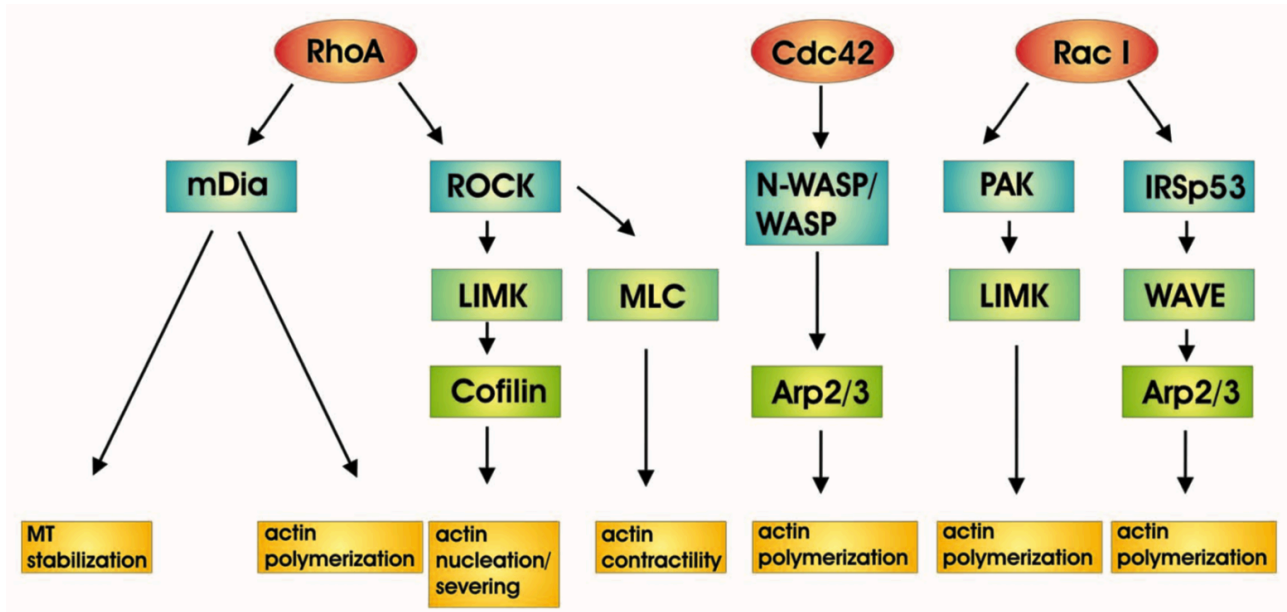


FIG. 1.5 DOWNSTREAM EFFECTOR TARGETS OF RHO FAMILY OF GTPASES

Adapted from Spiering and Hodgson, 2011.

1.5 The NFκB signalling pathway

NFκB-mediated transcription plays a critical role in the regulation of immune responses, apoptosis and cell survival, hence are centrally implicated as mediators of cancer initiation and progression. NFκB activation leads to the transcription of a wide range of genes encoding for inflammatory cytokines, cell-cycle modulators, survival signals, growth and angiogenic factors, all positive drivers in the tumour environment. The fine tuned balance between NFκB activation and control is lost during pathological conditions such as cancer and chronic inflammation (Grivennikov et al., 2010).

1.5.1 NFκB subunits

The mammalian NFκB family consists of five subunits: p65 (RelA), RelB, c-Rel, p50 (NFκB1) and p52 (NFκB2) (**Fig. 1.6**). Unlike other subunits, NFκB1 and NFκB2 are synthesised as precursors (p105 and p100) which are proteolytically cleaved to p50 and p52, respectively. The various NFκB subunits are capable of forming homo- and hetero-dimers as they share structurally similar Rel homology domains (RHD) essential for dimerisation and cognate DNA interactions (May and Ghosh, 1997).

In most quiescent cells, these dimers are collectively held inactive in the cytoplasm by binding to inhibitor of κ B proteins (I κ B). These inhibitors are characterised by their ankyrin repeat domains, which associate with the DNA-binding domains of the NF κ B subunits, making them transcriptionally inactive. The precursors p105 and p100 contain ankyrin repeats which act as internal inhibitors prior to cleavage and maturation. In contrast to other NF κ B subunits, p50 and p52 do not contain transactivation domains (Marienfeld et al., 2003). Consequently when p50 and p52 dimers bind to NF κ B elements of gene promoters, they will be inactive and act as transcriptional repressors (Hayden and Ghosh, 2012). However, when p50 or p52 are bound to a subunit containing a transactivation domain, such as p65 or RelB, they will act as a transcriptional activator. One atypical member of the I κ B family, Bcl-3 also contains transactivation domains and can complex p50 and p52 dimers, rendering them transcriptionally active (Fujita et al., 1993). NF κ B subunits also contain phosphorylation sites and other post-translational modifications that play a role in activation and/or crosstalk with other signalling pathways (Oeckinghaus and Ghosh, 2009).

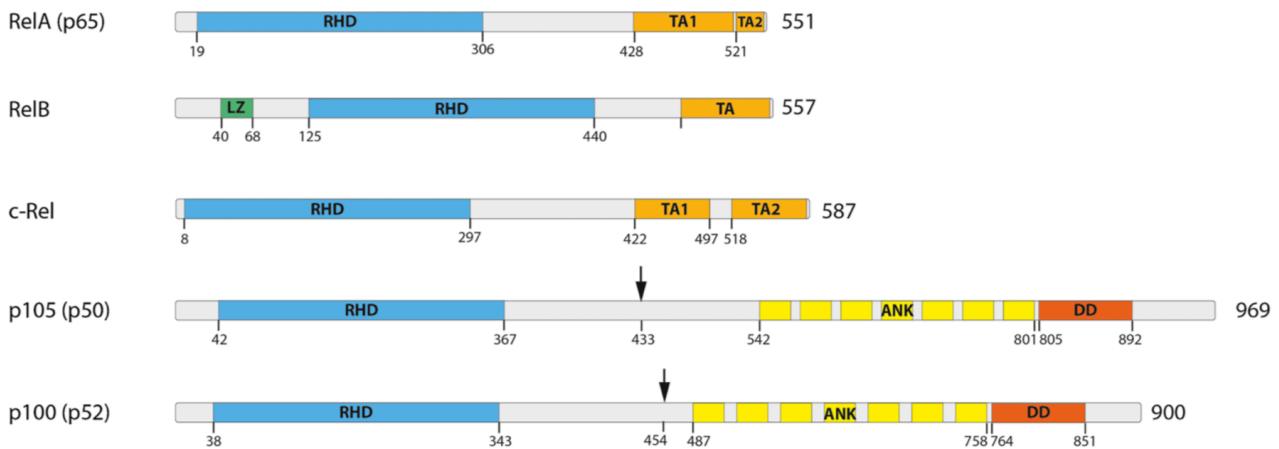


FIG. 1.6 THE FIVE SUBUNITS OF THE MAMMALIAN NF κ B FAMILY.
Figure adapted from Hoesel and Schmid, 2013.

1.5.2 Mechanisms activating NF κ B signalling pathways

Typically, activation of NF κ B subunits involves either the release from the I κ B molecules or by cleavage of the p100 and p105 inhibitory ankyrin repeat domains. Proteasomal degradation of the I κ B inhibitors requires prior polyubiquitination of the target molecules with lysine-48 linked ubiquitin chains. In order for the ubiquitination enzymes to carry out this process, it must first recognise a specific double

phosphorylation signature on the substrate. This is catalysed by a complex containing I κ B kinases (IKK α and IKK β) and at least one non-catalytic accessory protein (NEMO) (**Fig. 1.c**) (Hayden and Ghosh, 2008). This I κ B kinase (IKK) complex is able to bind additional components, respond to upstream signalling molecules and can be activated by a great variety of stimuli. The varying activation mechanisms guarantee that different stress situations can induce the catalytic activity of IKKs, leading to the liberation and activation of NF κ B signalling.

The canonical activation pathway (**Fig. 1.7a**) involves excitatory signals mediated through toll-like receptors (TLRs), interleukin-1 receptor (IL1R), tumour necrosis factor receptor (TNFR) and antigen receptors. Typical molecules that stimulate signalling include tumour necrosis factor alpha (TNF α), lipopolysaccharides (LPS) and interleukin-1 beta (IL1B) (Perkins and Gilmore, 2006). Stimulation through these receptors leads to the activation of the IKK2 complex and subsequently phosphorylates I κ B α . The non-canonical activation pathway (**Fig. 1.7b**) signals through a different class of receptors including B-cell activation factor (BAFFR), lymphotoxin β -receptor (LTBR), CD40, receptor activator for nuclear factor kappa B (RANK), TNFR2 and Fn14 (Sun, 2011). This process results in the activation of the NF κ B inducing kinase NIK, which phosphorylates and activates IKK1. IKK1 induces phosphorylation of p100 resulting in its ubiquitination and partial degradation to p52 (Xiao et al., 2001). In many cases, p100 is associated with RelB, so the proteolytic processing of p100 induces the formation of the transcriptionally active RelB-p52 complex. The atypical activation pathway (**Fig. 1.7c**) involves the activation of the IKK complex after genotoxic stress via the ATM checkpoint kinase, resulting in the ubiquitination of NEMO and subsequent NF κ B signalling.

After NF κ B dimers are liberated from the inhibitory I κ B proteins, they localise to the nucleus and the RHDs are free to bind their cognate DNA-sequences in the enhancer elements of gene promoters. Depending on the accessibility determined by the epigenetic mechanism of the cell type, thousands of potential target genes could become transcriptionally activated upon NF κ B pathway activation. Termination of NF κ B transcriptional activity is primarily achieved through NF κ B up-regulating its own inhibitors of the I κ B family in a negative feedback loop, until complete inactivation back to background levels (Pahl, 1999).

1.5.3 NFkB in cancer

NFkB is constitutively active in many cancers and subsequently exerts a variety of pro-tumourigenic functions. The immune system appear to play a role in protecting against malignant cells with dysregulated NFkB as immune-suppressed individuals exhibit a higher risk of cancer (Smyth et al., 2006). NFkB activation has been associated with the up-regulation of anti-apoptotic genes, promotion of proliferation, as well as inducing the release of pro-inflammatory cytokines (Guttridge et al., 1999). It has been postulated that neutrophils of the innate immunity that release reactive oxygen species to kill invading pathogens could cause DNA-damage and promote genetic mutations that trigger tumour initiation as a side effect (Liou and Storz, 2010). Moreover, NFkB signalling has been shown to contribute towards cancer progression through mediating EMT and metastatic progression (Huber et al., 2004). Finally, NFkB can also control tumour angiogenesis via up-regulation of VEGF and its receptors (Yoshida et al., 1999).

Direct mutations of NFkB genes have been found in lymphoid malignancies with amplifications or point mutations of RelA in B-cell lymphomas, chromosomal truncations of the NFKB2 gene in other lymphomas (Neri et al., 1991). Furthermore, mutations of other members of the NFkB signalling pathway including Bcl-3 and c-Rel have also been detected in B-cell leukemias (Rayet and G elinas, 1999). In solid tumours, direct mutations of NFkB are rarer, but transgenic mice studies have demonstrated direct contributions of the NFkB signalling pathway to the development of colorectal tumours (Greten et al., 2004).

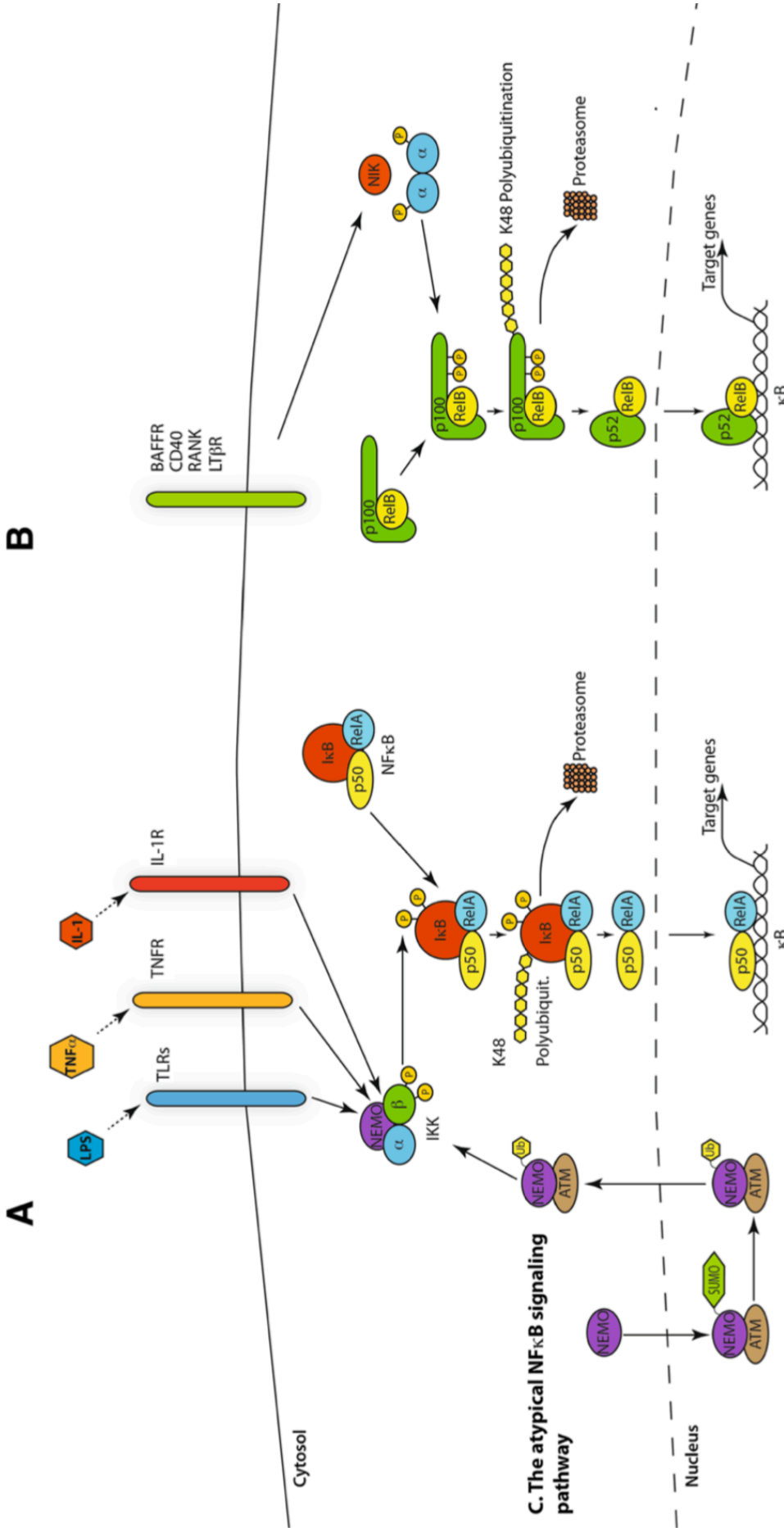


FIG. 1.7 THE CANONICAL, NON-CANONICAL AND THE ATYPICAL NF κ B SIGNALLING PATHWAYS

a. Canonical NF κ B signaling is activated by LPS, TNF α , IL1 and their respective receptors through a wide range of adapter proteins and kinases, this leads to the activation of IKK in the IKK complex, which in turn phosphorylates I κ B on ser32 and ser36. This is a prerequisite event for polyubiquitination, which results in the proteasomal degradation of I κ B. NF κ B dimers can then be translocated to the nucleus and activate transcription. **b.** Non-canonical NF κ B signaling can be signaled through BAFFR, RANK, LTBR, leading to activation of IKK α by the NIK. IKK α can then phosphorylate p100 on ser866 and ser870, which leads to polyubiquitination of p100 and its subsequent proteasomal processing to the active form which can then activate transcription. **c.** Atypical NF κ B signaling is activated by genotoxic stress which leads to translocation of NEMO to the nucleus where it is sumoylated and then ubiquitinated. This process is mediated by the ATM checkpoint kinase. NEMO and ATM can then return to the cytosol where they activate IKK β . Figure adapted from Hoesel and Schmid, 2013.

1.6 B-cell lymphoma 3 (Bcl-3)

Bcl-3 was first identified in cases of B-cell lymphocytic leukaemia as a translocation into the immunoglobulin alpha-locus on chromosome 19 (van Krieken et al., 1990). It is an atypical member of the I κ B family of proteins and despite being structurally similar to the other family members, it serves a separate function (Wulczyn et al., 1992). Both p50 and p52 dimers are transcriptionally inactive as they lack transactivation domains, however Bcl-3 is able to heterocomplex with these homodimers, providing two transactivation domains and subsequently drive transcription (Fujita et al., 1993). Bcl-3 interacts with both p50 and p52 and is able to activate both the canonical and non-canonical NF- κ B pathways. Bcl-3 is able to cleave cytosolic inactive p105 and complex with active p50 homodimers and facilitate its translocation into the nucleus (Watanabe et al., 1997).

1.6.1 Bcl-3 interactions

The physiological signalling cascades leading to activation of Bcl-3 has yet to be fully characterised, but its up-regulation has been reported in response to a number of cytokines including TNF- α (Heissmeyer et al., 1999), IL4 (Rebollo et al., 2000), IL1 (Elliott et al., 2002), IL6 (Brocke-Heidrich et al., 2006), IL10 (Kuwata et al., 2003), adiponectin (Folco et al., 2009) and IL12 (Valenzuela et al., 2005). These cytokines are all associated with the induction of diverse signalling pathways such as AP1 (Rebollo et al., 2000) and STAT3 (Maldonado et al., 2010). Similar to other members of the NF κ B family, Bcl-3 is regulated by p50 as well as itself, generating an auto-regulatory loop to terminate its activity (Brasier et al., 2001). Deubiquitination of ubiquitin chains at lysine 63 by the cylindromatosis gene product, CYLD, is able to regulate and prevent accumulation of Bcl-3 in the nucleus (Wickström et al., 2010).

Although the state of Bcl-3 phosphorylation will not be investigated within the scopes of this project, it is nevertheless an important aspect to consider. Bcl-3 exists as a phospho-protein in many cancers (Viatour et al., 2004) and unphosphorylated Bcl-3 acts as a classical I κ B-like inhibitor and removes p50/p52 from bound DNA (Fujita et al., 1993). A recent study showed that Akt, Erk2 and IKK1/2 phosphorylated Bcl-3 and phosphorylation of Ser33 by Akt switched K48 ubiquitination to K63 ubiquitination and promoted Bcl-3 nuclear localisation and stabilisation. Phosphorylation by Erk2 and

IKK1/2 of Ser114 and Ser446 facilitated the recruitment of Bcl-3 to DNA by turning on its transcriptional coregulator capabilities and it was shown that phosphorylation of these serines were key to the maintenance of cellular proliferation and migration (Wang et al., 2017). This study highlighted the importance of phospho-Bcl-3 and linked Akt and MAPK pathways to NF κ B signalling through Bcl-3 (Fig.1.8) and provided some key mechanistic insight into how Bcl-3 functioned as an oncogene.

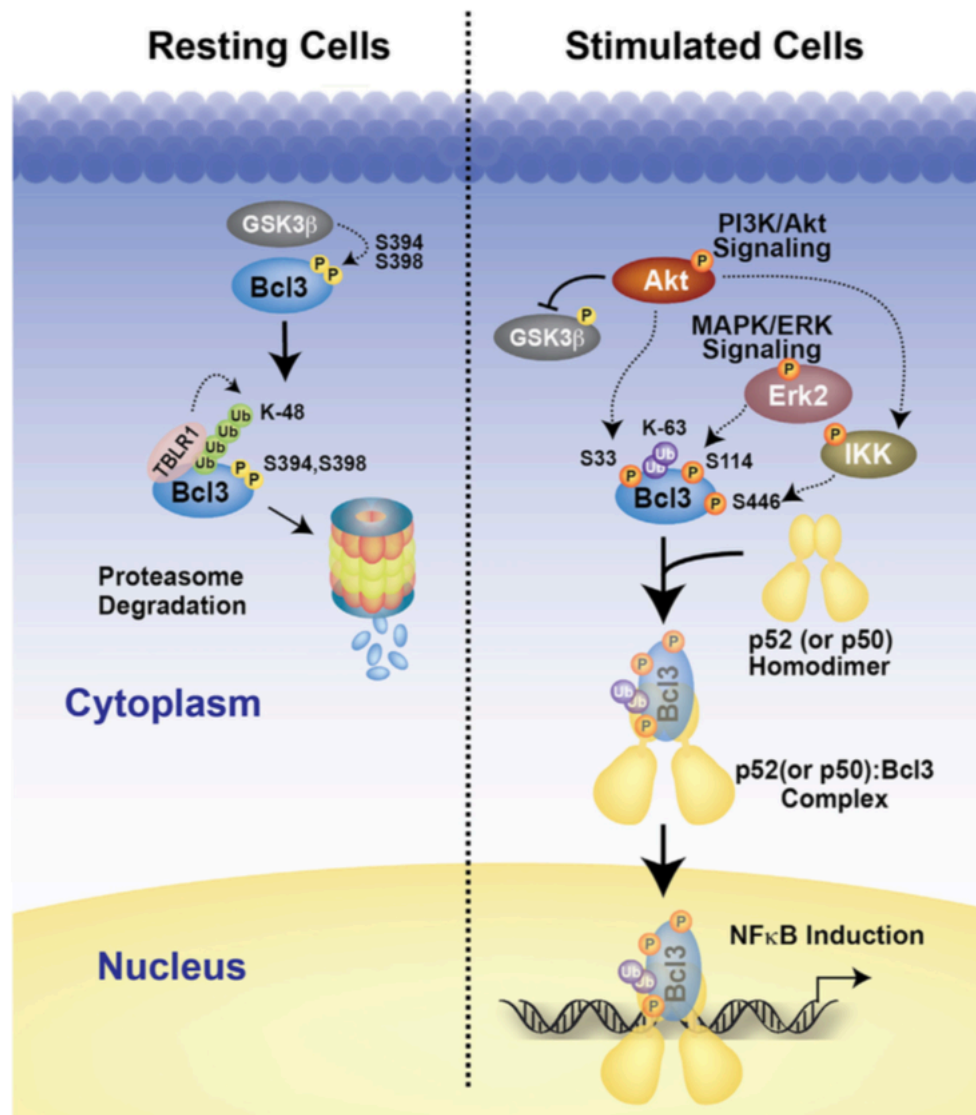


FIG. 1.8 MODEL OF BCL-3 ACTIVATION.

In resting cells, Bcl-3 undergoes continuous degradation, but upon LPS stimulation, Akt is activated through the PI3K pathway and stabilises Bcl-3. Figure adapted from Wang et al., 2017.

In additions to NFkB gene products, Bcl-3 has also been shown to associate with B3BP, a protein implicated in DNA damage responses (Watanabe et al., 2003), Lck, a tyrosine kinase expressed in haematological malignancies (Zhao et al., 2005), and ERRA α and PGC-1 α , proteins involved in metabolism (Yang et al., 2009). Recent studies have also reported interactions with CtBP1, a transcriptional repressor (Choi et al., 2010), IRS3, an insulin receptor substrate (Kabuta et al., 2010) and Bcl-10, a protein involved in apoptosis induction (Chan et al., 2010). All of these interactions and their physiological consequences have not been extensively studied, but highlights the widespread functions linked with Bcl-3 signalling.

1.6.2 Bcl-3 related malignancies

Since the discovery of Bcl-3 involvement in B-cell chronic leukemias, it has been found to be translocated in other haematological malignancies such as small lymphocytic lymphoma, Burkitt-like lymphoma as well as diffuse large cell lymphoma (Au et al., 2002). Furthermore, its overexpression without translocation has been identified in multiple subtypes of both non-Hodgkin and Hodgkin lymphomas (Schlette et al., 2005). Its dysregulation has also been reported in a large number of solid tumours including breast cancer (Cogswell et al., 2000), nasopharyngeal carcinoma (Thornburg et al., 2003), and colorectal cancer (Choi et al., 2010) and has since been largely accepted as a proto-oncogene. The most common alteration found in solid tumours is Bcl-3 overexpression and no translocations in the Bcl-3 locus has been found. This suggests the mechanism of deregulation is likely to be due to upstream activating signal cascades and/or epigenetic mechanisms. Since NFkB is commonly constitutively active in tumours it is likely Bcl-3 dysregulation could be due to aberrant NFkB activation (Karin et al., 2002).

The underlying mechanism of its oncogenicity is not yet fully understood, however Bcl-3 in complex with p52 has been shown to promote cell proliferation and survival *in vitro* through cyclin D1 up-regulation (Westerheide et al., 2001). Bcl-3 has a reciprocal relationship with the tumour suppressor p53 and induction of p53 can result in cyclin D1 inhibition resulting from reduced Bcl-3 levels. As previously mentioned, work done with human breast cancer MCF-7 cells showed that by overexpressing Bcl-3, it resulted in suppression of p53 induction following DNA damage, leading to a reduced apoptosis response (Kashatus *et al.*, 2006).

Elevated Bcl-3 levels is not only pathogenically specific to cancer and has been implicated in immune cell functions. Patients with inflammatory bowel disease have exhibited high Bcl-3 expression in colonic T cells and this correlated positively with disease manifestation. Mice with T-cell specific Bcl-3 overexpression developed severe colitis caused by pro-inflammatory immune infiltration attributed to defective Treg cell function and development (Reißig et al., 2017). Bcl-3 overexpression was also shown to be a novel regulator of non-alcoholic fatty liver disease or otherwise known as hepatic steatosis. Hepatocytes overexpressing Bcl-3 led to pronounced metabolic alterations, characterised by de novo lipogenesis and uptake, decreased hydrolysis and export of fatty acids. This was accompanied by an augmented inflammatory milieu, liver cell injury, as well as decreased insulin sensitivity (Gehrke et al., 2016). These recent studies highlighted the potential prognostic value of Bcl-3 not only in cancer, but also diseases such as colitis and non-alcoholic steatohepatitis.

1.6.3 Bcl-3 in breast cancer

Up-regulation of Bcl-3 in human breast cancer was first observed by Cogswell *et al.* when nuclear extracts of primary tumour samples, breast carcinoma cell lines and normal adjacent breast tissue were analysed for NFκB activation. RNA levels for NFκB-regulated genes indicated Bcl-3, c-Rel, p50 and p52 were all elevated compared to adjacent non-tumorigenic tissue (Cogswell *et al.*, 2000). Bcl-3 overexpression was also able to augment the development of an oestrogen-independent phenotype *in vivo* in an ER+ MCF-7 murine model. The same study also found elevated levels of Bcl-3 as well as activated NFκB signalling in oestrogen-independent MCF-7/LCC1 cells compared to oestrogen-dependent parental controls (Pratt *et al.*, 2003).

The C-terminal binding protein 1 (CtBP1) has been identified as a binding partner of Bcl-3 and it is a repressor of pro-apoptotic genes, such as p21 and NOXA. A strong positive correlation was found between Bcl-3 protein levels and CtBP1 in breast cancer patients. Binding of Bcl-3 to CtBP1 blocks its ubiquitination and prevents its degradation. It has also been shown that CtBP1 is able to stabilise Bcl-3 and further enhance its transrepressive functions (Keutgens *et al.*, 2010). Aberrant overexpression of Bcl-3 subsequently results in cells becoming resistant to apoptotic stimuli and helps to explain progression to cancer (Choi *et al.*, 2010).

1.6.4 Bcl-3 as a therapeutic target for metastasis

The metastatic process is multistep and fundamentally relies on the migration of tumour cells from the primary to secondary sites. Current standard of care for metastatic disease remains focusing on improving quality of life, but it has long been argued that existing therapies aimed at regressing primary tumours should be complemented with anti-metastatic agents aimed at preventing the initial or ongoing dissemination of disease (Sleeman and Steeg, 2010). However, to ensure successful translation into the clinic, such interventions must overcome the problems of non-selective toxicity and cellular plasticity, whereby tumours are able to evade inhibition of specific migration pathways by adopting alternative modes of migration (Gandalovicova et al., 2017). Despite some promising advances in this area, such as the next generation ROCK inhibitors (Sadok et al., 2015) and agents targeting the actin cytoskeleton (Zhang et al., 2012), ongoing issues of toxicity and efficacy justifies further search for novel targets of multi-modal migration.

Bcl-3 has shown early promise as a new anti-metastatic target in the pre-clinical setting and it has recently been implicated in progression and resistance to therapy in a number of solid tumour types (Legge et al., 2019). Its nuclear expression has been associated with colorectal cancer metastasis and high Bcl-3 expression has been correlated with reduced metastasis-free survival (Puvvada et al., 2010). Bcl-3 suppression. In breast cancer, high expression has been attributed to a reduction in metastasis-free survival (Chen et al., 2016) and in a recent transgenic mouse study featuring HER2+ mammary tumours resulted in significant reductions in pulmonary metastasis without disruptions to regular cell homeostasis, highlighting Bcl-3 inhibition as a potential clinical therapeutic option (Wakefield et al., 2013). More importantly, complete deletion of Bcl-3 in these mouse models was well tolerated with only minor disruptions to the immunological compartments (Schwarz et al., 1997). While it has been previously shown that Bcl-3 inhibition was able to reduce metastatic migration in a TNBC cell line murine model and despite recent promising advances, the precise mechanisms detailing the oncogenicity of Bcl-3 has yet to be fully characterised. Therefore we set out to further investigate the roles of Bcl-3 in TNBC as an anti-metastatic target and determine its effects on tumour proliferation, amoeboid, collective and mesenchymal-like cell migration, as well as seeking to identify the underlying signalling pathways by performing global gene expression.

1.6.5 Development of a small molecule inhibitor of Bcl-3

We modelled the interaction of Bcl-3 with the NF κ B subunits p50 and p52 to identify possible interaction areas on the surface of Bcl-3 that could be targeted by small molecules. A suitable novel binding pocket was identified between ANK6 and ANK7 ankyrin repeats in the Bcl-3 backbone (**Fig. 1.9**). In silico screening was performed to identify small molecules that would bind to this area and 10 hit compounds were selected from the SPEC database. We tested these compounds in an indirect sandwich ELISA to determine which compound had the highest efficacy at inhibiting p50 and p52 binding to Bcl-3. Using this top hit as a structural scaffold for the activity relationship between subunits, we were able to design and synthesise a novel small molecule compound with equivalent or greater biological potency.

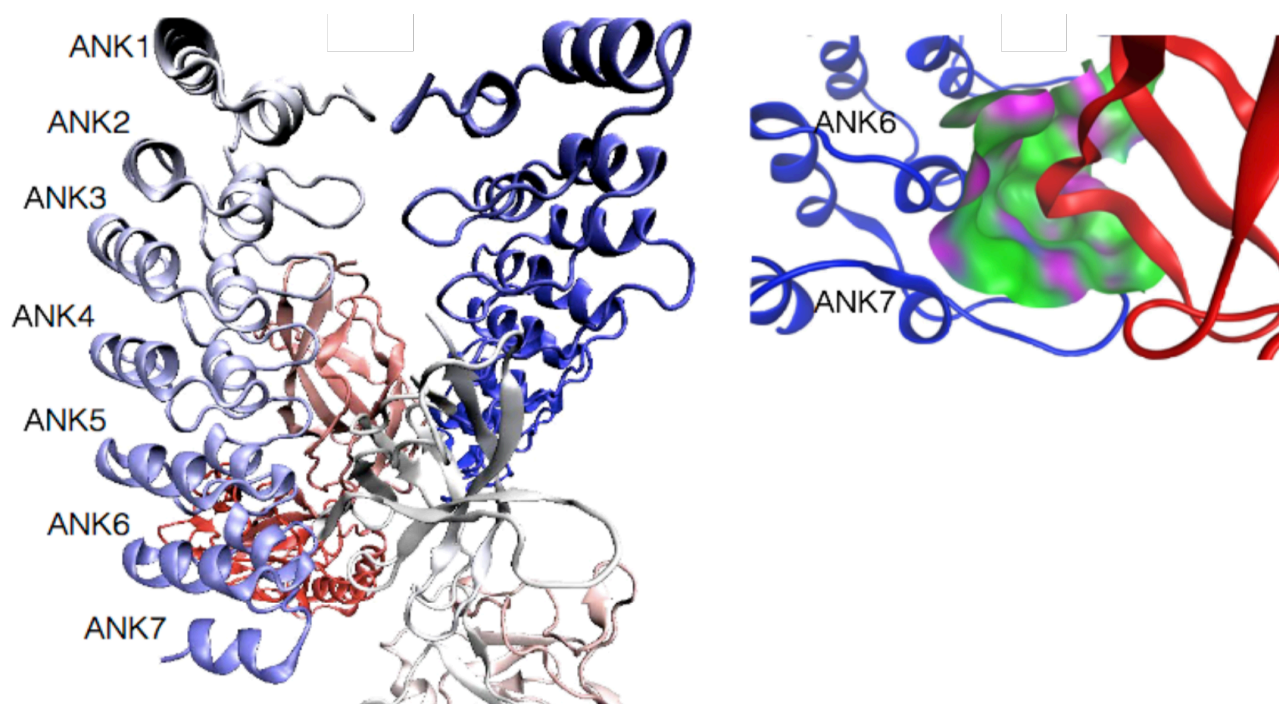


FIG. 1.9 BCL-3 SMALL MOLECULE BINDING SITES

Molecular dynamics were assessed using Bcl-3/p50 heterodimers to identify suitable small molecule binding sites. The contact area positioned between the ANK6 and ANK7 domain of Bcl-3 was determined to be a unique binding motif and subsequently used for in silico screening of small molecule compounds (Adapted from Soukupova, 2013, unpublished).

1.7 Project Aims

- Investigate the functional effects of both Bcl-3 suppression as well as up-regulation through ectopic protein overexpression in a panel of TNBC cell lines

TNBCs are an important clinical subtype and they do not respond effectively to traditional endocrine or targeted therapies. Bcl-3 is considered a proto-oncogene and its suppression has been postulated to be therapeutic in a number of solid cancers. Therefore it is possible for Bcl-3 suppression to have potential therapeutic efficacy in TNBCs.

- Confirm the *in vitro* and *in vivo* efficacy of novel small molecule Bcl-3 inhibitor compounds.

In vitro efficacy using our Bcl-3 inhibitors have been shown in a number of breast cancer cell lines. It is logical to demonstrate *in vivo* efficacy using luciferase xenograft models in athymic nude mice. Robust animal data is a vital prerequisite for adoption into human clinical trials. The Bcl-3 inhibitors have shown no significant cytotoxicity in animals and this is one advantage over traditional cytotoxic chemotherapies.

- Investigate the transcriptional changes following Bcl-3 suppression to identify potential mechanisms of action.

Affymetrix DNA microarray analysis using GeneChip 2.1 was carried out on RNA from the TNBC cell line MDA-MB-231-Luc. The samples will be from Bcl-3 siRNA treated, as well as Bcl-3 inhibitor treated cells and their appropriate controls. This will hopefully give us a starting point for elucidating a possible transcriptional mechanism and it is hypothesised that there will be some mechanistic overlap between the two different methods of Bcl-3 suppression.

Chapter 2:

Materials & Methods

2 Materials and Methods

2.1 Cell culture

2.1.1 Experimental cell lines

The human breast cancer cell lines used in this study were acquired from commercial sources and their descriptions are outlined below:

MDA-MB-231-Luc-D3H2LN (Caliper, Life Sciences)

This epithelial cell line was derived from pleural effusion of adenocarcinoma from a human patient with ER-, PR-, ERBB2- breast cancer. It overexpresses epidermal growth factor (EGF) receptors as well as transforming growth factor alpha (TGF alpha) receptors. It was passaged from a spontaneous lymph node metastasis from a D3H1 mammary fat pad tumour and transfected with pGL3 control red (SV40-luc) and pSV40/Zeo. It expresses *in vitro* bioluminescence of approximately 189-208 photos/sec/cell, subject to imaging and culturing conditions.

MDA-MB-231 (ATCC HTB-26)

This is a highly metastatic, human basal epithelial cell line isolated from an adenocarcinoma pleural effusion. The cells are triple-negative with a ER-, PR-, ERBB2-expression profile. It strongly overexpress EGFR.

MDA-MB-436 (ATCC HTB-130)

This epithelial cell line was derived from pleural effusion of adenocarcinoma from a human patient with ER-, PR-, ERBB2- breast cancer and has a BRCA1 5396 + 1G>A splice donor mutation in exon 20 site (Elstrodt et al., 2006).

SUM149PT (Asterand)

This epithelial cell line was derived from invasive ductal carcinoma from a human patient with ER-, PR-, ERBB2- inflammatory breast cancer. It over-expresses epidermal growth factor (EGF) receptors and carries the 2288delT mutations of BRCA1 (Elstrodt et al., 2006).

MCF10a (ATCC CRL-10317)

This is a mammary epithelial cell line and has been considered as a model of non-tumourigenic mammary cells. They were derived from mammary tissue from a 36-year old woman in good health and this immortalised cell line can grow in culture with a stable, near diploid karyotype with modest genetic modifications typical of culture adapted breast epithelial cells.

HCC1954 (ATCC CRL-2338)

This is an epithelial mammary cell line derived from a 61-year old female with TNM stage IIA, grade 3, ductal carcinoma disease. This cell lines is poorly differentiated and was initiated in 1995. It over-expresses HER2 and is negative for ER and PR.

2.1.2 Maintenance of cell lines

The following culture conditions were used for:

MDA-MB-231, MDA-MB-231-Luc-D3H2LN, MDA-MB-436, HCC1954

Cultured with Roswell Park Memorial Institute (RPMI) 1640 medium supplemented with GlutaMAX (ThermoFisher Scientific), and heat-inactivated Fetal Bovine Serum (Gibco) at a final concentration of 10%.

SUM149PT

Cultured with Ham's F-12 (ThermoFisher) medium supplemented with heat-inactivated Fetal Bovine Serum (Gibco) at a final concentration of 5%, HEPES (Gibco) at 10mM, Hydrocortisone (Sigma-Aldrich) at 1ug/mL, and Insulin (Sigma-Aldrich) at 5ug/mL.

MCF10a

Cultured with Dulbecco's modified Eagle's medium nutrient mixture FG12 (Invitrogen) supplemented with 5% Horse Serum (Sigma-Aldrich, Dorset, UK), Penicillin at 50u/mL (Invitrogen), Epidermal Growth Factor at 20ng/mL (Sigma-Aldrich), Hydrocortisone at 0.5mg/mL (Sigma-Aldrich), Cholera Toxin at 100mg/mL (Sigma-Aldrich) and insulin at 10 µg/mL (Sigma-Aldrich).

All cell lines were incubated at 37°C and 5% CO₂ in T25 tissue culture flasks (Nunc) and were routinely passaged every 4-7 days at split ratios of 1:5-1:10 when they

became 90% confluent. Growth media was completely aspirated using a vacuum and cells gently washed with PBS. The PBS was removed and 1mL of 0.25% Trypsin/EDTA (ThermoFisher) was added to the flask followed by incubation at 37°C for 5-10mins. Once cells were detached, the appropriate split ratio was performed by discarding a set amount of cell suspension. The remaining volume of cell suspension was made up to 5mLs with complete growth medium.

2.1.3 Cell counting and seeding

Cells were trypsinised using 0.25% Trypsin/EDTA and counted using an automated Luna cell counter (LogosBiosystems). Single cells were counted by adding 10uL of cell suspension to the Luna cell counting slide, and inserted into the machine. Cells were then diluted with the appropriate amount of culture medium before being seeded into the specific culture plates depending on the assay being performed.

2.1.4 Long term frozen storage of cell lines

A confluent T75 flask of cells were trypsinised and resuspended in 10mLs of complete medium and spun down at 1200RPM for 5 mins. The supernatant was then removed and cells resuspended in 5mLs of complete medium containing 10% DMSO (Sigma-Aldrich) before being aliquoted into 1mL cryotubes (Nunc) and transferred to a freezing container (ThermoFisher). This container was then stored at -80°C overnight and cryotubes subsequently transferred to liquid nitrogen for long term storage.

2.1.5 Raising cells lines from frozen storage

Cell lines were transferred from liquid nitrogen storage into dry ice before being thawed in a warm 37°C water bath until cells were defrosted. Cell suspension was then transferred into a 15mL falcon (Nunc) containing 4mL of complete growth medium and centrifuged at 1200RPM for 3 mins. The supernatant was aspirated, pellet resuspended in normal growth medium before being transferred into a T25 culture flask and incubated at the correct culturing conditions.

2.2 Transfection and drug treatment of cell lines

2.2.1 Single siRNA transfection

Tubes containing 5nmol of siRNA were briefly centrifuged to collect the pellets at the bottom of the tubes. siRNA pellets were resuspended in 250uL of RNase-free 1x siRNA buffer to make up the desired final concentration of 20uM. The solutions were then placed on an orbital shaker for 30 mins at room temperature before being aliquoted and frozen at -20°C. The concentration of siRNA was verified using UV spectrophotometry at 260nm and 5uM = 66.5 ng/uL.

Transfection of siRNA was performed on cells that reached 70% confluent using Lipofectamine 3000 (Invitrogen) and serum-free Opti-MEM (Invitrogen) medium. Different volumes of reagent were calculated depending on the total culture medium held by each different cell culture plate (**Tab. 2.1**). The correct volume of siRNA was diluted in Opti-MEM in a 1.5mL Eppendorf tube before Lipofectamine 3000 was added. The siRNA mixture was then vortexed for 5 seconds and left to incubate at RT for 5 mins. Lipofectamine-siRNA complexes were then added on top of adherent cells in the appropriate volume of growth medium to give a final siRNA concentration of 20nM (**Tab. 2.2**). Cells were cultured for 48h before harvest. Transfections were controlled for by using a pool of scrambled siRNA designed for minimal targeting of human genes, which allowed us to determine the baseline cellular response in RNAi experiments. Bcl-3 knockdown efficiency was measured by assessing both mRNA and proteins levels following transfection and the final siRNA concentration of 20nM resulted in consistent 90% reductions in Bcl-3 expression.

Tissue culture plate type	Culture medium	Opti-MEM medium	Final siRNA concentration	Volume of 20uM siRNA	Lipofectamine 3000
12-well	1.125mL	125uL	20nM	1.25uL	2.5uL
6-well	2.25mL	250uL	20nM	2.5uL	5uL
T25 flask	4.5mL	500uL	20nM	5uL	10uL

TABLE 2.1 TRANSFECTION CONCENTRATION FOR SIRNA

siRNA	Target sequence (5'-3')	Catalogue Number
Human control ON-Target plus SMART pool	UGGUUUACAUGUCGACUAA UGGUUUACAUGUUGUGUGA UGGUUUACAUGUUUUCUGA UGGUUUACAUGUUUUCUUA	D-001810-10
Human Bcl-3 ON-Target plus SMART pool	UGGUUUACAUGUUUUCUUA UGGUUUACAUGUUUUCUUA GCGCAAUAGUACUCCGGCA GCCGGGAGCUCGACAUCUA	L-003874-00-0005

TABLE 2.2 SEQUENCES OF SIRNA

2.2.2 Bcl-3 plasmid constructs

Plasmids containing either wild type (WT) Bcl-3 or the Bcl-3 ANK M123 (**Fig. 4.1**) non-binding mutant sequences contained within a FLAG-tagged pcDNA 3.1 backbone vector were gifted from Dr. Alain Chariot (Interdisciplinary Cluster for Applied Genoproteomics, University of Liège, Belgium).

2.2.3 Transfection of NFkB reporter and Bcl-3 plasmids

For transfection of the NFkB luciferase reporter or Bcl-3 plasmids, 1×10^4 cells were seeded into 12-well plates (Costar) in normal growth media and left to settle overnight. Wells were transfected with either 900ng of 3x kB luciferase reporter plasmid and 100ng of pcDNA 3.1-LacZ plasmid or 500ng of Bcl-3 plasmid using the appropriate amounts of Lipofectamine 3000, p3000 reagent and Opti-MEM (**Tab. 2.3**).

Transfection reagent	NFkB Reporter	WT Bcl-3/ANK/pcDNA plasmids
DNA plasmid	1000ng	500ng
Lipofectamine 3000	2uL	2uL
p3000 reagent	4uL	4uL
Opti-MEM	100uL	100uL

TABLE 2.3 NFkB LUCIFERASE REPORTER ASSAY TRANSFECTION VOLUMES

2.2.4 Generation of stable overexpression clones

Stably transfected cells overexpressing either WT Bcl-3, the Bcl-3 ANK mutant or empty control pcDNA vector were selected by continuous addition of G418 (Sigma) to the culture medium. Under selective conditions, resistant cells that carry the plasmid vectors

will outgrow the non-resistant cells, resulting in a stable polyclonal population of overexpression cells. 500ug/mL of G418 was used to select for resistant cells within the first 7 days and subsequently the stable cell lines were cultured in media with 250ug/mL of G418.

2.2.5 Drug treatments

Novel small molecule inhibitor compounds, JS6, 15F and CB1 were designed and synthesised to disrupt the interaction of Bcl-3 with p50 and p52 homodimers. They were synthesised by Cinzia Bordoni, Cardiff University and stored in powder form at RT. Each compound was diluted in an appropriate volume of fresh DMSO (Sigma) to a stock concentration of 100mM (**Tab 2.4**). Compounds were then aliquoted and frozen at -20°C until use and each compound was discarded following 2 freeze-thaw cycles. When treating cells, each compound was diluted in the appropriate volume of complete growth media to the required concentration, with DMSO being diluted at the same ration to act as blank vehicle controls.

Compound	Molecular weight	DMSO volume per mg	Final concentration
JS6	371.41	26.9uL	100mM
CB1	401.43	24.9uL	100mM
15F	383.44	26.1uL	100mM

TABLE 2.4 LIST OF NOVEL BCL-3 INHIBITORS

2.3 Cell based functional assays

2.3.1 Migration assays

2.3.1.1 Wound-healing assay

In order to assess collective migration in cancer cell lines, the wound-healing assay was performed. Cell were seeded at 1×10^5 cells/well in 12-well plates and left to settle overnight. Once cells have reached 70% confluence, they were transfected with Bcl-3 siRNA and incubated for 48 hours. Two separate wounds were then created on the confluent cell monolayer using 200uL pipette tips (Anachem) before culture media was gently removed and cells washed with PBS. Fresh media was replaced before place

holder locations were marked on the bottom of the plate using a permanent marker to define areas to be recorded. Images were captured on an inverted microscope (Leica) at each of the different marks before cells were left to incubate for the appropriate length of time relevant for each experiment.

2.3.1.2 Fluoroblok migration assay

In order to assay amoeboid-like single cell migratory capacities of cancer cell lines, the Fluoroblok migration assay plate (Corning) was used. Following relevant experimental pre-treatment of cells defined by individual experiments, cells were harvested and suspended in phenol red free growth medium (Invitrogen) without FBS. Cells were diluted to a concentration of 1×10^5 cells/mL and 50uL per well of cells were seeded into the top chambers of the 96-well Fluoroblok assay plate. To stimulate chemotaxis migration across the pored membrane, 200uL of phenol red free growth medium with 10% FBS was added to the bottom chambers. After 24h incubation, the top and bottom chambers were detached and the growth medium removed from the bottom wells. The top chamber was then carefully reassembled and 200uL of 1uM Calcein AM (eBioscience) in PBS was added to the bottom chambers and incubated for 1 hour at 37°C. Post-incubation the fluorescence intensity of each well was read at 500nm from the bottom side using the Clariostar plate reader (BMG Labtech).

2.3.1.3 Single cell migration assay

In order to assess the mesenchymal-like single cell migratory capacities of cancer cell lines, the ability of singular cancer cells were monitor in real-time. Cells were seeded into 6-well plates at a density of 1×10^5 cells/well and left to settle overnight before being treated with siRNA for 48h. Cells were then removed, counted and re-seeded in Leibovitz's L-15 medium (Invitrogen), at a low density of 5×10^4 cells/well into 12-well plates. Once cells have settled overnight, they were placed into a time-lapse incubation chamber (Leica) pre-warmed to 37°C with 5% CO₂ and left to equilibrate for 1 hour. Each well was then located using the "mark and find" software tool, 4 different areas tracked and cells were monitored over a period of 18 hours with photos being taken every 10 minutes. The first 50 images equating to 8 hours of elapsed time, was exported as a .tiff image sequence, which were then converted into an 8-bit grayscale image sequence using ImageJ. The sequence

was then opened in the CellTracker software and cell movement tracks for each cell quantified and analysed manually.

2.3.2 Colony formation assay

This assay tested the clonogenicity of individual cancer cells and assessed their ability to survive, proliferate and clonally expand into small colonies. Cells were seeded at the low density of 250 cells/mL in 6-well format in complete growth medium and incubated for 10 days. Quantification of colonies involved aspiration of culture media, washing the cells gently with PBS, followed by fixation of colonies with glutaraldehyde (6% v/v) and staining with crystal violet (0.5% w/v) for 15mins at RT. The crystal violet solution was then removed and cells were thoroughly washed under running tap water to completely remove excess staining. Colonies were then imaged and quantified using the GelCount plate reader.

2.3.3 CellTiter-Blue assay

The CellTiter-Blue cell viability assay (Promega) is a homogenous, fluorescence based method for assessing cell viability. This reagent assayed the ability of living cells to convert a redox dye, resazurin, into the fluorescent end product resorufin. Nonviable cells rapidly lose metabolic capacity and thus do not generate a fluorescent signal. The assay involved adding a single nontoxic reagent directly to the medium of cultured cells and after an incubation step of 1 hour at 37°C, viability data is recorded using a plate reader based on the intensity of fluorescence at 560/590nm. 20uL of reagent was added for every 100uL of growth medium.

2.3.4 Realtime-glo assay

The RealTime-Glo MT Cell Viability Assay (Promega) incorporates non-lytic NanoLuc Luciferase and MT Cell Viability substrates to cell media during time of plating. The assay reagents then diffused into cells where it was reduced to form a NanoLuc substrate, which exited the cells and was used by NanoLuc Luciferase in the media. This assay was used to quantify cell population growth because metabolically active cells could reduce the substrate and light produced was directly proportional to the number of viable

cells in culture. The non-lytic and rapid response of the assay allowed for accurate and continued measurements of cell proliferation over time.

2.3.5 NFkB luciferase reporter assay

The NFkB activity of cells was quantified using a luciferase reporter plasmid. Cells were transfected with the reporter using conditions previously mentioned (Refer to 2.2.2) following Bcl-3 siRNA knockdown or inhibitor treatment. Cells were seeded into clear bottom black walled 96-well plates (Corning Inc., Lowell, US) in antibiotic free culture media ($1-2 \times 10^5$ cells/mL). After 24 hours, cells were transfected with reporter plasmids using Lipofectamine LTX reagent (Invitrogen) according to manufacturer's protocol. The NFkB reporter plasmid pLTRX-Luc (10 ng/well) was used with pcDNA3.1-LacZ plasmid (10 ng/well) to normalize for transfection efficiency. For positive and negative controls respectively, 10ng of pGL3control or pGL3basic were transfected in place of the reporter plasmid. After 48 hours post-transfection cell were lysed using Glo-lysis buffer and analysed using Beta-glo and Bright-glo according to manufacturer's protocol (Promega). Luminescence relative to LacZ was read using a Flurostar Optima plate reader (BMG Labtech) and displayed as relative light units (RLU).

2.3.6 DAPI cell cycle assay via flow cytometry

In order to determine cell cycle progression, flow cytometry was used to sort based on the intensity of the nuclear DNA marker DAPI. This allows us to determine the total DNA content of each individual cell, and this data can be aggregated to calculate the stages of the cell cycle. Cells were harvested, counted and diluted in PBS to a concentration of 1×10^6 cells/mL, cells were then pelleted and resuspended in 5uL/mL DAPI solution (ThermoFisher Scientific) in 0.01% IGEPAL CA-630 (Sigma) in PBS and incubated for 5 mins at RT. Cells were stored on ice and shielded from light.

Before DAPI stained cells were analysed, each sample was filtered through a 40um cell strainer (BD Biosciences) into flow cytometry collection tubes (BD) to ensure a robust single cell suspension. Flow cytometry was carried out on the LSRFortessa flow cytometer (BD) and analysed using the FlowJo software. Cells were gated by FSC-area/SSC-area and by FSC-area/FSC-height in order to obtain a single cell population and remove

artefacts and doublets. Single cells were then analysed by plotting histograms using the DAPI-area curves to determine the DNA content of the cell.

2.3.7 Caspase-glo -3/-7 assay

The Caspase-Glo 3/7 assay (Promega) is a homogenous, luminescent assay that measured caspase-3 and -7 activities. The assay contained a pro-luminescent caspase-3/7 substrate with the tetrapeptide sequence DEVD, in a reagent optimised for caspase activity, luciferase activity and cell lysis. Cleavage of substrate released aminoluciferin and resulted in the production of light and luminescence was proportional to the amount of caspase activity present. Media was aspirated from wells of a 96-well plate and 50uL of caspase-glo was added per well, which lysed the cells and allowed luminescence representative of caspase activity to be measured using a plate reader.

2.3.8 Mammosphere assay

A reliable and cost efficient assay involving the formation of anoikis resistant mammospheres is able to demonstrate the presence of a stem-like cell population. 1×10^3 cancer cells were disaggregated and transferred from an adherent monolayer setting into a non-adherent, serum-free epithelial growth medium (MEBM, Lonza, Slough, UK), supplemented with B27 (Invitrogen), 20 ng/ml EGF (Sigma), Insulin (Sigma), and hydrocortisone (Sigma), in a 96-well condition. After at least 7 days incubation, the number of mammospheres formed were imaged and quantified.

2.4 Protein analysis

2.4.1 Protein extraction from cells

Cells were chilled on ice, media was completely aspirated and an appropriate amount of ice-cold PBS was added. Cells were mechanically removed using a cell scraper and pelleted at 1200RPM at 4°C for 5 mins, supernatant was discarded. Cells were either stored at -80°C or protein extraction carried out immediately with the addition of an appropriate amount of RIPA buffer (150mM sodium chloride (Fisher Scientific), 1% v/v Nonidet-P40 (Roche), 0.5% w/v sodium deoxycholate (Sigma), 0.1% w/v sodium dodecyl sulphate (SDS; Sigma), 50mM Tris (Sigma), pH8) containing 1:100 protease and

phosphatase inhibitor cocktail (Cell Signalling Technologies, MA, USA) and incubated on ice for 30 minutes. Lysate was then centrifuged at 13k RPM for 15 minutes at 4°C to pellet cell debris and the protein supernatant was aliquoted into fresh tubes for protein quantification.

For colP: Adherent cell lines were cultured in 60mm dishes under normal conditions prior to protein harvest. Aspirate cell culture media, wash cells with ice cold PBS, discard PBS and repeat wash; keeping cells chilled on ice at all times. Add 1mL of PBS, scrap cells, transfer to 1.5mL micro-centrifuge tube and spin pellet cells at 4°C. Discard PBS and re-suspend cell pellet in 400uL of pre-chilled lysis buffer (20mM HEPES pH7.9, 100mM NaCl, 20% glycerol, 1mM MgCl₂, 0.5mM EDTA, 0.1mM EGTA, 1% NP-40). Place on ice for 30-45 mins and pellet insoluble material by centrifugation at 13k RPM for 10 mins at 4°C. Remove and store the total protein lysate supernatant at -80°C.

2.4.2 Nuclear and cytoplasmic protein extraction

Cell pellets were resuspended in 200uL of NEBA buffer (10mM HEPES pH7.9, 10mM KCl, 0.1mM EDTA pH8, 0.1mM EGTA pH8) with protease inhibitors and incubated on ice for 15 mins. 10uL of 10% NP-40 were added and samples vortexed for 30 sec. Samples were then centrifuged at 10k RPM for 30 sec and the resulting supernatant is the cytoplasmic protein fraction. 100uL of NEBC buffer (10% glycerol, 20mM HEPES pH7.9, 0.4M NaCl, 1mM EDTA pH8, 1mM EGTA pH8) was added to the resulting invisible protein pellet, vortexed and placed on ice for 30 mins. This was then spin at 13k RPM at 4°C for 5 mins and resulting supernatant will be the nuclear protein fraction. Measure the protein concentration of the cytoplasmic protein fraction using the BCA assay and the nuclear protein fraction using the Bradford assay.

2.4.3 Quantification of protein

Protein concentrations were determined using the Pierce BCA protein assay kit (ThermoFisher Scientific) according to the manufacturers instructions. Protein standards were prepared by diluting 2mg/mL BSA in PBS to produce a range of 7 known concentrations (2mg/ml, 1mg/ml, 0.5mg/ml, 0.25mg/ml, 0.125mg/ml, 0.0625mg/ml, and 0mg/ml) and 10µL of these standards or of sample were added to 100µL of solution containing BCA protein assay reagent A and BCA protein assay reagent B in a ratio of 50:1

in a 96 well plate. Samples were mixed and then incubated at 37°C for 30 minutes before being analysed on a Flurostar Optima plate reader (BMG Labtech, Bucks, UK) at 562nm. The standards were used to generate a standard curve from which the concentration of protein in each sample could be extrapolated.

2.4.4 Coimmunoprecipitation

Prepare 75mg protein A-sepharose bead (GE Healthcare Life Sciences) suspension in 50mL of water. Spin down at 13k RPM for 3 mins and repeat suspension-spin process once more. Resuspend beads in 2mL of water and store at 4°C. Pre-clear cell lysates by adding 100uL of bead suspension to 200uL of lysates; agitate at 4°C for 30-45 mins. Spin down at 13k RPM for 3 mins and transfer supernatant, discarding pelleted beads. Add 10uL of Bcl-3 primary antibody and 5uL of p50 antibody to separate aliquots of 100uL lysate. Incubate overnight at 4°C under agitation.

Add 100uL of bead suspension to each lysate and incubate at 4°C under agitation for 2h. Spin down at 13k RPM for 3 mins and aspirate supernatant. Re-suspend beads in 1mL of lysis buffer and re-spin down and aspirate supernatant. Repeat this wash 2 more times. After the final wash add the appropriate 5x Laemmli buffer, mix and boil at 95°C for 5 mins.

2.4.5 Western Blotting

2.4.5.1 Protein sample preparation

25µg of protein was diluted in RIPA buffer to a final volume of 8µL. 2 µL of 5x laemmli buffer (0.125M Tris-HCL pH6.8, 4% w/v SDS, 40% v/v glycerol, 0.1% w/v bromophenol blue (Sigma), 6% v/v beta- mercaptoethanol (Sigma) in ddH2O) was added to each sample. Prior to gel loading, the samples were heated to 95°C for 5 minutes to denature proteins.

2.4.5.2 Gel electrophoresis

Precast gels were purchased from BioRAD (4–20% Mini-PROTEAN® TGXTM Precast Protein Gels) and placed in the Mini-Protean III (Bio-Rad) electrophoresis tank

and immersed in Tris-Glycine-SDS running buffer (Biorad). Protein molecular weight marker (PageRuler, ThermoFisher) was loaded into the first and last lane of each gel and prepared protein samples were loaded into the appropriate remaining wells. The samples were resolved down gels for approximately 45-60 minutes at 150V until the dye front reached the bottom of the gel.

2.4.5.3 Membrane transfer

After electrophoresis, gels were removed carefully from plastic cassettes using a specific tool (BioRad). They were kept moist by dripping running buffer onto them and excess gel was trimmed. They were then placed into a membrane system purchased from BioRAD in the correct orientation (Trans- Blot® TurboTMPVDF, BioRAD) before being rolled to remove any air bubbles in Trans-Blot® TurboTM Transfer System (BioRAD) Cassettes. Cassettes were then placed in to the Trans-Blot® TurboTMSystem and run on a MIXED MW protocol for 7 minutes.

2.4.5.4 Blocking and primary antibody incubation

Once Western transfer is completed, sandwiches were disassembled and membranes washed 3 x 5 mins in PBST (1 x PBS solution (Fisher): 5 tablets 500mL dH₂O with 0.5mL Tween (Sigma)) before being incubated in blocking buffer (5% w/v non-fat milk powder (Marvel): 0.75g in 15 mL PBST per transfer membrane) with agitation for 1h. The membranes were then transferred to 30mL universal tubes (Fisher) containing 2mL of the desired primary antibody (**Tab. 2.5**) diluted in 5% w/v non-fat milk powder (Marvel) in PBST. Membranes were incubated in the primary antibody solution overnight at 4°C on a roller.

Antibody	Dilution	Supplier	Species	Molecular Weight
Bcl-3	1:200	Proteintech (23959-1-AP)	Rabbit Polyclonal	48-60kDa
p50	1:500	Cell Signalling #3035	Rabbit	50kDA active 120kDA precursor

TABLE 2.5 PRIMARY ANTIBODIES USED IN WESTERN BLOTTING

2.4.5.5 Detection and quantification

Membranes were then washed 3 x 5 mins in PBST and transferred to a 30mL tube containing 2mL of the appropriate rabbit horseradish peroxidase-conjugated secondary antibody (Dako) diluted 1:2000 in 5% BSA in PBST. Membranes were incubated in secondary antibody at room temperature for 1 hour on a roller. Finally, membranes were washed 3 x 5 mins in PBST. Antibody binding was detected using ECL prime detection reagent (Amersham) before being developed in a BioRad Chemidoc MP Imaging System. Digital images were then quantitated by densitometry using the program Image J.

2.4.6 Immunofluorescence

Cells were plated into wells of a 24-well plate atop an ethanol-UV sterilised glass coverslip and allowed to seed overnight. The culture media was then removed, cells gently rinsed with PBS before fixation with 500uL of warm PBS diluted 4% formaldehyde for 15 mins at room temperature. The fixative was then aspirated and cells rinsed three times with PBS for 5 mins each time. Cells were then permeabilised and blocked in 300uL 1% BSA PBS/Triton 0.3% for 1h to minimise background staining. Following blocking, the blocking solution was replaced with 300uL of primary antibody (**Tab. 2.6**) made up in blocking buffer and incubated overnight at 4C on a rocker. The primary antibody was then aspirated and cells rinsed three times in PBS 5 mins each time. Cells were then incubated with 300uL fluorochrome-conjugated secondary antibody diluted in blocking buffer for 1-2h in the dark at room temperature. Following secondary incubation cells were rinsed once more with PBS for 5 mins and stained with DAPI (5uL/mL) diluted in PBS for 20 mins at room temperature. Cells were rinsed three times with PBS, coverslips were dip rinsed in water before being mounted onto glass slides on top of 2uL of Mowiol (Sigma-Aldrich) mounting solution.

Antibody	Dilution	Species	Origin
Ki67	1:200	Mouse monoclonal	NCL-L-Ki67-MM1 (Leica Novocastra)
Phospho-Histone (Ser10) H3	1:400	Rabbit	#9701 (Cell Signalling)
Anti-mouse 488	1:200	Goat	Abcam
Anti-rabbit 488	1:200	Goat	Abcam

TABLE 2.6 LIST OF ANTIBODIES USED FOR IMMUNOFLUORESCENCE

2.5 RNA analysis

2.5.1 RNA extraction

Harvested cells were pelleted at 1200RPM for 5 mins before being lysed in 350uL of RLT buffer (Qiagen) and placed on ice for immediate RNA extraction or stored frozen at -80°C. RNA extraction was performed using the Qiagen RNEasy kit following the exact manufacturer instructions. The concentration and purity of RNA was analysed using a nanodrop 3000 spectrophotometer (Thermo Scientific).

2.5.2 cDNA synthesis

Previously extracted RNA was synthesised into cDNA using the QuantiTect Reverse Transcription kit (Qiagen). Frozen RNA template was thawed on ice along with the gDNA Wipeout buffer, Quantiscript Reverse Transcriptase, Quantiscript RT buffer and RT primer mix. 1ug of RNA was diluted in 2uL of gDNA Wipeout buffer and RNase-free water to a total volume of 14uL and incubated for 2 mins at 42°C before being placed immediately on ice. The master mix (**Tab 2.7**) was used for each reaction and incubated for 30 mins at 42°C followed by 3 mins at 95°C to inactivate the reverse transcriptase. The cDNA product was then either immediately used or stored at -20°C.

Component	Volume per 1ug reaction
Quantiscript Reverse Transcriptase	1uL
Quantiscript RT Buffer, 5x	4uL
RT Primer Mix	1uL

TABLE 2.7 CDNA SYNTHESIS MASTER MIX REAGENTS

2.5.3 Quantitative-real time-polymerase chain reaction (qRT-PCR)

2.5.3.1 Primer acquisition

All primers were bought from ThermoFisher Scientific from their online inventoried TaqMan gene expression assay search tool and were selected to target human sequences (**Tab. 2.8**). Each primer was chosen to carry a FAM-reporter dye with the exception of

ACTB controls, which carried the VIC-reporter dye, so multiplex PCR reactions could be performed.

Gene target	Assay ID
Bcl-3	Hs00180403_m1
ACTB	Hs99999903_m1
TNFA	Hs00174128_m1
IL1B	Hs01555410_m1
FOS	Hs00171851_m1
EGR1	Hs00152928_m1
ESM1	Hs00199831_m1
IL6	Hs00985639_m1
CDH2	Hs00983056_m1
MDM2	Hs00540450_s1
IL10	Hs00961622_m1

TABLE 2.8 TAQMAN GENE EXPRESSION ASSAY PROBES

2.5.3.2 qRT-PCR reaction

All qRT-PCR reactions were designed to incorporate both the target gene probe as well as the ACTB control probe. This control was selected as a housekeeping gene and its expression levels are generally found to remain constant across different cell lines and can therefore be used to normalise target application based on the amount of cDNA added. A RNase-free water reaction with no templates was also run alongside to control for the presence of DNA contamination.

The TaqMan Universal Master Mix II, with UNG (ThermoFisher Scientific) was used in each experiment and this includes the AmpliTaq gold DNA polymerase, dNTPs (with dUTP), ROX passive reference dye, Uracil-N glycosylase (UNG) and optimised buffer components. The TaqMan master mix was added to the target and ACTB probes as well as enough RNase-free water to make up each individual target condition (**Table 2.9**). Either 18uL or 8uL of master mix was added to either 96 or 384-well plates before cDNA was added to each well.

Once all components were added then the plates were sealed with Micro AMP optical adhesive film (Applied Biosystems) before being shaken for 30 seconds and spun down for 1 min at 1200RPM. Assay plates were then run on a QuantStudio 7 Real-Time PCR machine (Applied Biosystems) set to: initial denaturation at 95°C for 10 mins, 40 cycles of 95°C for 15 seconds (denaturation), and 60°C for 1 minute (annealing/elongation).

qRT-PCR component	Volume per well for 96-well plate	Volume per well for 384-well plate
Target primer probe 20x (FAM)	1uL	0.5uL
ACTB primer probe 20x (VIC)	1uL	0.5uL
TaqMan master mix 2x	10uL	5uL
RNase-free water	6uL	3uL
cDNA	2uL	1uL
Total	20uL	10uL

TABLE 2.9 QRT-PCR REACTION COMPONENT MIX

2.5.3.3 qRT-PCR data analysis

Data retrieve from the QuantStudio 7 can be directly uploaded to the Thermo cloud service which allows use to view relative gene expression quantification once a reference sample is selected. The target Ct values are subtracted from ACTB control Ct values for each individual well to create a Δ Ct value, which is then averaged by the experimental triplicates for each sample. The relative value for the difference in transcription between samples can then be calculated as a difference between the Δ Ct of samples and a reference sample, giving us the $\Delta\Delta$ Ct value. This value is then calculated as $2^{-\Delta\Delta Ct}$ to give us the relative fold change which can then be transformed to a log10 scale. Statistical significance is derived by assessing the overlap between the 95% confidence intervals.

2.6 Animal experiments

2.6.1 Licensing

All animal procedures were carried out in accordance with guidelines set by the UK Home Office in compliance with the Animals Scientific Procedures Act of 1986 under the UK HO personal licence number: I20ACBDE4

2.6.2 Animals

For immune-compromised animal xenograft experiments, Athymic Nude (Hsd:Athymic Nude-Foxn1nu) mice were obtained from Harlan Laboratories (Indianapolis, US). Animals were acquired at six to eight weeks of age and maintained in individually ventilated cages (Allentown Inc. NJ, US) with a 12hr day/night cycle. Mice received a Teklad global 19% protein extruded rodent diet (Harlan Laboratories) and water *ad libitum*. All food, drink, saw dust and water bottles were sterilised by autoclaving prior to use. All procedures and animal husbandry was performed within a laminar flow hood (Allentown).

2.6.3 Experimental models

2.6.3.1 Subcutaneous orthotopic xenograft tumour model

Prior to transplantation, cells were either treated under the conditions of interest or grown to 70-80% confluency before being trypsinised and disaggregated into single cell suspension. Cells were washed in 5mLs RPMI media containing no additives (Invotrogen, Paisley, UK) and spun at 1200RPM for 5 minutes three times before being prepared at the required concentrations (1×10^6 cells in 100 μ l) in a mix of 50% RPMI with no additives and 50% Matrigel (ThermoFisher) that had been thawed overnight at 4°C and kept on ice until transplantation. Cells were injected in the subcutaneous tissue bilaterally on the dorsum of mouse and allowed to grow.

2.6.3.2 Tail vein xenograft tumour model

Experimental metastases were established by intravenous injection of 2×10^5 MDA-MD-231-Luc cells. Cells were suspended in 100 μ L of RPMI media and injected via the tail vein of 8-week old female Hsd: Athymic Nude-Foxn 1^{nu} mice (Harlan Laboratories)

2.6.4 In vivo treatment of mice

For some experiments mice were treated *in vivo* with either JS6, 15F, CB1 or DMSO control. Mice were also treated with Bcl-3 inhibitors at a concentration of either 3.5mg/kg via intraperitoneal injection or 20mg/kg via oral gavage. These dosing regimes were determined through outsourced pharmacokinetics experiments investigating the drug

concentration in circulating plasma over time. Drugs were prepared by diluting powdered compound in DMSO. The DMSO was controlled for by using the same concentration of DMSO injected into mice at the same time. Mice were weighed and drug dose determined by the relative animal weight (**Tab. 2.10**).

Mouse weight (g)	Volume of CB1 (uL)
17	148
18	157
19	166
20	174
21	183
22	192
23	201
24	209
25	218
26	227
27	235
28	244
29	253
30	262
31	270
32	279

TABLE 2.10 INJECTED DRUG VOLUME BASED ON ANIMAL WEIGHT FOR 3.5MG/KG

2.6.5 Tumour monitoring and measurements

Mice were inspected at least twice weekly for tumours via palpation and measurements were taken with digital calipers (Fisher Scientific, Loughborough, UK). The size of tumours was calculated as volume in mm³ using the formula: Volume = (Length x (Width²))/2.

2.6.6 Imaging of luciferase expressing tumour metastasis model

Metastatic progression to distal organs was assessed through bioluminescence imaging with the IVIS Spectrum In Vivo Imaging System (Perkin Elmer). Prior to imaging, an intraperitoneal injection of 100µL D-luciferin was administered to each animal. The mice were then anaesthetised with 2.5% isoflurane, oxygen mix and imaged with the charge-coupled IVIS camera device selecting an exposure time of 2 minutes. Luminescence signal was measured through region of interest selection and quantified as total flux

(photon count) overlaying corresponding grayscale photographs (**Fig. 5.10**) and composite images were analysed using the Living Image software (Xenogen Bioscience Corp).

2.7 Affymetrix DNA Microarray GeneChip array analysis

Affymetrix Exon Expression experiment analysis was carried out in the GeneSpring GX Pathway Architect software. The ExonRMA summarisation algorithm was performed on all projects with the baseline set to the median of all samples. The samples were quality checked by assessing the PCA values to ensure appropriate clustering. Probe sets were filtered based on their signal intensity values and 43590 out of 48144 entities had values between 20 and 100 percentile for Bcl-3 knockdown experiment and 43889 out of 48144 for CB-1 drug treatment experiment. The Benjamini and Hochberg False Discovery Rate multiple testing correction was performed to determine corrected p-values and entities were filtered based on a cut-off of $p\text{-value} < 0.05$. 4229 out of 43590 entities satisfied the corrected p-value cut-off for Bcl-3 knockdown experiment and 127 out of 43889 for CB-1 drug treatment experiment.

2.7.1 Gene function analysis with the PANTHER classification system

The PANTHER website was accessed at <http://www.pantherdb.org>. The input file was prepared as a simple text file (.txt) with gene symbols as the first column and log fold change values as the second column in order to use the statistical enrichment test. The gene list was uploaded to the PANTHER tool system and homo sapiens was selected as the list type. The appropriate test type was then selected and analysis carried out.

2.8 Statistical analysis

Error bars on all graphs represent standard error of the mean. Unpaired student's T-tests were performed within the GraphPad Prism software unless stated otherwise to query statistical significance for all normally distributed data sets.

Chapter 3: Results

Investigating Bcl-3 Knockdown
using small interfering RNA (siRNA)
in TNBC Cell Lines

3.1 Introduction

B-cell lymphoma 3 (Bcl-3) is a proto-oncogene in the region adjacent to the t(14;19) (q32; q13) translocation first identified in a subset of patients with chronic lymphocytic leukaemia (CLL) (Ohno et al., 1990). Bcl-3 binds to p50 and p52 dimers on DNA, providing these complexes with a transactivation domain which subsequently drives transcription (Bours et al., 1993). Bcl-3 has been implicated in both innate and adaptive immunity (Zhang et al., 2007). In numerous hematopoietic and solid tumours, including breast cancer, Bcl-3 has been shown to be up-regulated and associated with tumour development and progression (Maldonado and Melendez-Zajgla, 2011).

Bcl-3 is often highlighted as an oncogene through its regulation of cell cycle or apoptosis at the gene expression or protein level during cancer development. The cylindromatosis (CYLD) protein binds and deubiquitinates Bcl-3 and prevents its nuclear accumulation. In cylindromas and other cancers featuring reduced CYLD, increased nuclear Bcl-3 accumulation induces transcription of genes such as cyclin D1 and N-cadherin through interactions with p50 and p52 homodimers (Massoumi et al., 2009). Bcl-3 has also been shown to stabilise the c-Myc protein and promote colorectal cancer development by regulating ERK signalling (Liu et al., 2013). Bcl-3 was further reported to promote colorectal tumourigenesis through activation of AKT signalling (Urban et al., 2016). These studies demonstrate the various novel roles Bcl-3 has in tumour development and progression by being a trans-activator or trans-repressor within NFkB signalling pathways. A recent study has demonstrated the ability of Bcl-3 to regulate metastasis of mouse mammary cancer cells. Bcl-3 knockout MMTV-Neu mice had significantly reduced secondary lung metastasis with no effect on primary tumour growth (Wakefield et al., 2013). This was supported by Chen et al., who confirmed that Bcl-3 played a role in pulmonary metastasis in human breast cancer. Despite numerous studies highlighting the oncogenic properties of Bcl-3 up-regulation, and the identification of oncogenic pathways associated with Bcl-3 mediated oncogenesis (Chen et al., 2016), the underlying cellular mechanisms surrounding its oncogenicity remains largely unknown.

Triple-negative breast cancers (TNBC) are characterised by tumours that do not express oestrogen receptor (ER), progesterone receptor (PR), or HER2 receptors. They represent real clinical challenges, as these cancers do not respond well to traditional endocrine therapy or targeted agents. Typically, TNBCs feature earlier metastatic events

compared with other breast cancer subtypes, as well as a shorter period from the time of recurrence until death (Kim et al., 2009). This presents a hurdle for clinicians who are tasked with palliating an incurable disease and extending patient life when possible.

Given the previously published association between Bcl3 and metastatic breast cancer (Chen et al., 2016), the main aims in this chapter were to further explore and characterise the roles of Bcl-3 in human cancer progression, specifically in the context of TNBC, an aggressive, increasingly metastatic subtype of human breast cancers that often features poor clinical prognoses. We investigated the effects of Bcl-3 siRNA knockdown in a panel of four human triple negative breast cancer cell lines, contrasted with one nonmalignant human mammary epithelial cell line. Following Bcl-3 knockdown, we looked at the biological outcomes in a number of *in vitro* cell-based assays to quantify cell population change, proliferative markers, cell cycle, apoptosis, stemness, clonogenicity, migration and NFkB activity. We also carried out an *in vivo* xenograft experiment to assess the effect of Bcl-3 suppression in a mouse metastasis model. An Affymetrix microarray experiment was subsequently performed to profile global gene expression changes and help explain and piece together mechanisms pertaining to these biological outcomes.

3.2 Bcl-3 expression in breast cancer cell lines

A panel of triple negative breast cancer cell lines, MDA-MB-436, SUM149, MDA-MB-231 and the highly metastatic MDA-MB-231 sub-line MDA-MB-231-Luc were selected and their relative Bcl-3 protein (**Fig. 3.1a**) and RNA (**Fig. 3.1b**) expression levels were profiled by western blotting and qRT-PCR. We chose these experimental cell lines as they are all extensively studied and well characterised in the current literature and provided good representation for modelling TNBCs. The HER2+ HCC1954 cell line which was found to features comparatively high Bcl-3 expression in our previous studies was used as a positive control. Within the triple negative cell lines, MDA-MB-436 expressed the highest Bcl-3 levels, followed by MDA-MB-231-Luc with just less than half Bcl-3 RNA levels, followed by MDA-MD-231 with another halving, and finally SUM149 have similar Bcl-3 levels to MDA-MD-231. The non-malignant MCF10a cell line expressed the lowest quantities of Bcl-3.

3.3 Bcl-3 siRNA knockdown had no observable effects on bulk cellular monolayer morphology and knockdown was stable up to 96h

We were interested in whether Bcl-3 knockdown had any discernible effects on the monolayer morphology of the cell lines through bright-field phase-contrast microscopy. It was also important to optimise and confirm the duration of Bcl-3 knockdown as siRNA only has a transient effect and wears off over time.

The five chosen breast cancer cell lines were each transfected with either Bcl-3 or scrambled control siRNA for 48h, 72h or 96h, before being imaged by bright-field microscopy and total cellular RNA was harvested (**Fig. 3.2**). qRT-PCR for Bcl-3 was then performed for each time-point and Bcl-3 expression was shown to be significantly lowered at all time-points up to 96h. Thus suppression of Bcl3 by siRNA was stable for up to 4 days. The time taken for levels to return to normal was not determined.

Each cell line exhibited distinct cellular morphologies. MDA-MB-436 cells (**Fig. 3.2a**) appeared fibroblastic, displaying a mesenchymal-like morphology with hyper-elongated cellular processes and an almost complete lack of cell-cell adhesion, traits which are associated with highly migratory cells. SUM149 cells (**Fig. 3.2d**) had a more 'cobblestone'-like appearance in confluency, similar to MCF10A (**Fig. 3.2e**), with clear evidence of cell-adhesions, while MDA-MB-231 subtypes (**Fig. 3.2b&c**) had an intermediate mesenchymal-like morphology. Bright-field images taken at 96h showed no significant cellular morphological differences between Bcl-3 knockdown and that of the scrambled control in any of the cell lines tested.

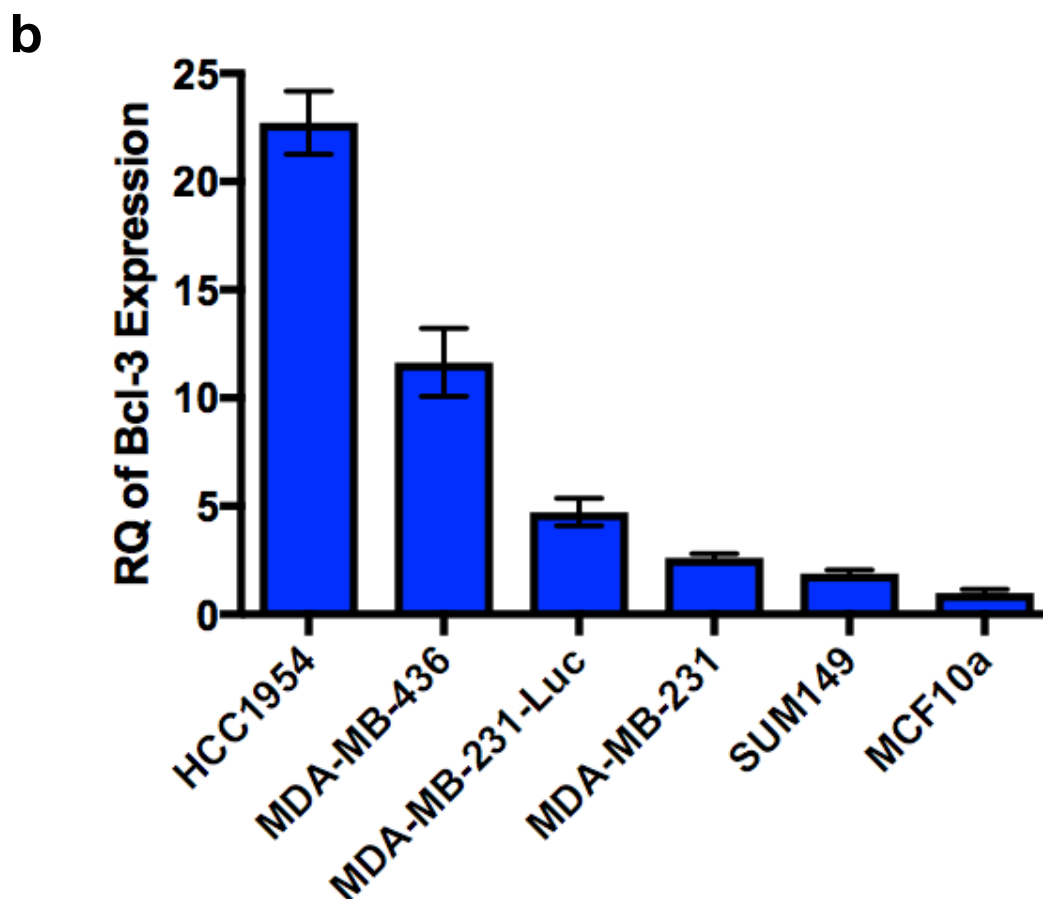
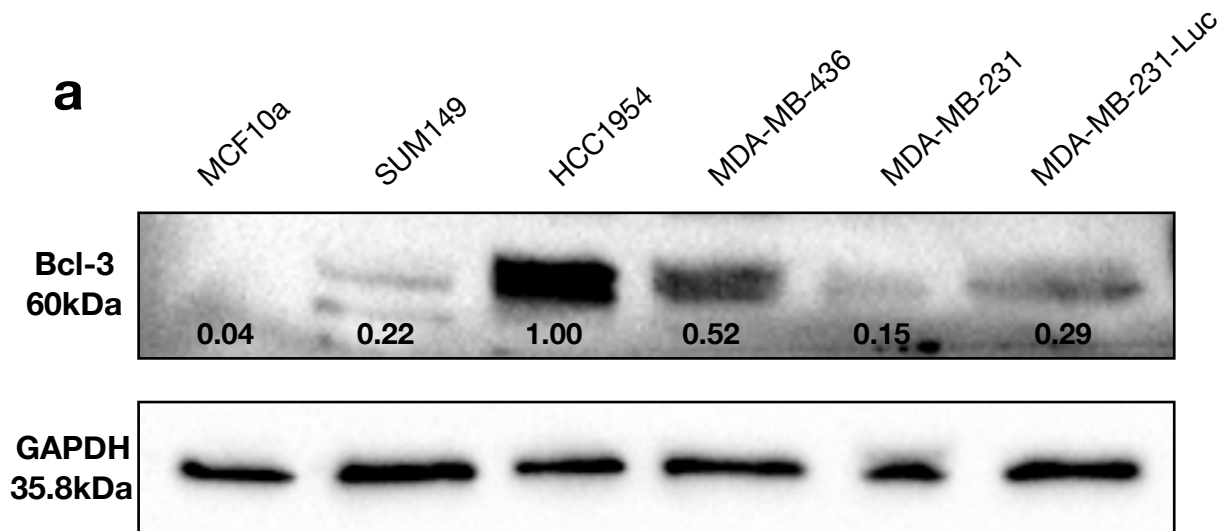
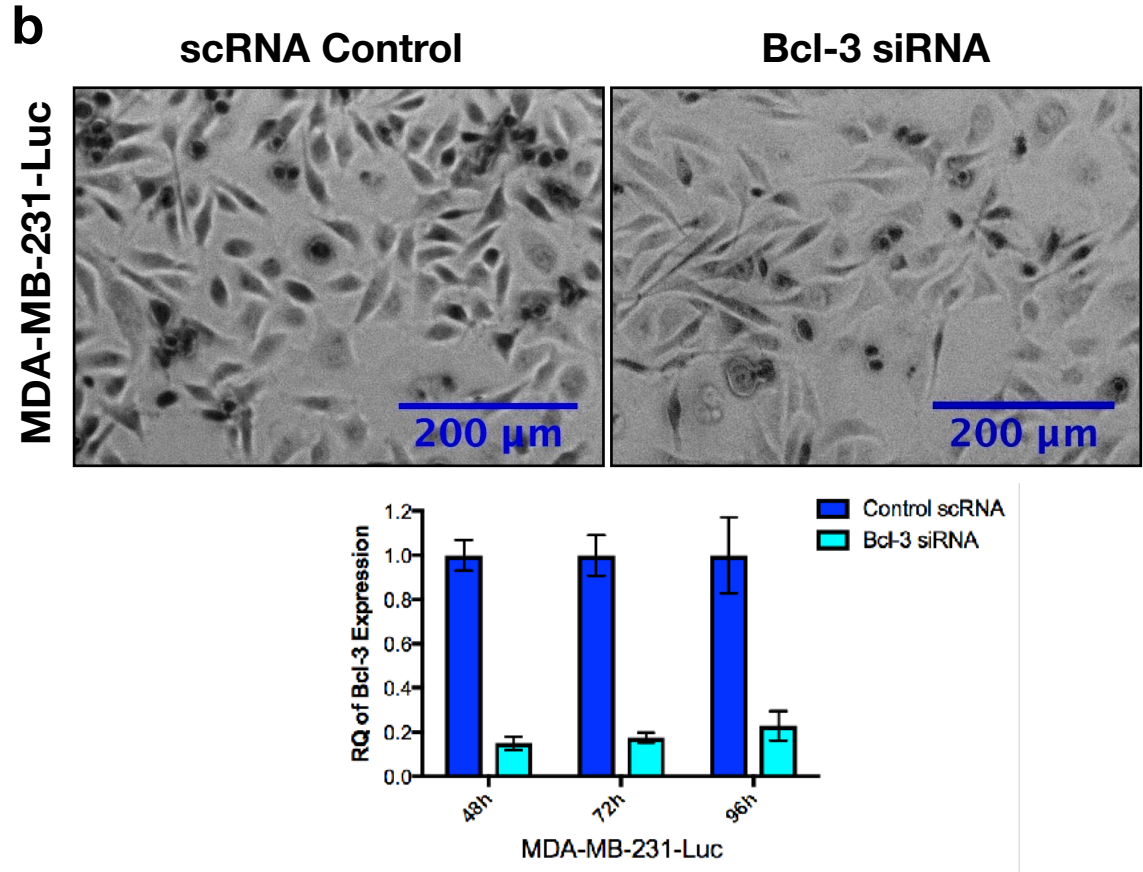
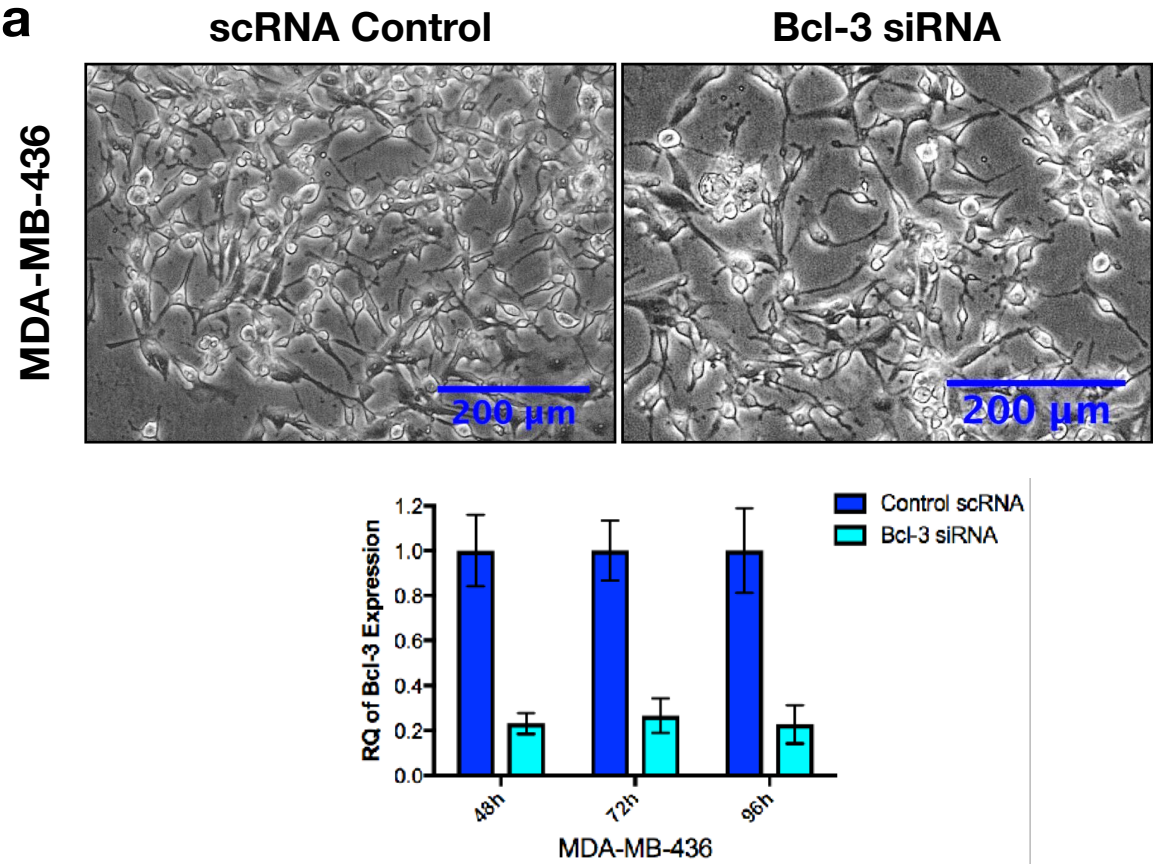
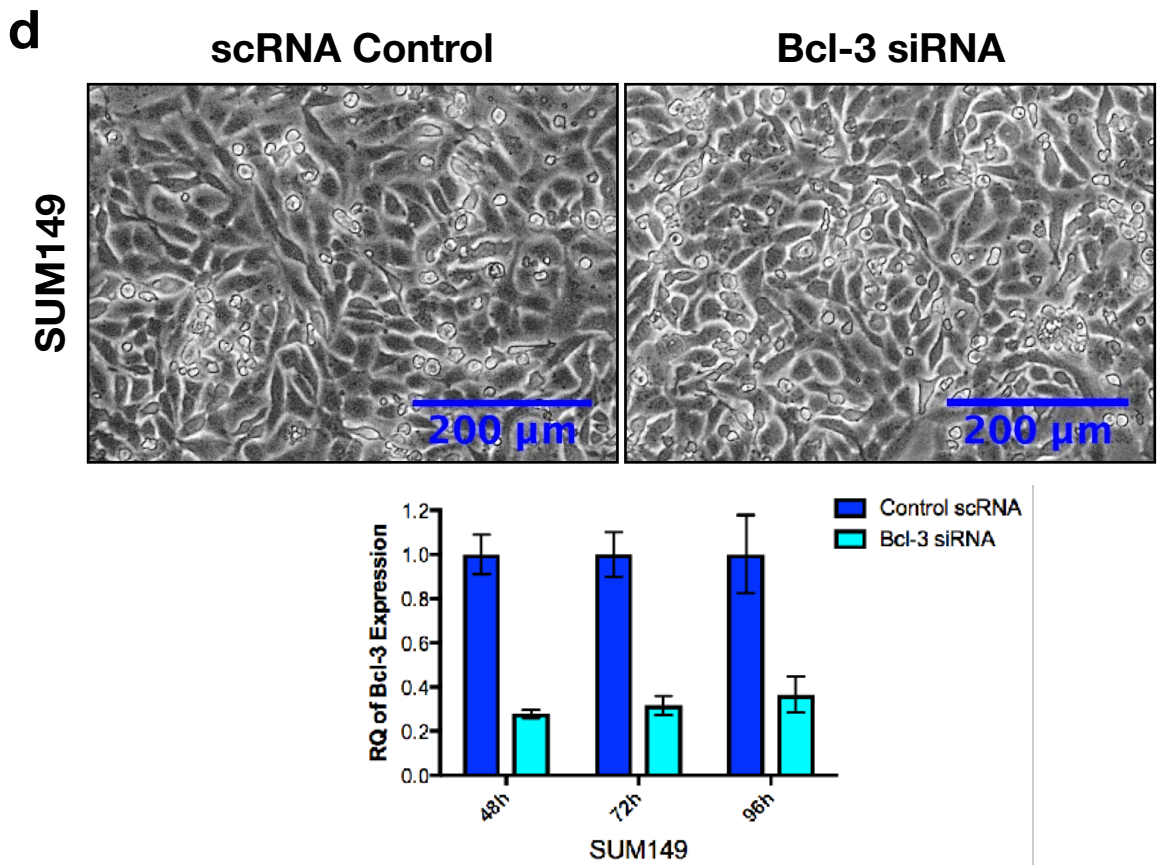
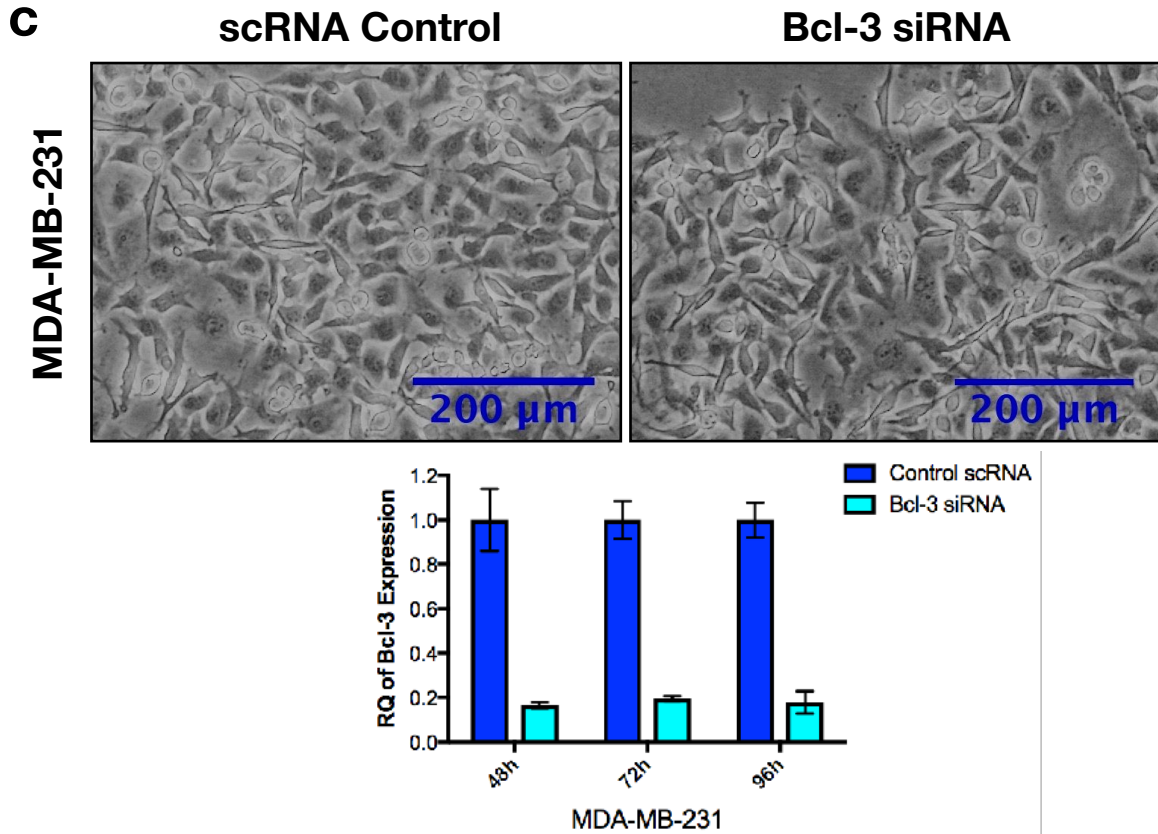


FIG. 3.1 RELATIVE BCL-3 PROTEIN AND RNA EXPRESSION IN BREAST CANCER CELL LINES.

a. Cell lines were cultured under standard conditions and total protein extraction and western blotting for Bcl-3 was carried out, using GAPDH as the loading control. Average relative densities are estimated. Image shown is representative of 3 independent westerns. **b.** Total cellular RNA was extracted and Bcl-3 expression quantified using Taqman qRT-PCR and relative gene expression normalised to beta-actin (ACTB). Error bars represent \pm SEM of 3 independent experiments.





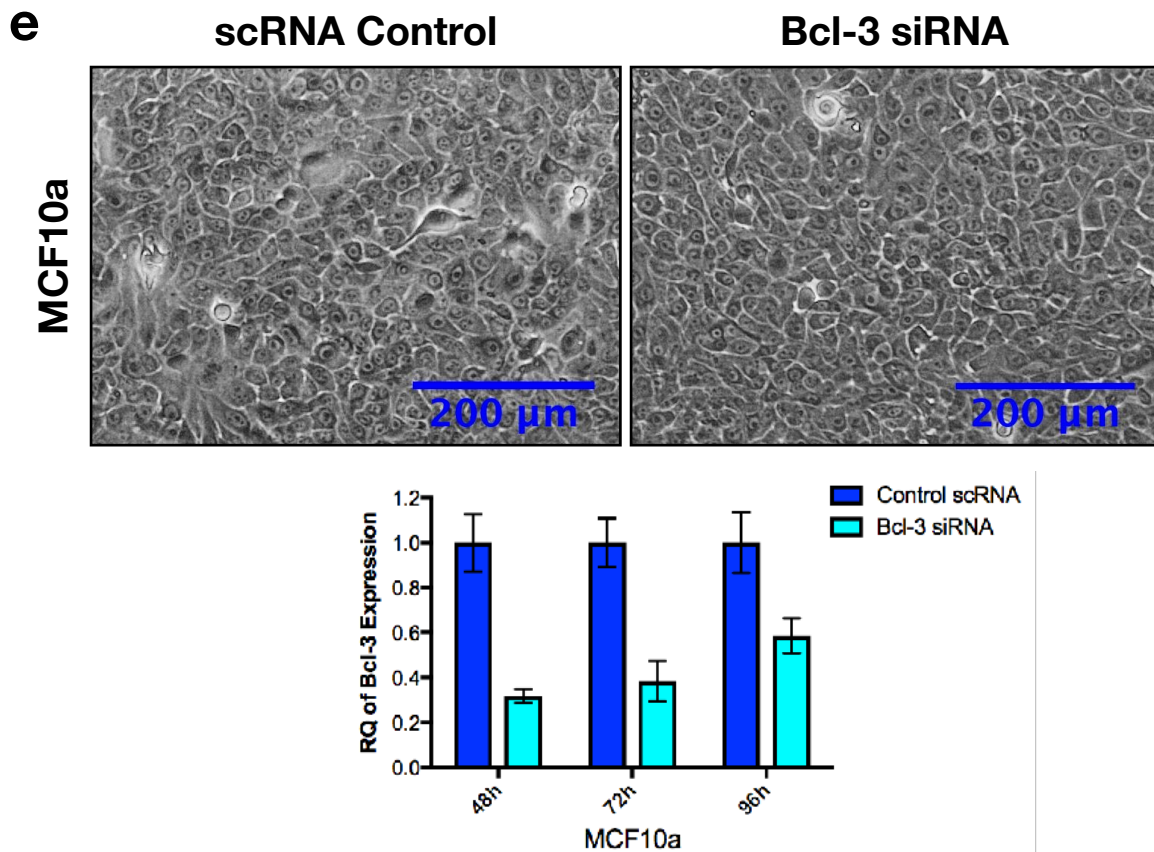


FIG. 3.2 BCL-3 SIRNA KNOCKDOWN HAD NO EFFECTS ON BULK MONOLAYER MORPHOLOGY AND KNOCKDOWN WAS STABLE UP TO 96H

Representative bright-field microscopy images following 96h knockdown with either Bcl-3 or scrambled control siRNA and qRT-PCR for Bcl-3 RNA expression following 48h, 72h or 96h knockdown for **a.** MDA-MB-436 **b.** MDA-MB-231-Luc **c.** MDA-MB-231 **d.** SUM149 **e.** MCF10a breast cancer cell lines. Error bars represent \pm SEM of 3 independent experiments.

3.4 Bcl-3 siRNA knockdown significantly reduced cell population growth in TNBC cell lines but not in the non-malignant MCF10a cell line

One of the primary characteristics of an oncogene is the ability to promote cell population growth and it is known that Bcl-3 positively drives proliferation in a number of different cancer types (Maldonado and Melendez-Zajgla, 2011). Therefore we hypothesised that knocking it down will inhibit growth in TNBCs.

The breast cancer cell line panel were transfected with either Bcl-3 or scrambled control siRNA for 48h, plated into assay plates and cell population growth measured using RealTime-Glo MT Cell Viability Assay (Promega). In this assay, non-lytic NanoLuc Luciferase and MT Cell Viability substrates were added to cell media during time of plating. The assay reagents then diffused into cells where it was reduced to form a NanoLuc substrate, which exited the cells and was used by NanoLuc Luciferase in the media. This assay was used to quantify cell population growth because metabolically active cells could reduce the substrate and light produced was directly proportional to the number of viable cells in culture. The non-lytic and rapid response of the assay allowed for accurate and continued measurements of cell proliferation over time.

By 72h all four TNBC cell lines showed a significant reduction in cell population growth following Bcl-3 siRNA knockdown (**Fig 3.3a-d**). This growth effect was most prominent in the MDA-MB-231 (**Fig 3.3c**) and MDA-MB-231-Luc (**Fig 3.3b**) cell lines as significant cell growth reductions could already be seen from 24h and 48h respectively. There was no growth reduction in the non-malignant MCF10a cell line following Bcl-3 siRNA knockdown (**Fig. 3.3e**).

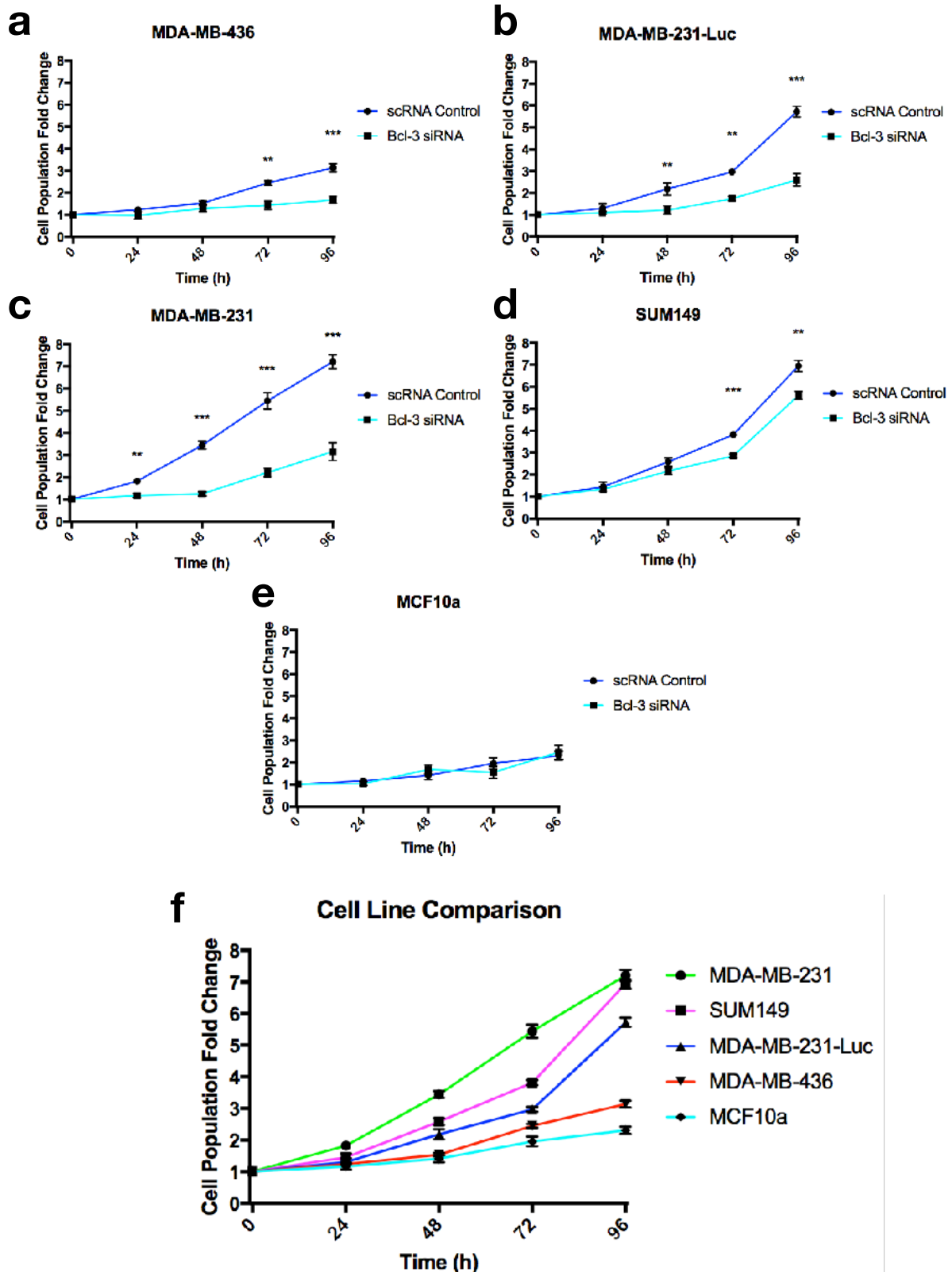


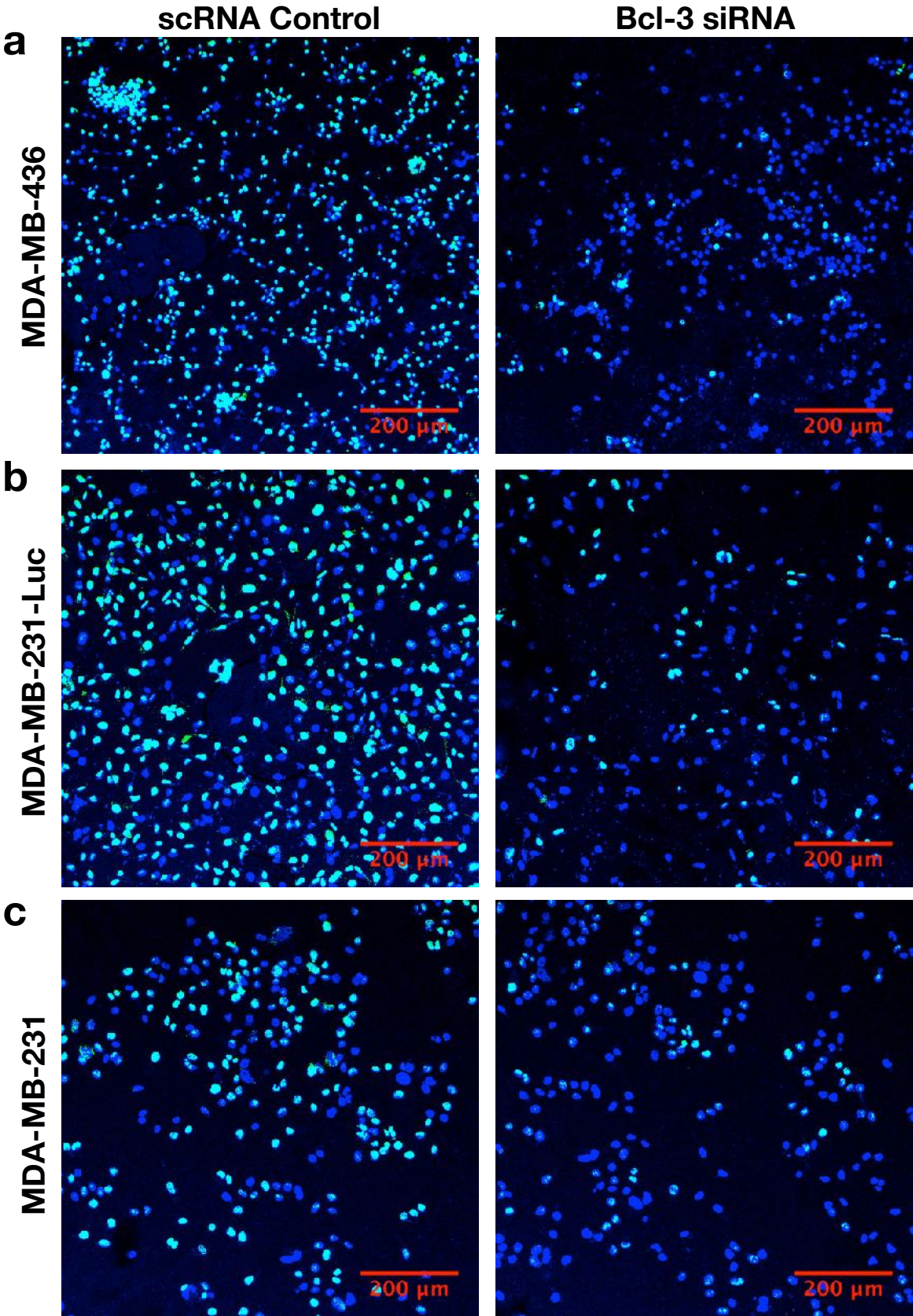
FIG. 3.3 BCL-3 SIRNA KNOCKDOWN REDUCED CELL POPULATION FOLD CHANGE OVER TIME RELATIVE TO THE SCRNA CONTROL

a. MDA-MB-436 **b.** MDA-MB-231-Luc **c.** MDA-MB-231 **d.** SUM149 **e.** MCF10a cell lines were knockdown with either Bcl-3 or scrambled control siRNA for 48h, plated into 96-well plates and cell population growth assayed using RealTime-Glo Assay. The results at each timepoint were normalised to their corresponding values at 0 hours and plotted as cell population fold change increases over time. **f.** Graph comparing cell population growth between different cell lines. Error bars represent \pm SEM of 3 independent experiments. (T-test, * $p < 0.05$, ** $p < 0.01$, *** $p < 0.001$)

3.5 Bcl-3 siRNA knockdown significantly reduced Ki67 expression in TNBC cell lines but not in the non-malignant MCF10a cell line

To confirm whether the effects on growth seen in the cell viability assay manifested in a reduction in cell proliferation, we investigated the proportion of cells undergoing cell division. Ki67 is a nuclear protein associated with cellular proliferation and a commonly used proliferative marker (Scholzen and Gerdes, 2000). Ki67 is present during all active phases of the cell cycle (G1, S, G2, and mitosis), but is absent in resting or quiescent cells (G0) (Bruno and Darzynkiewicz, 1992). Cellular content of Ki67 protein markedly increases during cell progression through S phase (Darzynkiewicz et al., 2015).

The breast cancer cell line panel were transfected with either Bcl-3 or scrambled control siRNA for 48h, plated onto coverslips, PFA fixed and immunofluorescence staining for Ki67 was performed. Bcl-3 knockdown significantly reduced the fraction of Ki67 positive cells in all TNBC cell lines but had no effect on the non-malignant MCF10a cell line, which comparatively had a much lower basal Ki67 expression (**Fig 3.4f**).



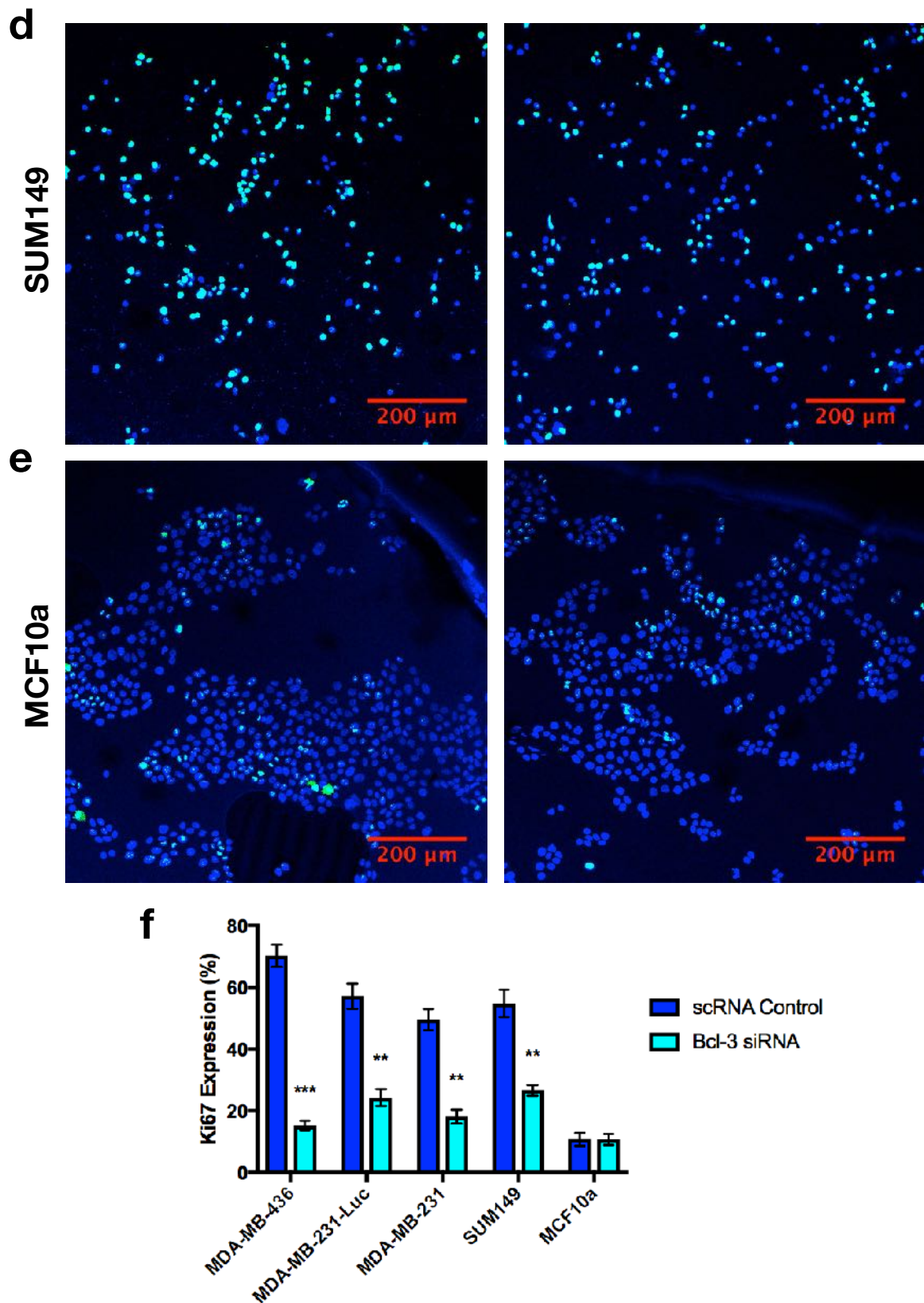


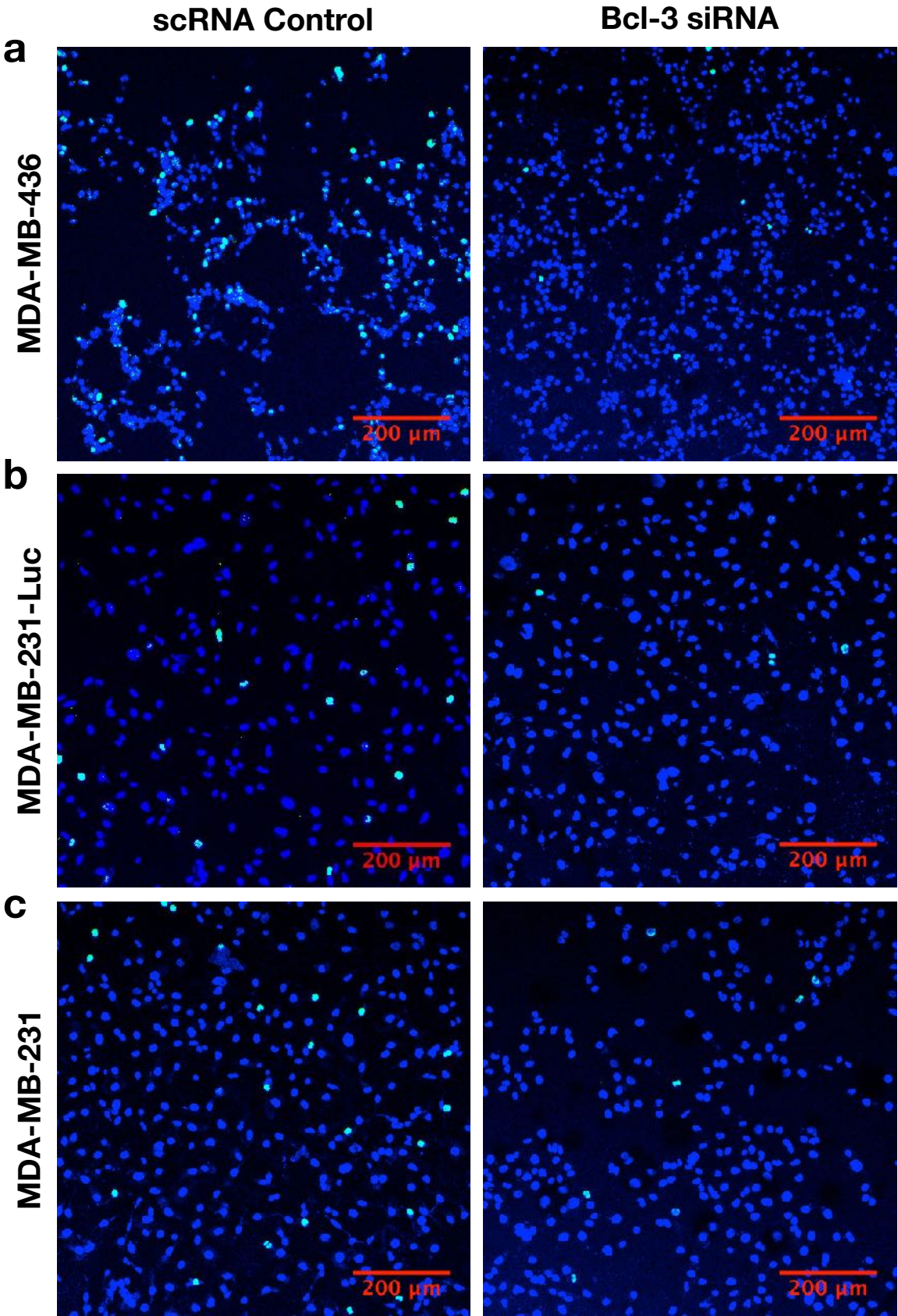
FIG. 3.4 BCL-3 SIRNA KNOCKDOWN REDUCED KI67 EXPRESSION

Representative immunofluorescence images of **a.** MDA-MB-436 **b.** MDA-MB-231-Luc **c.** MDA-MB-231 **d.** SUM149 **e.** MCF10a cells were knockdown with either Bcl-3 or scrambled control siRNA for 48h, plated onto coverslips, PFA fixed and immunofluorescent-stained for Ki67. **f.** Graph comparing Ki67 expression between knockdowns and different cell lines. Error bars represent \pm SEM of 3 independent experiments. (T-test, *= $p < 0.05$, **= $p < 0.01$, ***= $p < 0.001$)

3.6 Bcl-3 siRNA knockdown significantly reduced phosph-Histone H3 (ser10) expression in TNBC cell lines but not in the non-malignant MCF10a cell line

To compliment our Ki67 findings, phospho-histone H3 (pHH3) immunofluorescence staining was carried out. pHH3 is a recently described immuno-marker specific for cells undergoing mitosis. The phosphorylation of Histone H3 plays an important role in gene expression, chromatin remodelling, chromosome condensation and cell division (Hans and Dimitrov, 2001). Histone H3 phosphorylation is always heavily associated with metaphase, and H3 phosphorylation at serine 10 is coupled with mitotic chromosome segregation and condensation during both mitosis and meiosis (Hendzel et al., 1997). Upon exit of mitosis and meiosis global dephosphorylation of H3 takes place during anaphase (Dai et al., 2005). Due to the narrower window of expression in the cell cycle this marker detects a smaller proportion of cells than Ki-67.

The breast cancer cell line panel were transfected with either Bcl-3 or scrambled control siRNA for 48h, plated onto coverslips, PFA fixed and immunofluorescence staining for pHH3 was performed. Bcl-3 knockdown was able to significantly reduce the fraction of pHH3 positive cells in all TNBC cell lines but had no effect on the non-malignant MCF10a cell line, which comparatively had a much lower basal pHH3 expression (**Fig 3.5f**).



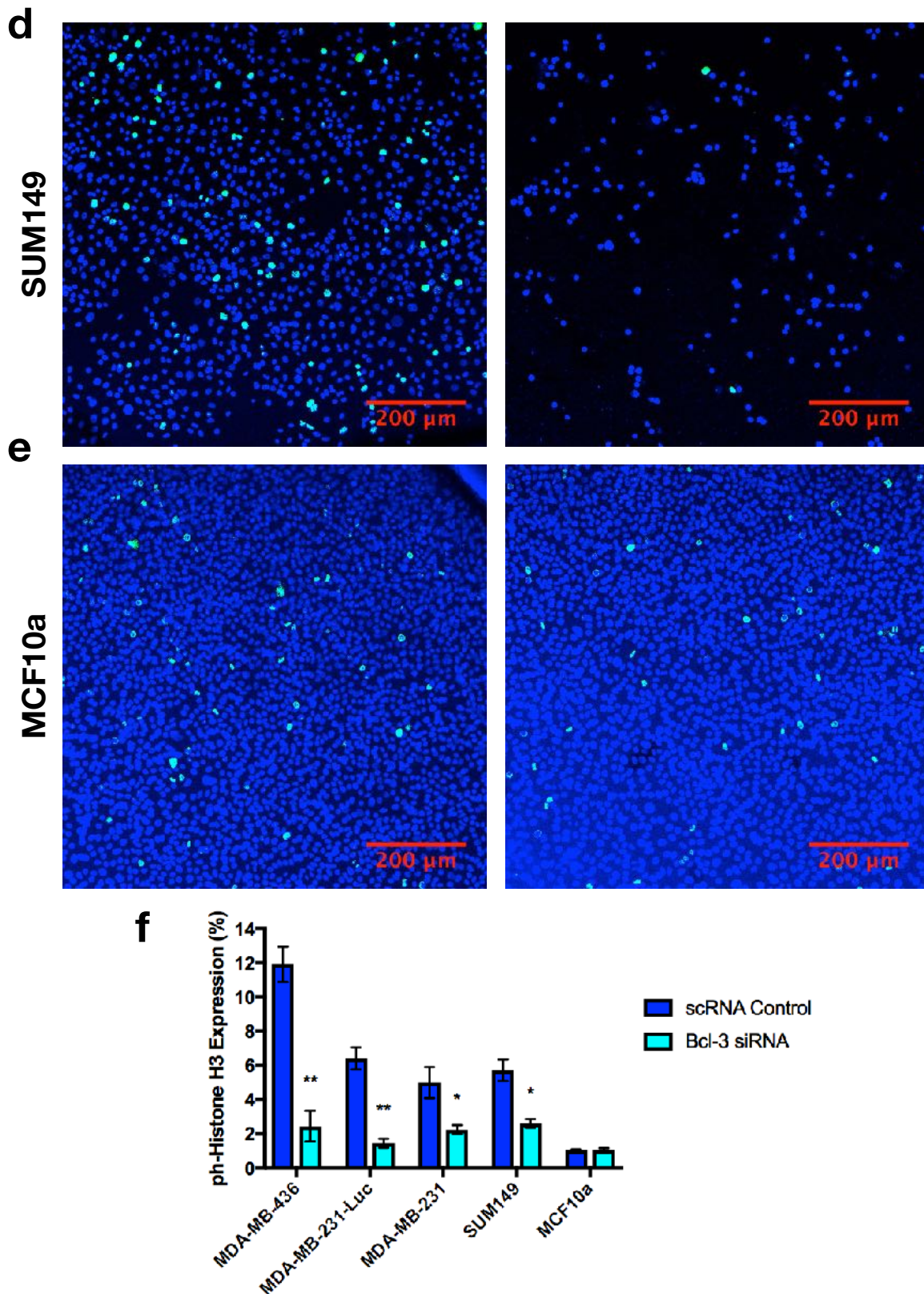


FIG. 3.5 BCL-3 SIRNA KNOCKDOWN REDUCED PHOSPHO-HISTONE H3 (SER10) EXPRESSION
 Representative immunofluorescence images of **a.** MDA-MB-436 **b.** MDA-MB-231-Luc **c.** MDA-MB-231 **d.** SUM149 **e.** MCF10a cells were knockdown with either Bcl-3 or scrambled control siRNA for 48h, plated onto coverslips, PFA fixed and immunofluorescent-stained for phospho-Histone H3. **f.** Graph comparing Ki67 expression between knockdowns and different cell lines. Error bars represent \pm SEM of 3 independent experiments. (T-test, $*$ = $p < 0.05$, $**$ = $p < 0.01$, $***$ = $p < 0.001$)

3.7 Effects of Bcl-3 siRNA knockdown on the cell cycle

In order to further confirm and explain the effects seen on cell growth, we investigated the effects of Bcl-3 knockdown on stages of the cell cycle. A common approach for determining cell cycle stage is through measurement of cellular DNA content. This allows the discrimination of cells in the G₀/G₁, S, and G₂/M phases of the cell cycle. DNA is stained with the fluorescent DAPI dye and cellular fluorescence is measured by flow cytometry. The intensity of integrated fluorescence for each cell is expected to be in stoichiometric relationship to DNA content and thereby can be used to determine cell cycle stage. The DNA content frequency histograms can be deconvoluted using FlowJo, a computer program used for single-cell flow cytometry analysis (Darzynkiewicz et al., 2001). Internucleosomal DNA fragmentation is one of the hallmarks of apoptosis as low molecular weight DNA fragments are extracted during cell staining in aqueous solution. This results in a subG₁ peak as the apoptotic cells are identified on the DNA content frequency histograms as cells with fractional DNA content thus providing an additional assessment of Bcl3's effects on cell viability (Kajstura et al., 2007).

MDA-MB-436 cells were transfected with either Bcl-3 or scrambled control siRNA for 48h before being permeabilised with NP-40 and stained with DAPI. Single-cell DNA content was measured using flow cytometry and cell cycle stages calculated. Bcl-3 knockdown cells had a 25% significantly increased subG₁ population, which was balanced by significant reductions in all other G₀/G₁, S and G₂/M populations (**Fig 3.6a**).

MDA-MB-231-Luc cells were transfected with either Bcl-3 or scrambled control siRNA for 48h before being permeabilised with NP-40 and stained with DAPI. Single-cell DNA content was measured using flow cytometry and cell cycle stages calculated. Bcl-3 knockdown cells had a significantly decreased G₂/M population (**Fig 3.7a**).

MDA-MB-231 cells were transfected with either Bcl-3 or scrambled control siRNA for 48h before being permeabilised with NP-40 and stained with DAPI. Single-cell DNA content was measured using flow cytometry and cell cycle stages calculated. Bcl-3 knockdown cells had a significantly increased G₀/G₁ and decreased G₂/M population (**Fig 3.8a**).

SUM149 cells were transfected with either Bcl-3 or scrambled control siRNA for 48h before being permeabilised with NP-40 and stained with DAPI. Single-cell DNA content was measured using flow cytometry and cell cycle stages calculated. Bcl-3 knockdown cells had a significantly increased G0/G1 and decreased S, and G2/M populations (**Fig 3.9a**).

MCF10a cells were transfected with either Bcl-3 or scrambled control siRNA for 48h before being permeabilised with NP-40 and stained with DAPI. Single-cell DNA content was measured using flow cytometry and cell cycle stages calculated. Bcl-3 knockdown cells did not have significantly different cell cycle populations compared to control (**Fig 3.10a**).

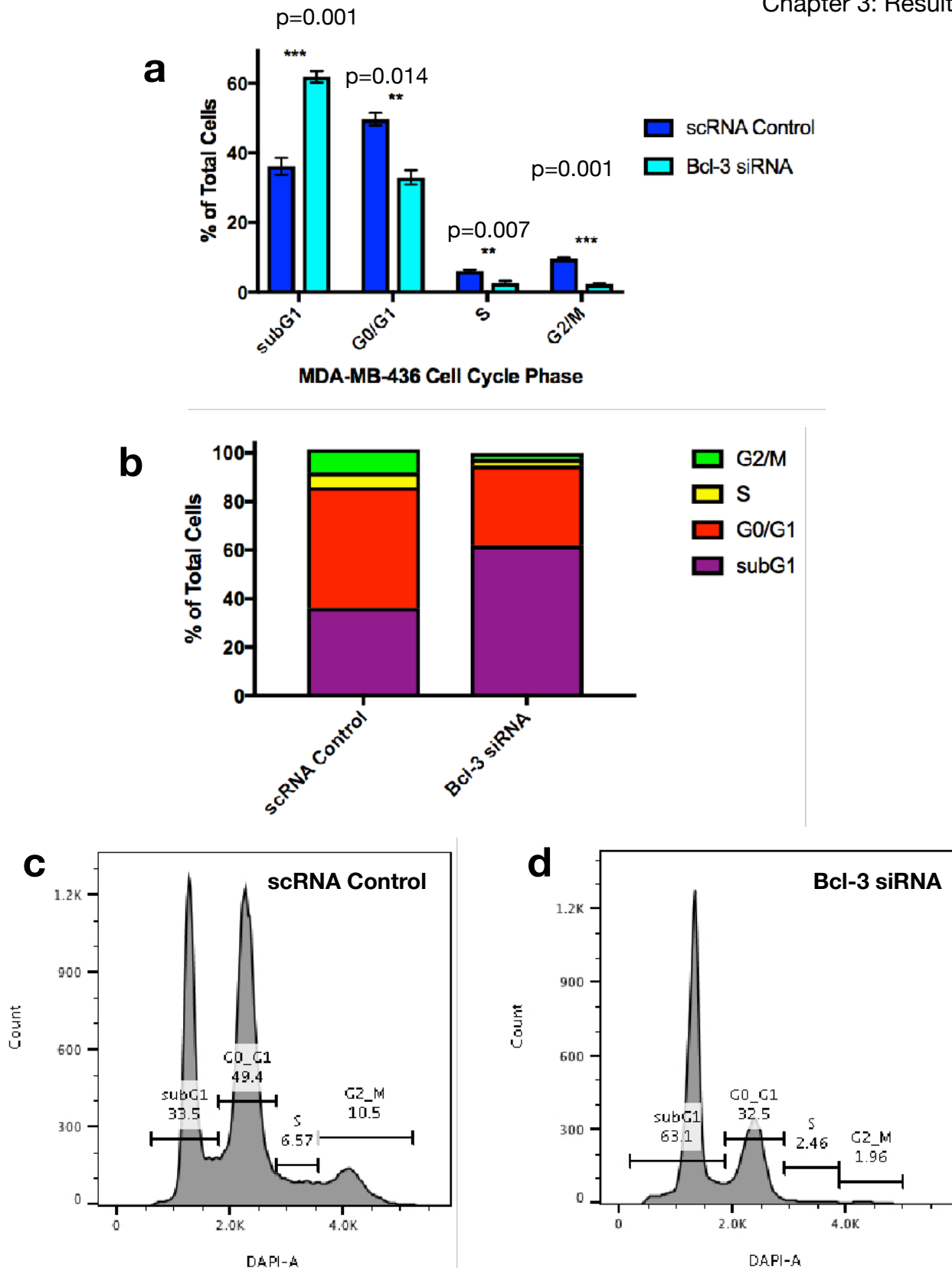


FIG. 3.6 BCL-3 SIRNA KNOCKDOWN IN MDA-MB-436 INCREASED THE SUBG1 POPULATION WHILE DECREASING THE G0/G1, S, AND G2/M POPULATIONS

MDA-MB-436 cells were transfected with either Bcl-3 or scrambled control siRNA for 48h before being permeabilised with NP-40 and stained with DAPI. Single-cell DNA content was measured using flow cytometry and cell cycle stages calculated. **a.&b.** Percentage of cells in each cell cycle. **c.&d.** Representative histograms detailing cell cycle stage distribution. Error bars represent \pm SEM of 3 independent experiments. (T-test, * $p < 0.05$, ** $p < 0.01$, *** $p < 0.001$)

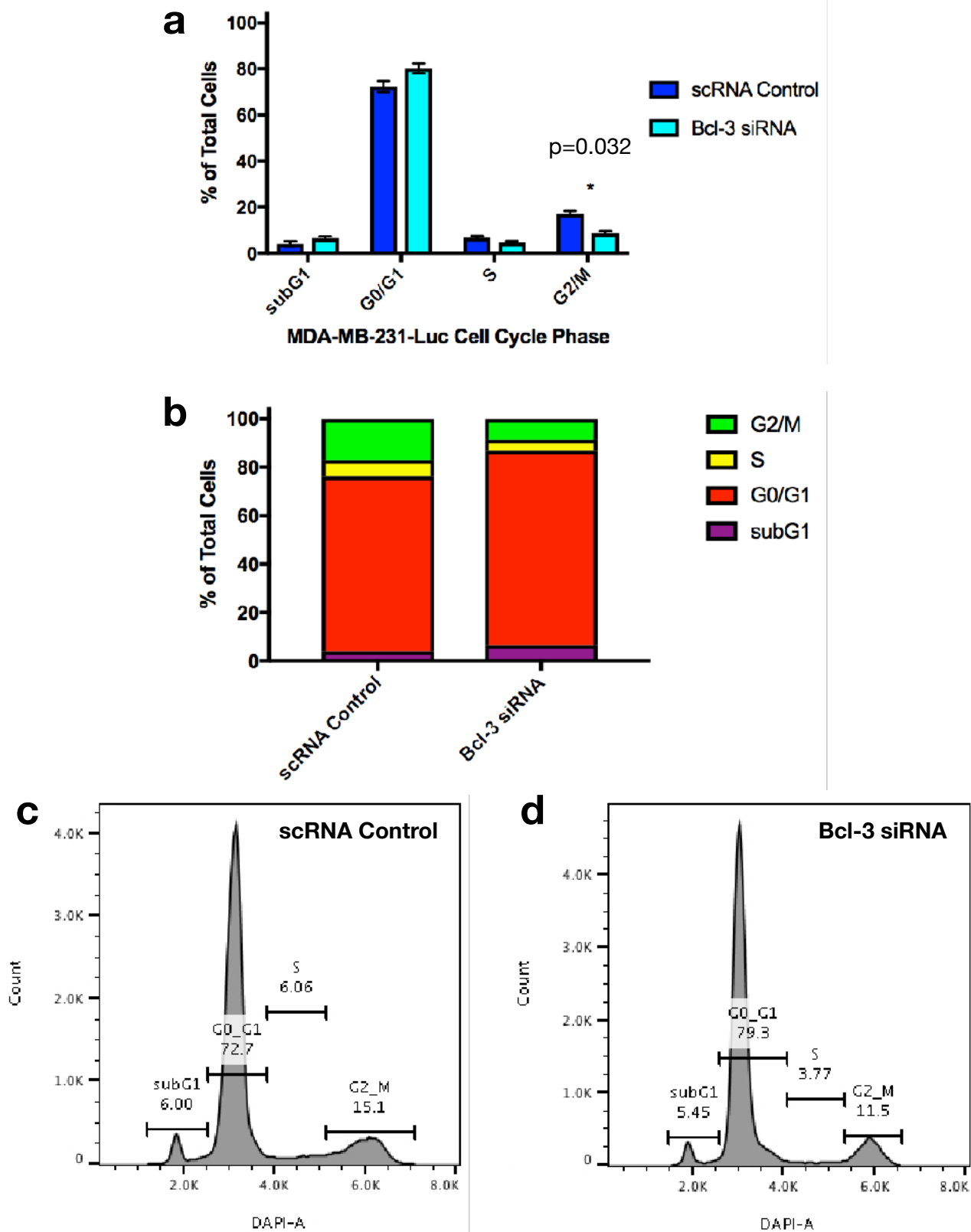


FIG. 3.7 BCL-3 SIRNA KNOCKDOWN IN MDA-MB-231-LUC DECREASED THE G2/M POPULATION
 MDA-MB-231-Luc cells were transfected with either Bcl-3 or scrambled control siRNA for 48h before being permeabilised with NP-40 and stained with DAPI. Single-cell DNA content was measured using flow cytometry and cell cycle stages calculated. **a.&b.** Percentage of cells in each cell cycle. **c.&d.** Representative histograms detailing cell cycle stage distribution. Error bars represent \pm SEM of 3 independent experiments. (T-test, *= $p < 0.05$, **= $p < 0.01$, ***= $p < 0.001$)

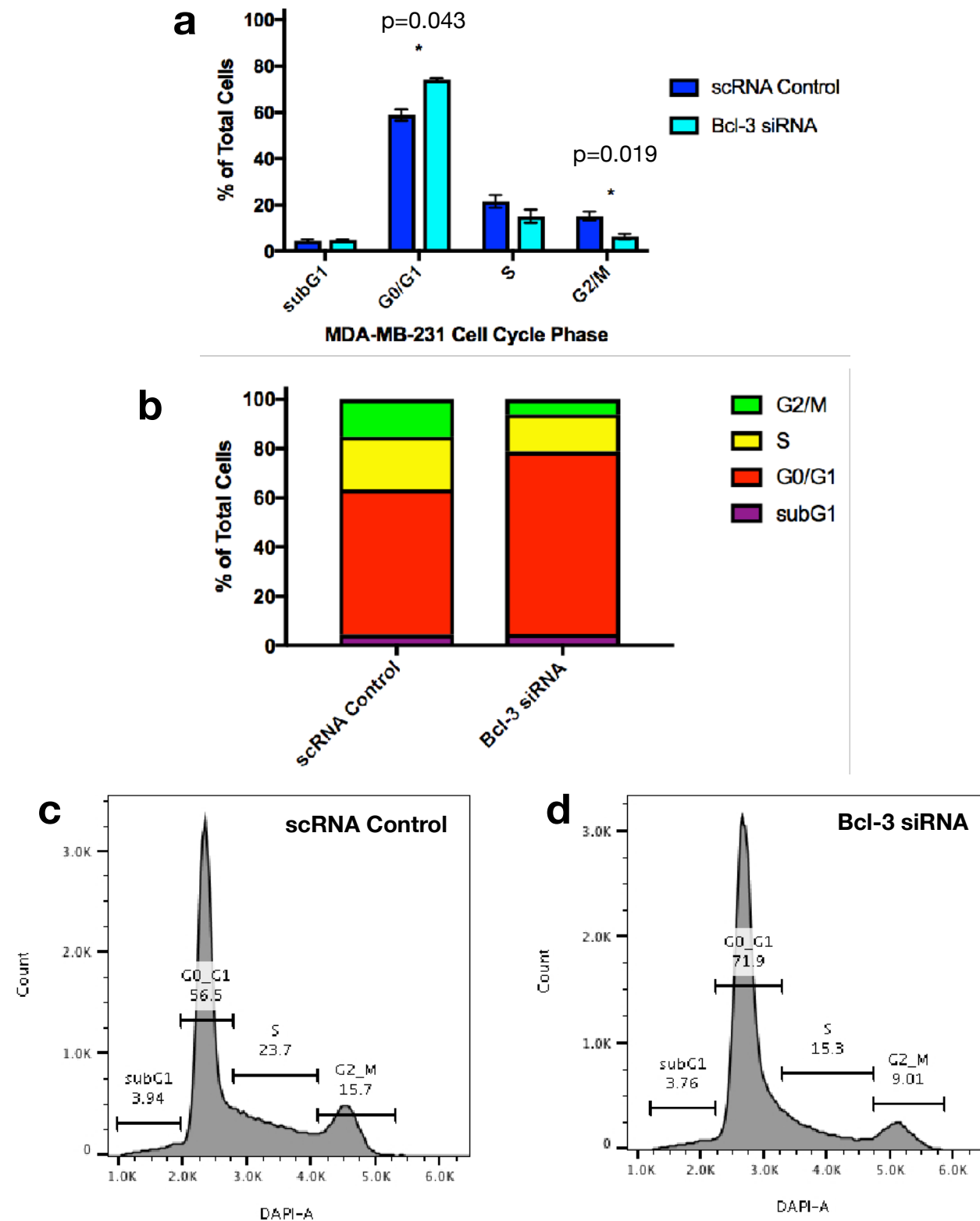


FIG. 3.8 BCL-3 SIRNA KNOCKDOWN IN MDA-MB-231 INCREASED THE G0/G1 AND DECREASED THE G2/M POPULATIONS

MDA-MB-231 cells were transfected with either Bcl-3 or scrambled control siRNA for 48h before being permeabilised with NP-40 and stained with DAPI. Single-cell DNA content was measured using flow cytometry and cell cycle stages calculated. **a.&b.** Percentage of cells in each cell cycle. **c.&d.** Representative histograms detailing cell cycle stage distribution. Error bars represent \pm SEM of 3 independent experiments. (T-test, *= $p < 0.05$, **= $p < 0.01$, ***= $p < 0.001$)

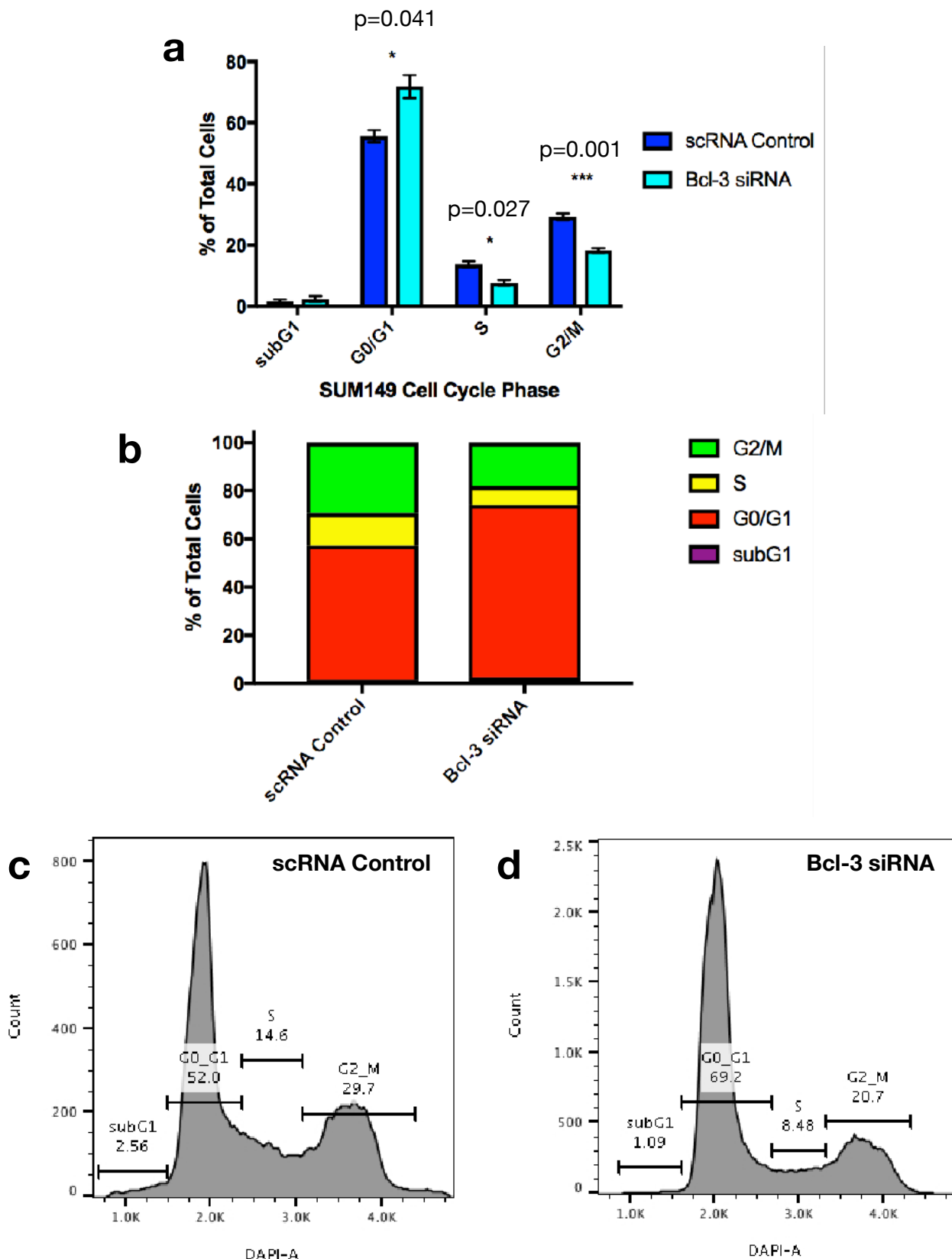


FIG. 3.9 BCL-3 SIRNA KNOCKDOWN IN SUM149 INCREASED THE G0/G1 AND DECREASED THE S, AND G2/M POPULATIONS

SUM149 cells were transfected with either Bcl-3 or scrambled control siRNA for 48h before being permeabilised with NP-40 and stained with DAPI. Single-cell DNA content was measured using flow cytometry and cell cycle stages calculated. **a.&b.** Percentage of cells in each cell cycle. **c.&d.** Representative histograms detailing cell cycle stage distribution. Error bars represent \pm SEM of 3 independent experiments. (T-test, *= $p < 0.05$, **= $p < 0.01$, ***= $p < 0.001$)

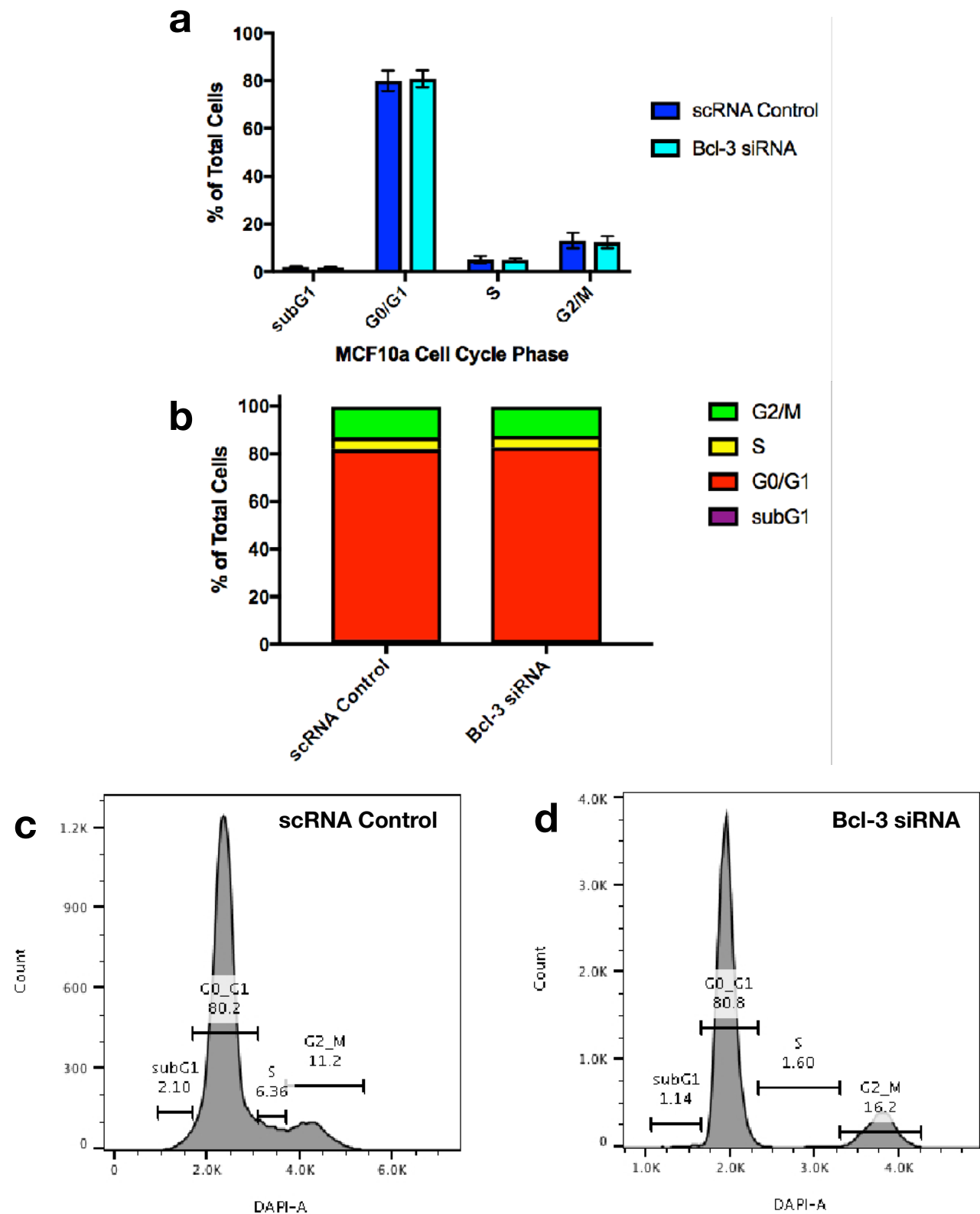


FIG. 3.10 BCL-3 SIRNA KNOCKDOWN IN MCF10A DID NOT AFFECT THE CELL CYCLE

MCF10a cells were transfected with either Bcl-3 or scrambled control siRNA for 48h before being permeabilised with NP-40 and stained with DAPI. Single-cell DNA content was measured using flow cytometry and cell cycle stages calculated. **a.&b.** Percentage of cells in each cell cycle. **c.&d.** Representative histograms detailing cell cycle stage distribution. Error bars represent \pm SEM of 3 independent experiments. (T-test, *= $p < 0.05$, **= $p < 0.01$, ***= $p < 0.001$)

3.8 Bcl-3 siRNA knockdown significantly increased caspase-3/-7 activity in TNBC cell lines but not in the non-malignant MCF10a cell line

Apart from cellular proliferation another key contributor to overall cell population growth is the rate of cellular apoptosis or other forms of programmed cell death. In light of the results highlighting a high sub-G1 population in MDA-MB-436s, which is indicative of apoptotic bodies, we wanted to specifically assay the rate of apoptosis in our cell line panel. Cell lines were transfected with either Bcl-3 or scrambled control siRNA for 48h before being lysed and assayed for caspase-3/7 activity using the Caspase-Glo 3/7 assay (Promega). This is a homogenous, luminescent assay that measures caspase-3 and -7 activities. These members of cysteine aspartic acid-specific protease (caspase) family plays key effector roles in apoptosis in mammalian cells (Thornberry and Lazebnik, 1998). The assay contains a pro-luminescent caspase-3/7 substrate with the tetrapeptide sequence DEVD, in a reagent optimised for caspase activity, luciferase activity and cell lysis. Cleavage of substrate releases aminoluciferin and results in the production of light and luminescence is proportional to the amount of caspase activity present.

Bcl-3 knockdown significantly increased caspase-3/7 activity in all TNBC cell lines (**Fig 3.11**). A 35% increase was observed in the MDA-MB-436, a 140% increase in the MDA-MB-231-Luc, a 110% increase in MDA-MB-231 and 160% increase in SUM149. There was no change in the caspase-3/7 activity of the non-malignant MCF10a cell line.

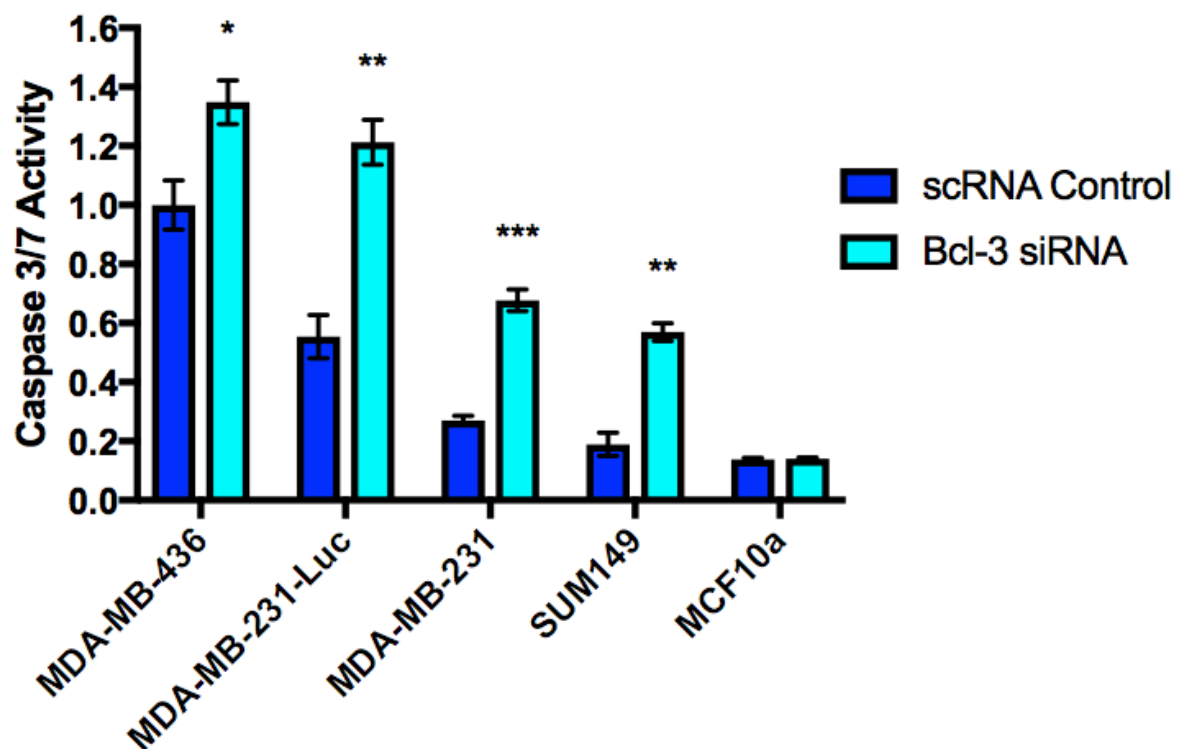


FIG. 3.11 BCL-3 SIRNA KNOCKDOWN INCREASED CASPASE-3/7 ACTIVITY IN TNBC CELL LINES
Cell lines were transfected with either Bcl-3 or scrambled control siRNA for 48h before being lysed and assayed for caspase-3/7 activity. Error bars represent \pm SEM of 3 independent experiments. (T-test, *= $p < 0.05$, **= $p < 0.01$, ***= $p < 0.001$)

3.9 Bcl-3 siRNA knockdown did not affect mammosphere numbers but significantly reduced mammosphere size in TNBC cell lines

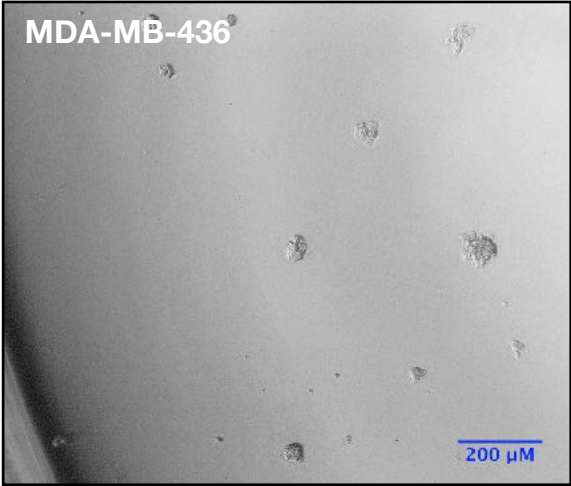
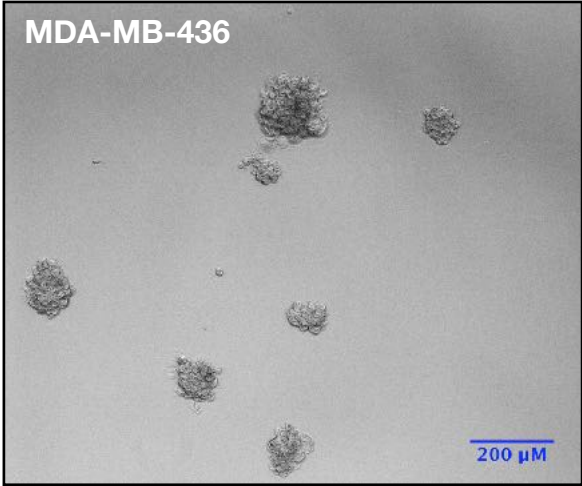
Recent research has focused on a small population of tumour cells termed cancer stem-like cells (CSCs) for their characteristics of self-renewal and are associated with tumour initiation and development. Breast cancer recurrence rates are close to 40% and evidence suggests this could be due to remaining CSCs following either incomplete elimination of primary tumour, or through their inherent resistance to adjuvant therapy. The gold standard for CSC self-renewal is in vivo transplantation. However a reliable and cost efficient in vitro assay involving the formation of anoikis resistant mammospheres is also able to demonstrate the presence of a stem-like cell population (Shaw et al., 2012). We wanted to investigate whether Bcl-3 played any roles in promoting CSC formation or stem-like properties as this would certainly contribute to the increased tumourigenicity associated with an oncogene.

Cell lines were transfected with either Bcl-3 or scrambled control siRNA for 48h before being disaggregated into single cells and plated into non-adherent mammosphere plates, cultured for 10 days and total mammosphere numbers and size quantified. Bcl-3 knockdown did not affect the number of spheres formed but for the MDA-MB-436, MDA-MB-231-Luc and MDA-MB-231 cell lines average sphere sizes were significantly lower (**Fig 3.12f**). We did not carry out a second passage as sphere formation numbers were not affected in the primary passage, suggesting Bcl-3 did not act upon mechanisms pertaining to propagation of a stem-like population.

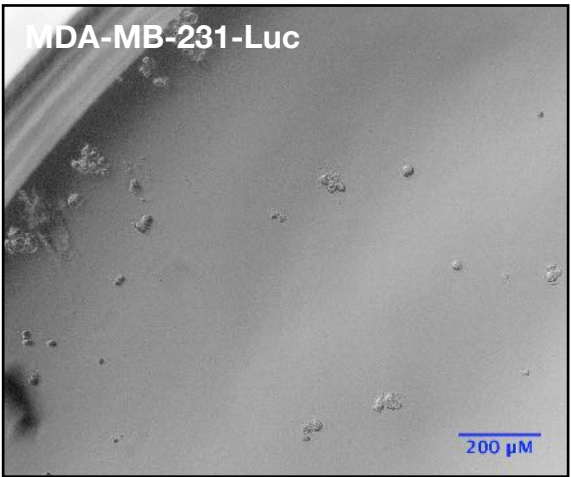
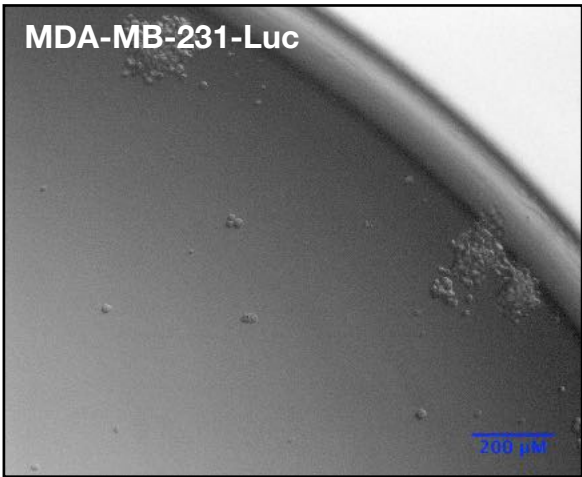
scRNA Control

Bcl-3 siRNA

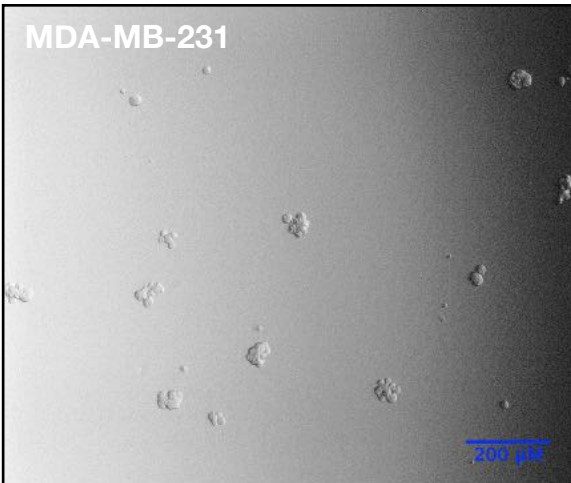
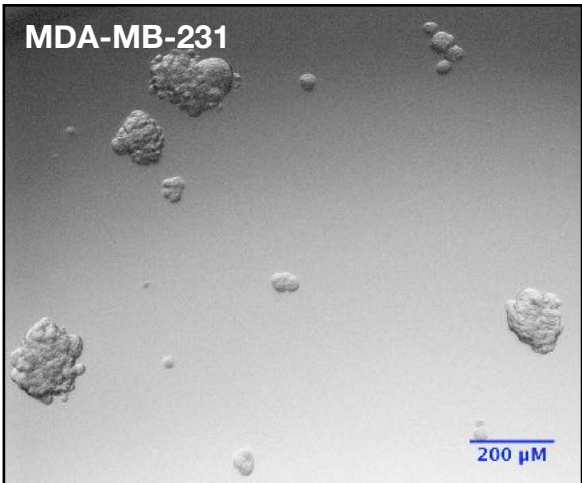
a



b



c



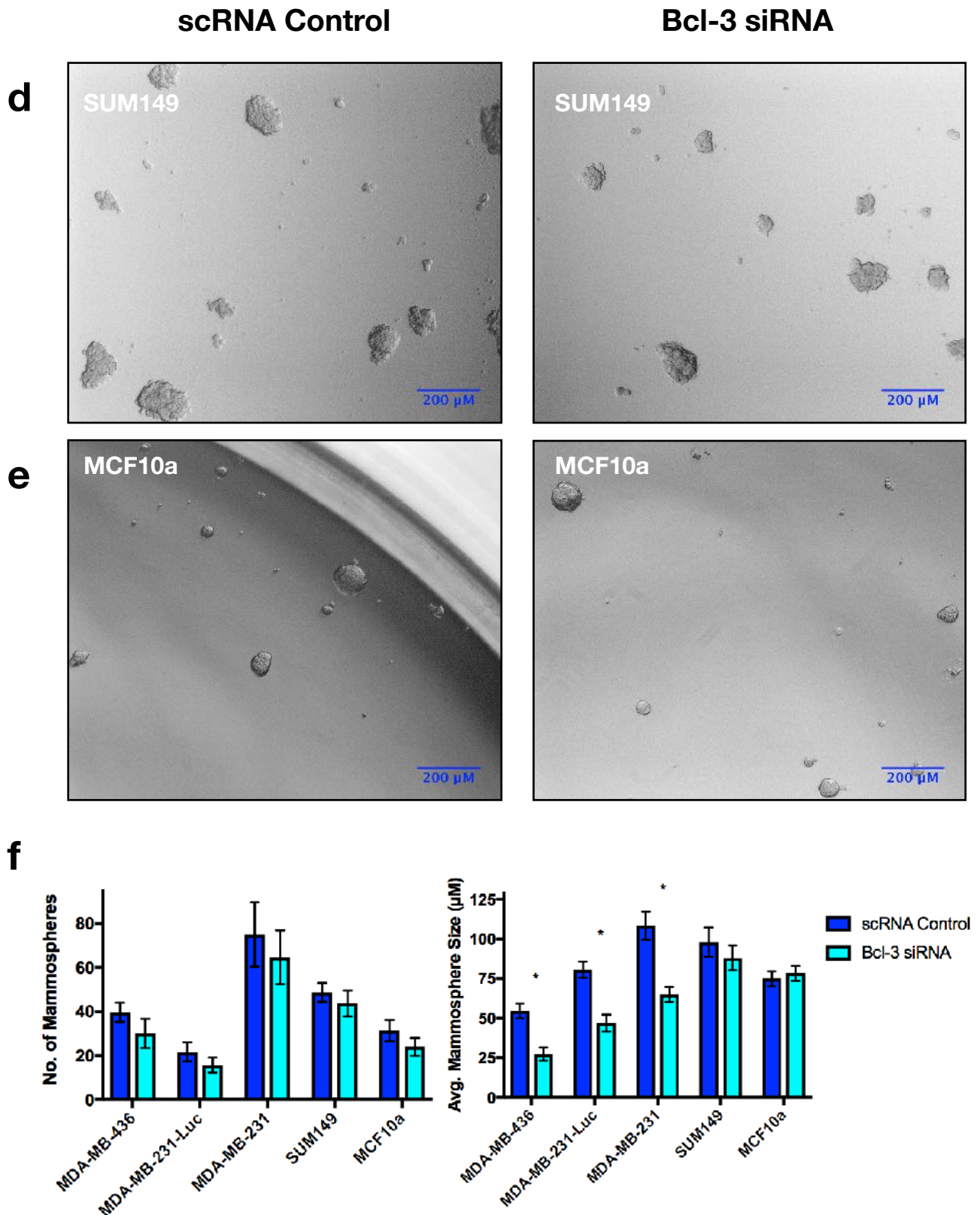


FIG. 3.12 BCL-3 SIRNA KNOCKDOWN DID NOT AFFECT MAMMOSPHERE NUMBERS BUT SIGNIFICANTLY REDUCED MAMMOSPHERE SIZE

Cell lines were transfected with either Bcl-3 or scrambled control siRNA for 48h before being disaggregated into single cells and plated into non-adherent mammosphere plates and cultured for 10 days. Representative bright-field microscopy images for **a.** MDA-MB-436 **b.** MDA-MB-231-Luc **c.** MDA-MB-231 **d.** SUM149 **e.** MCF10a cell lines. **f.** Total mammosphere numbers and average mammosphere sizes for each cell line. Error bars represent \pm SEM of 3 independent experiments. (T-test, *= $p < 0.05$, **= $p < 0.01$, ***= $p < 0.001$)

3.10 Bcl-3 siRNA knockdown significantly impaired clonogenic survival in TNBC cell lines but not the non-malignant MCF10a cell line

Colony formation or otherwise known as clonogenic assay is an in vitro cell survival assay based on the ability of a single cell to grow into a colony. Colonies are defined as containing at least 50 cells and this assay tests the ability of every cell in the plated population to undergo unlimited division. This assay is typically used to determine cell reproductive death following treatment with ionising radiation or cytotoxic agents as only a fraction of seeded cells retain the capacity to produce colonies (Franken et al., 2006). As Bcl-3 knockdown appeared to affect cellular proliferation and promoted apoptosis, it made sense to also investigate its effect on clonogenicity.

Cell lines were transfected with either Bcl-3 or scrambled control siRNA for 48h before being plated at low densities and cultured for 10 days. Colonies were then fixed with glutaraldehyde (6% v/v), stained with crystal violet (0.5% w/v), imaged using a plate scanner and colonies quantified. Bcl-3 knockdown in all TNBC cell lines resulted in impaired clonogenic potential as there were significant reductions in both total colony number as well as average colony size. There were no effects on clonogenicity in the non-malignant MCF10a cell line.

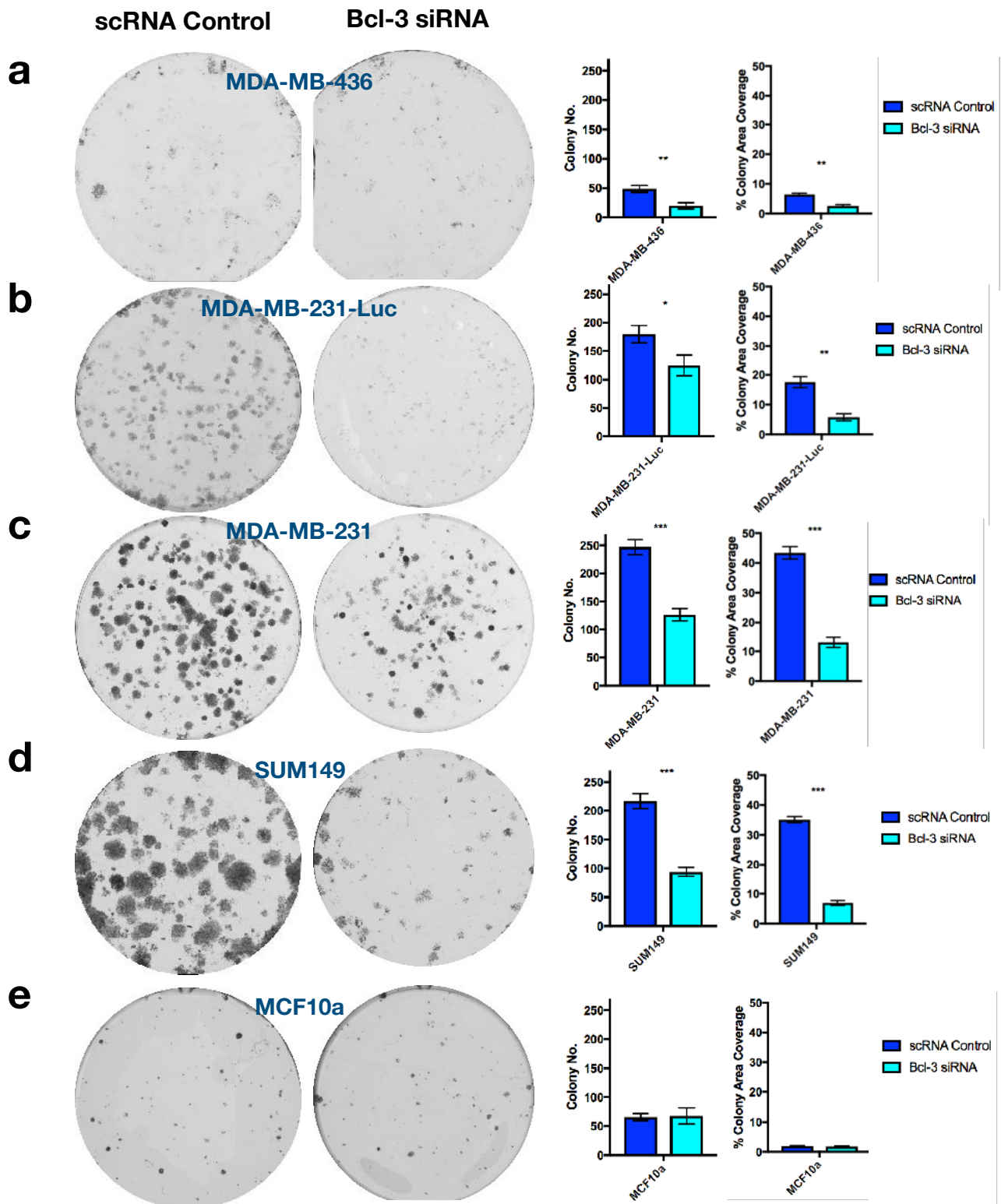


FIG. 3.13 BCL-3 SIRNA KNOCKDOWN SIGNIFICANTLY IMPAIRED CLONOGENIC SURVIVAL

Clonogenic potential was tested by transfecting cell lines with either Bcl-3 or scrambled control siRNA for 48h before being plated at low density in a colony formation assay and cultured for 10 days before being fixed and stained with crystal violet. Representative images, total colony number and average colony coverage for **a.** MDA-MB-436 **b.** MDA-MB-231-Luc **c.** MDA-MB-231 **d.** SUM149 **e.** MCF10a cell lines. Error bars represent \pm SEM of 3 independent experiments. (T-test, *= $p < 0.05$, **= $p < 0.01$, ***= $p < 0.001$)

3.11 Effects of Bcl-3 siRNA knockdown on cellular migration

Recently it has been shown elevated Bcl-3 expression was associated with higher metastatic potential and reduced metastasis-free survival. Bcl-3 was linked to increased cell motility through regulation by TGF- β signalling and stabilisation of SMAD3 (Chen et al., 2016). Bcl-3 was also demonstrated to regulate the metastasis of mouse breast cancer cells (Wakefield et al., 2013). In light of the significance of Bcl-3 surrounding metastasis, we wanted to investigate its roles in several different forms of cellular migration. Three different assays were used to assess collective, amoeboid-like and mesenchymal-like single cell migration.

3.11.1 Bcl-3 siRNA knockdown significantly inhibited collective migration in wound-healing assay in TNBC cell lines but not the non-malignant MCF10a cell line

The wound-healing assay is a simple, inexpensive, and one of the earliest developed methods to study directional collective in vitro cell migration. The basic steps involve creating a “wound” or scratch with a pipette tip in a confluent cell monolayer, capturing images at the beginning and at regular intervals during cell migration to close the wound, and comparing images to quantify the migration rate of cells (Rodriguez et al., 2005). Cell lines were transfected with either Bcl-3 or scrambled control siRNA for 48h before a scratch was made on a confluent monolayer using a 200 μ L pipette tip and cells cultured for a further 48h. Bright-field microscopy images were captured at 12h, 24h, 36h and 48h time-points and percentage wound closure was calculated using ImageJ.

Bcl-3 siRNA knockdown significantly reduced the collective migratory capacity of this cell line at all time-points and by the final 48h time-point the knockdown wound closure was ~15% less than that of the control (**Fig. 3.14c**). Bcl-3 siRNA knockdown significantly reduced the collective migratory capacity of this cell line at all time-points and by the final 48h time-point the knockdown wound closure was ~60% less than that of the control (**Fig. 3.15c**). Bcl-3 siRNA knockdown significantly reduced the collective migratory capacity of this cell line at all time-points and by the final 48h time-point the knockdown wound closure was ~50% less than that of the control (**Fig. 3.16c**). Bcl-3 siRNA knockdown significantly reduced the collective migratory capacity of this cell line at all time-points and by the final 48h time-point the knockdown wound closure was

~35% less than that of the control (**Fig. 3.17c**). Bcl-3 siRNA knockdown did not reduce the collective migratory capacity of this cell line at all time-points (**Fig. 3.18c**).

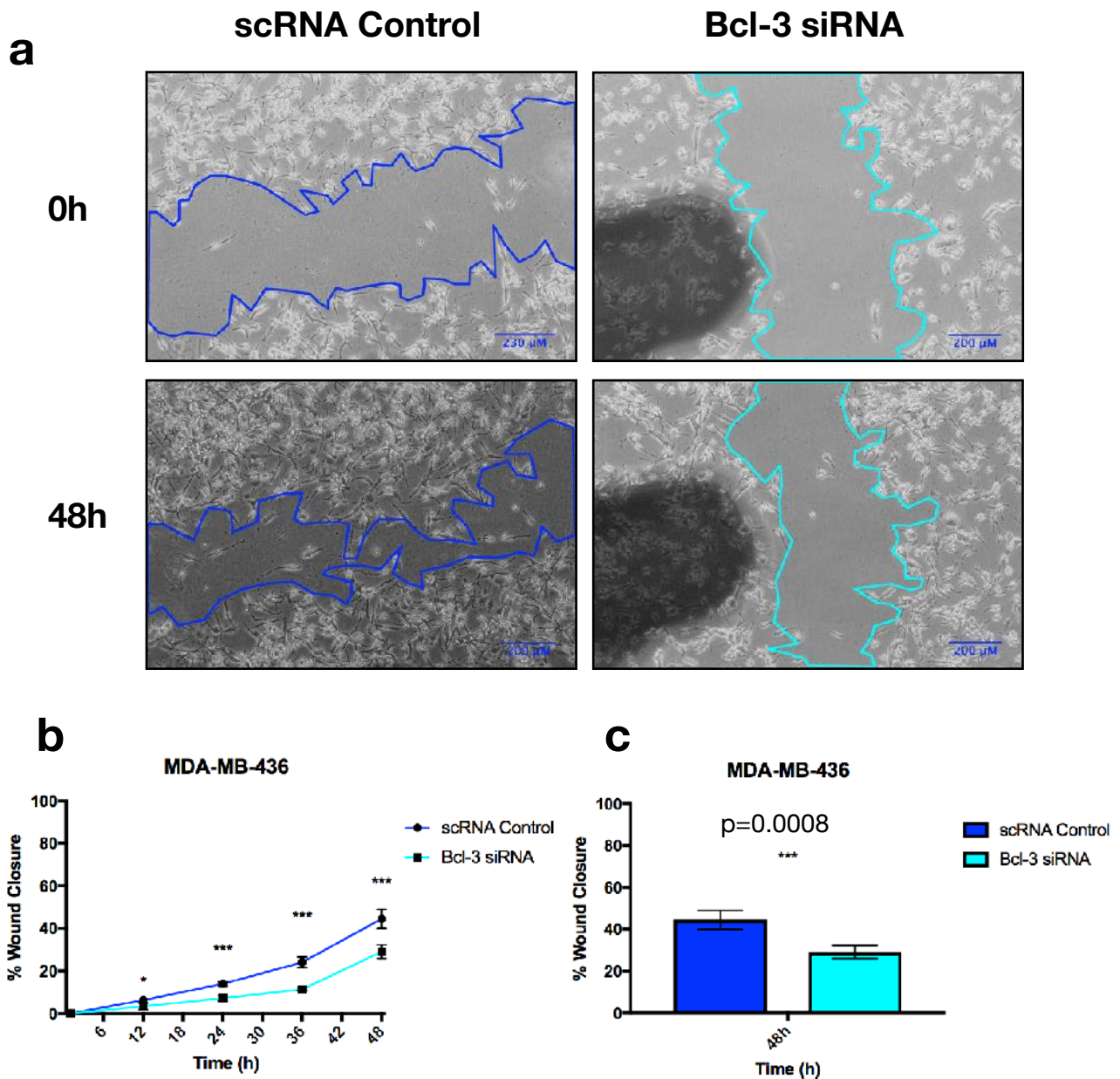


FIG. 3.14 BCL-3 SIRNA KNOCKDOWN SIGNIFICANTLY INHIBITED COLLECTIVE MIGRATION IN MDA-MB-436

The wound-healing assay was used to investigate collective migration in MDA-MB-436. The cell line was transfected with either Bcl-3 or scrambled control siRNA for 48h before a scratch was made on a confluent monolayer using a 200 μ L pipette tip and cells cultured for a further 48h with images being taken every 12h. **a.** Representative images showing the scratch at 0h and 48h. **b.** Total scratch area quantified using ImageJ and % wound closure calculated for 12h, 24h, 36h and 48h time-points. **c.** % wound closure at 48h time-point. Error bars represent \pm SEM of 3 independent experiments. (T-test, ***= $p < 0.001$)

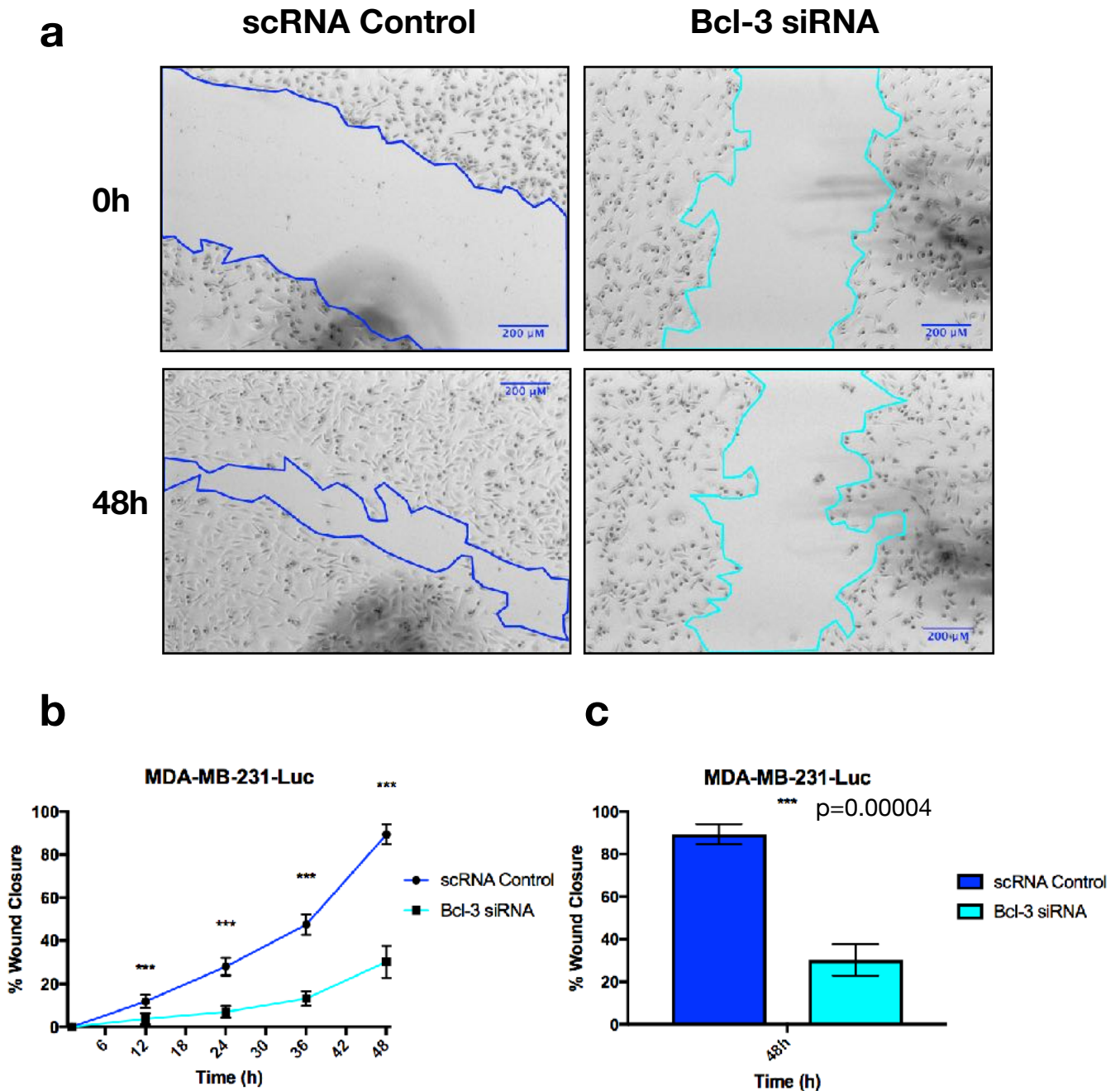


FIG. 3.15 BCL-3 SIRNA KNOCKDOWN SIGNIFICANTLY INHIBITED COLLECTIVE MIGRATION IN MDA-MB-231-LUC

The wound-healing assay was used to investigate collective migration in MDA-MB-231-Luc. The cell line was transfected with either Bcl-3 or scrambled control siRNA for 48h before a scratch was made on a confluent monolayer using a 200 μ L pipette tip and cells cultured for a further 48h with images being taken every 12h. **a.** Representative images showing the scratch at 0h and 48h. **b.** Total scratch area quantified using ImageJ and % wound closure calculated for 12h, 24h, 36h and 48h time-points. **c.** % wound closure at 48h time-point. Error bars represent \pm SEM of 3 independent experiments. (T-test, ***= $p < 0.001$)

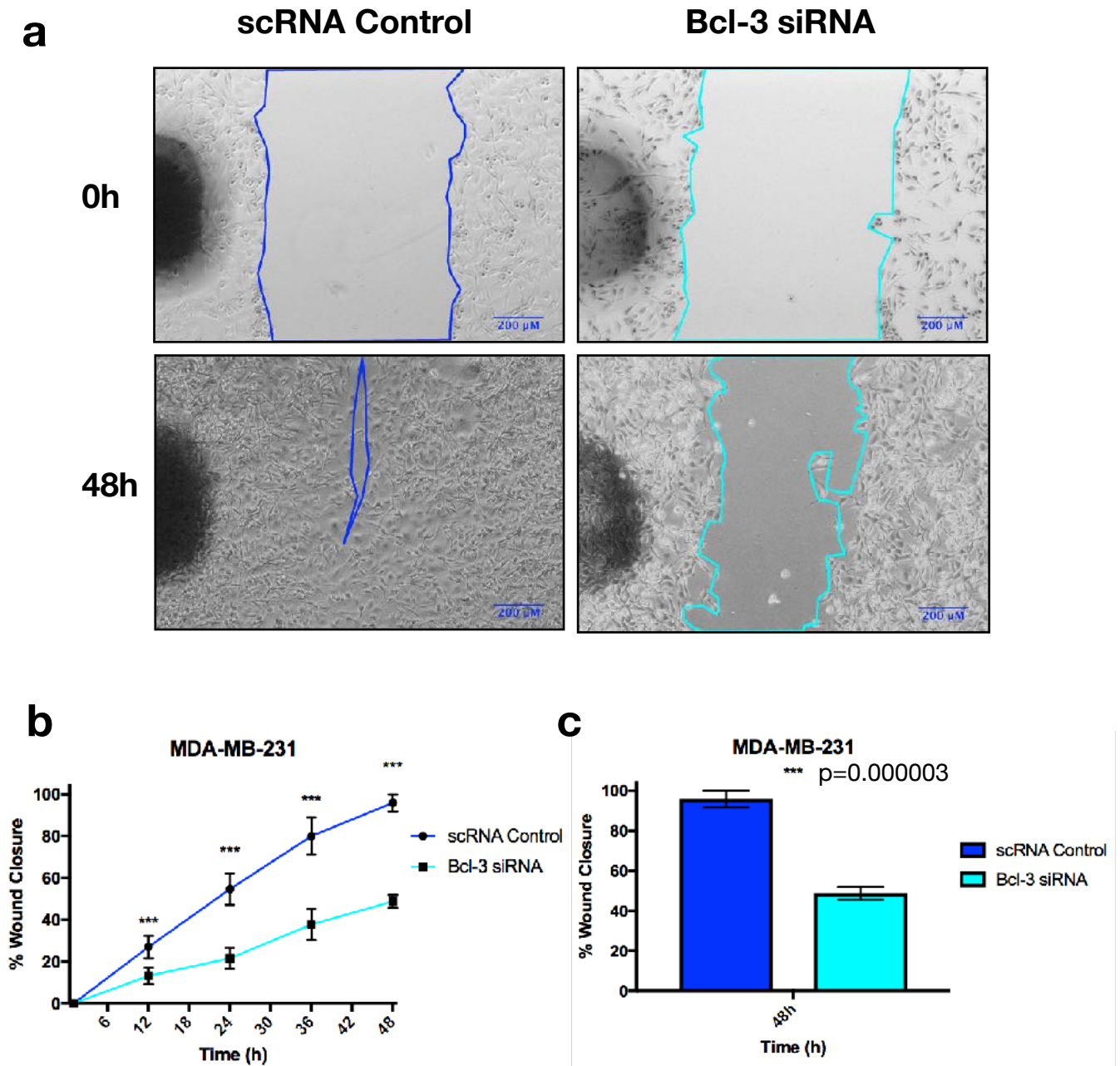


FIG. 3.16 BCL-3 SIRNA KNOCKDOWN SIGNIFICANTLY INHIBITED COLLECTIVE MIGRATION IN MDA-MB-231

The wound-healing assay was used to investigate collective migration in MDA-MB-231. The cell line was transfected with either Bcl-3 or scrambled control siRNA for 48h before a scratch was made on a confluent monolayer using a 200 μ L pipette tip and cells cultured for a further 48h with images being taken every 12h. **a.** Representative images showing the scratch at 0h and 48h. **b.** Total scratch area quantified using ImageJ and % wound closure calculated for 12h, 24h, 36h and 48h time-points. **c.** % wound closure at 48h time-point. Error bars represent \pm SEM of 3 independent experiments. (T-test, ***=p<0.001)

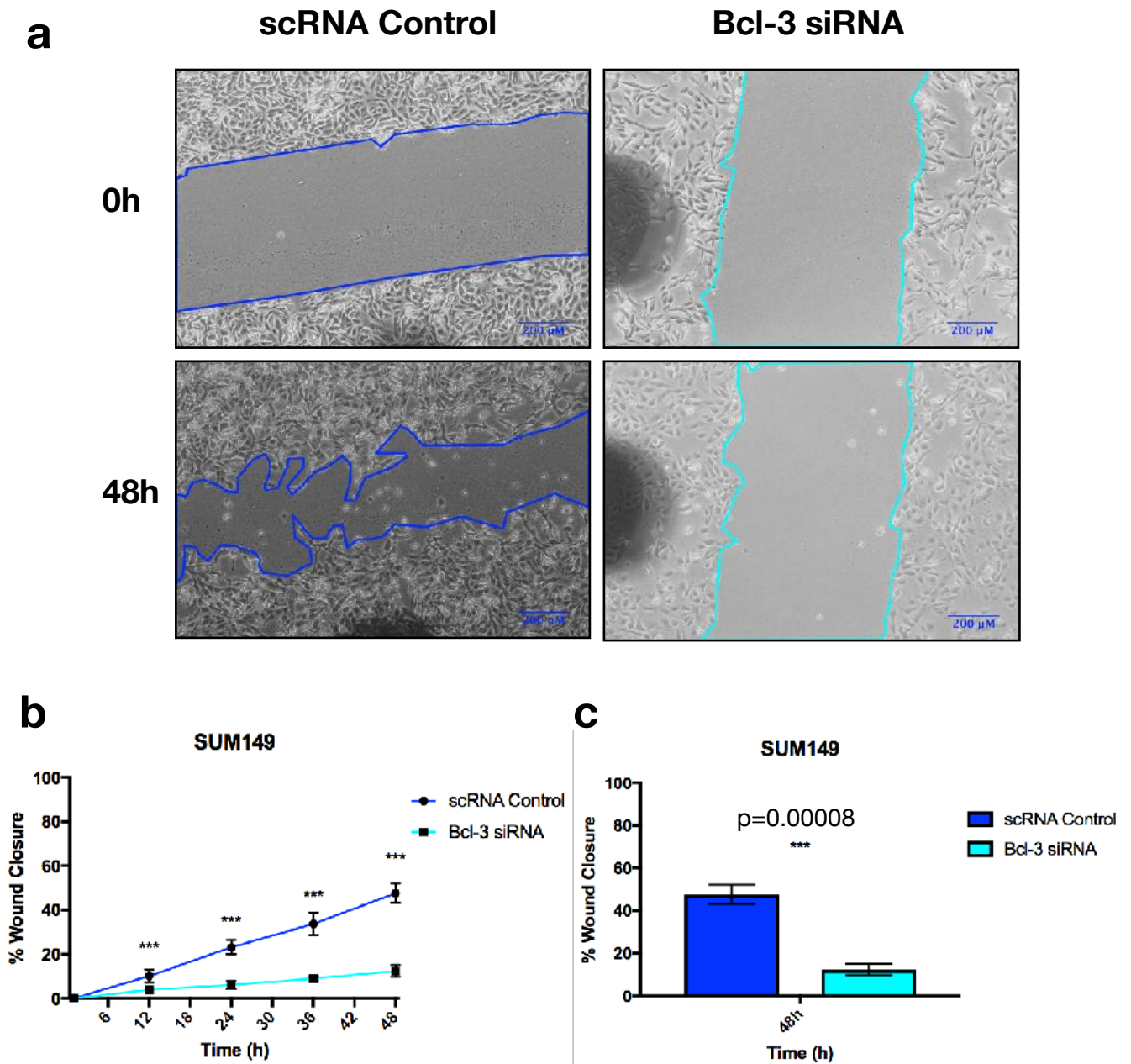


FIG. 3.17 BCL-3 SIRNA KNOCKDOWN SIGNIFICANTLY INHIBITED COLLECTIVE MIGRATION IN SUM149

The wound-healing assay was used to investigate collective migration in SUM149. The cell line was transfected with either Bcl-3 or scrambled control siRNA for 48h before a scratch was made on a confluent monolayer using a 200 μ L pipette tip and cells cultured for a further 48h with images being taken every 12h. **a.** Representative images showing the scratch at 0h and 48h. **b.** Total scratch area quantified using ImageJ and % wound closure calculated for 12h, 24h, 36h and 48h time-points. **c.** % wound closure at 48h time-point. Error bars represent \pm SEM of 3 independent experiments. (T-test, ***= $p < 0.001$)

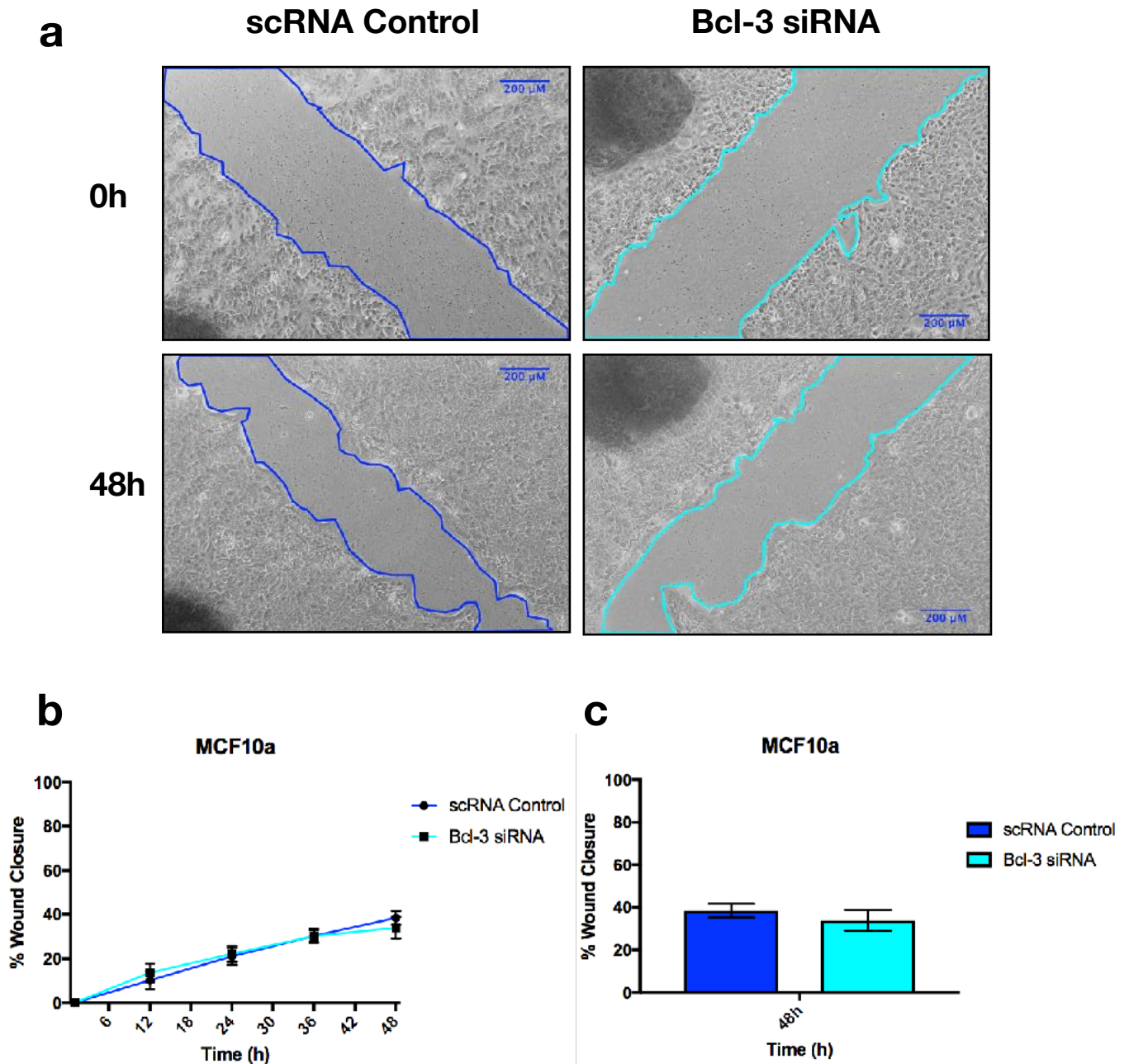


FIG. 3.18 BCL-3 SIRNA KNOCKDOWN DID NOT AFFECT COLLECTIVE MIGRATION IN MCF10A

The wound-healing assay was used to investigate collective migration in MCF10a. The cell line was transfected with either Bcl-3 or scrambled control siRNA for 48h before a scratch was made on a confluent monolayer using a 200 μ L pipette tip and cells cultured for a further 48h with images being taken every 12h. **a.** Representative images showing the scratch at 0h and 48h. **b.** Total scratch area quantified using ImageJ and % wound closure calculated for 12h, 24h, 36h and 48h time-points. **c.** % wound closure at 48h time-point. Error bars represent \pm SEM of 3 independent experiments.

3.11.2 Bcl-3 siRNA knockdown significantly inhibited amoeboid-like single cell migration in TNBC cell lines but not the non-malignant MCF10a cell line

The hallmark of metastatic cells is their ability to invade through the basement membrane and migrate to other parts of the body. Using the BD FluoroBlok system we were able to look at chemotaxis, movement in response to a chemical gradient and amoeboid-like cell motility. It consists of a 96-well insert plate with 8.0 micron pore size polyethylene terephthalate (PET) membranes. Subsequent quantification of cell migration is achieved by labelling with the fluorescent dye calcein AM and measuring fluorescence of migrated cells. Since the BD FluoroBlok membrane effectively blocks the passage of light from 490-900nm at >99% efficiency, fluorescently labelled cells that have not migrated past the membrane are not detected by a bottom-reading plate reader.

Cell lines were transfected with Bcl-3 or scrambled control siRNA for 48h before being plated into the top well of a FluoroBlok assay plate and left to migrate for 24h across a chemotactic gradient. Bcl-3 knockdown was able to significantly inhibit 20-30% of the amoeboid-like migratory capacity of TNBC cell lines but had no effect in the non-malignant MCF10a cell line (**Fig. 3.19**).

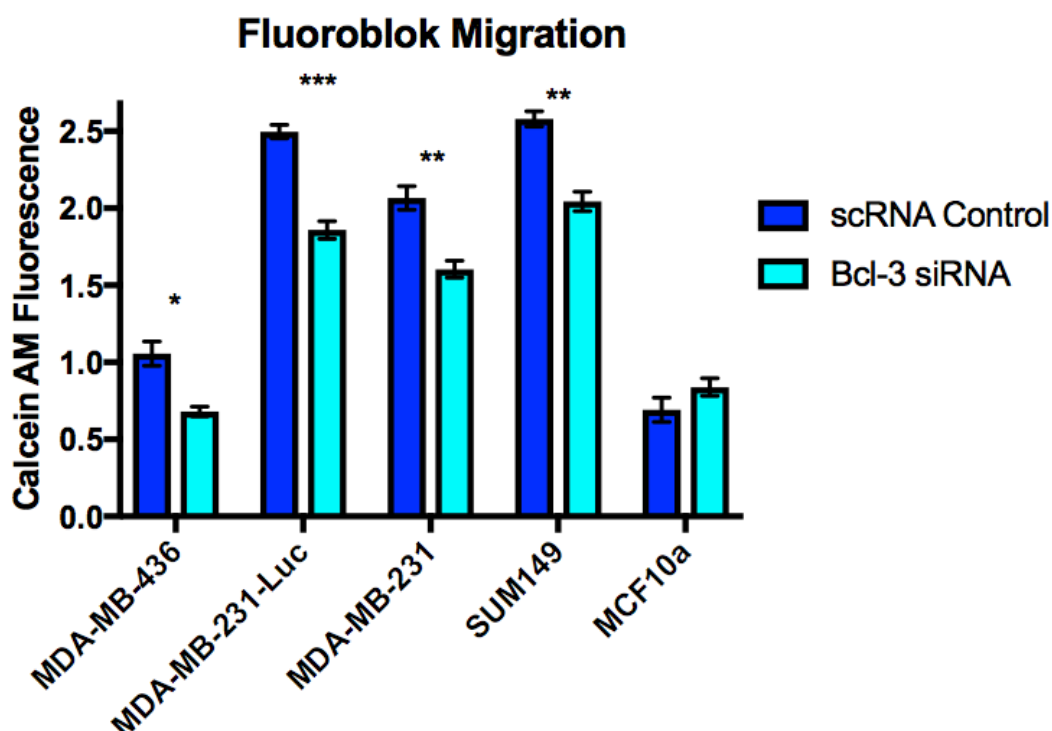


FIG. 3.19 BCL-3 SIRNA KNOCKDOWN SIGNIFICANTLY INHIBITED AMOEBOID-LIKE SINGLE CELL MIGRATION IN TNBC CELL LINES

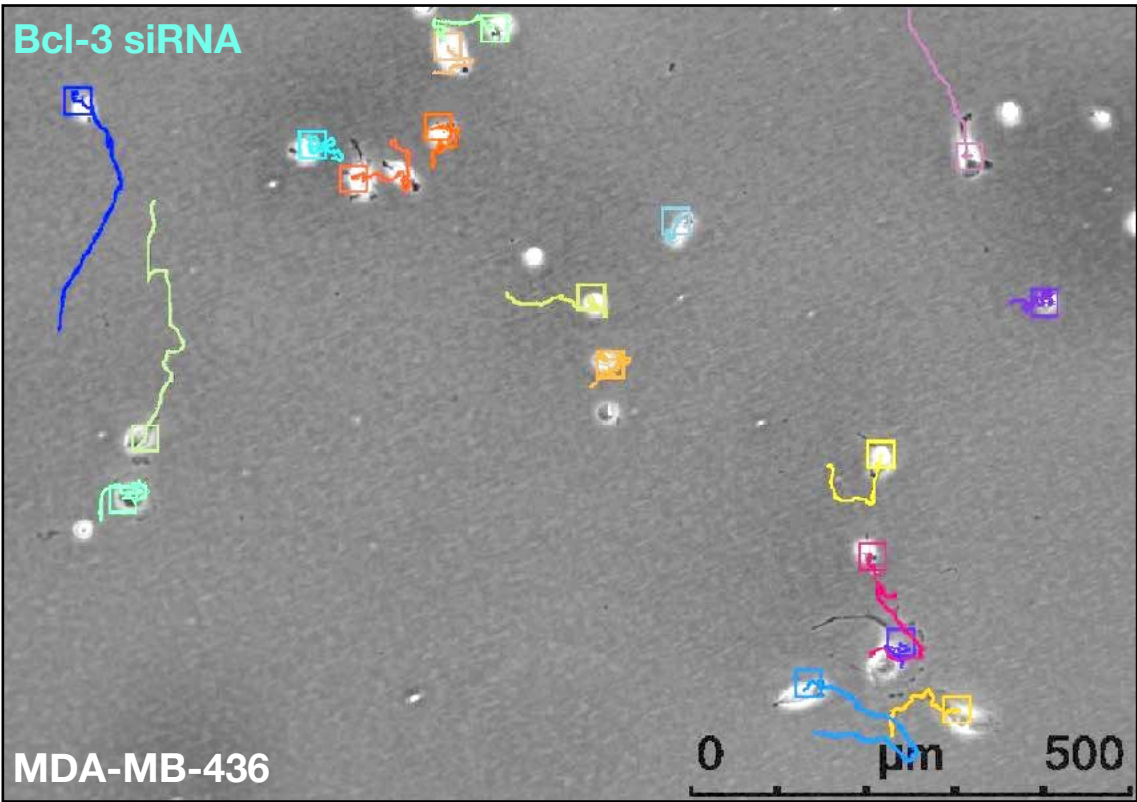
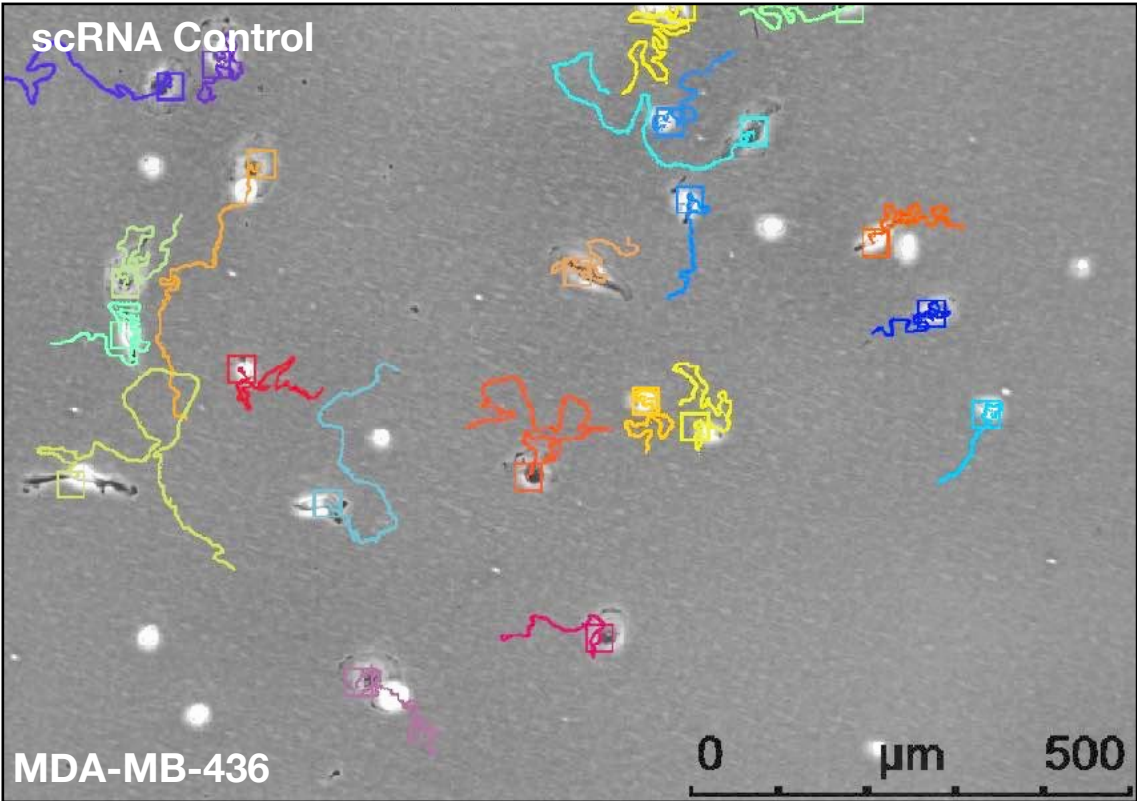
The FluoroBlok assay was used to investigate amoeboid-like migration of cell line panel. Cells were transfected with either Bcl-3 or scrambled control siRNA for 48h before being plated into the top well of a FluoroBlok assay plate and left to migrate for 24h across a chemotactic gradient. Cells were stained with calcein AM and fluorescence intensity at 500nm was quantified by a bottom-reading plate reader. Error bars represent \pm SEM of 3 independent experiments. (T-test, *= $p < 0.05$, **= $p < 0.01$, ***= $p < 0.001$)

3.11.3 Bcl-3 siRNA knockdown significantly inhibited mesenchymal-like single cell migration in TNBC cell lines but not the non-malignant MCF10a cell line

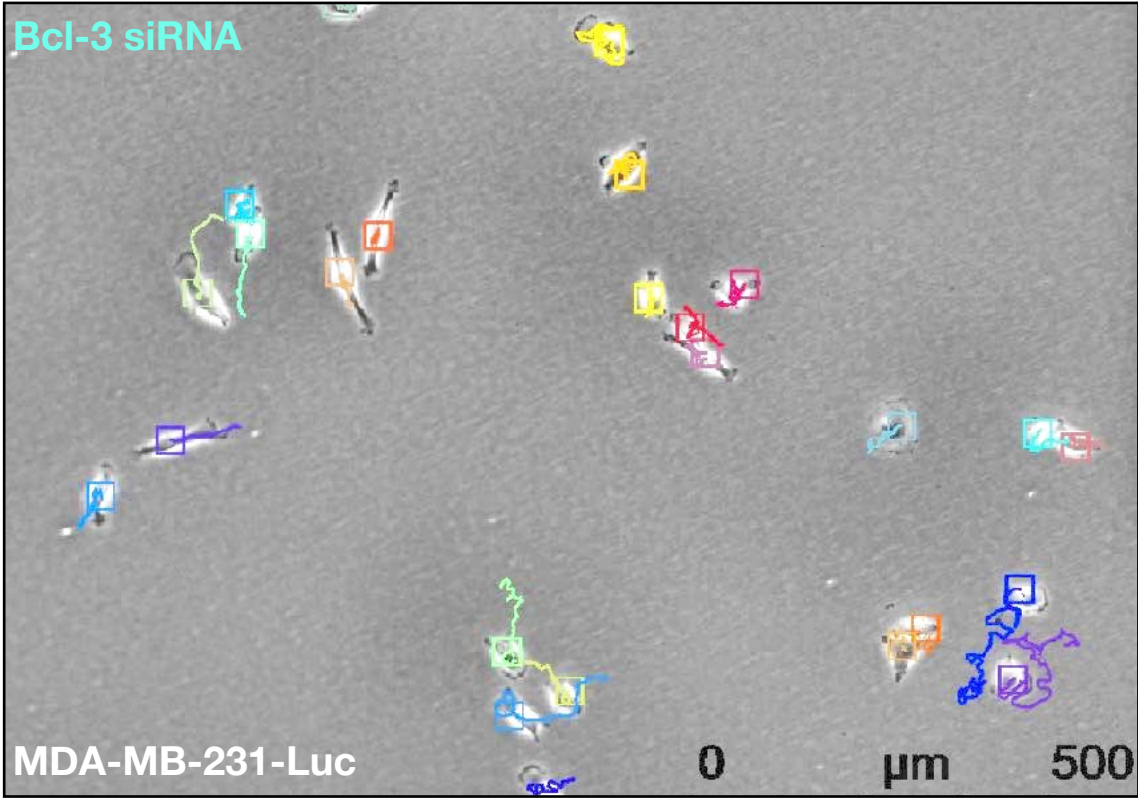
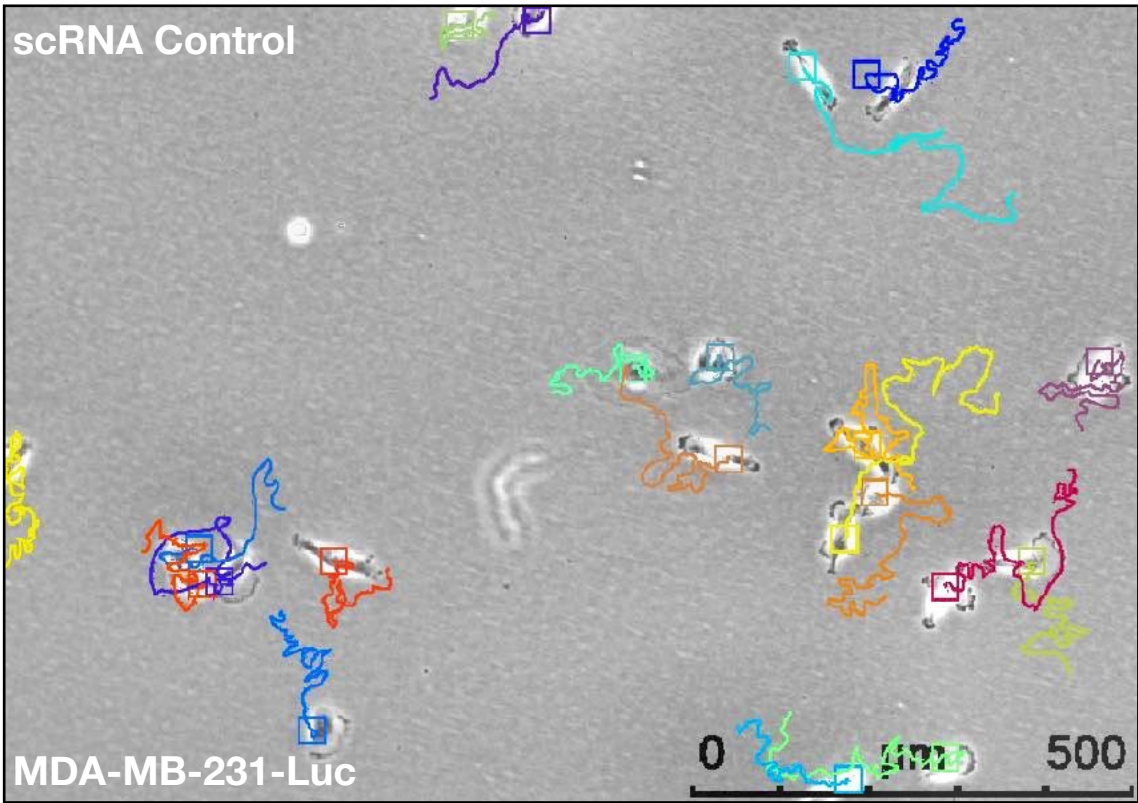
In metastatic cancer, cells must be able to invade across physiological barriers and migrate effectively in a single cell mesenchymal manner. By seeding cells at low densities we were able to quantify single cell migration using a time-lapse incubator chamber over the course of 12h with images being taken every 10 min. Cell lines were transfected with Bcl-3 or scrambled control siRNA for 48h, plated into 12-well plates and imaged.

Bcl-3 siRNA knockdown significantly reduced the average distance travelled by single cells over the course of 12h in MDA-MB-436 by ~70%, MDA-MB-231-Luc by ~45% and MDA-MB-231 by ~25% (**Fig. 3.20e**). Average distance travelled from origin at 0h was also reduced by a comparable amount over the course of 12h (**Fig. 3.20d**).

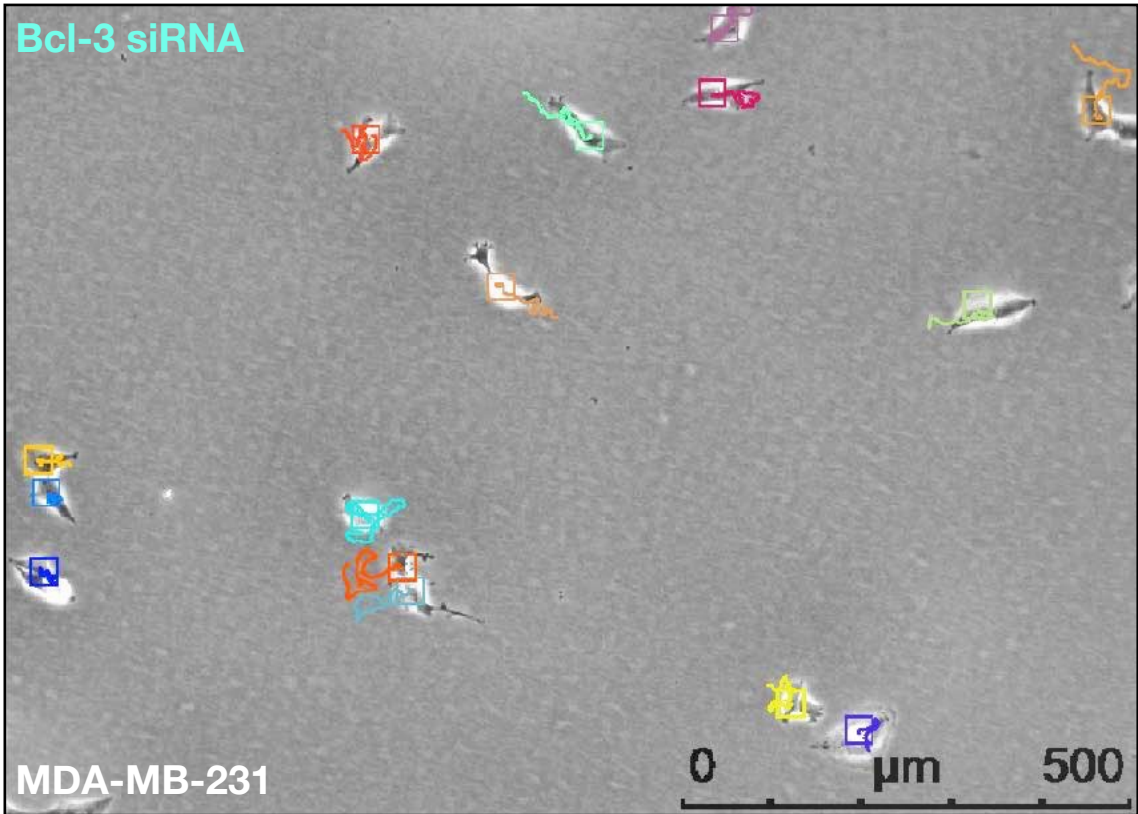
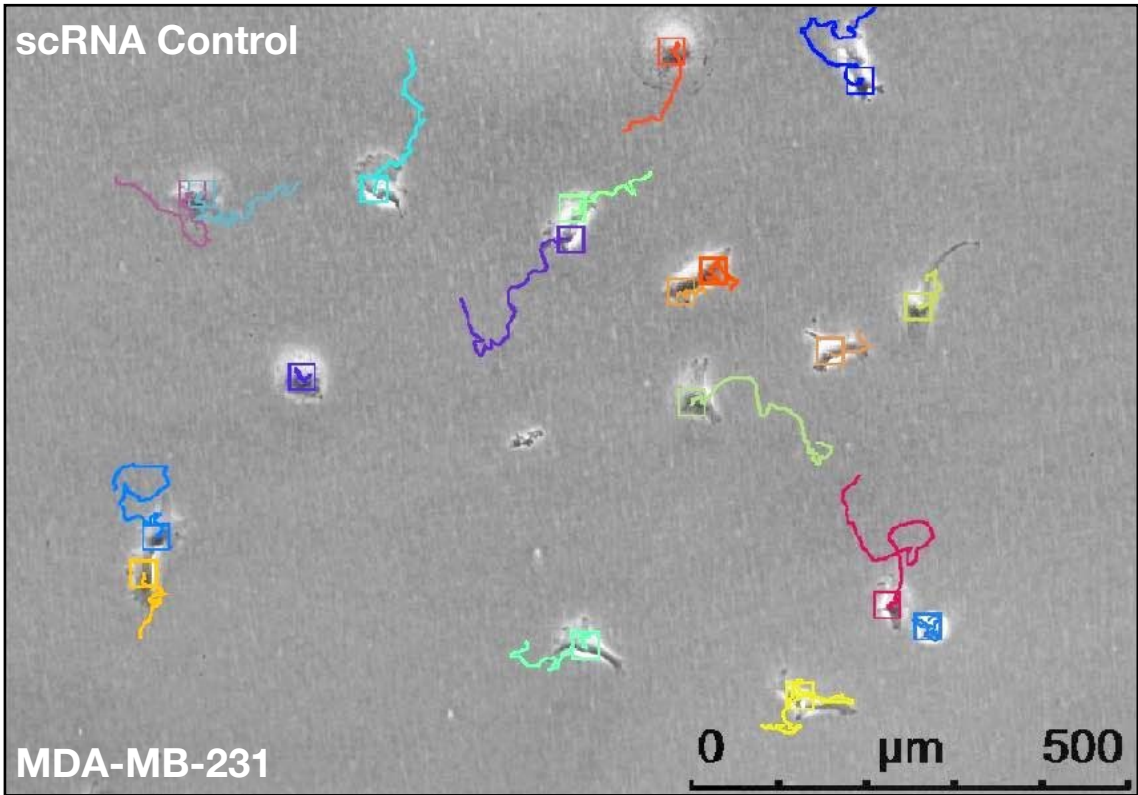
a



b



C



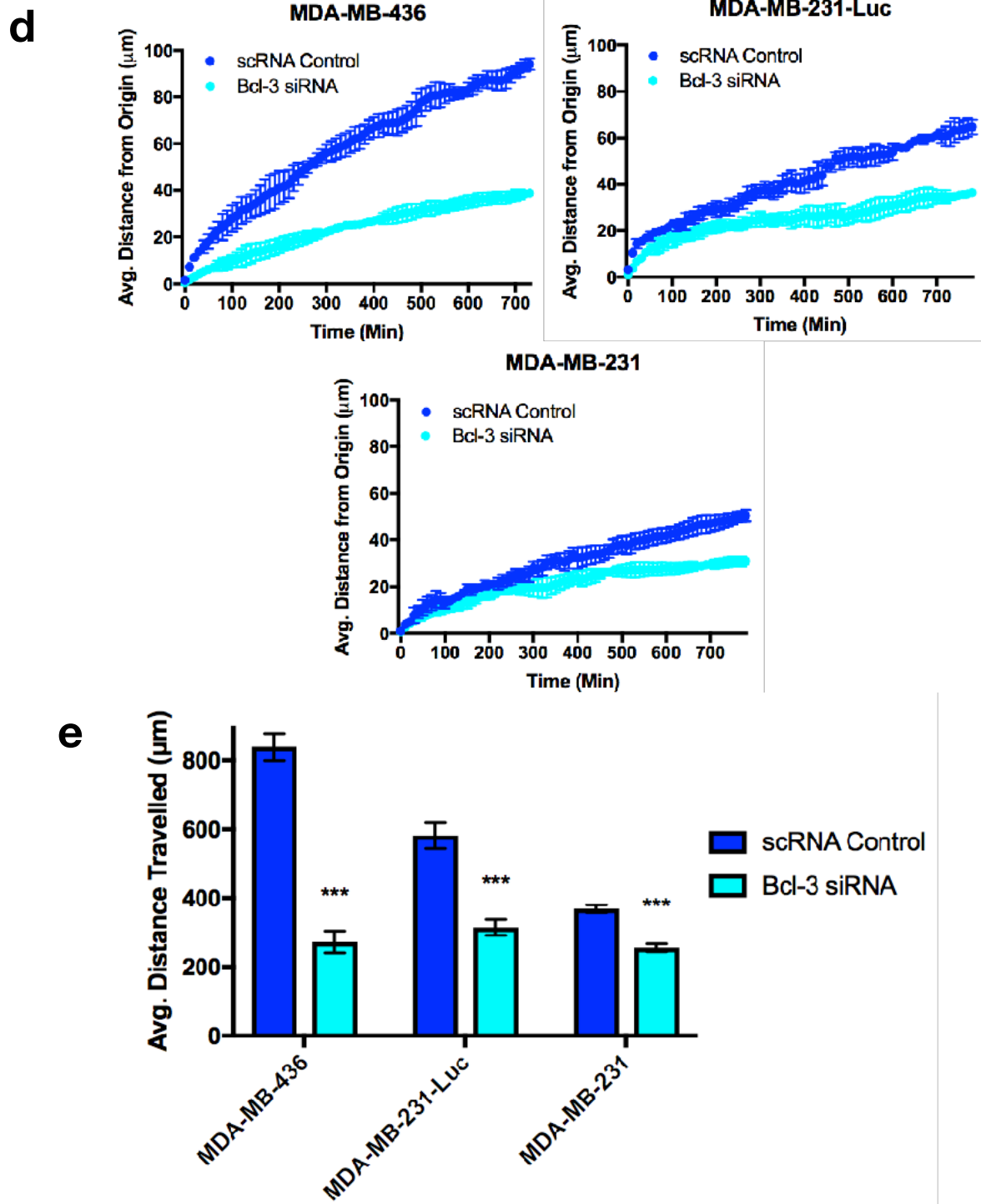


FIG. 3.20 BCL-3 SIRNA KNOCKDOWN SIGNIFICANTLY INHIBITED MESENCHYMAL-LIKE SINGLE CELL MIGRATION IN TNBC CELL LINES

The single cell migration assay was used to investigate the 2D motility of the cell line panel. Cells were transfected with either Bcl-3 or scrambled control siRNA for 48h before being plated low densities and single cell migration was quantified by tracking the motility path of each cell using a time-lapse incubator chamber over the course of 12h with images captured every 10 min. Representative images of motility paths of single cells over 12h for Bcl-3 siRNA knockdown and scrambled control in **a**. MDA-MB-436 **b**. MDA-MB-231-Luc **c**. MDA-MB-231. **d**. Average distance travelled away from origin for Bcl-3 knockdown and control cells. **e**. Average distance travelled after 12h for Bcl-3 knockdown and control cells. Error bars represent \pm SEM of 3 independent experiments. (T-test, *= $p < 0.05$, **= $p < 0.01$, ***= $p < 0.001$)

3.12 Bcl-3 siRNA knockdown significantly inhibited NFkB activity

The activity of NFkB signalling in cultured cells can be monitored using a luciferase NFkB reporter plasmid vector. This reporter contains a firefly luciferase gene under the control of multiple NFkB transcriptional responsive elements (TRE) located upstream of a minimal promoter. The nucleotide binding sequence for these NFkB TREs are GGGACTTCC.

Cells were transfected with either Bcl-3 or scrambled control siRNA for 24h before being further transfected with the luciferase NFkB reporter plasmid, LacZ control plasmid and cultured for another 24h. Cells were then lysed and NFkB activity measured as luminescence using a plate reader. NFkB activity was then normalised to LacZ luminescence to control for transfection efficiency. Bcl-3 knockdown significantly inhibited NFkB activity in all cell lines (**Fig. 3.21**).

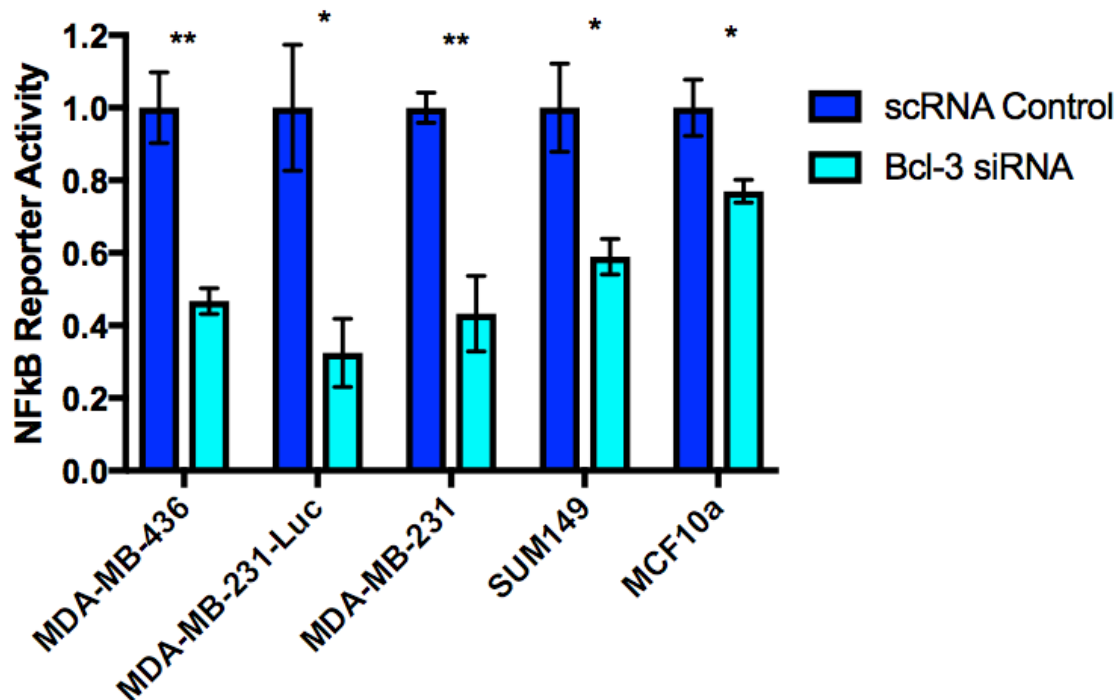


FIG. 3.21 BCL-3 SIRNA KNOCKDOWN SIGNIFICANTLY INHIBITED NFKB ACTIVITY

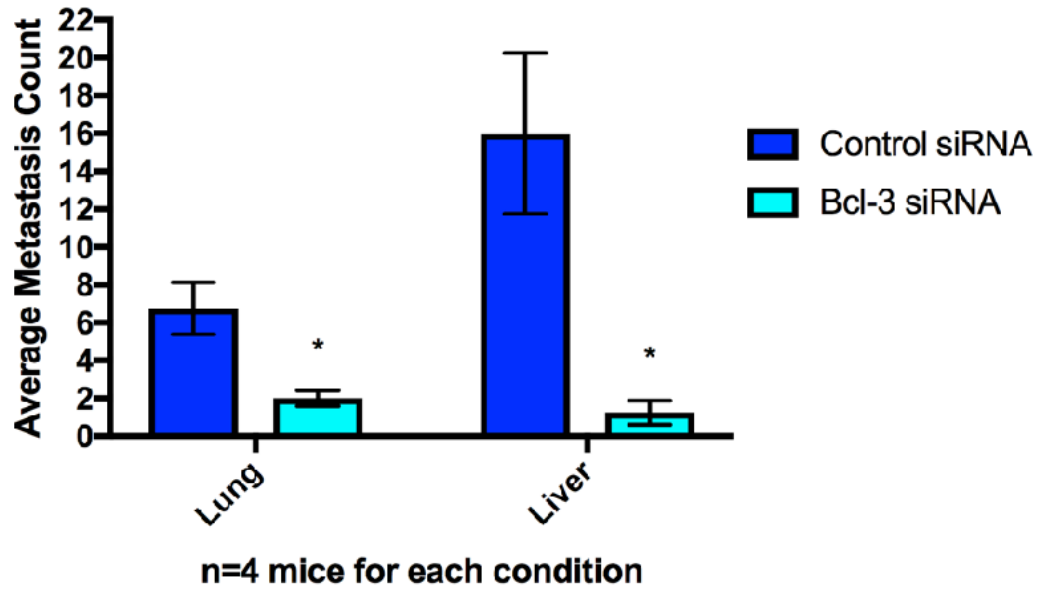
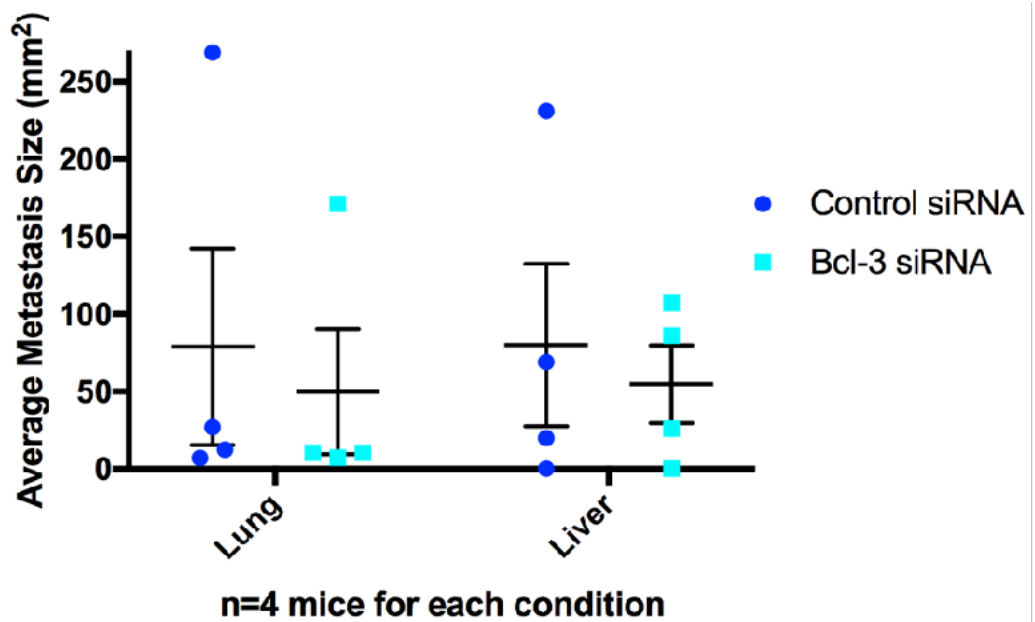
A luciferase NFkB reporter plasmid was used to quantify NFkB levels in the cell line panel. Cells were transfected with either Bcl-3 or scrambled control siRNA for 24h before being further transfected with the luciferase NFkB reporter plasmid, LacZ control plasmid and cultured for another 24h. Cells were then lysed and NFkB activity measured as luminescence using a plate reader. NFkB activity was then normalised to LacZ luminescence to control for transfection efficiency. Error bars represent \pm SEM of 3 independent experiments. (T-test, $*=p<0.05$, $**=p<0.01$, $***=p<0.001$)

3.13 Bcl-3 knockdown reduced metastatic occurrence in a murine tail vein xenograft metastasis model

Xenograft modelling has served as a robust method for researching genetic drivers of cancer and determining the potential efficacy of cancer therapies. The capacity to propagate human cancer cell lines and tissues in mice was first catalysed with the discovery of T-cell deficient athymic nude (nu/nu) mice and T- and B-cell deficient combined immunodeficient (scid/scid) mice (Flanagan, 1966; Bosma and Carroll, 1991). Since then many additional immunocompromised mouse models have become established such as the more recent NOD-scid IL2Rgamma(null) mice (otherwise known as NSG mice) (Shultz et al., 2005).

Direct injection of breast cancer cells via the tail vein (TV) vasculature provides a quick and easy method for studying the later stages of the metastatic process. This is especially the case for aggressive cell lines that proliferate rapidly and take long periods of time to metastasise, if at all from the orthotopic site. Although we skip some natural biological steps the primary tumour must take in order to produce distal metastases, it had been shown that TV tumours exhibited no gene profile differences to that of metastases generated by orthotopic tumours. Hence this is a relevant model for the study of breast cancer metastasis (Rashid et al., 2013).

MDA-MB-231 cells transfected with either Bcl-3 or scrambled control siRNA for 48h were injected intravenously via the lateral tail vein (2×10^5 cells in 100 μ l of RPMI media) in 6 week old female Hsd: Athymic Nude-Foxn 1^{nu} mice (Harlan Laboratories). Animals were culled and necropsy performed at 45 days post surgery. Xenograft tissue were fixed, embedded in paraffin blocks, serial sections cut and H&E slides generated for metastases quantification through histological analysis. (**Fig. 3.22c**) Bcl-3 knockdown significantly decreased the number of metastases identified in both the lungs and liver. (**Fig. 3.22a**) The average metastases size between the two conditions was not found to be significantly different (**Fig. 3.22b**). There were attempts to generate stably inducible shRNA Bcl-3 knockdown cell line clones, but these cell attempts were unsuccessful.

a**b**

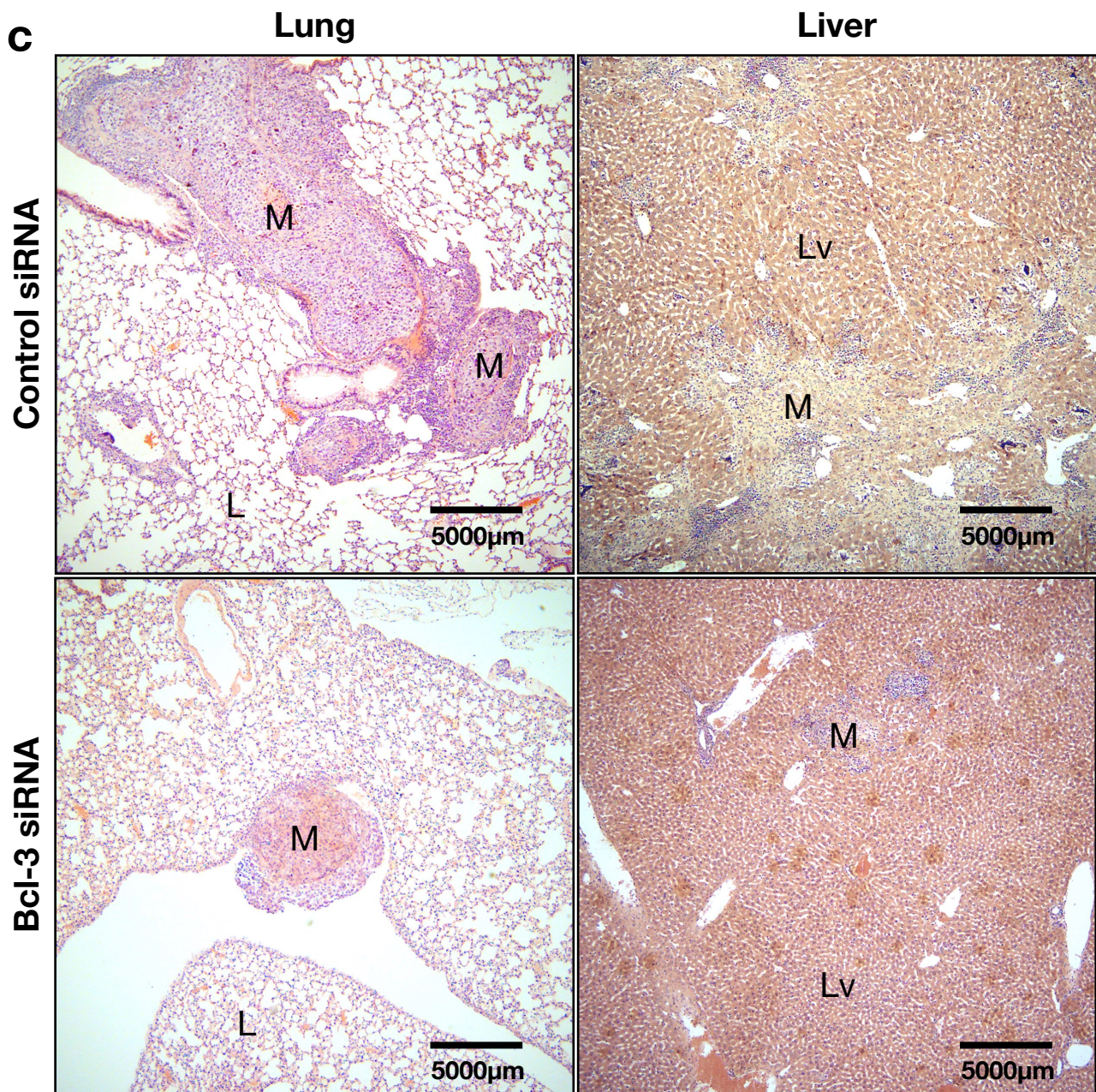


FIG. 3.22 BCL-3 KNOCKDOWN REDUCED METASTATIC OCCURRENCE IN A MURINE TAIL VEIN XENOGRRAFT METASTASIS MODEL

MDA-MB-231 cells transfected with either Bcl-3 or scrambled control siRNA for 48h were injected intravenously via the lateral tail vein (2×10^5 cells in $100 \mu\text{l}$) in 6 week old female Hsd: Athymic Nude-Foxn 1^{nu} mice (Harlan Laboratories). Animals were culled and necropsy performed at 45 days post surgery. Xenograft tissue were fixed, embedded in paraffin blocks, serial sections cut and H&E slides generated for metastases quantification through histological analysis. **a.** Average metastasis count and **b.** Average metastasis size in the lung and liver for control siRNA cohort ($n=4$) and Bcl-3 siRNA cohort ($n=4$). Error bars represent \pm SEM of 4 independent mice. (T-test, $*=p<0.05$, $**=p<0.01$, $***=p<0.001$) **c.** Haematoxylin and eosin (H&E) staining of mouse lung and liver sections with representative metastatic tumours. M = Metastasis, L = Normal lung parenchyma, Lv = Normal liver tissue.

3.14 Affymetrix DNA microarray analysis of Bcl-3 siRNA knockdown

We knew from our previous experiments that Bcl-3 knockdown led to a decrease in overall NFkB output. Building upon this knowledge, we carried out global gene expression profiling to further our understanding of Bcl-3 mediated transcriptional signalling. An Affymetrix DNA GeneChip microarray experiment was carried out using mRNA extracted from MDA-MD-231-Luc cells treated with either Bcl-3 or scrambled control siRNA for 48h. Experimental data were normalised and analysed using GeneSpring GX Pathway Architect software. Genes were filtered based on their corrected p-values and a statistical cut off of 0.05 was chosen. 4229 out of 43590 genes satisfied this cut off.

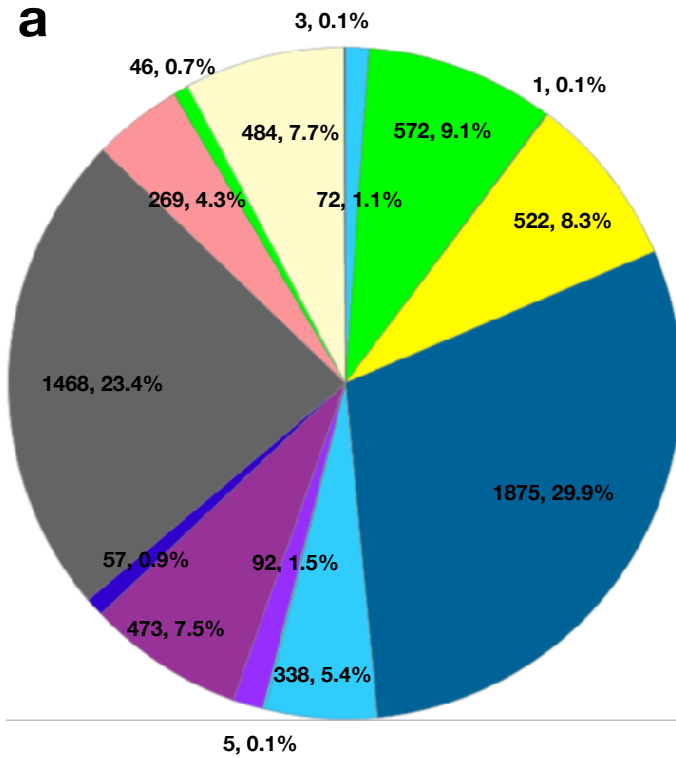
3.14.1 Gene function analysis of significantly up/down-regulated genes following Bcl-3 siRNA knockdown using the PANTHER classification system

The PANTHER (protein annotation through evolutionary relationship) classification system is designed as an online based platform for comprehensive analysis of gene function on genome-wide scale. The PANTHER system is composed of three functional modules. The core module is a large protein library that contains all protein-coding genes from 82 organisms, each annotated with ontology terms. The second is a pathways module with all pathways connected to individual proteins and linked to phylogenetic information and statistical models. The last module is a website tool suite that contains a collections of bioinformatic tools and software allowing users to visualise, analyse and interpret genome-wide experimental data (Mi et al., 2013).

Using the gene analysis tool that can be accessed directly from the PANTHER home page we can input a list of genes and quantitative data for analysis. The PANTHER data recognises a number of identifiers and in our case we used the gene symbol and log fold change data. The gene list can be analysed in a number of ways. The functional classification tool analyses input genes, stratifies them by biological processes, molecular functions, cellular components, pathways and displays them in either a gene list or pie chart. The statistical overrepresentation tool compares the input genes to a reference gene list and determines whether a particular ontology class or pathway of genes is over

or underrepresented. The statistical enrichment test uses the Mann-Whitney test to consider the numerical values associated with each gene to determine whether there are trends within an ontology class or pathway. It looks for significant coordinated effects across all the relevant ratios to test whether an up- or down-regulation is unlikely to be accounted for by random chance. PANTHER functional classification, statistical overrepresentation and statistical enrichment analyses were carried out on the 4229 significant gene hits and stratified by biological process, pathways, molecular function and cellular components. **(Fig.3.23)**

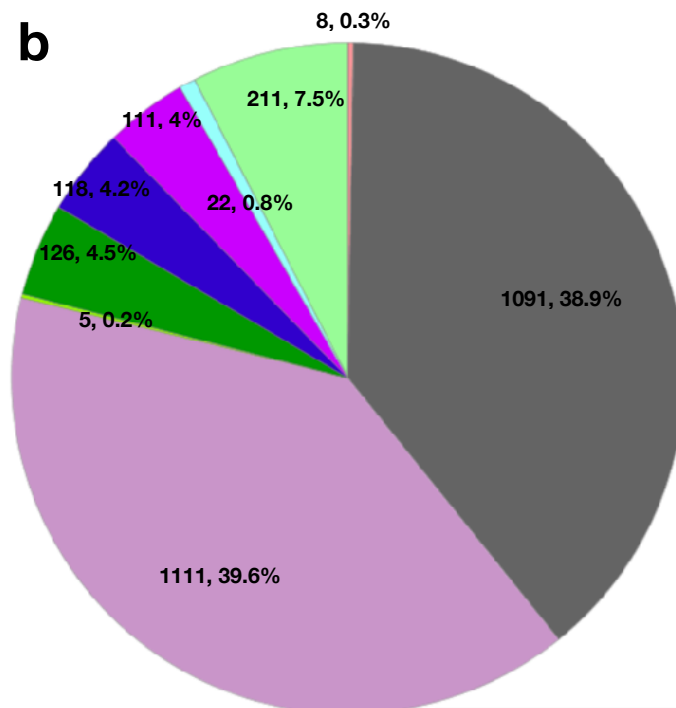
a



PANTHER Biological Processes

- [biological adhesion \(GO:0022610\)](#)
- [biological regulation \(GO:0065007\)](#)
- [cell killing \(GO:0001906\)](#)
- [cellular component organization or biogenesis \(GO:0071840\)](#)
- [cellular process \(GO:0009987\)](#)
- [developmental process \(GO:0032502\)](#)
- [growth \(GO:0040007\)](#)
- [immune system process \(GO:0002376\)](#)
- [localization \(GO:0051179\)](#)
- [locomotion \(GO:0040011\)](#)
- [metabolic process \(GO:0008152\)](#)
- [multicellular organismal process \(GO:0032501\)](#)
- [reproduction \(GO:0000003\)](#)
- [response to stimulus \(GO:0050896\)](#)
- [rhythmic process \(GO:0048511\)](#)

b



PANTHER Molecular Function

- [antioxidant activity \(GO:0016209\)](#)
- [binding \(GO:0005488\)](#)
- [catalytic activity \(GO:0003824\)](#)
- [channel regulator activity \(GO:0016247\)](#)
- [receptor activity \(GO:0004872\)](#)
- [signal transducer activity \(GO:0004871\)](#)
- [structural molecule activity \(GO:0005198\)](#)
- [translation regulator activity \(GO:0045182\)](#)
- [transporter activity \(GO:0005215\)](#)

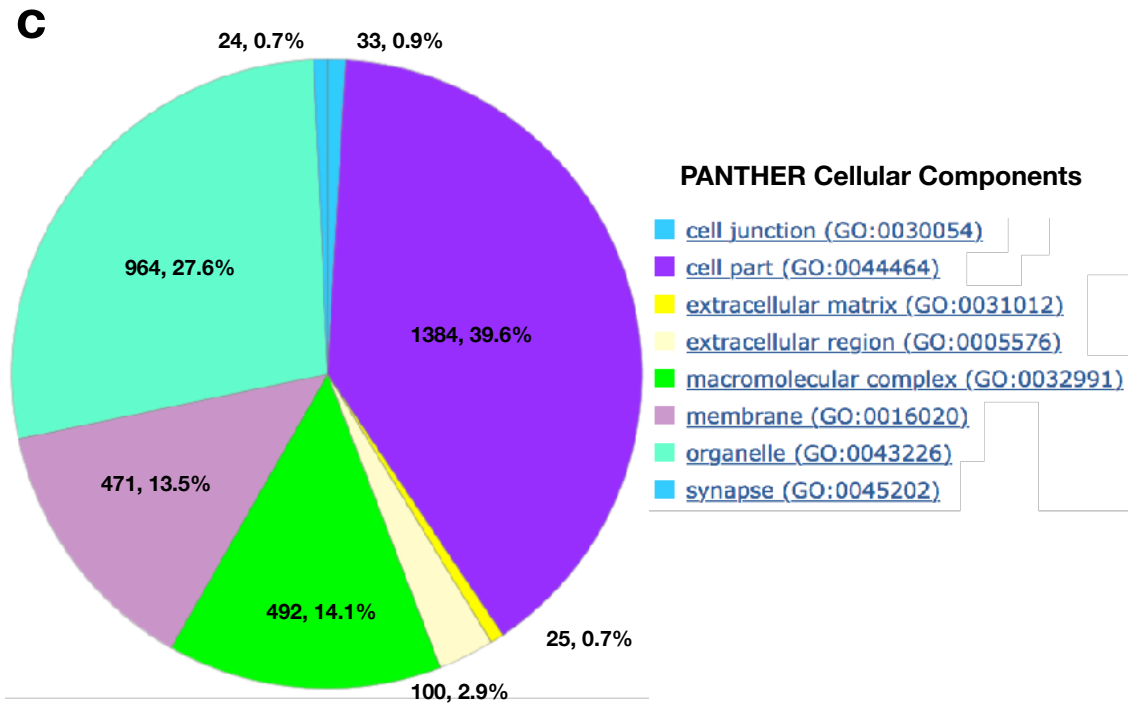


FIG. 3.23 PANTHER FUNCTIONAL CLASSIFICATION TOOL FOR BCL-3 SIRNA KNOCKDOWN

Genes found to be significantly up/down-regulated (p -value <0.05) in the MDA-MB-231-Luc, 48h Bcl-3 siRNA knockdown Affymetrix microarray experiment were used to perform PANTHER functional classification. Result of analyses are visualised as pie charts with information within each wedge detailing the number of genes and percent of genes against total hits for **a.** PANTHER biological processes **b.** PANTHER Molecular Function **c.** PANTHER Cellular Components.

PANTHER Biological Processes	H.Sapiens Ref List	Bcl3 siRNA	Expected	Fold Enrichment	FDR<0.05
cellular process	8247	1875	1657.47	1.13	1.79E-08
cell cycle	723	182	145.31	1.25	3.37E-02
cytokinesis	138	55	27.74	1.98	4.44E-04
apoptotic process	336	92	67.53	1.36	4.92E-02
metabolic process	5878	1468	1181.35	1.24	6.05E-16
nitrogen compound metabolic process	2524	614	507.27	1.21	1.17E-04
biosynthetic process	1745	452	350.71	1.29	1.70E-05
catabolic process	1176	302	236.35	1.28	1.13E-03
carbohydrate metabolic process	320	96	64.31	1.49	5.86E-03
protein glycosylation	105	36	21.1	1.71	4.27E-02
cellular component organisation or biogenesis	2099	522	421.85	1.24	9.93E-05
cellular component morphogenesis	423	119	85.01	1.4	8.74E-03
cytoskeleton organisation	404	119	81.2	1.47	2.88E-03
localisation	2012	473	404.37	1.17	8.66E-03
protein transport	736	186	147.92	1.26	2.93E-02
anion transport	241	70	48.44	1.45	3.70E-02
nucleobase-containing compound metabolic process	2797	662	562.14	1.18	5.87E-04
RNA metabolic process	1570	389	315.54	1.23	1.40E-03
transcription from RNA polymerase II promoter	774	206	155.56	1.32	2.86E-03
phosphate-containing compound metabolic process	1595	439	320.56	1.37	8.35E-08
intracellular signal transduction	1071	272	215.25	1.26	3.77E-03
immune system process	669	92	134.45	0.68	2.85E-03
complement activation	94	2	18.89	0.11	1.03E-04
B cell mediated immunity	94	1	18.89	0.05	2.04E-05
G-protein coupled receptor signaling pathway	456	44	91.65	0.48	6.40E-06
single-multicellular organism process	1665	268	334.63	0.80	2.81E-03
cell recognition	105	4	21.10	0.19	4.96E-04
system process	1020	150	205.00	0.73	1.63E-03

PANTHER Molecular Function	H.Sapiens Ref List	Bcl3 siRNA	Expected	Fold Enrichment	FDR<0.05
nucleic acid binding	1625	390	326.59	1.19	1.29E-02
transcription factor binding transcription factor activity	236	71	47.43	1.5	2.86E-02
binding	4911	1091	987.01	1.11	7.45E-03
cytoskeletal protein binding	320	101	64.31	1.57	1.85E-03
actin binding	139	48	27.94	1.72	1.95E-02
ligase activity	227	74	45.62	1.62	5.75E-03
ubiquitin-protein ligase activity	80	30	16.08	1.87	3.76E-02
transferase activity	1325	400	266.3	1.5	8.80E-11
kinase activity	625	210	125.61	1.67	1.46E-08
enzyme regulator activity	405	114	81.4	1.4	1.97E-02
catalytic activity	4217	1111	847.53	1.31	1.57E-16
hydrolase activity	1844	463	370.61	1.25	2.39E-04
pyrophosphatase activity	663	173	133.25	1.3	2.21E-02
phosphatase activity	201	74	40.4	1.83	3.91E-04
receptor activity	1128	126	226.70	0.56	3.27E-10
G-protein coupled receptor activity	309	33	62.10	0.53	3.38E-03
signal transducer activity	960	118	192.94	0.61	1.48E-06

PANTHER Cellular Component	H.Sapiens Ref List	Bcl3 siRNA	Expected	Fold Enrichment	FDR<0.05
organelle	3910	964	785.83	1.23	6.33E-09
endosome	132	45	26.53	1.7	1.86E-02
vacuole	196	64	39.39	1.62	7.64E-03
cytoskeleton	600	156	120.59	1.29	1.90E-02
actin cytoskeleton	203	63	40.8	1.54	1.97E-02
nucleus	1943	498	390.5	1.28	6.23E-06
nucleoplasm	392	115	78.78	1.46	3.80E-03
endoplasmic reticulum	412	113	82.8	1.36	1.85E-02
intracellular	5262	1335	1057.55	1.26	1.75E-16
cytoplasm	3171	817	637.3	1.28	2.23E-10
protein complex	1796	422	360.96	1.17	1.85E-02
extracellular region	673	100	135.26	0.74	1.75E-02

PANTHER Pathways	H.Sapiens Ref List	Bcl3 siRNA	Expected	Fold Enrichment	FDR<0.05
p53 pathway feedback loops 2	51	25	10.25	2.44	0.011
VEGF signalling pathway	68	33	13.67	2.41	0.004
p53 pathway	89	39	17.89	2.18	0.005
Apoptosis signalling pathway	120	52	24.12	2.16	0.001
TGF-beta signalling pathway	97	39	19.49	2	0.013
Integrin signalling pathway	190	67	38.19	1.75	0.005
Angiogenesis	173	60	34.77	1.73	0.012
Gonadotropin-releasing hormone receptor pathway	237	72	47.63	1.51	0.049

TAB. 3.1 PANTHER STATISTICAL OVERREPRESENTATION TEST FOR BCL-3 SIRNA KNOCKDOWN

Genes found to be significantly up/down-regulated (p -value<0.05) in the MDA-MB-231-Luc 48h Bcl-3 siRNA knockdown Affymetrix microarray experiment were used to perform the PANTHER Statistical Overrepresentation test. The Bcl-3 knockdown gene list was compared to a reference human gene list and whether a particular biological process, pathway, molecular function or cellular component is over or underrepresented is determined and fold enrichment calculated. Tables represent broad categories from the enriched or depleted biological processes, molecular functions, cellular components and pathways. Fisher's Exact test with FDR multiple test correction is used to determine statistical significance and only those with FDR of <0.05 is shown.

3.14.1 PANTHER statistical overrepresentation analysis

Numerous genes associated with biological processes were both significantly over and underrepresented following Bcl-3 siRNA knockdown (**Tab 3.1**). The enriched subsets include genes involved in cell cycle, cytokinesis, apoptosis, cellular metabolism, catabolism, protein glycosylation, cellular component biogenesis, cytoskeleton organisation, localisation of proteins and anions, transcription associated metabolism, phosphate-containing compound metabolism and intracellular signal transduction. The depleted subsets include genes involved in immune process such as complement activation and B-cell mediated immunity, G-protein coupled receptor signalling pathways, various system processes such as cell recognition.

Numerous genes associated with molecular functions were both significantly over and underrepresented following Bcl-3 siRNA knockdown (**Tab 3.1**). The enriched subsets include genes involved in transcription factor binding, actin and cytoskeletal protein binding, ubiquitin-protein ligase activity, transferase activity, catalytic activity including phosphatases and hydrolase. The depleted subsets include genes involved in the activity G-protein coupled receptors and signal transducers.

Numerous genes associated with cellular components were both significantly over and underrepresented following Bcl-3 siRNA knockdown (**Tab 3.1**). The enriched subsets include genes associated with the nucleoplasm, actin cytoskeleton, vacuoles, endosomes, endoplasmic reticulum, intracellular cytoplasm, and protein complexes. Genes associated with the extracellular region were depleted.

Numerous pathways were both significantly overrepresented following Bcl-3 siRNA knockdown (**Tab 3.1**). The enriched subsets include genes associated p53, apoptosis, VEGF signalling, TGF-beta signalling, integrin signalling, angiogenesis and gonadotropin-releasing hormone receptor pathways.

3.14.2 PANTHER statistical enrichment analysis

Following statistical enrichment analysis the following genes associated with biological processes were found to be significantly down-regulated: multicellular

organismal processes, system development, signal transduction and cell communications. (**Tab 3.2**)

Following statistical enrichment analysis the following genes associated with molecular functions were found to be significantly down-regulated, activity of structural molecules, motor activity and cytoskeletal protein binding. (**Tab 3.2**)

Following statistical enrichment analysis genes associated with the cytoskeleton were found to be significantly down-regulated. (**Tab 3.2**)

Following statistical enrichment analysis genes associated with apoptosis signalling, purine metabolism and activin beta signalling pathways were significantly up-regulated. Genes associated with pyridoxal-5-phosphate biosynthesis, 5-HT degradation and cytoskeletal regulation by Rho GTPase pathways were significantly down-regulated. (**Tab 3.2**)

PANTHER Biological Process	#	+/-	P value
multicellular organismal process (GO:0032501)	269	-	0.004
system development (GO:0048731)	93	-	0.024
signal transduction (GO:0007165)	482	-	0.011
cell communication (GO:0007154)	555	-	0.023

PANTHER Molecular Function	#	+/-	P value
structural molecule activity (GO:0005198)	111	-	0.013
motor activity (GO:0003774)	26	-	0.002
cytoskeletal protein binding (GO:0008092)	101	-	0.001

PANTHER Cell Component	#	+/-	P value
cytoskeleton (GO:0005856)	156	-	0.004

PANTHER Pathway	#	+/-	P value
Apoptosis signalling pathway (P00006)	52	+	0.006
Purine metabolism (P02769)	3	+	0.008
Pyridoxal-5-phosphate biosynthesis (P02759)	2	-	0.032
Activin beta signalling pathway (P06210)	2	+	0.039
5-Hydroxytryptamine degradation (P04372)	8	-	0.043
Cytoskeletal regulation by Rho GTPase (P00016)	27	-	0.045

TAB. 3.2 PANTHER STATISTICAL ENRICHMENT TEST FOR BCL-3 SIRNA KNOCKDOWN

Genes found to be significantly up/down-regulated (p -value <0.05) in the MDA-MB-231-Luc 48h Bcl-3 siRNA knockdown Affymetrix microarray experiment were used to perform the PANTHER Statistical Enrichment test. This test uses the Mann-Whitney test to consider the Log fold-change associated with each gene to determine whether there are trends within an ontology class or pathway. It looks for significant coordinated effects across all the relevant ratios to test whether an up- or down-regulation is unlikely to be accounted for by random chance. Tables represent classes from enriched biological processes, molecular functions, cellular components and pathways with a p -value of <0.05 .

3.15 Discussion

Bcl-3 is generally accepted to be a putative proto-oncogene and its up-regulation has been identified and associated with many solid tumours, including breast cancer. We tested four triple negative breast cancer (TNBC) cell lines and found they all expressed significantly higher Bcl-3 than a nonmalignant human mammary epithelial cell line, MCF10a (**Fig. 3.1**). We wanted to investigate how Bcl-3 knockdown affected the cellular characteristics of these TNBCs and whether it influenced oncogenic or metastatic potential. We optimised conditions to robustly suppress its expression using siRNA for at least 96h. There were no observable effects on bulk monolayer cellular morphology over this time course (**Fig. 3.2**).

3.15.1 Bcl-3 regulated cellular proliferation through modulation of the cell cycle

Following Bcl-3 knockdown we observed changes in a number of cellular phenotypic outputs. There were significant reductions in cell population turnover and we saw reduced growth rates in all four TNBC cell lines following ectopic suppression of Bcl-3. Despite this predicted effect on proliferation when Bcl-3 was ectopically suppressed, interestingly the baseline growth or proliferation rates for TNBCs inversely correlated with endogenous Bcl-3 levels (**Fig. 3.3f**). MDA-MB-436s expressed the highest Bcl-3 yet had the slowest growth, while MDA-MB-231s and SUM149s had comparatively low Bcl-3, but proliferated almost 2.5-fold faster over the course of 96h. If Bcl-3 was a classically dominant oncogene, simplistically we would expect to correlate higher expression with increased growth rates. However these results suggest there are other dominant factors contributing to overall cell growth. Grow rates of the nonmalignant MCF10a cell line was not affected by Bcl-3 knockdown.

Ki67 is a commonly used proliferative marker and is present during all active cell cycle phases. Phospho-histone H3 (ser10) is a cell marker specific for mitosis. Bcl-3 knockdown was able to significantly reduce expression of both Ki67 and pHH3 in all four TNBC cell lines, but not in MCF10a (**Fig. 3.4f + 3.5f**). This supports the notion that Bcl-3 influences proliferation by modulating aspects of the cell cycle and helps explain the growth suppression effects previously seen. However if we compared Ki67 and pHH3 expression with relative growth rate between the controls, there was a seemingly inverse

correlation. MDA-MB-436s expressed the highest Ki67 and pHH3 but exhibited the slowest growth, while MDA-MB-231s grew the fastest but had the lowest comparative Ki67 and pHH3. Nevertheless endogenous Ki67 and pHH3 expression of these TNBCs did positively correlate with endogenous Bcl-3 levels. Similarly to Bcl-3, higher fractions of Ki67-positive cells can often correlate with a worsening clinical course of breast cancer and serve as a prognostic indicator for survival and tumour recurrence (Yerushalmi et al., 2010). pHH3 expression has also been reported to be of prognostic significance in many breast cancers (Skaland et al., 2007). These results supported the hypothesis of Bcl-3 acting as an oncogene as we were able to pair its higher expression with increased proliferative markers. However the underlying mechanism for the inverse relationship seen between proliferation and overall cell growth is addressed further below.

By staining and measuring cellular DNA content, we were able to determine snapshots of cell cycle stages and discriminate between cell fractions in the G0/G1, S and G2/M phases. Following Bcl-3 knockdown, all TNBC cell lines apart from MDA-MB-436 saw reduced in S and G2/M phases and increased G0/G1 phases. This suggested the slow down in proliferation previously seen is likely due to the shift in balance between the increased G0/G1 resting cell fraction and decreased S and G2/M dividing cell fractions. In MDA-MB-436, we observed an atypically high subG1 cell fraction (**Fig. 3.6a**). This is indicative of internucleosomal DNA fragmentations and a hallmark of an apoptotic population. Bcl-3 knockdown resulted in not only a reduction of G2/M and S, but also G0/G1, which was balanced by a drastic increase in the subG1 apoptotic cell fraction. This indicated Bcl-3 knockdown not only negatively regulated cell population change through a shift towards the resting G0/G1 population, but also through increasing the rate of apoptosis. The cell cycle of the nonmalignant MCF10a cell line was not affected by Bcl-3 knockdown.

PANTHER analyses of the knockdown Affymetrix data highlighted many statistically enriched and overrepresented genes associated with integrin signalling pathways (**Tab. 3.1**). Integrins are transmembrane receptors that facilitate cell to extracellular matrix adhesion and upon ligand binding they activate signal transduction pathways that mediate the cell cycle and also potentially apoptosis (Giancotti and Ruoslahti, 1999). These downstream signalling implications following Bcl-3 knockdown could provide potential mechanistic explanations for the observed changes to the cell cycle.

3.15.2 Bcl-3 regulated apoptosis signalling pathways

By directly assaying caspase-3/-7 activity we were able to show that Bcl-3 knockdown significantly increased their activation in all TNBC cell lines but not in MCF10a (**Fig. 3.11**). On top of this, MDA-MB-436 by far expressed the highest endogenous caspase activity when compared with the other cell lines. Hence when considering the overall rate of cell growth, one must consider the overall cell-turnover, the combined rate of proliferation and rate of cell death, this might help explain why MDA-MB-436 had the slowest cell growth rate despite having the highest Ki67 and pHH3 expression among the TNBCs. Interestingly, despite significantly increased of caspase-3/-7 activity in all TNBC cell lines following Bcl-3 knockdown, we only saw an increased subG1 apoptotic cell fraction in the MDA-MB-436. This could be explained by the presence of a time lag between when apoptosis signalling is first triggered following Bcl-3 suppression and the subsequent phenotype of accumulated cellular DNA fragmentation required to identify a subG1 population. It will be interesting to assess the effects on the cell cycle phases with time-points longer than 48h when Bcl-3 suppression is sustained.

PANTHER statistical enrichment analysis of the Affymatrix knockdown experiment revealed a total of 52 significantly altered genes falling within the apoptosis signalling pathway. The overall pathway genotype was up-regulation and this correlated with the increased apoptotic phenotypes seen within the triple negative cell line experiments. As expected, Caspase-3 (CASP3) and -7 (CASP7) were shown to be up-regulated 1.27-fold and 1.36-fold respectively. These members of the cysteine-aspartic acid protease family have central roles in the execution of apoptosis. Although caspase-9 (CASP9) was down-regulated 0.89-fold, it is unclear whether this was the active isoform 1 or isoform 2, a dominant-negative inhibitor of caspase-9, helping explain the increased downstream activation of caspase-3 and -7 (Li et al., 2017).

3.15.2.1 Bcl-3 protected against intrinsic mitochondria-mediated apoptosis

The expression of a wide number of Bcl-2 family proteins were altered following Bcl-3 knockdown. Bcl-2 apoptosis regulator (BCL2) and Bcl-2 like 1 (BCL2L1) were both

down-regulated 0.70-fold and 0.73-fold. These encode integral outer mitochondrial membrane proteins that antagonises apoptosis through regulation of mitochondrial membrane permeability (Delbridge et al., 2016). Bcl-2 interacting killer (BIK) was up-regulated 1.46-fold and this protein acts to sensitise and accelerate apoptosis. Pro-apoptotic protein BAK (BAK1) was up-regulated 1.34-fold and it induces apoptosis by opening mitochondrion voltage-dependent anion channels, and release of cytochrome c. Bcl-2 associate X apoptosis regulator (BAX) was up-regulated 1.19-fold and it heterodimerises with Bcl-2, antagonising its apoptosis repressing functions. Bcl-2 related ovarian killer (BOK) was up-regulated 1.18-fold and positively regulate intrinsic apoptosis through both TP53-, BAX-, BAK1-dependent and independent manners. Bcl-2 family apoptosis regulator (MCL1) was up-regulated 1.32-fold and is involved in the regulation of survival and apoptosis. The longest MCL1 isoform 1 is anti-apoptotic, but the alternatively spliced shorter isoform 2 and 3 promotes apoptosis and are death-inducing (Yang-Yen et al., 2015). Tumour protein P53 (TP53) was up-regulated 1.07-fold and encodes a potent tumour suppressor mediating apoptosis through stimulation of BAX and FAS or repression of Bcl-2 (Kasthuber and Lowe, 2017).

Mitogen-activated protein kinase kinase 3 (MAP2K3), mitogen-activated protein kinase kinase 4 (MAP2K4), mitogen-activated protein kinase kinase kinase 4 (MAP4K4) and mitogen-activated protein kinase kinase 7 (MAP2K7) were all up-regulated 1.20-fold, 1.17-fold, 1.23-fold and 1.09-fold respectively. These encode kinases that activate MKK/JNK signalling pathways involved in mitochondrial death signalling (Otto et al., 2012). Apoptotic peptidase activating factor 1 (APAF1) was up-regulated 1.28-fold and it encodes a protein component of the oligomeric apoptosome which activates caspase-9 stimulating the caspase cascade that executes apoptosis (Shakeri et al., 2017). Mitogen-activated protein kinase 1 (MAPK1) was up-regulated 1.03-fold and mitogen-activated protein kinase 3 (MAPK3) was down-regulated 0.81-fold. These encode essential serine/threonine kinase components of the MAPK/ERK signal transduction pathway which mediate diverse biological functions including apoptosis (Upadhyay et al., 2013).

A recent study investigating the pathogenesis of gliomas found elevated Bcl-3 levels compared to normal brain tissues. Bcl-3 silencing in U251 cells saw prominent reductions in proliferation, cell cycle arrest in G1 phase, increased apoptosis and inhibition of in vivo tumour growth. Mechanistically it was found Bcl-3 positively associated with an abundance of STAT3, p-STAT3 and downstream targets of the STAT3

pathways including BCL2, MCL1 and cyclin D1. When they knocked down STAT3, the oncogenic effects mediated by Bcl-3 was found to be abolished. Their findings suggest that Bcl-3 oncogenicity seem to be mediated through STAT3 signalling pathways in gliomas (Wu et al., 2016). In light of the gene changes linked to the intrinsic apoptosis pathways in our TNBC cell line, it would be interesting to investigate STAT3 pathways to see if there are shared mechanistic links. Taken together with all of the pro-apoptotic gene changes seen relating to the Bcl-2 family of proteins, we propose that the effect of Bcl-3 knockdown in TNBCs is at least in part driven, or augmented by the intrinsic mitochondria-mediated apoptosis pathway. These results seem to indicate that Bcl-3 plays a critical role in protecting TNBCs against activation of this particular pathway.

3.15.2.2 Bcl-3 protected against stress induced apoptosis

Various genes implicated in the cellular stress response were found to be altered following Bcl-3 knockdown. Heat shock 70kDA protein 1A (HSPA1A), 1B (HSPA1B) and 2 (HSPA2) were all down-regulated 0.75-fold, 0.75-fold and 0.82-fold. These encode molecular chaperones involved in the protection of the proteome from stress induced apoptosis (Daugaard et al., 2007). Activating transcription factor 6 (ATF6) and 6 beta (ATF6B) were up-regulated 1.10-fold and 1.22-fold. These encode atypical transcription factors that act as transmembrane proteins embedded in the ER involved in the unfolded protein response (UPR) pathway following ER stress (Thuerauf et al., 2007).

These gene changes suggest that Bcl-3 is involved in regulation of the cellular stress threshold required to trigger an apoptotic cascade. It is possible knockdown led to the lowering of this threshold and primed the cancer cells for apoptosis in response to existing environmental stressors. Further experiments will have to be carried out to investigate whether this is the case. It will be interesting to assay cell viability and the proportion of cells that undergo apoptosis following varied culturing conditions, such as changes in temperature, oxygen or carbon dioxide content or even chemotherapeutics.

3.15.2.3 Bcl-3 and the extrinsic receptor-mediated apoptosis pathways

Although the most conclusive changes following Bcl-3 knockdown were associated with the intrinsic mitochondria-mediated apoptosis pathway, a number of

interesting changes in genes associated with the extrinsic receptor-mediated pathways were also observed. TNF receptor superfamily member 10a (TNFRSF10A), 10b (TNFRSF10B) and 10d (TNFRSF10D) were all up-regulated 1.21-fold, 1.21-fold and 1.60-fold respectively. These encode apoptosis inducing receptors activated by the tumour necrosis factor-related apoptosis inducing ligand (TRAIL). Their up-regulation hints at perhaps a sensitisation for endogenous TRAIL-mediated apoptosis. TNF receptor superfamily member 10c (TNFRSF10C) was down-regulated 0.78-fold. This encodes a receptor containing an extracellular and transmembrane TRAIL-binding domain but no cytoplasmic death domain. Subsequently this receptor is not capable of inducing apoptosis and is thought to function as a competitive antagonistic receptor protecting cells from TRAIL-induced apoptosis (Micheau, 2018). Its down-regulation further suggests at an increased sensitivity for TRAIL-mediated apoptosis.

MAP kinase activating death domain (MADD) was down-regulated 0.89-fold and it encodes a death domain-containing adaptor protein that interacts with the death domain of TNF-alpha receptor 1 to activate mitogen-activated protein kinase (MAPK) and propagate apoptosis. Depending on alternative mRNA splicing, MADD can serve different regulatory roles. For example, isoform 1 and 2 induces apoptosis and decreases proliferation while isoform 5 increases proliferation and confers apoptosis resistance. Down-regulation of the anti-apoptotic isoforms could help explain the increase in apoptosis signalling, but further investigation is required before any conclusions can be drawn (Al-Zoubi et al., 2001). Receptor-interacting protein kinase 1 (RIPK1) was up-regulated 1.28-fold and encodes a protein that mediates both apoptosis and necroptosis through the TNF-alpha signalling pathway (Shan et al., 2018). Protein kinase C epsilon (PRKCE) and gamma (PRKCG) were down-regulated 0.87-fold and 0.72-fold. These encode PKC isoforms associated with up-regulation of NFkB signalling, enhanced apoptosis (Körner et al., 2013), and radiotherapy and chemotherapy resistance (Lu et al., 2014).

Despite the aforementioned pro-apoptotic gene changes seen following Bcl-3 knockdown, there are some key anti-apoptotic gene changes that may counteract their effectiveness. Activating transcription factor 7 (ATF7) was up-regulated 1.16-fold and plays important functions in early cell signalling by forming activatory heterodimers with JUN or FOS. Proto-oncogene c-jun (JUN) and c-fos (FOS) were both up-regulated 1.14-fold and 1.23-fold respectively and encodes nuclear phosphoproteins that forms

complexes with the JUN/AP-1 transcription factor. JUN and FOS are typically seen as survival factors and promoters of proliferation, though in some cases they have been shown to be associated with apoptosis (Durchdewald et al., 2009).

CASP8 and FADD like apoptosis regulator (CFLAR) was up-regulated 1.11-fold. This encodes a regulator of apoptosis that is structurally similar to caspase-8 and acts as an inhibitor of TNFRSF6 mediated apoptosis. Death domain containing protein CRADD (CRADD) was down-regulated 0.84-fold, this gene encodes an apoptotic adaptor molecule specific for caspase-2 and the FASL/TNF receptor-interacting protein RIP. In the presence of RIP and TRADD, CRADD recruits caspase-2 to the TNFR-1 signalling complex activating apoptosis (Fulda, 2013). AKT serine/threonine kinase 2 (AKT2) was up-regulated by 1.10-fold and this protein inhibits apoptosis by phosphorylation of MAP3K5 (Riggio et al., 2017). While it is clear Bcl-3 does play some roles in mediating extrinsic apoptosis, mixed changes in both pro- and anti-apoptotic genes suggested a more complex regulatory pathway.

3.15.3 Bcl-3 implicated in NFkB signalling

Using a NFkB reporter vector we were able to show that Bcl-3 knockdown led to a global reduction in pan-NFkB signalling in all cell lines (**Fig. 3.21**). This made sense as Bcl-3 plays an important role as a transactivator within NFkB signalling and we would expect its down-regulation to result in decreased p50 and p52 complex-mediated transcription. NFkB signalling is also closely linked with cellular processes such as proliferation and reduced pathway activities could help explain the slow down in proliferation seen previously following Bcl-3 suppression.

We were able to tease from the microarray analyses a few specific changes pertaining to the NFkB signalling pathway following Bcl-3 knockdown. Nuclear factor kappa B subunit 2 (NFkB2) and transcription factor RelB (RELB) were up-regulated 1.18-fold and 1.13-fold. These encode pleiotropic transcription factors involved in regulation of a wide range of biological processes including but not limited to apoptosis. A recent study found that RelB was consistently linked with Bcl-3 expression in colorectal cancers. NFkB2 and RelB complexes were shown to be able to bind directly to the promoter region of the Bcl-3 gene and upregulate its transcription (Tao et al., 2018). This could help explain the up-regulation of these two subunits following Bcl-3 knockdown as it could

perhaps be an attempted cellular feedback response to restore endogenous Bcl-3 balance.

Inhibitor of NFκB Kinase subunit beta (IKBKB) was down-regulated 0.79-fold and this encodes a protein that phosphorylates inhibitors of NFκB. These modifications allow polyubiquitination of the inhibitors, subsequent proteasomal degradation and activation of NFκB signalling (Schmid and Birbach, 2008). Inhibitor of NFκB kinase subunit (CHUK) was up-regulated by 1.25-fold and this encodes a member of the serine/threonine protein kinase family that acts as an inhibitor of NFκB transcription (Solt and May, 2008). NFκB inducing kinase (MAP3K14) was down-regulated 0.81-fold and encodes the serine/threonine mitogen-activated protein kinase kinase kinase 14. This is involved in the activation of non-canonical NFκB transcriptional activity (Malinin et al., 1997). It is clear from these findings that Bcl-3 is intricately tied to the balance of many different arms of NFκB signalling and the knockdown phenotype is the a result of many shifted downstream outputs.

3.15.4 Bcl-3 did not regulate cancer cell stemness but affected clonogenic survival

When we assayed for self-renewal and cancer stem-like cells, Bcl-3 knockdown did not affect the number of mammospheres formed in any of the TNBC cell lines. However the average mammosphere size in all cell lines apart from SUM149 and MCF10a were significantly smaller (**Fig. 3.12**). This suggested Bcl-3 is not specifically implicated in conferring anoikis resistance, nor the survival of a stem-like cell population. Smaller sphere sizes following knockdown is likely a carried forward effect of the growth reduction phenotype previously seen. We would have expected SUM149 spheres to be smaller, but it is possible for this cell line to have a stem population resistant to the growth impairing effects of Bcl-3 knockdown. MCF10a does not seem to be affected by Bcl-3 knockdown so it was unsurprising for their sphere numbers and size to also remain unchanged.

When clonogenic survival capabilities were assayed we saw a marked reduction in both the number of colonies formed as well as their size following Bcl-3 knockdown in all cell lines apart from MCF10a (**Fig. 3.13**). These effects can partly be explained by the reduced cell growth and increased apoptosis seen within the knockdown cell populations. Following knockdown, a greater proportion of cells plated into the colony formation assay

were apoptotic compared to controls, and the surviving clonal populations proliferated slower. Furthermore, the low cell plating density conditions of this assay appeared to further sensitise these effects, leading to an overall significant impairment of clonogenicity within the Bcl-3 knockdown cells. The nonmalignant MCF10a cell line did not exhibit any reduced clonogenicity.

3.15.5 Bcl-3 regulated various modes of migration potentially through Rho GTPases

The effects of Bcl-3 knockdown on three different migratory outputs were characterised in our panel of cell lines. We tested collective migration using the wound healing assay, amoeboid-like migration using the fluoroblok assay and mesenchymal-like migration using the single cell assay. In all TNBC cell lines, Bcl-3 knockdown was able to significantly inhibit all three forms of migration when compared to the scrambled control. The migratory phenotypes of the nonmalignant MCF10a cell line was not affected by Bcl-3 knockdown (**Fig. 3.14-3.20**).

PANTHER statistical enrichment analysis revealed 27 significantly altered genes falling within the cytoskeletal regulation by Rho GTPase pathway following Bcl-3 siRNA knockdown. This signalling pathway is primarily associated with cellular actin restructuring linked to cell motility. The general genotype following Bcl-3 knockdown was inhibitory and this correlates with the decreased migratory phenotype seen in the triple negative cell line experiments. In the next section we will discuss the significance and roles of the various altered genes within this signalling pathway following Bcl-3 knockdown (**Fig. 3.24**).

The Rho-related GTP-binding protein RhoB (RHOB) was up-regulated 1.32-fold. RhoB encodes a major member of the Rho GTPase family, it shares about 85% amino acid identity with RhoA and RhoC, but plays very biologically different roles. It has been well established in numerous studies that RhoA and RhoC are pro-tumourigenic in almost all cancers. However RhoB has unique post-translational modifications distinctive from RhoA and RhoC, contributing to a more dualistic role in cancer. While RhoA and RhoC can only be palmitoylated, RhoB can also undergo farnesylation (RhoB-F) or geranylgeranylation (RhoB-GG) and its pernylation state determines its function (Zandvakili et al., 2017). Farnesylated RhoB localises to the plasma membrane, promoting

cell growth, mediating effects of Ras actin cytoskeleton and activating NF κ B. In contrast geranylgeranylated RhoB localises to endosomes and induces apoptosis (Ju and Gilkes, 2018).

RhoB has been shown to “switch-off” EGF mitogenic signals by targeting activated EGF receptors to the lysosome (Gampel et al., 1999). It has also been shown to exert a negative regulatory influence on TGF- β -induced transcriptional activation (Engel et al., 1998) and this signalling pathway was one that was found to be statistically overrepresented following Bcl-3 knockdown. RhoB promoter activity was detected following genotoxic treatments indicating its role in the cellular response to DNA damage (Fritz and Kaina, 2000). Some studies have also shown that Ras actually down-regulates RhoB via EGFR, ErbB2 and AKT/PKB pathways (Jiang et al., 2004). Numerous subsequent studies began to reveal emerging evidence for a cancer suppressor role of RhoB by inhibiting in vitro cell proliferation, survival, invasion and metastasis and backed up by in vivo findings that RhoB depleted cells formed tumours less efficiently than cells expressing RhoB (Liu et al., 2001). RhoB depletion promoted 2D cell migration by altering β 1 integrin expression and hence focal adhesion dynamics and distribution (Ridley, 2013). In breast tumourigenesis it was shown that RhoB acted as a tumour suppressor until the tumour vasculature was established, in which then its angiogenic tumour promoter functions overrode the negative impact it had in tumour cells (Kazerounian et al., 2013).

Rho-related GTP-bind protein RhoJ (RHOJ) was down-regulated 0.70-fold and it has been associated with formation of f-actin rich structures and focal adhesions (Wilson et al., 2014). RHOJ is activated by VEGF, a signalling pathway found to be statistically overrepresented following Bcl-3 knockdown and also shown to be implicated in angiogenesis regulation (Kim et al., 2014). RhoJ depletion was able to attenuate hypoxia induced EMT (Liu et al., 2018).

The genes Diaphanous-related formin-1 (DIAPH1) and Diaphanous-related formin-3 (DIAPH3), members of the diaphanous subfamily of the formin family were down-regulated 0.75-fold and 0.74-fold respectively. DIAPH1 encodes a protein controlling cell shape, assembly of f-actin structures and stabilising microtubules. DIAPH3 is implicated in formin-dependent TGF- β signalling for EMT (Rana et al., 2018). Silencing of DIAPH3 was shown to destabilise microtubules and increased prostate and breast

cancer sensitivity to taxanes (Morley et al., 2015). Tubulin beta-4A chain (TUBB4A) was down-regulated 0.70-fold and Tubulin beta-6 chain (TUBB6) up-regulated 1.13-fold. These proteins encode members of the tubulin family which are major constituents of microtubules. They are likely downstream effectors of DIAPH1 and DIAPH3 signalling (Nami and Wang, 2018).

Rho-associated protein kinase 1 (ROCK1) was down-regulated 0.88-fold. It encodes a serine/threonine kinase regulated by upstream Rho GTPases and modulates cytoskeletal rearrangements processes including focal adhesion formation, cell motility and tumour cell invasion (Julian and Olson, 2014). Downstream of ROCK1 is LIM domain kinase 1 (LIMK1), which was down-regulated 0.83-fold. This is another serine/threonine kinase that regulates actin polymerisation via phosphorylation and inactivation of cofilin, preventing the cleavage of f-actin and stabilising the actin cytoskeleton. In this way LIMK1 regulates several actin-dependent biological processes including cell motility, cell cycle progression, and differentiation (Gorovoy et al., 2005). Following LIMK1 down-regulation, Cofilin 2 (CFL2) was found to be up-regulated 1.16-fold. Cofilin is a major component of intra-nuclear and cytoplasmic actin rods and reversibly controls actin polymerisation and depolymerisation. Slingshot protein phosphatase 2 (SSH2) which encodes a protein tyrosine phosphatase that dephosphorylates and activates cofilin, promoting actin filament depolymerisation was up-regulated 1.09-fold. Slingshot protein phosphatase 3 (SSH3), another member of the slingshot phosphatase family was found to be down-regulated 0.77-fold and it is likely to have inhibitory effects on cofilin activation (Kanellos and Frame, 2016).

Protein enabled homolog/MENA (ENAH) was found to be down-regulated 0.77-fold. It encodes an actin regulatory protein involved in a range of processes dependent on cytoskeleton remodelling and lamellipodial and filopodial dynamics in migrating cells. In invasive migratory tumour cells, ENAH imparts increased sensitivity to EGF and both invasive and protrusive capabilities are up-regulated (Gertler and Condeelis, 2011). Myosin heavy chain 9 (MYH9) was down-regulated 0.72-fold. This gene encodes a conventional non-muscle cytoplasmic myosin involved in cytokinesis, cell motility, cell shape, focal contact formation and lamellipodial retraction (Pecci et al., 2018).

Cell division control protein 42 homolog (CDC42) was down-regulated 0.66-fold following Bcl-3 knockdown. It is a major Rho GTPase family member upstream of many

actin polymerisation processes and commonly associated with promoting filopodial protrusions. However both Rho GTPase activating protein 1 (ARHGAP1) and Rho GTPase activating protein 8 (ARHGAP8) were down-regulated 0.90-fold and 0.81-fold respectively. These encode a family of proteins that activate Rho GTPase metabolising enzymes, converting Rho GTPase family proteins into the putatively inactive GDP-bound state. The down-regulation of these specific GAP proteins might be a feedback response due to the inhibitory effects of Bcl-3 knockdown and could help explain why we did not observe a significant down-regulation of other major Rho GTPase family members such as Rac1 or RhoA (J. Li et al., 2017).

p21-activated kinase 1 (PAK1) and p21-activated kinase 6 (PAK6) were both down-regulated 0.86-fold and 0.95-fold respectively. They encode serine/threonine p-21-activating kinases PAK protein family members which are effector proteins for CDC42. PAK1 and PAK6 signalling are important for cytoskeleton dynamics, cell adhesion, migration and vesicle-mediated transport processes. They are also involved in a wide range of other cellular functions and facilitates the full activation of Ras/RAF/MEK/ERK, PI3K/Akt/mTOR, MAPK and Wnt signalling pathways, which are implicated in cell cycle progression, cell survival, differentiation and proliferation. They can phosphorylate BAD and protect against apoptosis (Pérez-Yépez et al., 2018).

Despite CDC42 down-regulation, Neural Wiskott-Aldrich syndrome protein/N-WASP (WASL) was found to be up-regulated 1.10-fold. WASL is a scaffold protein that typically bind CDC42 and transduce signals from the cell surface to activate ARP2/3 complexes leading to actin nucleation, polymerisation and is involved in mitosis and cytokinesis. Actin-related protein 2/3 complex subunit 1A (ARPC1A), 1B (ARPC1B), and 4 (ARPC4), were up-regulated 1.18-fold, 1.24-fold and 1.11-fold respectively. Actin-related protein 2/3 complex subunit 3 (ARPC3) was down-regulated 0.87-fold. These changes in genes encoding subunits of the Arp2/3 protein complex are likely downstream effects of WASL signalling (Abella et al., 2016). Even though CDC42 was shown to be down-regulated following Bcl-3 knockdown, it is possible that Bcl-3 has an inhibitory effect on WASL signalling independent of CDC42 altering the cellular migration phenotype.

Profilin-2 (PFN2), down-regulated 0.90-fold, encodes an actin binding protein belonging to the profilin family which regulates actin polymerisation. PFN2 has been shown to enhance TGF- β 1-induced EMT and production of the angiogenic VEGF and

drive lung cancer growth and metastasis (Tang et al., 2015). These are both pathways found to be statistically overrepresented following Bcl-3 knockdown. PFN2 has also been shown to promote metastatic potential and stemness of HT29 colorectal cancer cells by regulating EMT and stemness related proteins (Kim et al., 2015). Myosin light chain kinase (MYLK), down-regulated 0.90-fold, encodes a calcium/calmodulin depended enzyme that phosphorylates myosin regulatory light chains to facilitate interactions with actin filaments to produce contractile activity (Shen et al., 2015). Beta-actin-like protein 2 (ACTBL2) down-regulated 0.79-fold, is an isomer of beta-actin and this was identified as a novel up-regulated protein in colorectal cancer (Ghazanfar et al., 2017). Actin, gamma-enteric smooth muscle (ACTG2), down-regulated 0.90-fold, is a component of the cytoskeleton, acts as mediators of internal cell motility and has also been shown to be involved in small intestinal neuroendocrine tumourigenesis (Edfeldt et al., 2016).

It is worth noting these changes in Rho GTPase signalling was derived from experimental Affymetrix microarray analysis of Bcl-3 siRNA knockdown in the MDA-MB-231-Luc cell line and other triple negative cell lines may respond differently. However the other TNBC cell lines used within this project had comparable experimental phenotypes following Bcl-3 knockdown so it is likely this analysis is at least somewhat representative, highlighting important mechanistic elements. Regardless, it is still important to confirm and validate whether there are similar genotypic responses following Bcl-3 knockdown in other TNBCs in future studies.

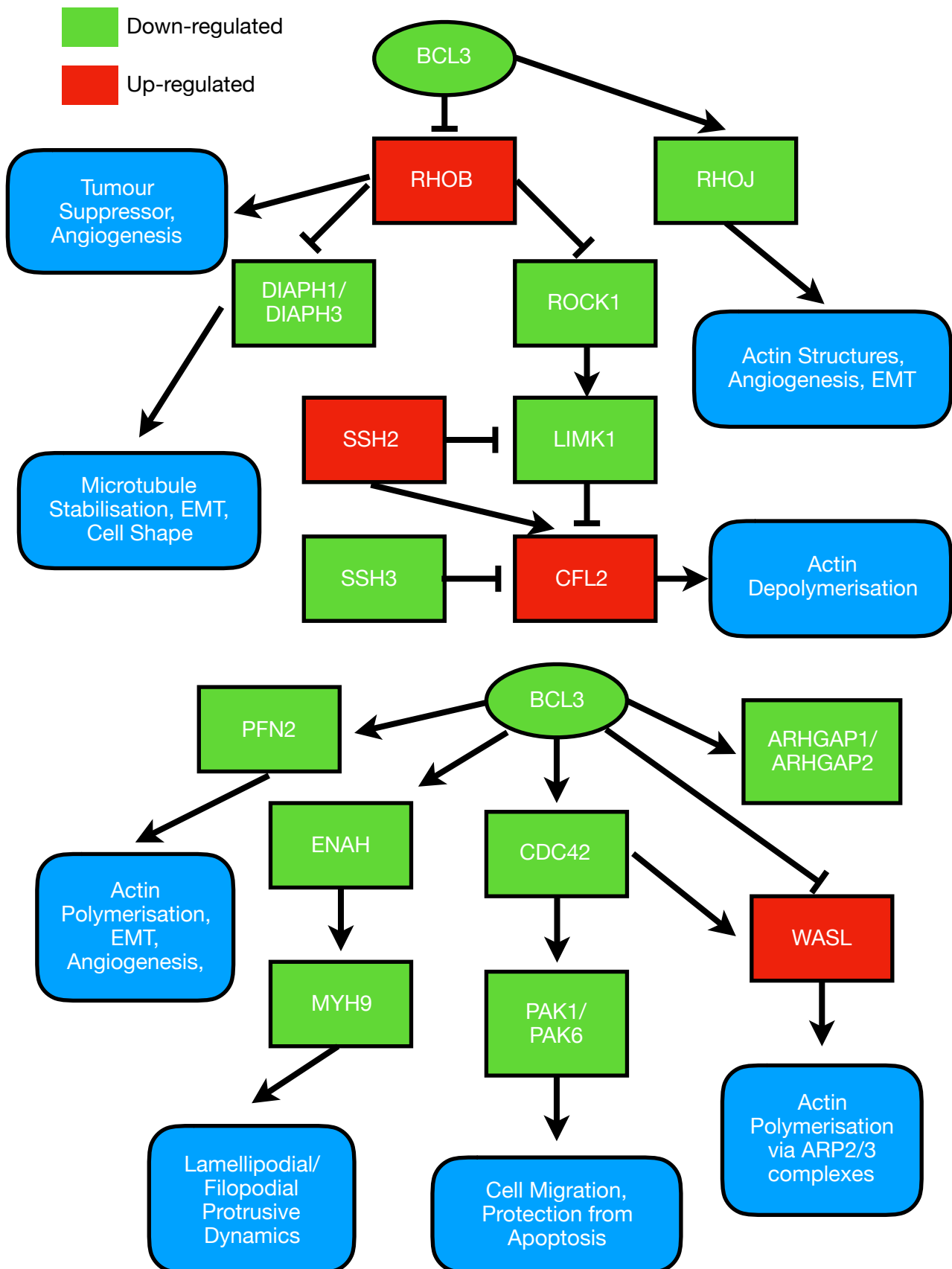


FIG. 3.24 BCL-3 REGULATES RHO GTPASES SIGNALLING PATHWAYS WHICH POTENTIALLY IMPACTS ON MIGRATION

Following Bcl-3 knockdown, numerous changes in Rho GTPase signalling pathways were observed. This figure plots out signalling pathway diagrams highlighting the interlinked downstream interactions associated with Bcl-3 and describes the main roles of each pathway.

3.15.6 Bcl-3 knockdown reduced metastatic occurrence in a murine tail vein xenograft metastasis model

In order to derive eventual clinical relevance it was important to investigate the effects of Bcl-3 knockdown in the context of an *in vivo* model. We chose a xenograft tail vein model as this was an effective technique at rapidly producing tumours that featured similar genetic profiles to metastases generated from orthotopic lesions (Rashid et al., 2013). It was found that when Bcl-3 knockdown cells were injected via the tail vein vasculature, significantly less total metastatic occurrences were found at point of necropsy. The total number of distinct tumours in both the lungs and liver were significantly lower compared to the control siRNA cell line.

Although there was no significant difference between the average tumour size between the two conditions, it is worth noting this does not necessarily disprove the efficacy of Bcl-3 knockdown. Firstly the effects of siRNA knockdown is only transient and Bcl-3 levels within tumours would have returned to endogenous levels over the course of the experiment. We did not hypothesise Bcl-3 suppression to lead to tumour regression, hence the seeded metastases would have continued to expand at varying rates. Depending on the timeframe of the experiment there might be a more optimal endpoint than 45 days in order to see a significant difference between the Bcl-3 knockdown and control tumours. For future *in vivo* studies it will prove more informative to use luciferase expressing tumour cell lines to enable us to image and measure tumour growth longitudinally without the need to cull and perform necropsy at a chosen experimental endpoint.

All in all these results supports the effects seen in the *in vitro* experiments as suppressing Bcl-3 had been shown to impair viability, clonogenicity, and migratory capabilities. Taken together these expected downstream effect all contributed towards and helped explain the reduction in metastatic occurrence. *In vivo* efficacy further highlights Bcl-3 as a promising therapeutic target.

3.15.7 Bcl-3 knockdown and other downstream implications

Aside from apoptosis and migration linked Rho GTPase signalling pathways, PANTHER analyses of the Affymetrix microarray data highlighted a number of other interesting outputs worthy of further investigation. Among the altered genes a higher than expected proportion belonged to those associated with metabolic processes such as nitrogen, purine and carbohydrate metabolism, protein glycosylation, and biosynthetic and catabolic processes. Bcl-3 dysregulation had been shown in a recent study to disrupt hepatocyte metabolism and contribute to liver steatosis (Gehrke et al., 2016). Changes in cellular metabolism could also have contributed some of the phenotype shifts we observed in the TNBC cell lines.

Various angiogenesis related genes, specifically those related to VEGF were also found to be significantly overrepresented. This data preliminarily suggests Bcl-3 may be implicated in this physiological process by acting through vascular endothelial growth factor (VEGF) signalling. VEGF is a protein involved in both vasculogenesis and angiogenesis and is a part of the system that provides oxygen to tissues under hypoxic conditions. The capability of tumours to recruit the formation of new blood vessels is a critical transitional step towards aggressive disease. Cancers that express VEGF are able to continue to grow and metastasise (Palmer and Clegg, 2014).

Altered genes pertaining to the TGF-beta signalling pathways were also found to be highly enriched and overrepresented, this included the significantly up-regulated activin-beta signalling pathway which belongs to the TGF-beta superfamily. TGF-beta in breast cancer is selectively associated with pulmonary metastasis and a recent paper demonstrated the role of Bcl-3 to serve as a critical regulator. Bcl-3 knockdown was shown to enhance degradation of Smad3 but not Smad2 following TGF-beta treatment and Bcl-3 was able to bind to Smad3 to prevent its ubiquitination and degradation (Chen et al., 2016). This study and the changes seen in our microarray experiment emphasises the importance of further investigating the diverse roles and mechanisms of Bcl-3 within metastatic breast cancers.

3.15.8 Concluding remarks

It was evident from the experimental results generated in this chapter that siRNA knockdown of Bcl-3 profoundly suppressed oncogenic outputs within TNBC cell lines. We saw reductions in overall cell population turnover, characterised by reduced proliferation as well as increased apoptosis, mostly likely mediated through the intrinsic mitochondria-associated signalling pathways. We demonstrated the effects of Bcl-3 on the various modes of cellular migration and microarray analysis associated this reduced motility with Rho GTPase signalling pathways. Furthermore none of the above mentioned effects were seen in the control non-tumourigenic MCF10a breast cancer cell line, suggesting the effects were likely specific to TNBC. Bcl-3 knockdown was also able to reduce *in vivo* metastatic occurrences in a murine tail vein xenograft model. Altogether our findings highlight Bcl-3 as an important contributor toward human TNBC progression, especially within the roles of metastasis and outline some interesting mechanistic pathways worthy of further study.

Chapter 4: Results

Investigating Ectopic Bcl-3 Overexpression in TNBC Cell Lines

4.1 Introduction

Bcl-3 is generally accepted in the literature as a proto-oncogene and its overexpression has been implicated in a wide range of solid tumours and haematological malignancies (Maldonado and Melendez-Zajgla, 2011). Breast cancers were one of the first to be associated with deregulated Bcl-3 as when compared with normal adjacent tissues, p52 and Bcl-3 were found to be significantly up-regulated (Cogswell et al., 2000). Although mechanisms of Bcl-3 oncogenicity have not yet been fully described, its up-regulation has often been linked with promotion of cellular proliferation and survival, as well as suppression of apoptosis. These processes have been shown to act through a number of pathways, such as promotion of cyclin D1 (Westerheide et al., 2001), suppression of the p53 response to DNA damage (Kashatus et al., 2006), as well as stabilisation of CtBP1 (Choi et al., 2010).

In the previous chapter we established the cellular effects of Bcl-3 suppression in a panel of TNBC cell lines. Here, we wanted to investigate the physiological effects of the opposite - ectopic overexpression. We hypothesised that if Bcl-3 were to act as a classical oncogene then its overexpression in the same panel of cell lines should have opposing effects to those seen with siRNA knockdown. Plasmid vectors containing wild type (WT) Bcl-3 constructs were generated by Dr. Alain Chariot's group (Interdisciplinary Cluster for Applied Genoproteomics, University of Liège, Belgium). Plasmids containing Bcl-3 binding mutant constructs, termed Bcl-3 ANK mutants were generated through mutagenesis of the second Bcl-3 ankyrin repeat (**Fig. 4.1**). The integrity of this structure is required for binding to p50 and p52, hence Bcl-3 proteins containing these mutations have disrupted Bcl-3-p50 and Bcl-3-p52 binding (Keutgens et al., 2010b). Overexpression of this Bcl-3 binding mutant was expected to lead to inhibition of Bcl-3 signalling as dimerisation of the ANK mutant with endogenous Bcl-3 would prevent the formation of transcriptionally active p50-/p52-Bcl-3 complexes. Our understanding of Bcl-3 structural interactions allows us to explore the effects of Bcl-3 inhibition through a different mechanism of suppression compared to the excision of Bcl-3 protein with siRNA in the previous chapter.

The main aims of this chapter were to generate TNBC cell lines stably overexpressing WT Bcl-3, as well as the non-binding ANK mutant and assess their effects on overall cellular phenotype. We used the same range of in vitro cell-based assays (fully

described in the previous chapter) to quantify cell population change, proliferative markers, cell cycle, apoptosis, stemness, clonogenicity, migration and NFkB activity. In vivo xenograft experiments were also carried out to assess the affects of Bcl-3 overexpression in mouse models. We hoped the results would further inform and progress our understanding of the role of Bcl-3 in the context of human TNBC.

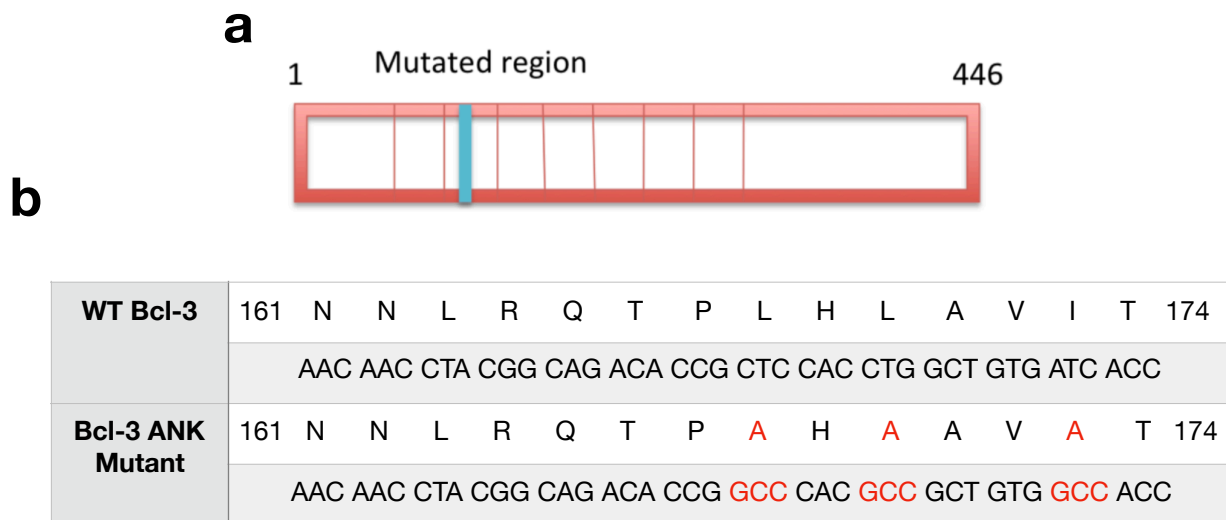


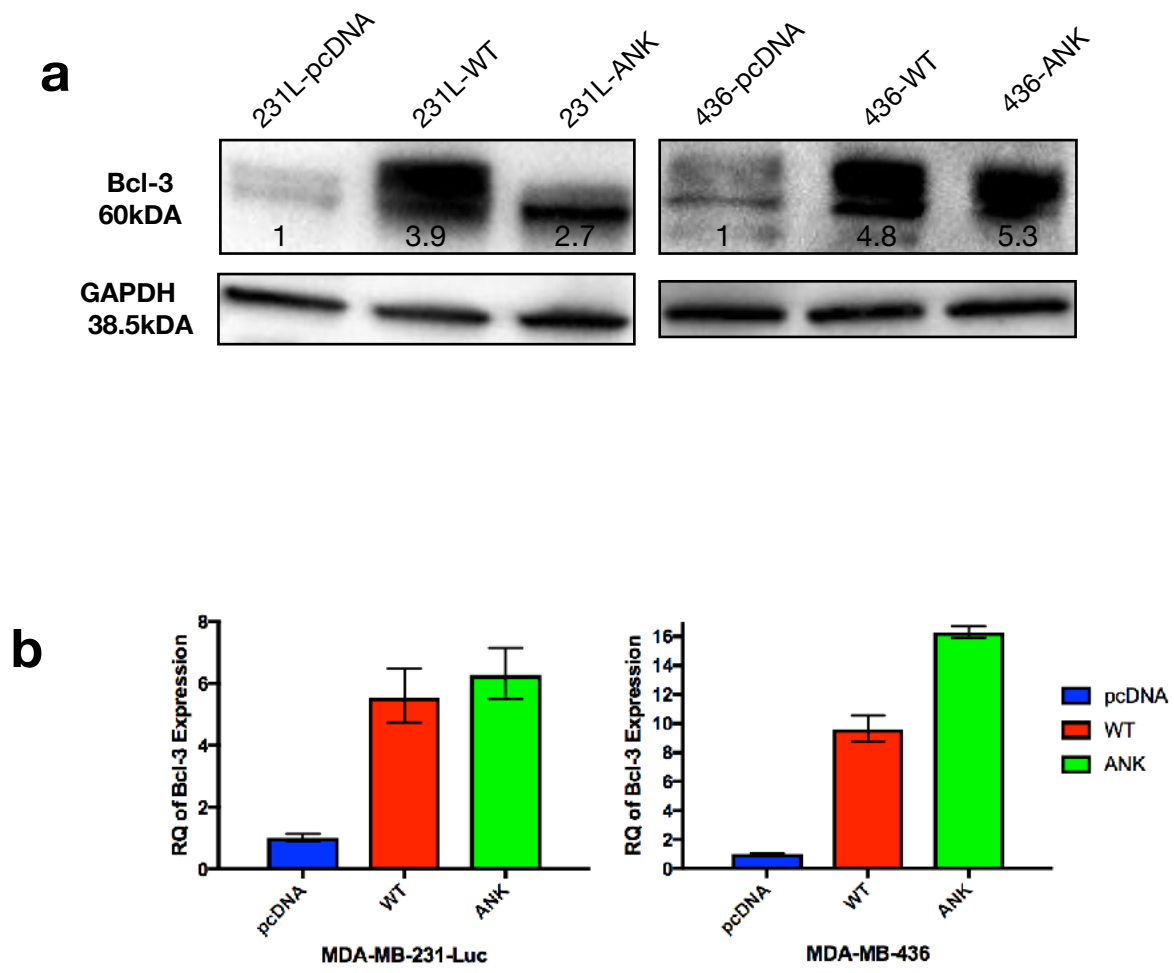
FIG. 4.1 BCL-3 CONSTRUCTS

a. Figure showing the position of the mutated region located at second Bcl-3 ankyrin repeat where a triple mutation is carried out to generate the ANK mutant construct. **b.** Table showing the corresponding Leucine (position 168), Leucine (position 170) and Isoleucine (position 173) in WT Bcl-3 being mutated into Alanines in the ANK mutant.

4.2 Generation of TNBC cell lines overexpressing ectopic Bcl-3

MDA-MB-231-Luc and MDA-MB-436 cell lines were transfected with the previously described WT Bcl-3 and Bcl-3 ANK mutant constructs as well as an empty pcDNA3.1 control vector. 24h post transfection the culture media for these lines were supplemented with Geneticin (G418) in order to select for plasmid expression. These newly generated recombinant cell lines were subsequently expanded and cultured under selection conditions for 1 week. Total protein (**Fig. 4.2a**) and RNA (**Fig. 4.2b**) were then extracted, western blotting and qRT-PCR carried out to characterise Bcl-3 expression. We observed expected increases in both Bcl-3 protein and RNA levels compared to pcDNA controls in both WT and ANK cell lines. For MDA-MB-231-Luc cells we saw a 5-6 fold overexpression of Bcl-3 and in MDA-MB-436 cells we saw a 9-16 fold overexpression.

Bcl-3 is thought to be predominantly active within the nucleus. In order to check the cellular localisation of our ectopic Bcl-3 constructs, cellular protein was separated into cytoplasmic and nuclear fractions. The cytoplasmic marker α -Tubulin and nuclear marker Lamin A/C were used to control for protein prep purity. By blotting for Bcl-3 in both fractions we can see both WT and ANK constructs were equally overexpressed in both cytoplasmic and nuclear compartments for both MDA-MB-231-Luc and MDA-MB-436 cell lines (**Fig. 4.2c**). These cell lines were cultured and maintained in G418 selection media and Bcl-3 levels were periodically checked every 5 passages by western blotting to confirm stability of overexpression.



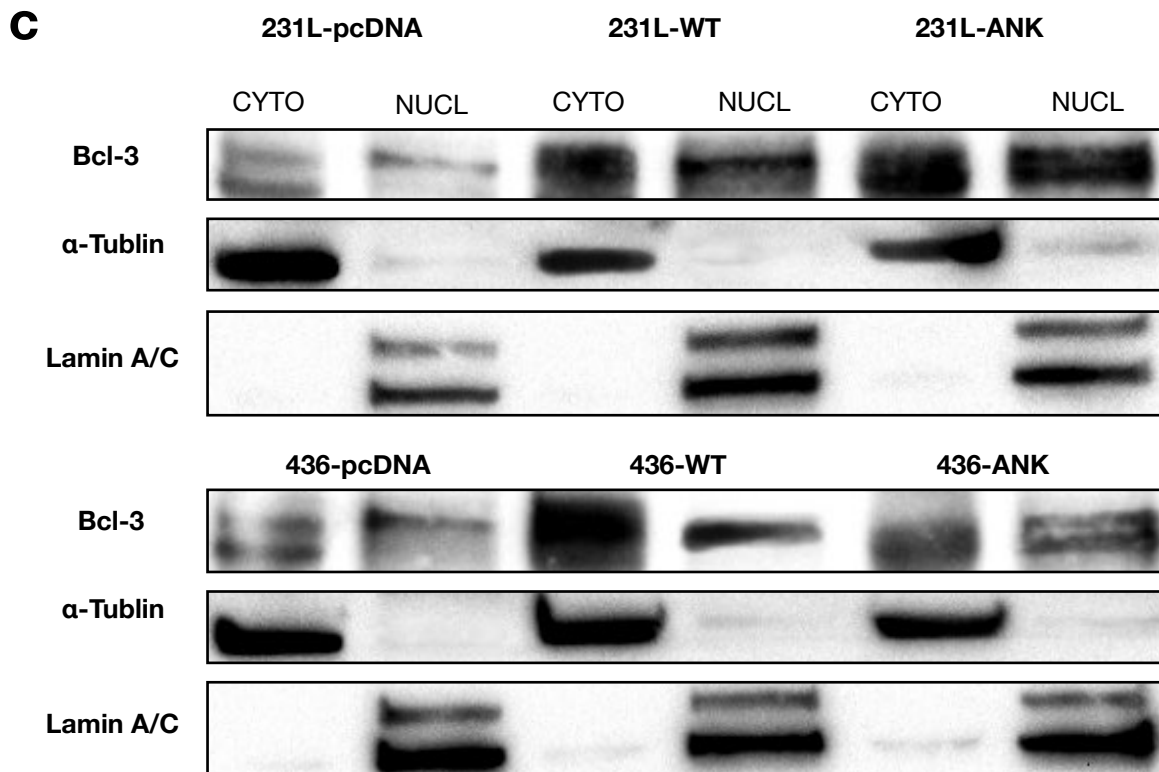


FIG. 4.2 RELATIVE BCL-3 PROTEIN RNA EXPRESSION AND CELLULAR LOCALISATION IN BREAST CANCER CELL LINES.

a. Cell lines were cultured under standard conditions, total protein was extracted and western blotting for Bcl-3 carried out, loading control = GAPDH. Relative densities estimated. **b.** Total cellular RNA was extracted and Bcl-3 expression quantified using Taqman qRT-PCR and relative gene expression normalised to beta-actin (ACTB). Error bars represent \pm SEM of 3 independent experiments. **c.** Cellular protein was separated into cytoplasmic and nuclear protein fractions and WB for Bcl-3 carried out, cytoplasmic marker = α -Tublin, nuclear marker = Lamin A/C. Images representative of 3 independent WBs.

4.3 Ectopic WT Bcl-3 overexpression reduced cell population growth

Due to the widely accepted oncogenic attributes of Bcl-3, we hypothesised that its ectopic overexpression would lead to accelerated cell population growth. MDA-MB-436 and MDA-MB-231-Luc cell lines stably expressing either WT Bcl-3, ANK mutant or control pcDNA constructs were plated into 96-well plates and cell population growth assayed using RealTime-Glo Assay (previously described in chapter 3.4) over the course of 96h. Surprisingly both TNBC cell lines overexpressing WT Bcl-3 exhibited a slow down in their cell population growth. Overexpression of the ANK Bcl-3 binding mutant also resulted in reduced cell growth for both of the TNBC cell lines (**Fig. 4.3**).

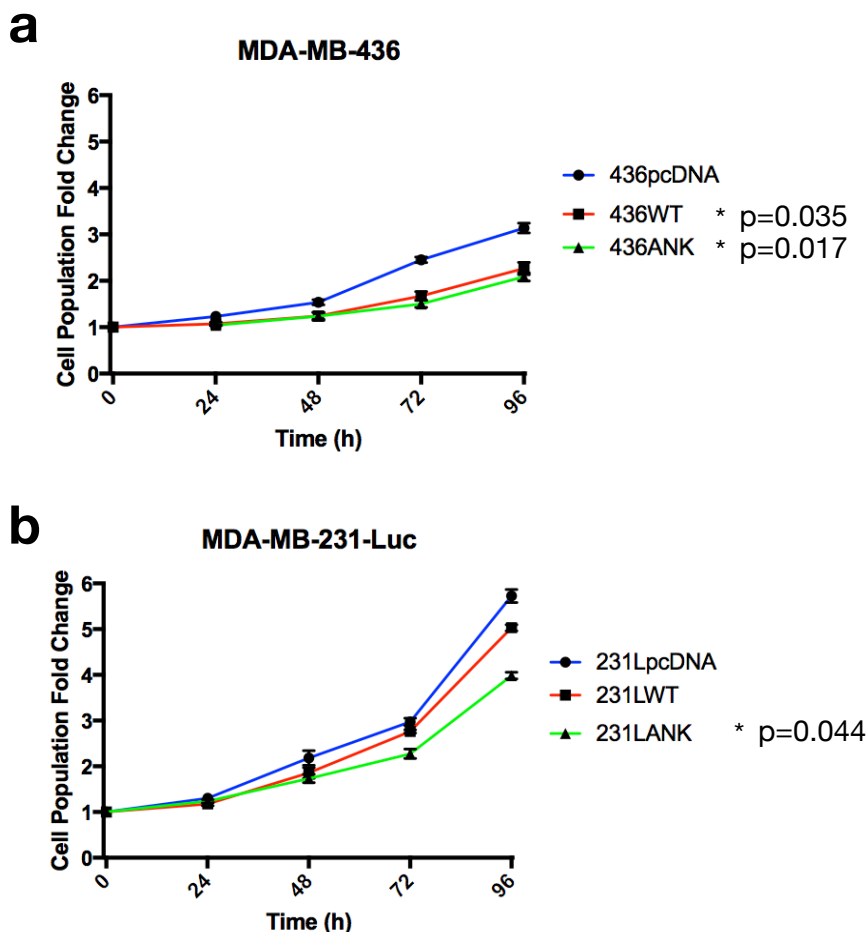


FIG. 4.3 ECTOPIC OVEREXPRESSION OF BCL-3 CONSTRUCTS REDUCED CELL POPULATION GROWTH

a. MDA-MB-436 **b.** MDA-MB-231-Luc cell lines stably expressing either WT Bcl-3, ANK mutant or pcDNA control constructs were plated into 96-well plates and cell population growth assayed using RealTime-Glo Assay. Error bars represent \pm SEM of 3 independent experiments.

4.4 Ectopic WT Bcl-3 overexpression increased Ki67 expression in -231-luc cells

To confirm whether the effects of reduced cell growth following overexpression as determined by the metabolism based viability assay was a result of reduced proliferation we stained for the proportion of cells undergoing cell division. Following immunofluorescent staining for the proliferative marker Ki67, overexpression of WT Bcl-3 resulted in a significant increase in the Ki67 population in MDA-MB-231-Luc cells. There were no significant changes in the MDA-MB-436 cell line though there was a slight trend for increased expression ($p=0.132$). Overexpression of the ANK mutant resulted in significant reductions of the Ki67 populations in both cell lines (**Fig. 4.4**).

4.5 Ectopic WT Bcl-3 overexpression increased pHH3 expression

To compliment our Ki67 results we also stained for phospho-histone H3 which specifically marks cells undergoing mitosis. This marker detects a smaller proportion of proliferating cells by targeting a narrower window within the cell cycle. Following immunofluorescent staining for the mitosis marker pHH3, overexpression of WT Bcl-3 resulted in an increase in the pHH3 population in both MDA-MB-231-Luc and MDA-MB-436 cell lines. Similarly to Ki67 expression in both of these TNBC cell lines, overexpression of the ANK binding mutant resulted in significantly reduced pHH3 expressions (**Fig. 4.5**).

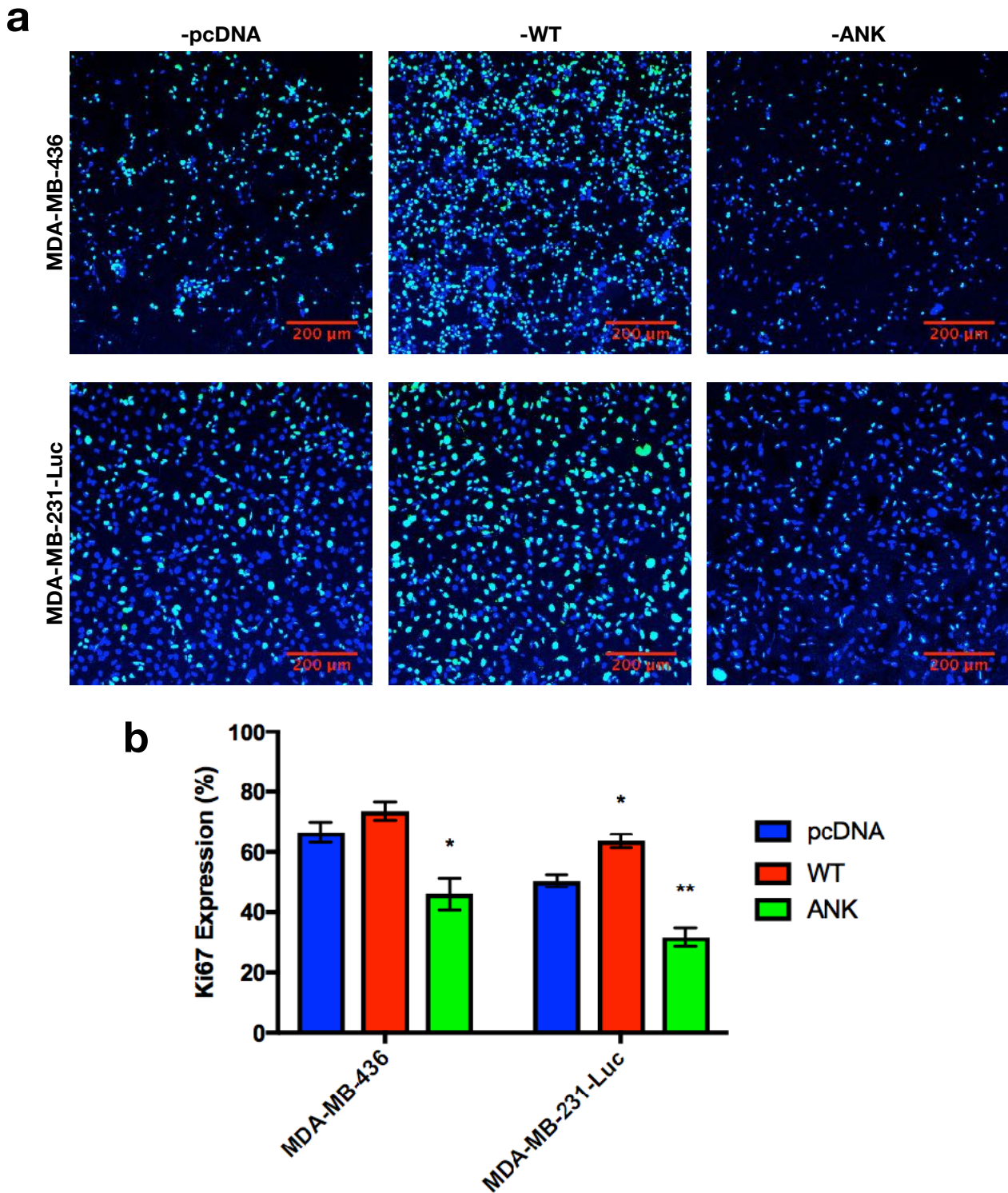


FIG. 4.4 ECTOPIC WT BCL-3 OVEREXPRESSION INCREASED KI67 EXPRESSION IN -231-LUC

Representative immunofluorescence images of **a**. MDA-MB-436 and MDA-MB-231-Luc cells stably expression WT Bcl-3, ANK mutant or pcDNA constructs were plated onto coverslips, PFA fixed and immunofluorescent-stained for Ki67. **b**. Graph comparing Ki67 expression between different cell lines and overexpression constructs. Error bars represent \pm SEM of 3 independent experiments. (T-test, *= $p < 0.05$, **= $p < 0.01$, ***= $p < 0.001$)

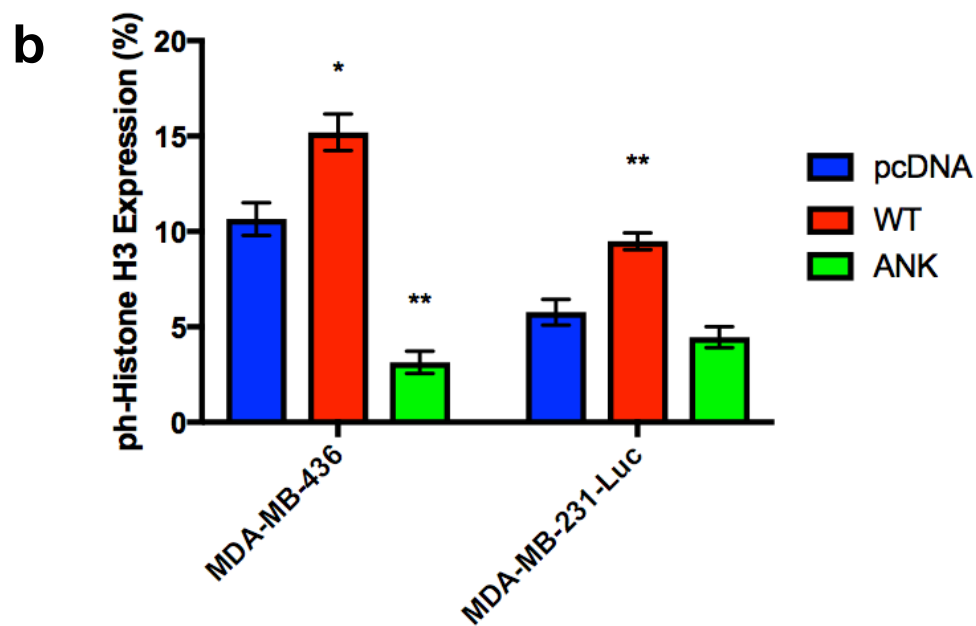
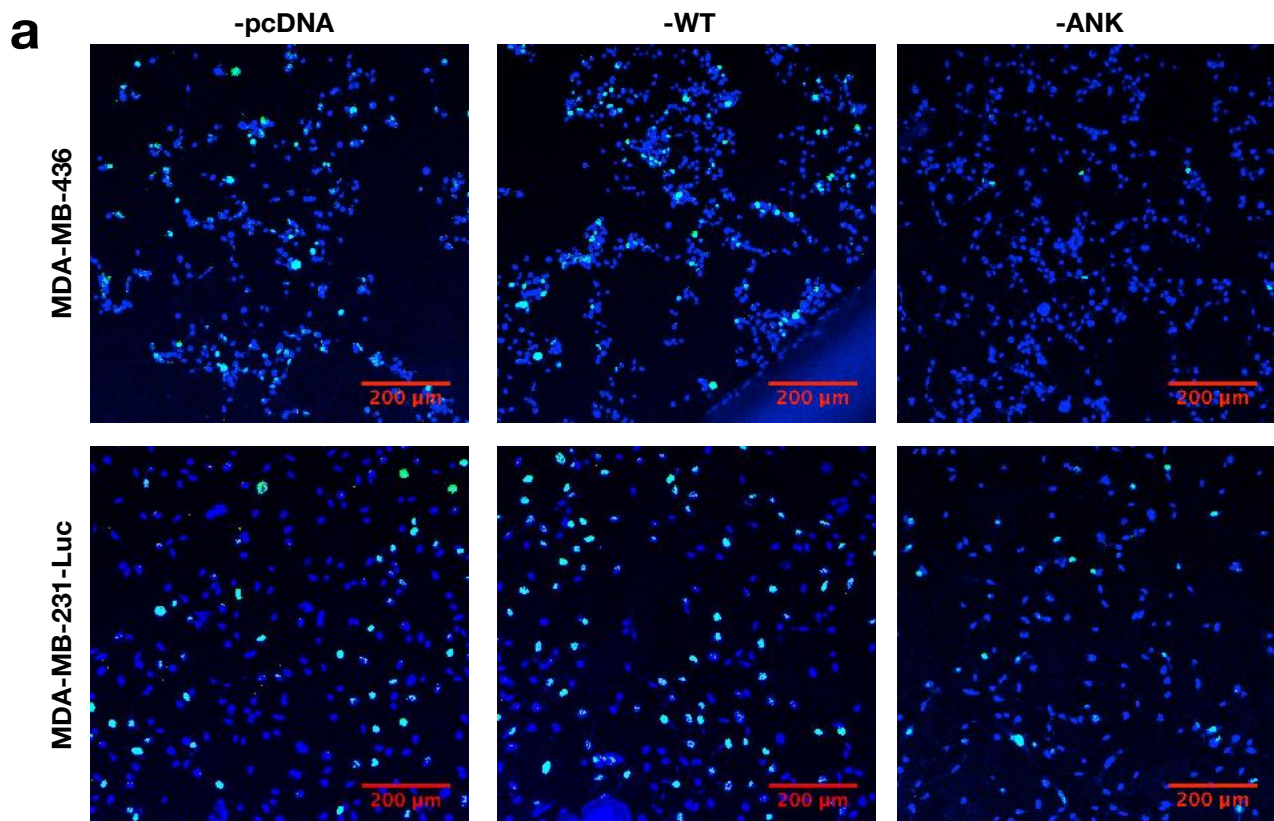


FIG. 4.5 ECTOPIC WT BCL-3 OVEREXPRESSION INCREASED PHH3 EXPRESSION

Representative immunofluorescence images of **a.** MDA-MB-436 and MDA-MB-231-Luc cells stably expression WT Bcl-3, ANK mutant or control pcDNA constructs were plated onto coverslips, PFA fixed and immunofluorescent-stained for pHH3. **b.** Graph comparing pHH3 expression between different cell lines and overexpression constructs. Error bars represent \pm SEM of 3 independent experiments. (T-test, *= $p < 0.05$, **= $p < 0.01$, ***= $p < 0.001$)

4.6 Effect of ectopic WT Bcl-3 overexpression on the cell cycle

By staining with fluorescent DAPI and quantifying total cellular DNA content we were able to discriminate between the different phases of the cell cycle. This provided us with additional information regarding the effect of Bcl-3 overexpression on the overall structure of the cell cycle. MDA-MB-436 and MDA-MB-231-Luc cells stably expressing WT Bcl-3, ANK mutant or control pcDNA constructs were permeabilised with NP-40 and stained with DAPI. Single-cell DNA content was measured using flow cytometry and cell cycle stages calculated. We were able to calculate a cell turnover index (CTI) reflective of the overall rate of cell growth as the ratio between the proliferative G2/M population to the apoptotic subG1 population.

4.6.1 Ectopic WT Bcl-3 overexpression in MDA-MB-436 increased the subG1 population and decreased the G0/G1 population

Overexpression of WT Bcl-3 in MDA-MB-436 resulted in a significant increase in the subG1 population which was balanced by a proportional reduction in the G0/G1 population. There was a trend of an increased G2/M population but the results were not significant ($p=0.140$). The CTI was calculated to be 0.688-fold significantly reduced compared to control ($p=0.0376$). Overexpression of the ANK mutant saw an increased subG1 population and decreased G0/G1 and G2/M populations. The CTI was calculated to be 0.372-fold significantly reduced compared to control ($p=0.001$) (**Fig. 4.6**).

4.6.2 Ectopic WT Bcl-3 overexpression in MDA-MB-231-Luc increased the subG1 population and decreased the G0/G1 population

Overexpression of WT Bcl-3 in MDA-MB-231-Luc resulted in a significant increase in the subG1 and G2/M populations which was balanced by a reduction in the G0/G1 population. The CTI was calculated to be 0.328-fold significantly reduced compared to control ($p=0.009$). Overexpression of the ANK mutant also resulted in an increased subG1 population and decreased G0/G1 and S populations. There was a trend of decreased G2/M but the results were not significant ($p=0.211$). The CTI was calculated to be 0.188-fold significantly reduced compared to control ($p=0.004$) (**Fig. 4.7**).

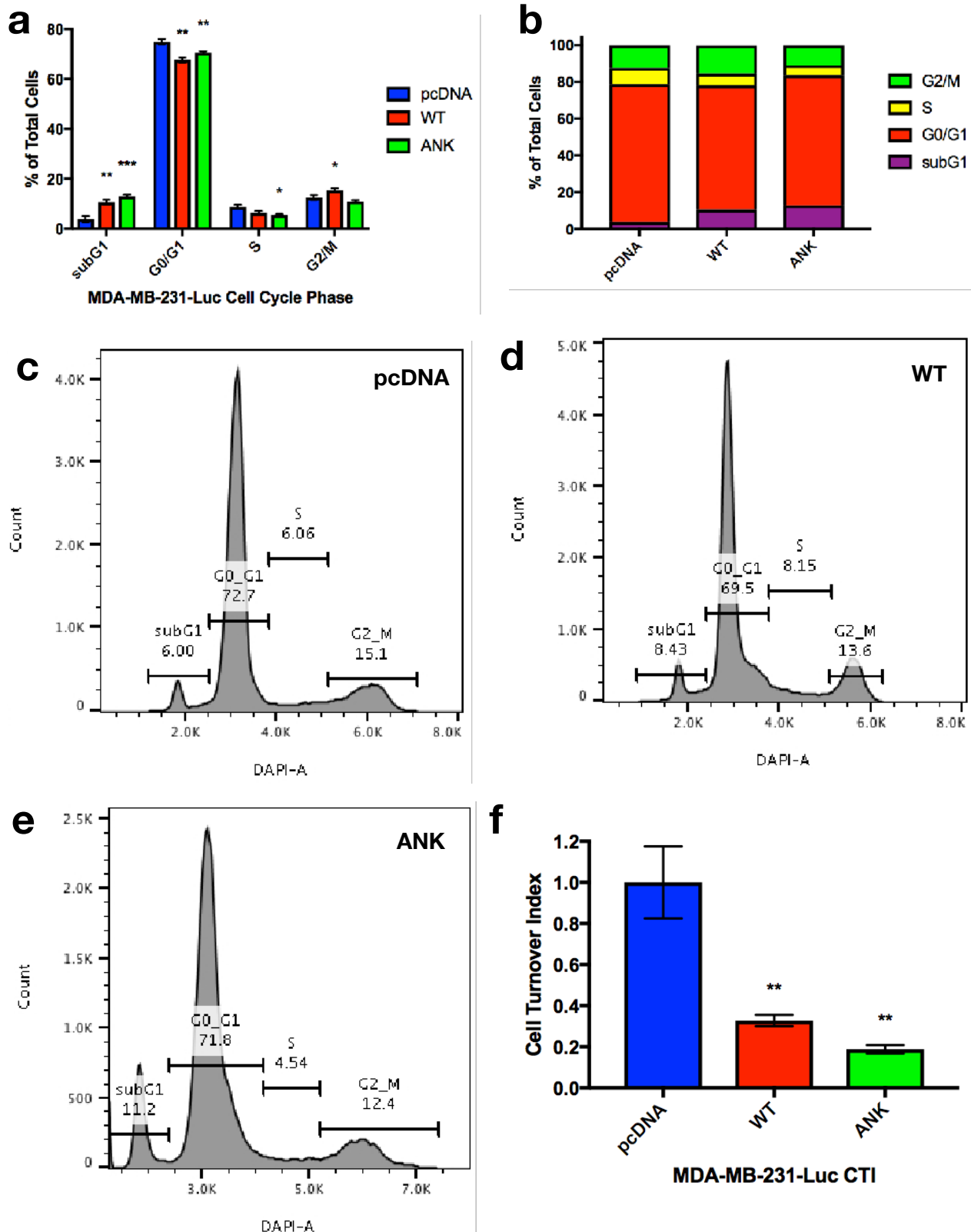


FIG. 4.6 ECTOPIC WT BCL-3 OVEREXPRESSION IN MDA-MB-436 INCREASED THE SUBG1 POPULATION AND DECREASED THE G0/G1 POPULATION

MDA-MB-436 cells stably expressing WT Bcl-3, ANK mutant or control pcDNA constructs were permeabilised with NP-40 and stained with DAPI. Single-cell DNA content was measured using flow cytometry and cell cycle stages calculated. **a.&b.** Percentage of cells in each cell cycle. **c.&d.&e.** Representative histograms detailing cell cycle stage distribution. **f.** Cell turnover index (CTI) calculated as the ratio of the proliferative G2/M population to the apoptotic subG1 population. Error bars represent \pm SEM of 3 independent experiments. (T-test, * p <0.05, ** p <0.01, *** p <0.001)

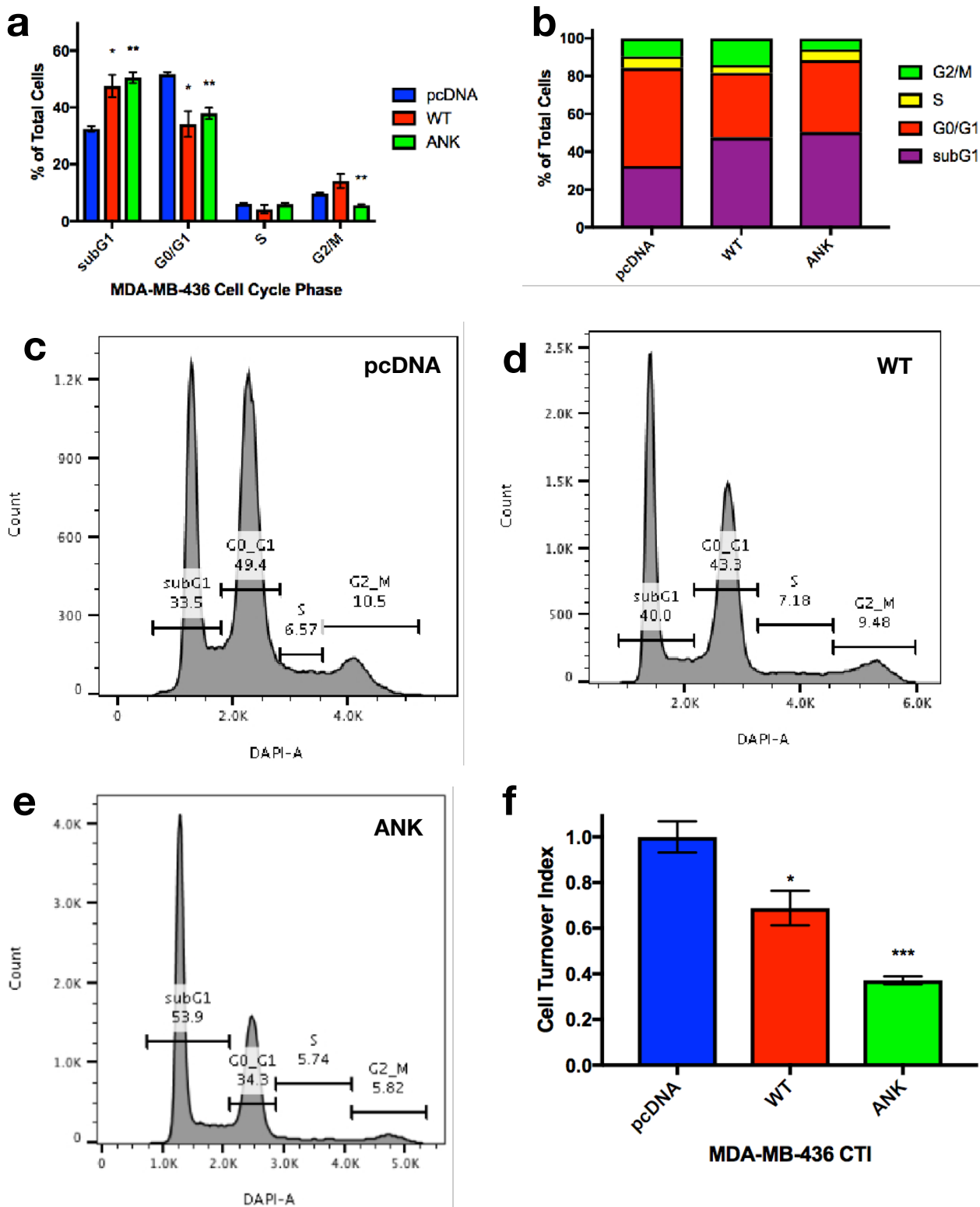


FIG. 4.7 ECTOPIC WT BCL-3 OVEREXPRESSION IN MDA-MB-231-LUC INCREASED THE SUBG1 AND G2/M POPULATIONS AND DECREASED THE G0/G1 POPULATION

MDA-MB-231-Luc cells stably expressing WT Bcl-3, ANK mutant or control pcDNA constructs were permeabilised with NP-40 and stained with DAPI. Single-cell DNA content was measured using flow cytometry and cell cycle stages calculated. **a.&b.** Percentage of cells in each cell cycle. **c.&d.&e.** Representative histograms detailing cell cycle stage distribution. **f.** Cell turnover index (CTI) calculated as the ratio of the proliferative G2/M population to the apoptotic subG1 population. Error bars represent \pm SEM of 3 independent experiments. (T-test, *= $p < 0.05$, **= $p < 0.01$, ***= $p < 0.001$)

4.7 Ectopic Bcl-3 overexpression increased caspase-3/7 activity

The presence of subG1 cell cycle populations is indicative of apoptotic bodies and we wanted another to quantify and validate the increased rate of apoptosis. MDA-MB-436 and MDA-MB-231-Luc cells stably expressing WT Bcl-3, ANK mutant or control pcDNA constructs were lysed and assayed for caspase-3/7 activity using the Caspase-Glo 3/7 assay (previously described in chapter 3.8). Ectopic overexpression of both WT Bcl-3 and the ANK mutant resulted in increased caspase 3/7 activity of roughly 1.5-fold for both MDA-MB-436 and MDA-MB-231-Luc cell lines (**Fig. 4.8**).

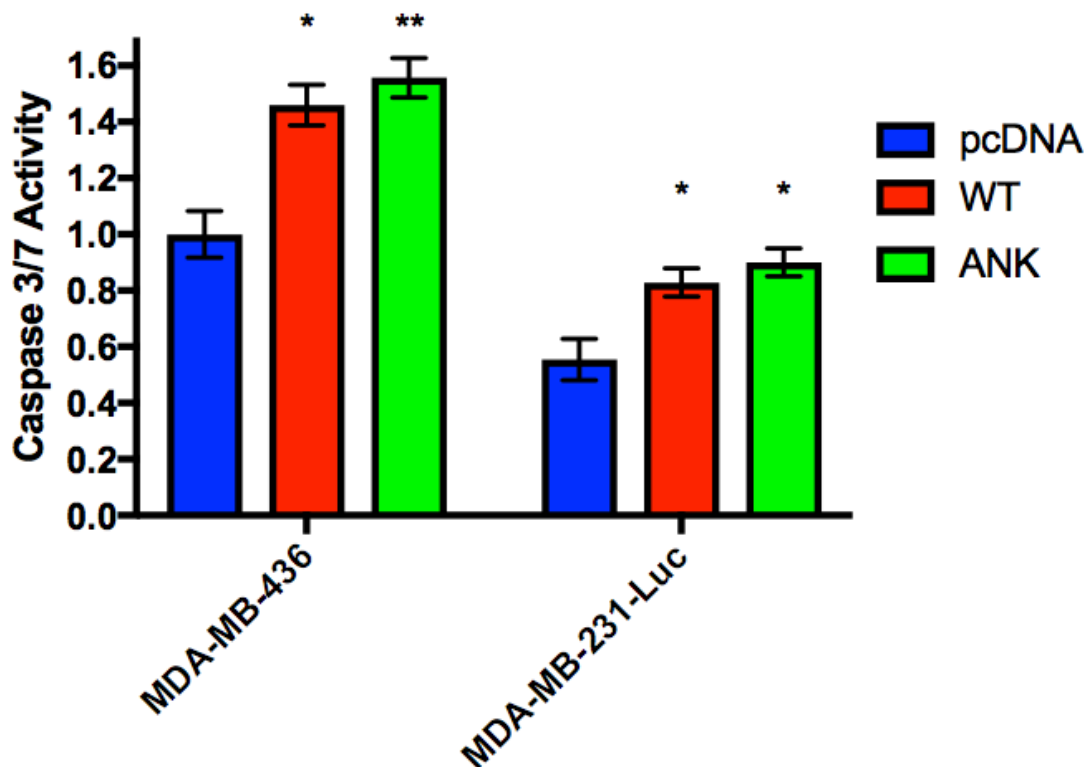


FIG. 4.8 ECTOPIC BCL-3 OVEREXPRESSION INCREASED CASPASE-3/7 ACTIVITY

MDA-MB-436 and MDA-MB-231-Luc cells stably expressing WT Bcl-3, ANK mutant or control pcDNA constructs were lysed and assayed for caspase-3/7 activity. Error bars represent \pm SEM of 3 independent experiments. (T-test, *= $p < 0.05$, **= $p < 0.01$, ***= $p < 0.001$)

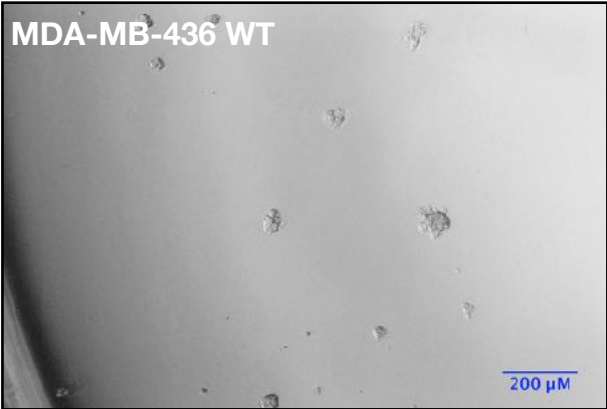
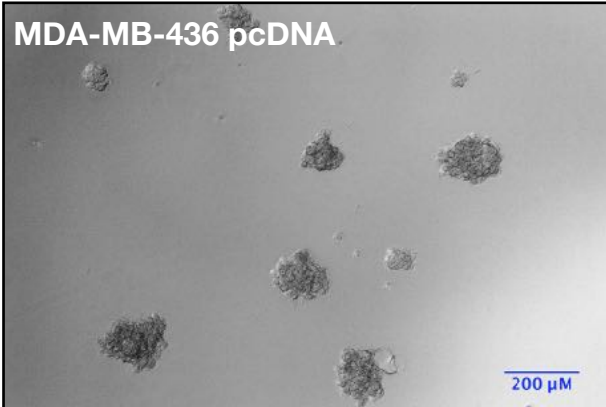
4.8 Ectopic Bcl-3 overexpression did not affect total mammosphere numbers but significantly reduced mammosphere size

We wanted to assess the whether Bcl-3 upregulation was able to promote anoikis resistance and increase the survival of a stem-like population as this attribute is commonly associated with oncogenicity. MDA-MB-436 and MDA-MB-231-Luc cells stably expressing WT Bcl-3, ANK mutant or control pcDNA constructs were disaggregated into single cells and plated into non-adherent mammosphere plates and cultured for 10 days and total mammosphere numbers and size quantified. Overexpression of both WT Bcl-3 and the ANK mutant in both TNBC cell lines did not affect total mammosphere numbers but resulted in significant reductions in average mammosphere size (**Fig. 4.9**).

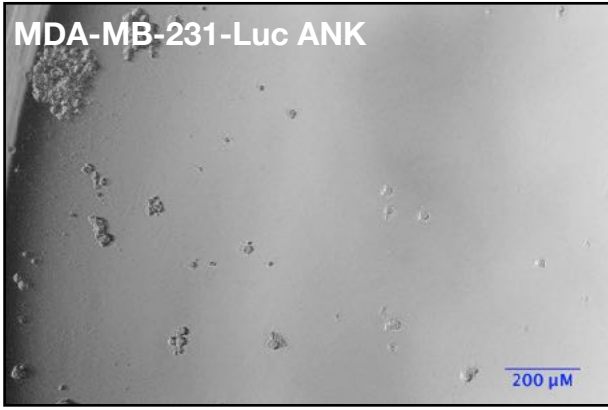
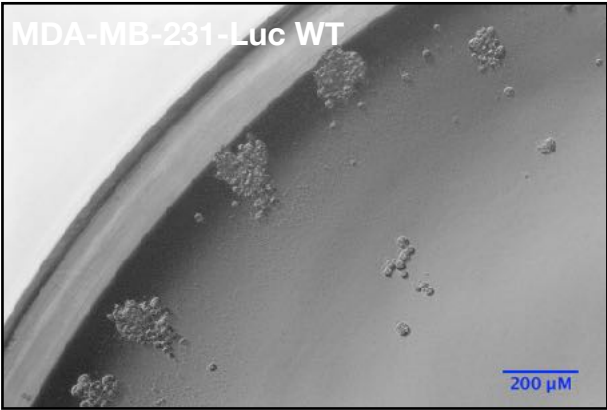
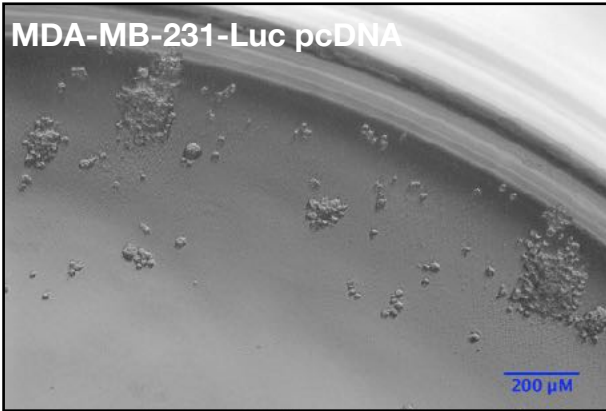
4.9 Ectopic Bcl-3 overexpression significantly impaired clonogenic survival

Clonogenic potential was tested by plating either MDA-MB-436 or MDA-MB-231-Luc cells stably expressing WT Bcl-3, ANK mutant or control pcDNA constructs at low density in a colony formation assay and cultured for 10 days. Colonies were then fixed with glutaraldehyde (6% v/v), stained with crystal violet (0.5% w/v), imaged using a plate scanner and colonies quantified. Overexpression of both WT Bcl-3 and the ANK mutant in both TNBC cell lines resulted in impaired clonogenic potential. There were significant reductions in both totally colony number, as well as average colony size with the effect being more pronounced in the ANK mutant (**Fig. 4.10**).

a



b



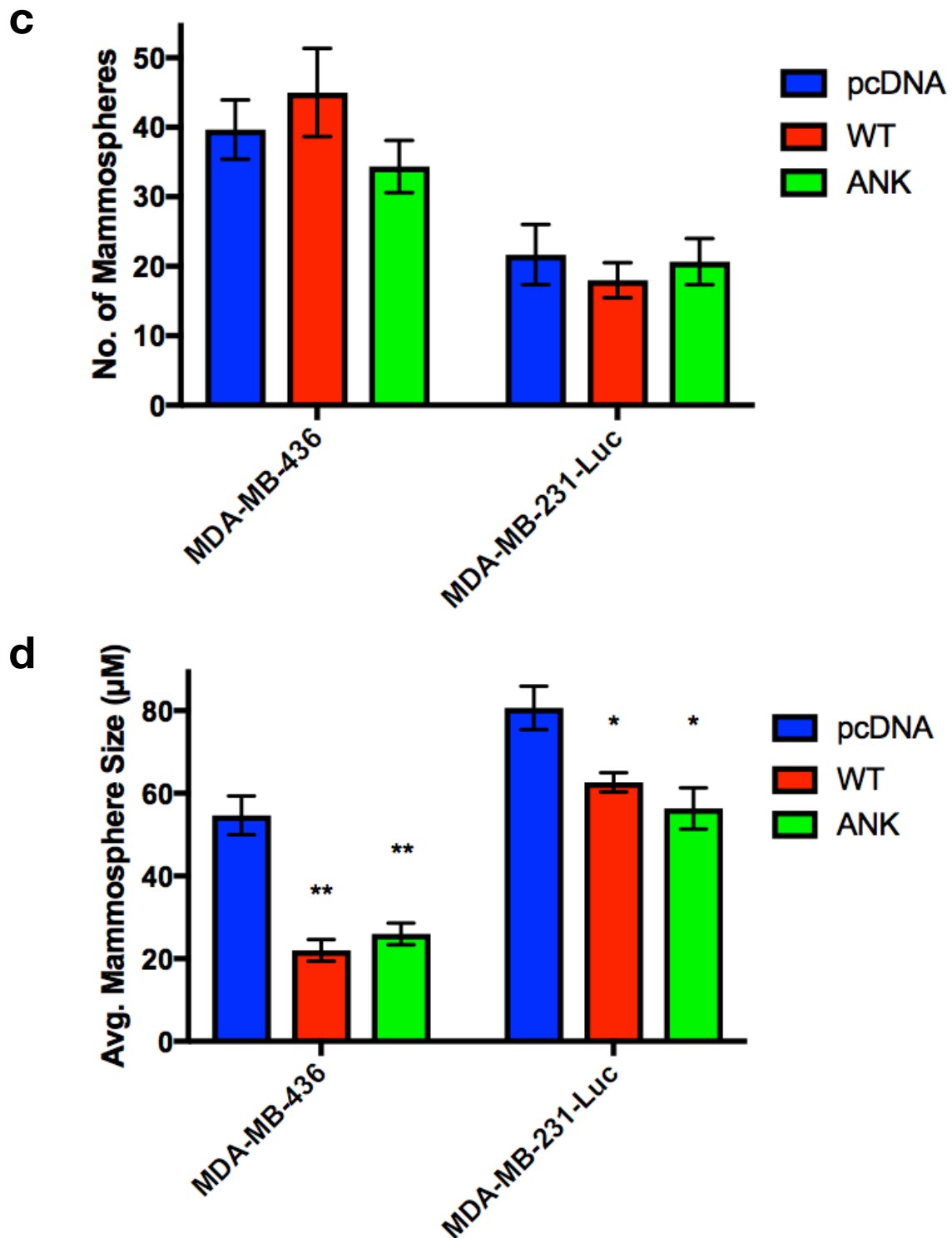


FIG. 4.9 ECTOPIC BCL-3 OVEREXPRESSION DID NOT AFFECT TOTAL MAMMOSPHERE NUMBERS BUT SIGNIFICANTLY REDUCED MAMMOSPHERE SIZE

MDA-MB-436 and MDA-MB-231-Luc cells stably expressing WT Bcl-3, ANK mutant or control pcDNA constructs were disaggregated into single cells and plated into non-adherent mammosphere plates and cultured for 10 days. Representative bright-field images for **a.** MDA-MB-436 **b.** MDA-MB-231-Luc **c.** Total mammosphere number. **d.** Average mammosphere size. Error bars represent \pm SEM of 3 independent experiments. (T-test, $*$ = $p < 0.05$, $**$ = $p < 0.01$, $***$ = $p < 0.001$)

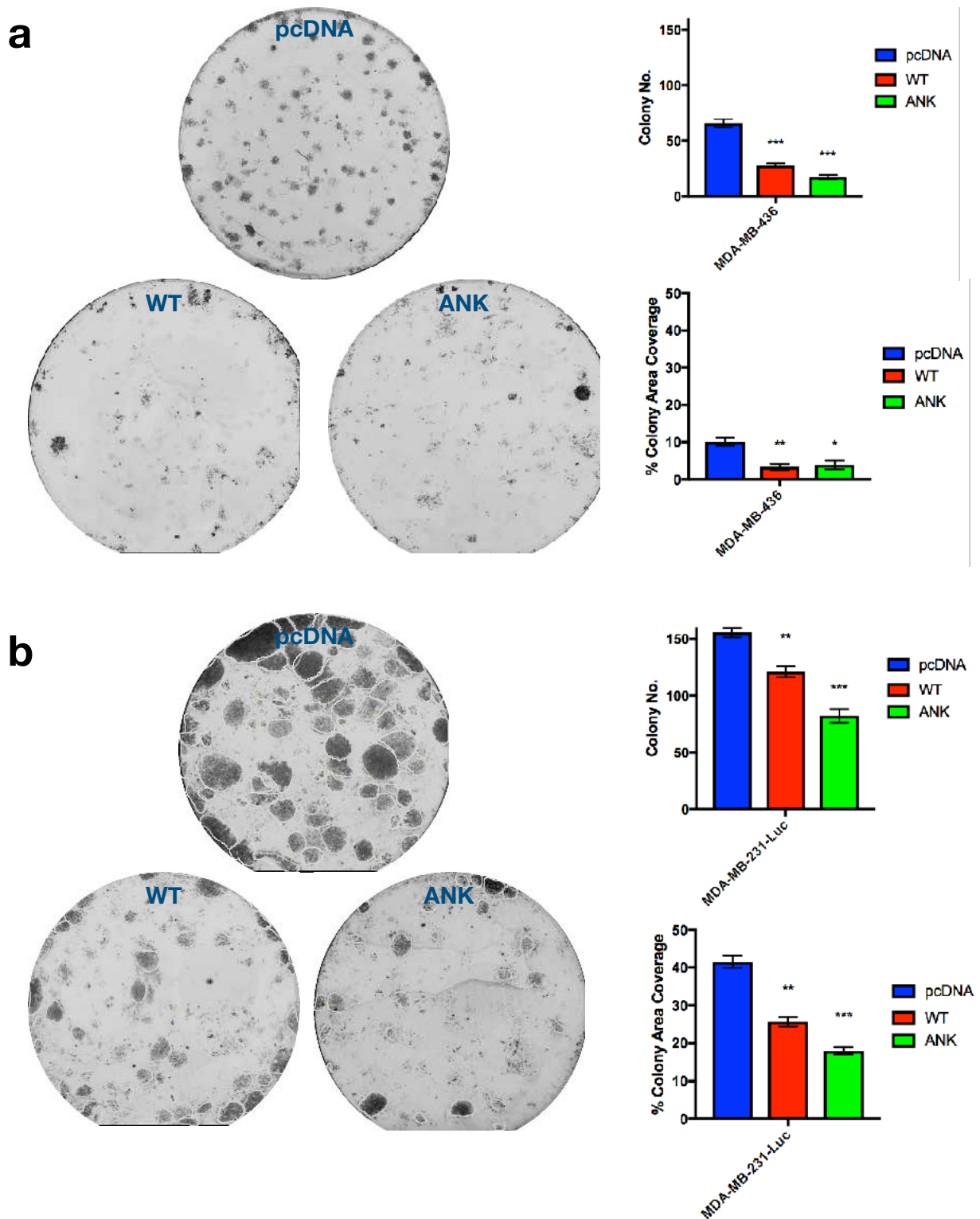


FIG. 4.10 ECTOPIC BCL-3 OVEREXPRESSION SIGNIFICANTLY IMPAIRED CLONOGENIC SURVIVAL
 Clonogenic potential was tested by plating either MDA-MB-436 or MDA-MB-231-Luc cells stably expressing WT Bcl-3, ANK mutant or control pcDNA constructs at low density in a colony formation assay and cultured for 10 days before being fixed and stained with crystal violet. Representative images, total colony number and average colony coverage for **a.** MDA-MB-436 **b.** MDA-MB-231-Luc. Error bars represent \pm SEM of 3 independent experiments. (T-test, $*=p<0.05$, $**=p<0.01$, $***=p<0.001$)

4.10 Effect of ectopic Bcl-3 overexpression on cellular migration

Similarly to the previous chapter 3.11, three different assays were used to assess the effect of Bcl-3 overexpression on collective, amoeboid-like and mesenchymal-like single cell migration in two TNBC cell lines.

4.10.1 Ectopic Bcl-3 overexpression significantly inhibited collective migration

The wound-healing assay was used to investigate collective migration in MDA-MB-436 and MDA-MB-231-Luc cells stably expressing WT Bcl-3, ANK mutant or control pcDNA constructs. Cells were cultured and a scratch was made on a confluent monolayer using a 200 μ L pipette tip and cells cultured for a further 48h. Bright-field microscopy images were captured at 12h, 24h, 36h and 48h time-points and percentage wound closure was calculated using ImageJ.

4.10.1.1 Ectopic Bcl-3 overexpression significantly inhibited collective migration in MDA-MB-436

Overexpression of both WT Bcl-3 and the ANK mutant resulted in an inhibition of collective migration over the course of 48h. The WT Bcl-3 and ANK mutant overexpression cell lines saw a 50% and 30% reduction respectively in wound closure capabilities by 48h (**Fig. 4.11**).

4.10.1.2 Ectopic Bcl-3 overexpression significantly inhibited collective migration in MDA-MB-231-Luc

Overexpression of both WT Bcl-3 and the ANK mutant resulted in an inhibition of collective migration over the course of 48h. The WT Bcl-3 and ANK mutant overexpression cell lines saw a 50% and 65% reduction respectively in wound closure capabilities by 48h (**Fig. 4.12**).

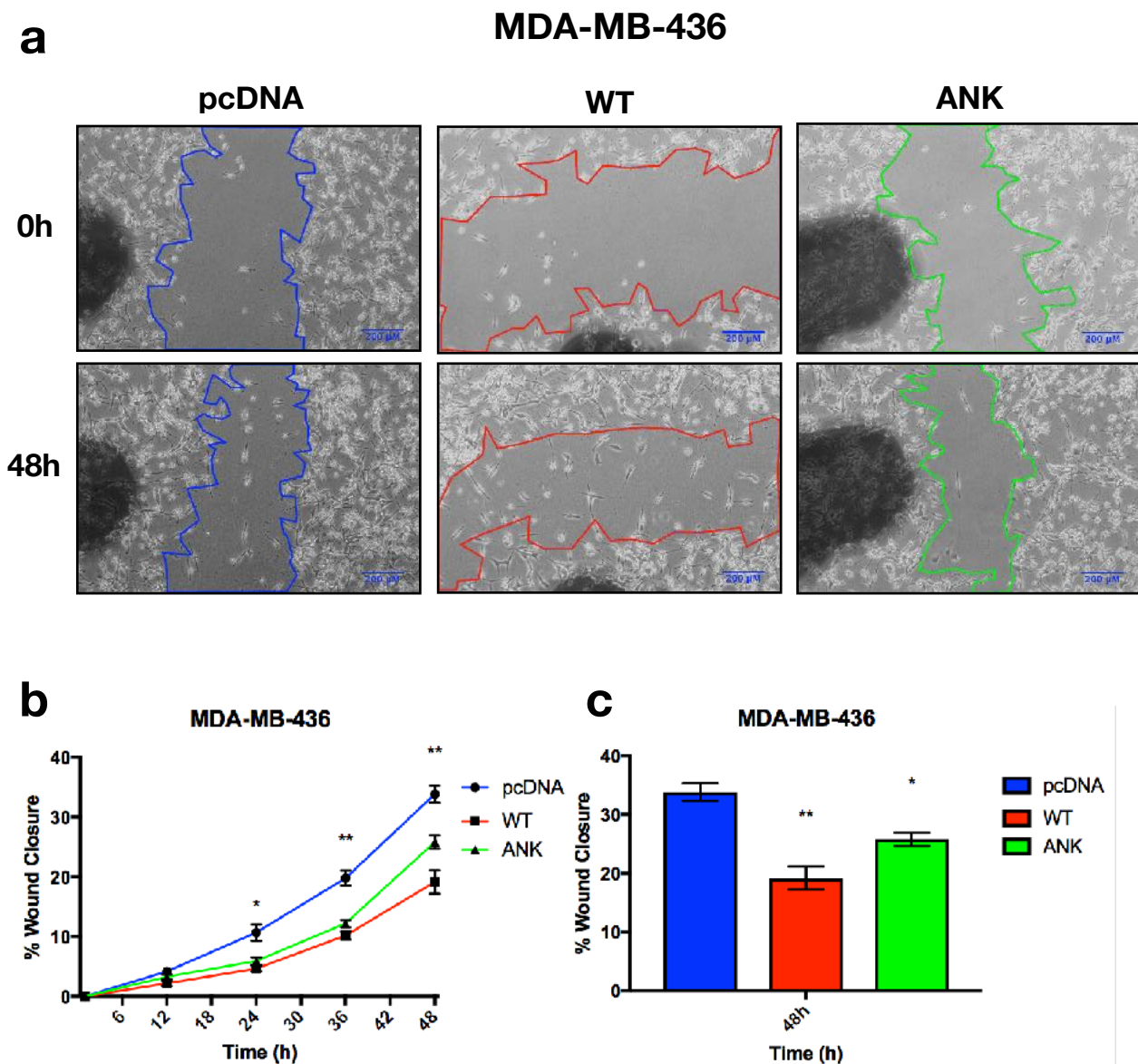


FIG. 4.11 ECTOPIC BCL-3 OVEREXPRESSION SIGNIFICANTLY INHIBITED COLLECTIVE MIGRATION IN MDA-MB-436

The wound-healing assay was used to investigate collective migration in MDA-MB-436 cells stably expressing WT Bcl-3, ANK mutant or control pcDNA constructs. A scratch was made on a confluent monolayer using a 200 μ L pipette tip and cells cultured for 48h with images being taken every 12h. **a.** Representative images showing the scratch at 0h and 48h. **b.** Total scratch area quantified using ImageJ and % wound closure calculated for 12h, 24h, 36h and 48h time-points. **c.** % wound closure at 48h time-point. Error bars represent \pm SEM of 3 independent experiments. (T-test, *= $p < 0.05$, **= $p < 0.01$, ***= $p < 0.001$)

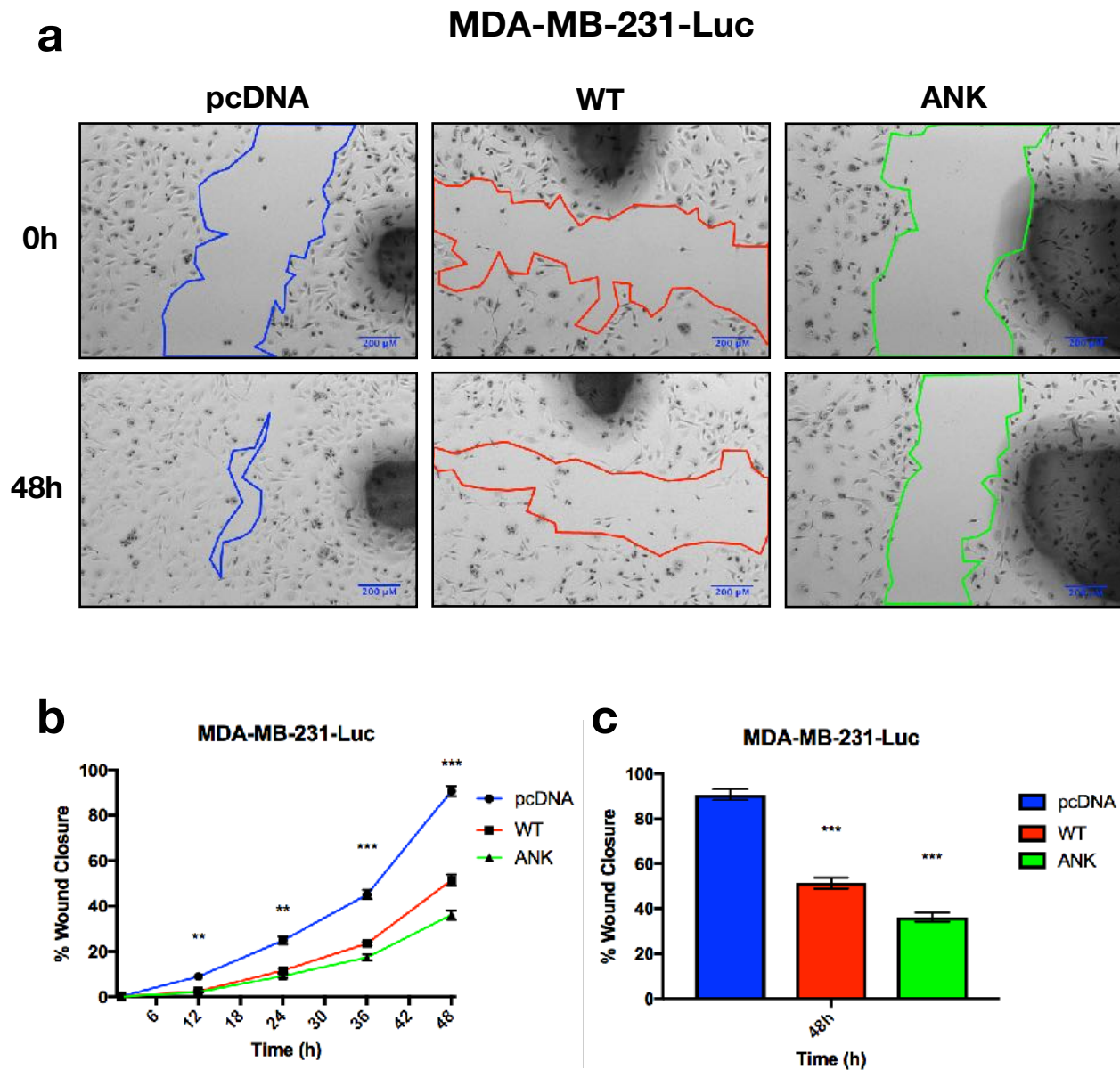


FIG. 4.12 ECTOPIC BCL-3 OVEREXPRESSION SIGNIFICANTLY INHIBITED COLLECTIVE MIGRATION IN MDA-MB-231-LUC

The wound-healing assay was used to investigate collective migration in MDA-MB-231-Luc cells stably expressing WT Bcl-3, ANK mutant or control pcDNA constructs. A scratch was made on a confluent monolayer using a 200 μ L pipette tip and cells cultured for 48h with images being taken every 12h. **a.** Representative images showing the scratch at 0h and 48h. **b.** Total scratch area quantified using ImageJ and % wound closure calculated for 12h, 24h, 36h and 48h time-points. **c.** % wound closure at 48h time-point. Error bars represent \pm SEM of 3 independent experiments. (T-test, *= p <0.05, **= p <0.01, ***= p <0.001)

4.10.2 Ectopic WT Bcl-3 overexpression increased amoeboid-like single cell migration

The FluoroBlok assay (described in chapter 3.11.2) was used to investigate amoeboid-like migration of MDA-MB-436 and MDA-MB-231-Luc cells stably expressing WT Bcl-3, ANK mutant or control pcDNA constructs. Cells were plated into the top well of a FluoroBlok assay plate and left to migrate for 24h across a chemotactic gradient. Cells were then stained with calcein AM and fluorescence intensity at 500nm was quantified by a bottom-reading plate reader. Overexpression of WT Bcl-3 resulted in a 20-30% increase in fluorescence intensity while the ANK mutant resulted in a 25-40% reduction (**Fig. 4.13**).

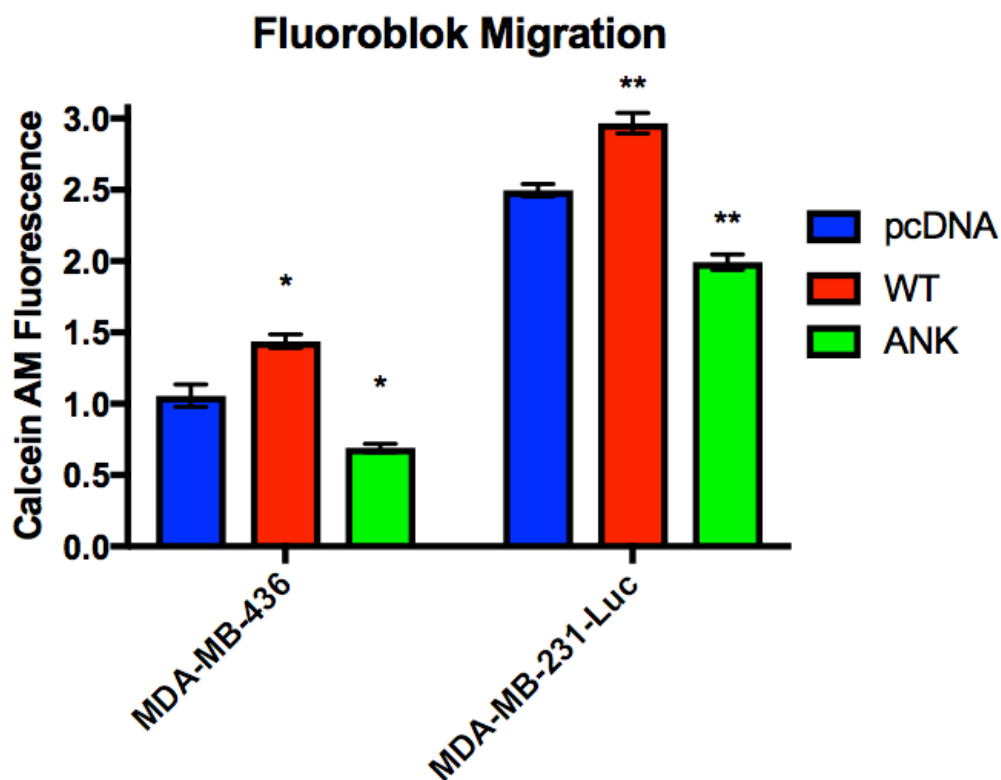


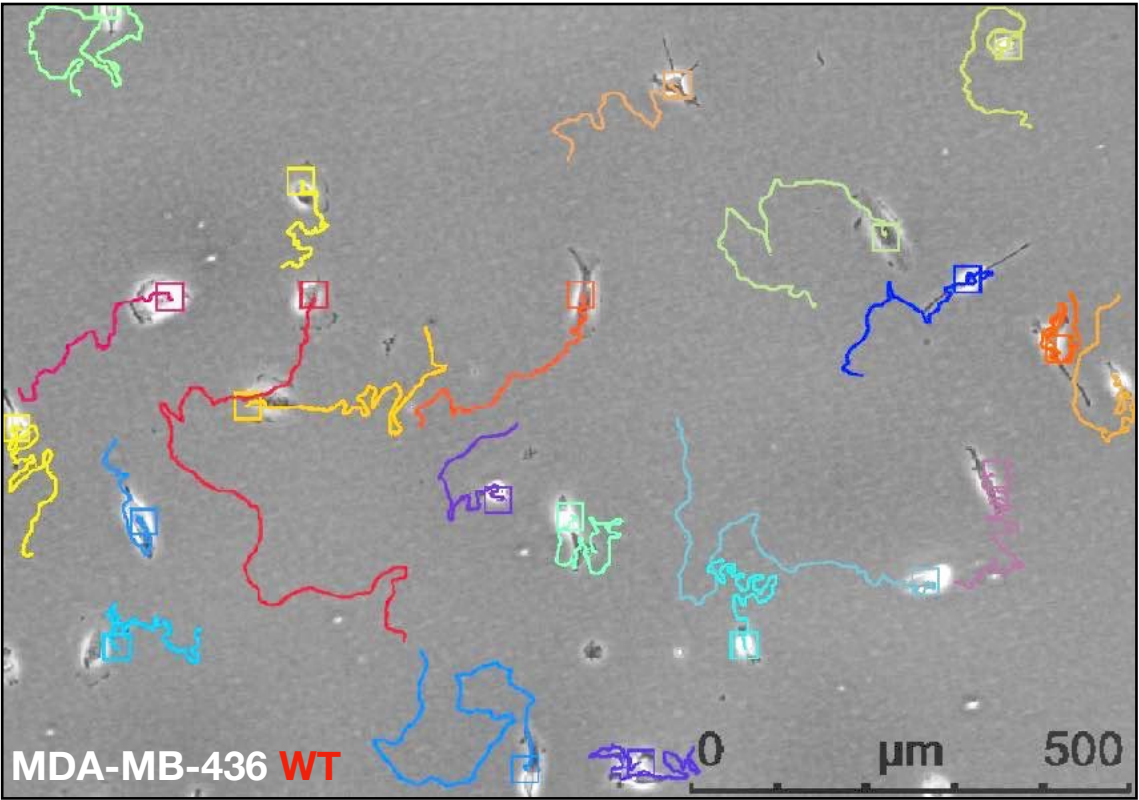
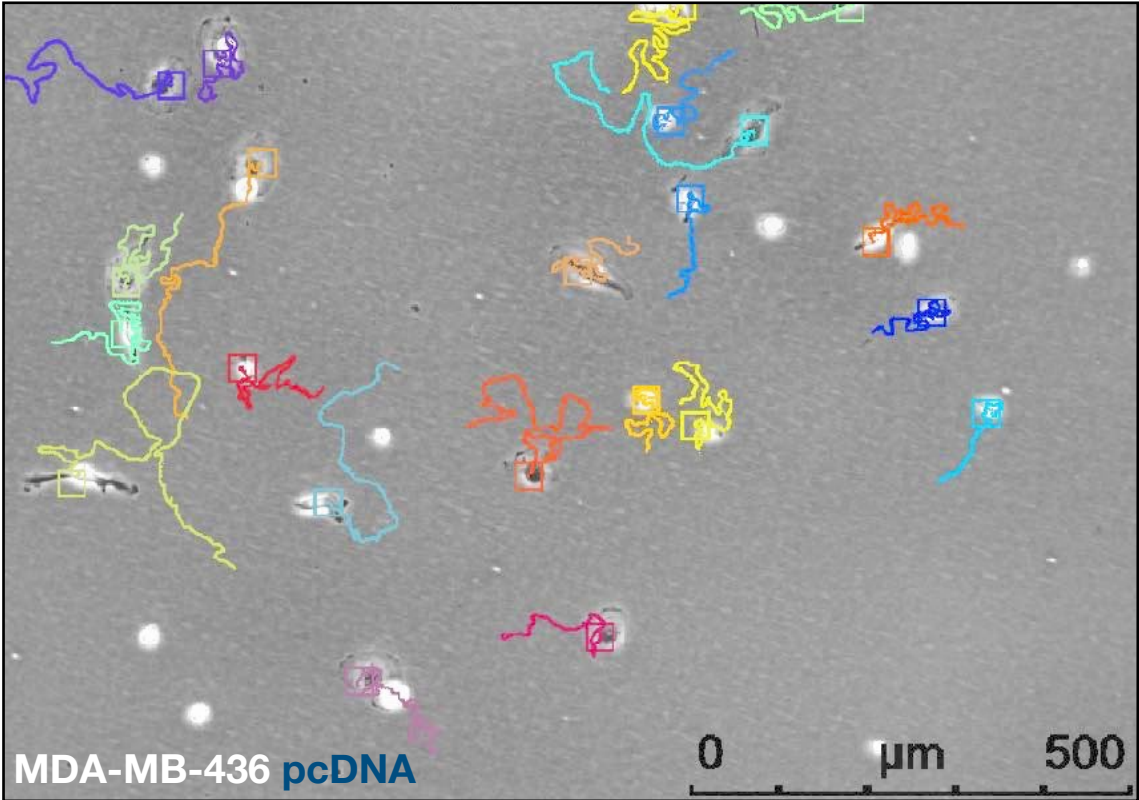
FIG. 4.13 ECTOPIC WT BCL-3 OVEREXPRESSION INCREASED AMOEBOID-LIKE SINGLE CELL MIGRATION

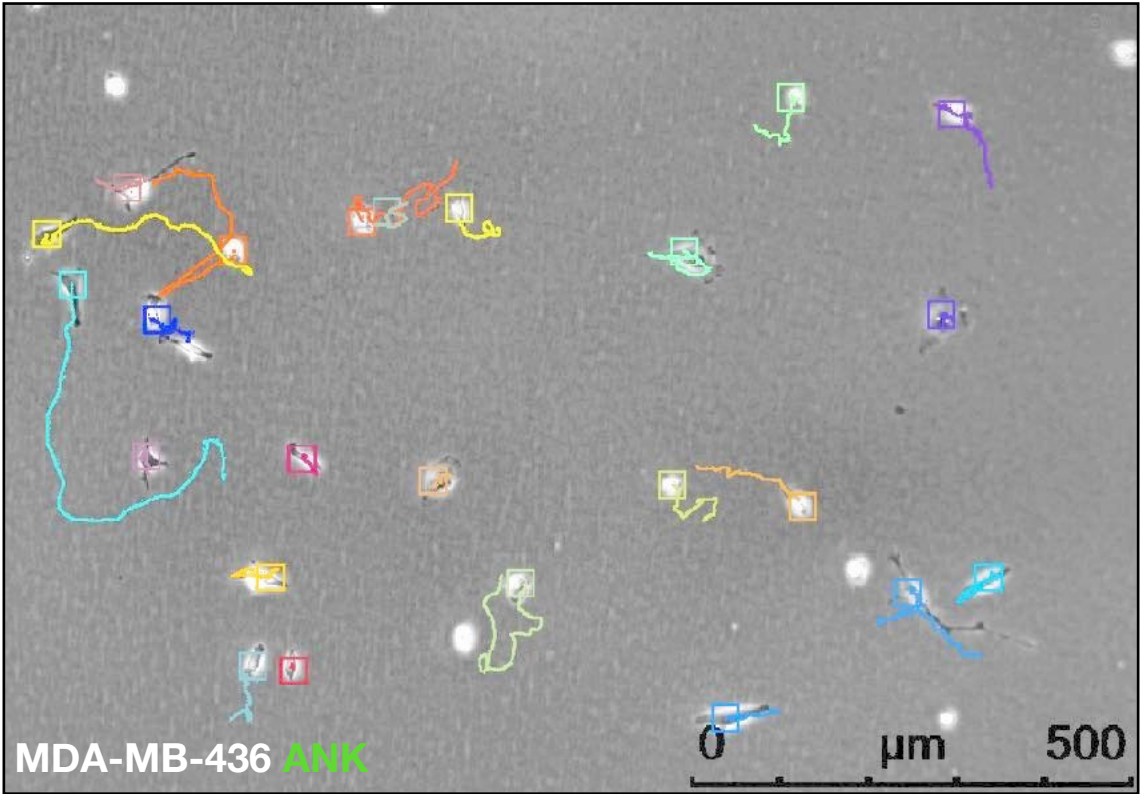
The FluoroBlok assay was used to investigate amoeboid-like migration of cell line panel. MDA-MB-436 and MDA-MB-231-Luc cells stably expressing WT Bcl-3, ANK mutant or control pcDNA constructs were plated into the top well of a FluoroBlok assay plate and left to migrate for 24h across a chemotactic gradient. Cells were stained with calcein AM and fluorescence intensity at 500nm was quantified by a bottom-reading plate reader. Error bars represent \pm SEM of 3 independent experiments. (T-test, *= $p < 0.05$, **= $p < 0.01$, ***= $p < 0.001$)

4.10.3 Ectopic Bcl-3 overexpression significantly increased mesenchymal-like single cell migration in the -231-Luc cell line

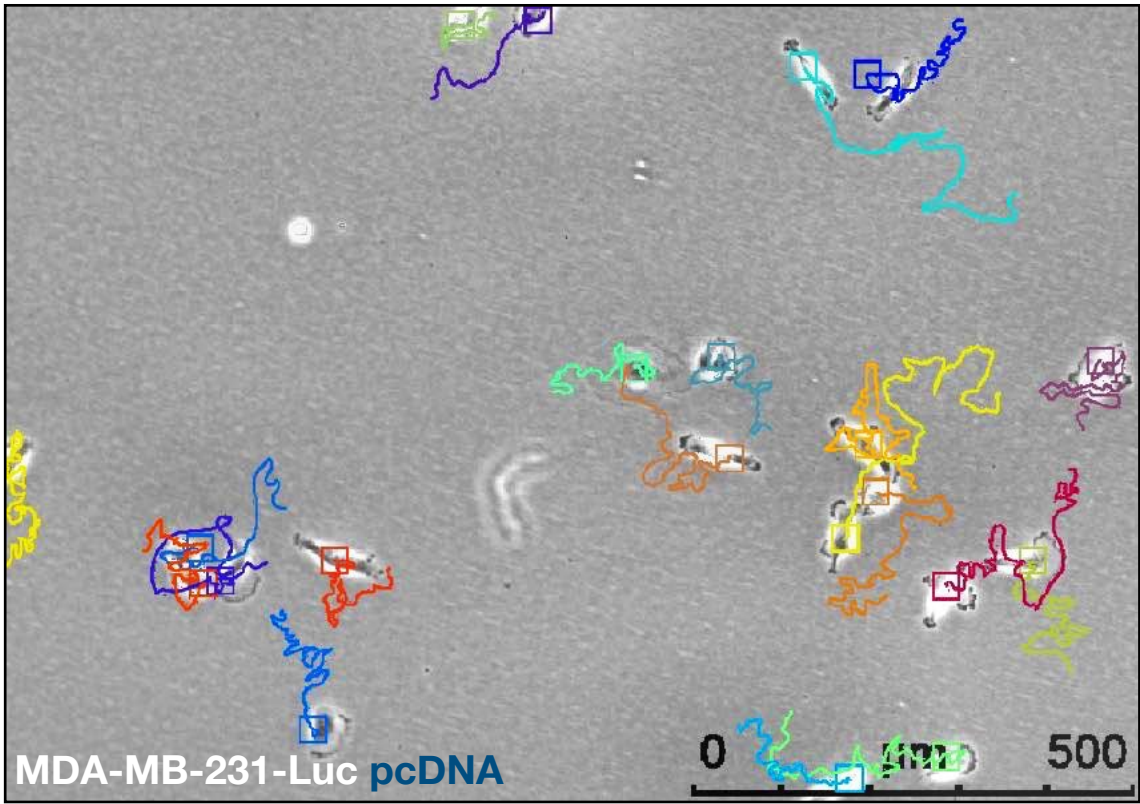
The single cell migration assay was used to investigate 2D motility of MDA-MB-436 and MDA-MB-231-Luc cells stably expressing WT Bcl-3, ANK mutant or control pcDNA constructs. Cells were plated at low densities and single cell migration quantified by tracking the motility path of each cell using a time-lapse incubator chamber over the course of 12h with images captured every 10 min. Overexpression of WT Bcl-3 resulted in a 15% increase in average distance travelled over the course of 12h in the -231-luc cell line, while the ANK mutant resulted in a 40-50% reduction in average distance travelled for both TNBC cell lines (**Fig. 4.14d**).

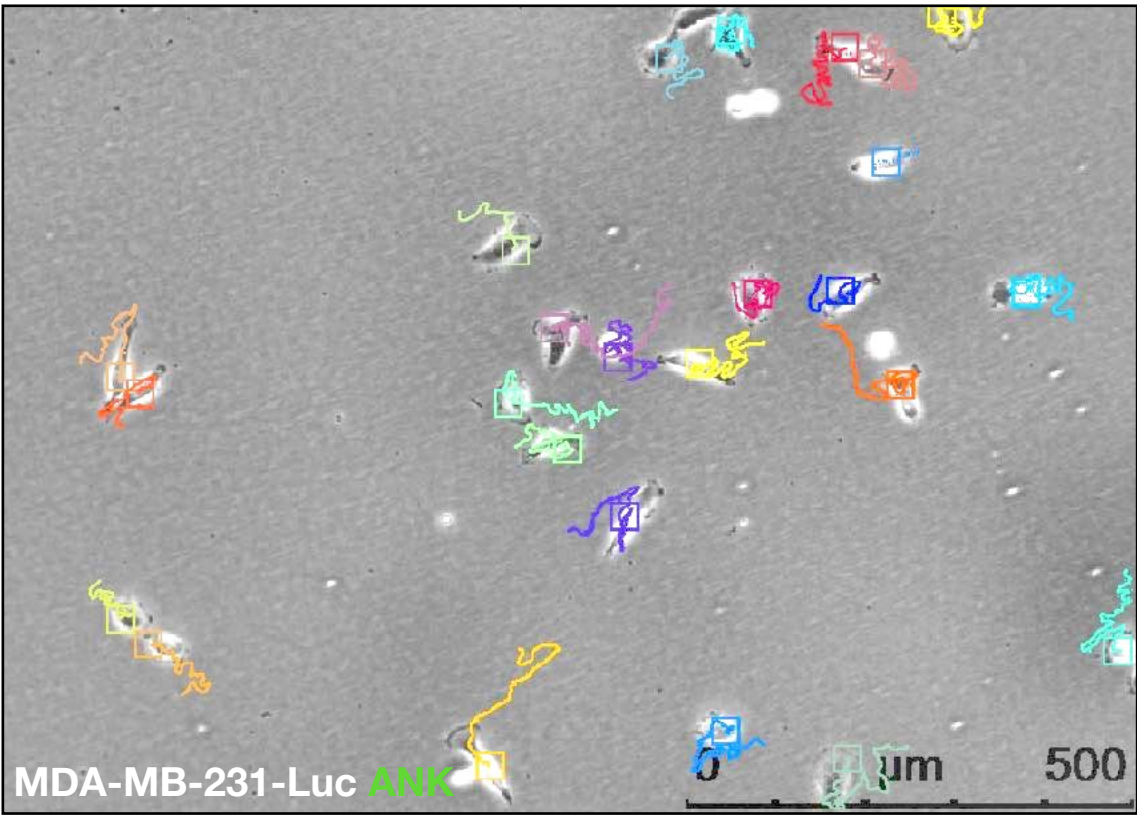
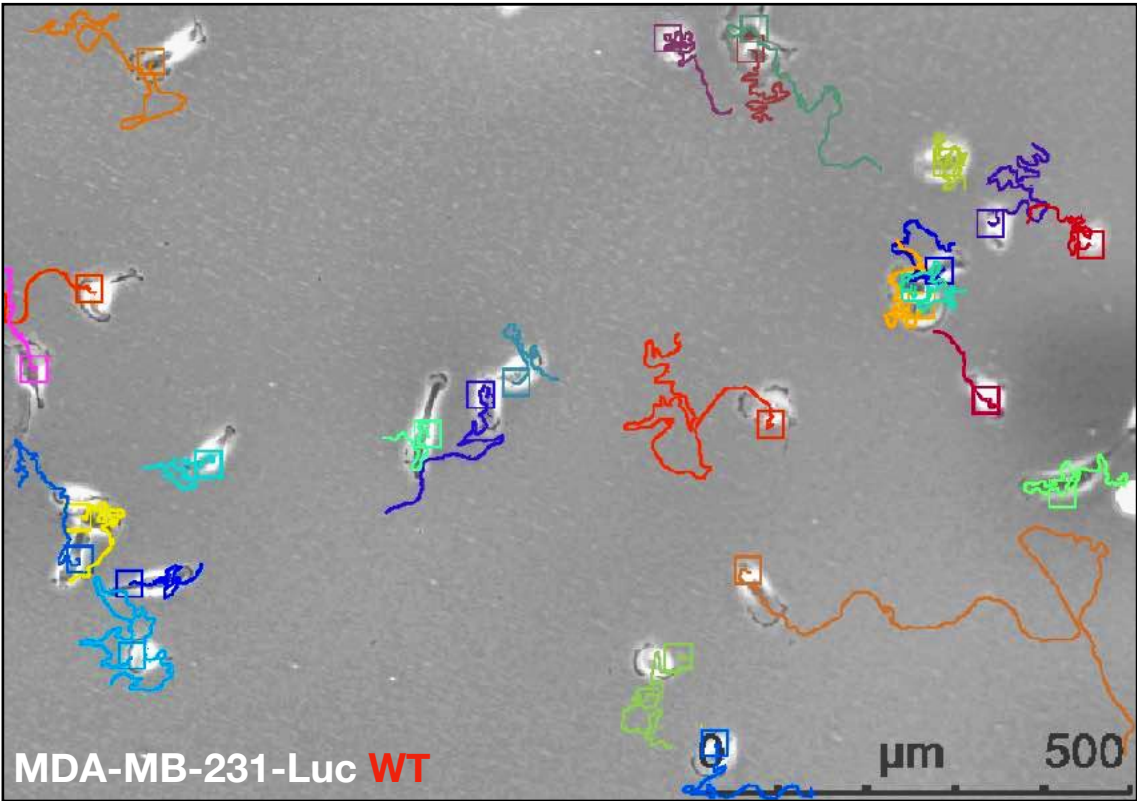
a





b





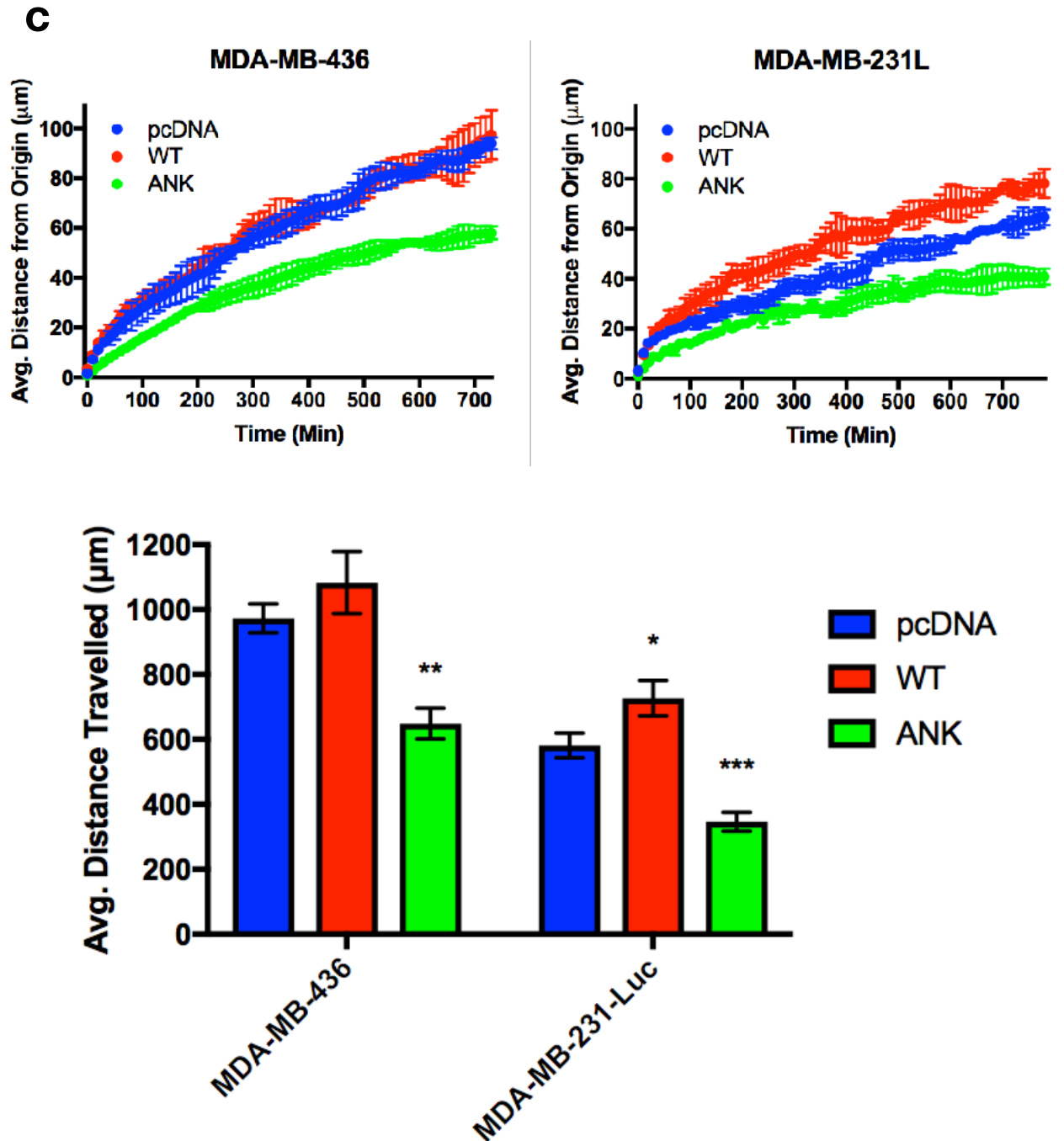


FIG. 4.14 ECTOPIC BCL-3 OVEREXPRESSION SIGNIFICANTLY INCREASED MESENCHYMAL-LIKE SINGLE CELL MIGRATION IN THE -231-LUC CELL LINE

The single cell migration assay was used to investigate 2D motility of MDA-MB-436 and MDA-MB-231-Luc cells stably expressing WT Bcl-3, ANK mutant or control pcDNA constructs. Cells were plated at low densities and single cell migration quantified using a time-lapse incubator chamber over the course of 12h with images captured every 10 min. Representative images of motility paths of single cells over 12h for **a.** MDA-MB-436 and **b.** MDA-MB-231-Luc cell lines. **c.** Average distance travelled away from origin. **d.** Average distance travelled after 12h. Error bars represent \pm SEM of 3 independent experiments. (T-test, *= $p < 0.05$, **= $p < 0.01$, ***= $p < 0.001$)

4.11 Ectopic overexpression of WT Bcl-3 increased NFkB activity

Since Bcl-3 is known to act through NFkB pathways (Bours et al., 1993) we wanted to verify the effect of overexpression on NFkB transcription activity. A luciferase NFkB reporter plasmid was used to quantify NFkB levels in MDA-MB-436 and MDA-MB-231-Luc cells stably expressing WT Bcl-3, ANK mutant or control pcDNA constructs. Cells were transfected with the reporter plasmid, LacZ control plasmid and cultured for 24h. Cells were then lysed and NFkB activity measured as luminescence readout using a plate reader. NFkB activity was then normalised to LacZ luminescence to control for transfection efficiency. Overexpression of WT Bcl-3 resulted a 20% increase in NFkB activity in both TNBC cell lines, while the ANK mutant resulted in a 30-40% decrease in NFkB activity (**Fig. 4.15**).

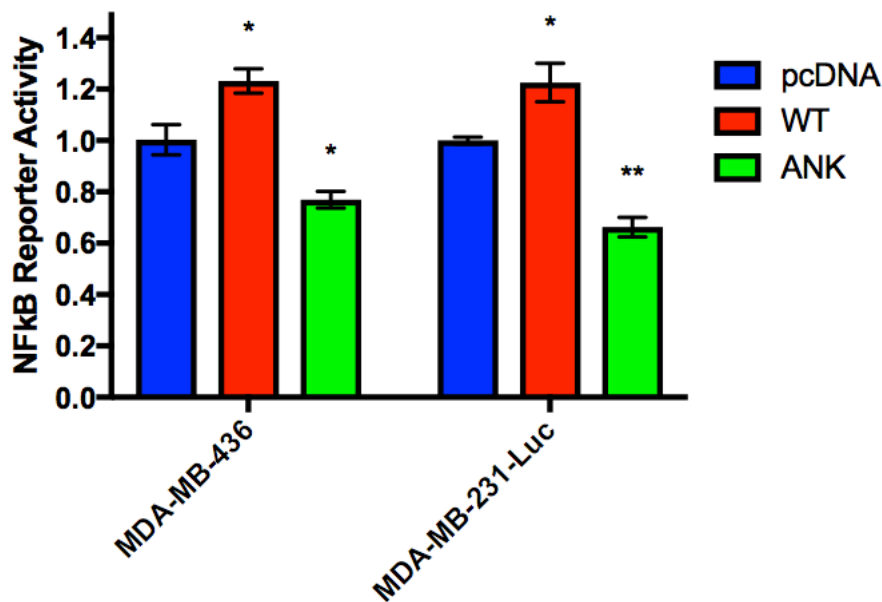


FIG. 4.15 ECTOPIC OVEREXPRESSION OF WT BCL-3 INCREASED NFkB ACTIVITY

A luciferase NFkB reporter plasmid was used to quantify NFkB levels in MDA-MB-436 and MDA-MB-231-Luc cells stably expressing WT Bcl-3, ANK mutant or control pcDNA constructs. Cells were transfected with the luciferase NFkB reporter plasmid, LacZ control plasmid and cultured for 24h. Cells were then lysed and NFkB activity measured as luminescence readout using a plate reader. NFkB activity was then normalised to LacZ luminescence to control for transfection efficiency. Error bars represent \pm SEM of 3 independent experiments. (T-test, *= $p < 0.05$, **= $p < 0.01$, ***= $p < 0.001$)

4.12 Effect of ectopic Bcl-3 overexpression in murine xenograft metastasis models

Several options were considered when developing relevant xenograft models including the site of injection and implantation. Orthotopic xenografts offers a complementary stromal microenvironment. Injecting into the mammary fat pad is a relatively simple procedure and allows for visible and measurable growth of our TNBC cell lines. But it is always worth noting there are distinct differences between the human and rodent mammary stroma and hormonal environments.

MDA-MB-231 cells stably expressing WT Bcl-3, ANK mutant or control pcDNA constructs were injected either orthotopically into both abdominal mammary fat pads bilaterally (1×10^6 cells in $100 \mu\text{l}$) or intravenously via the lateral tail vein (2×10^5 cells in $100 \mu\text{l}$) in 6 week old female Hsd: Athymic Nude-Foxn 1^{nu} mice (Harlan Laboratories). Orthotopic tumour growth was measured by palpation over 42 days and intravenous xenograft recipients were culled and necropsy performed at 45 days post surgery. Harvested xenograft tissue was then formalin fixed, embedded in paraffin blocks and H&E slides generated for histological analysis.

4.12.1 Ectopic overexpression of Bcl-3 exhibited a trend of reduced growth rates at the orthotopic site

Quantification of orthotopic MDA-MB-231 tumours revealed that overexpression of both WT Bcl-3 and the ANK mutant resulted in a trend of reduced growth rates compared to the pcDNA control over the course of 42 days. Final average tumour volumes for pcDNA control was 848mm^3 , WT Bcl-3 was 458mm^3 and ANK mutant was 524mm^3 (**Fig. 4.16**). The latency of tumour formation was noted by the first day post-surgery a palpable tumour was detectable and measured was found to be day 12 for the pcDNA control, day 14 for the WT Bcl-3 and day 17 for the ANK mutant.

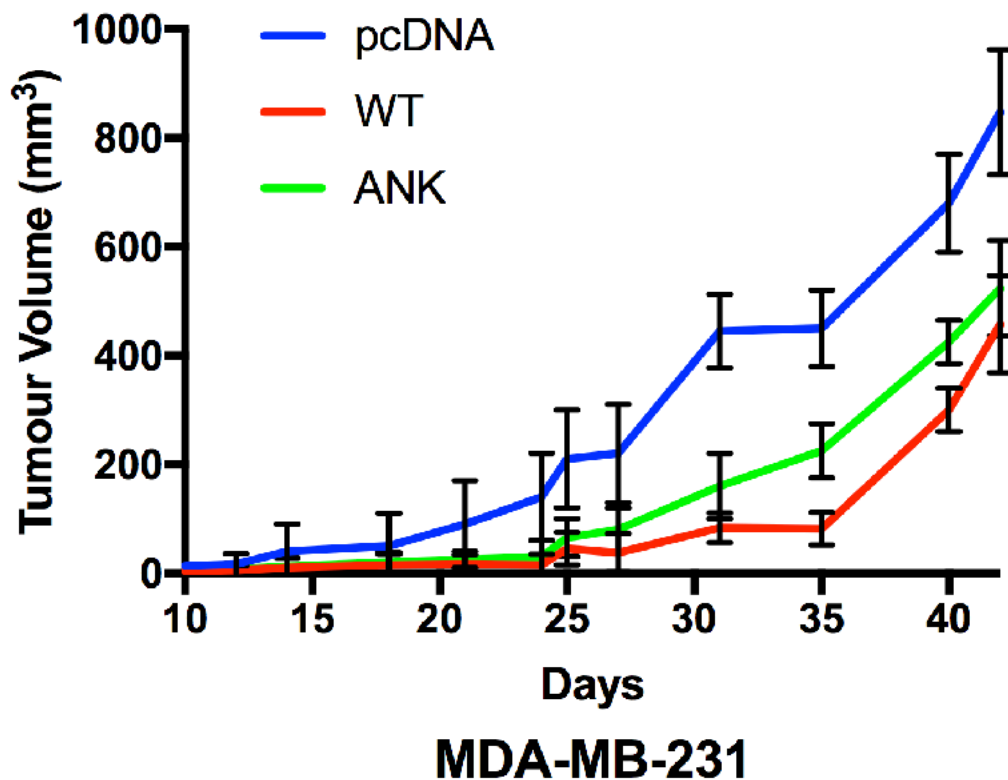


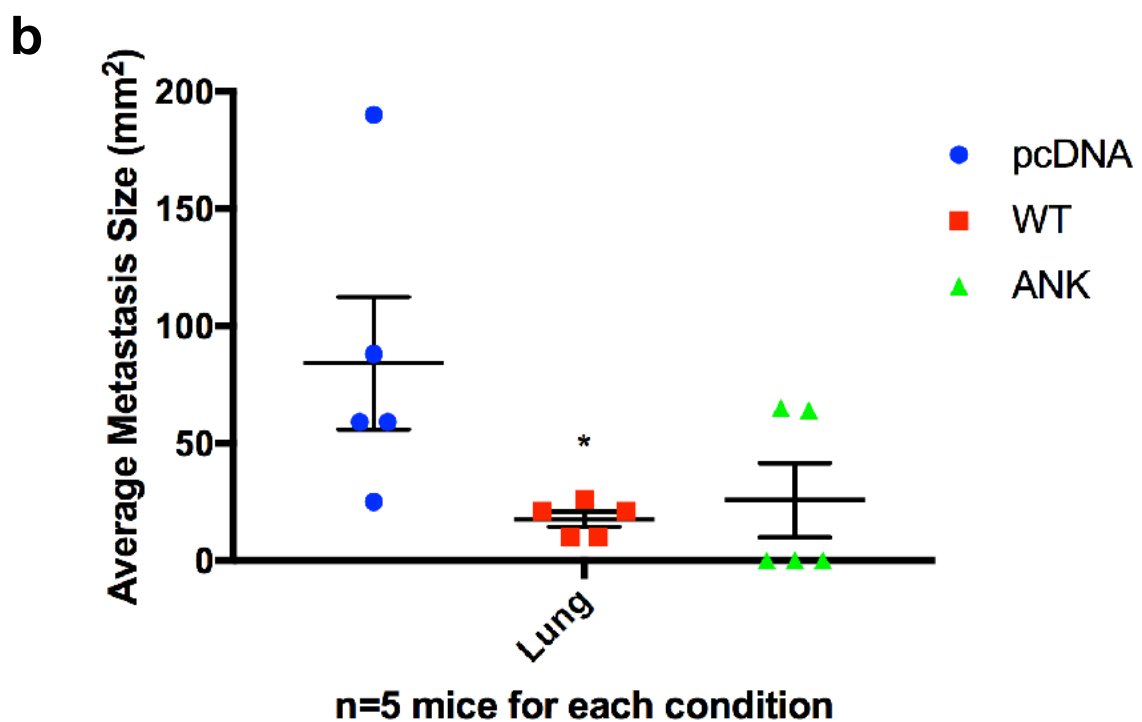
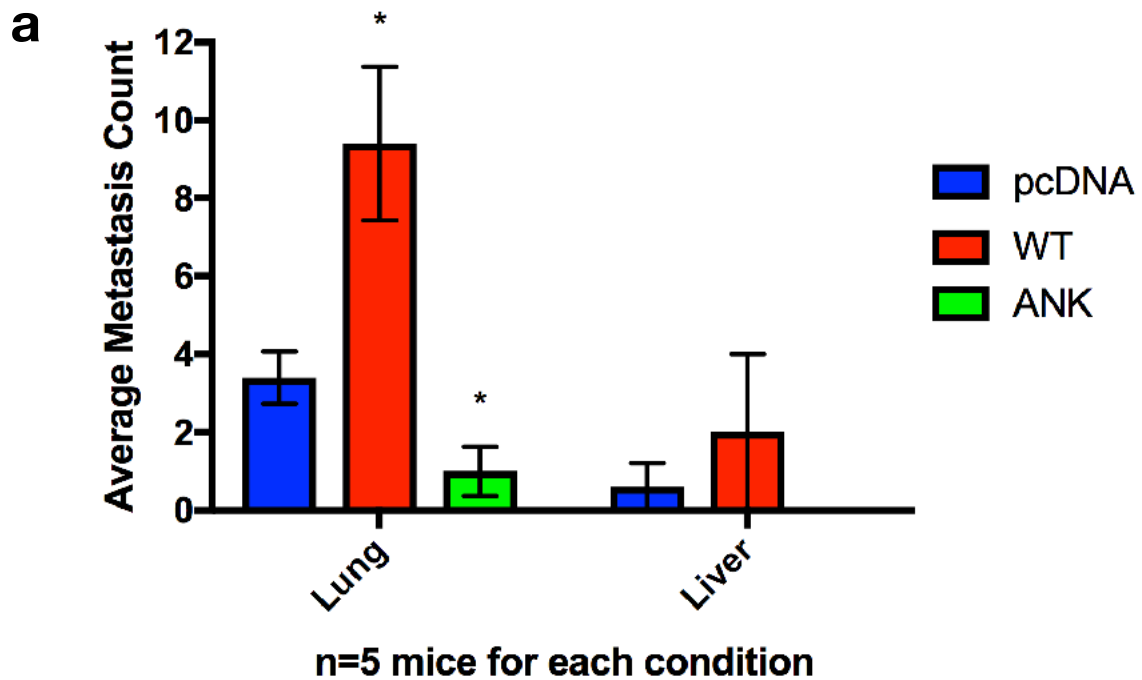
FIG. 4.16 ECTOPIC OVEREXPRESSION OF BCL-3 EXHIBITED A TREND OF REDUCED GROWTH RATES AT THE ORTHOTOPIC SITE

MDA-MB-231 cells stably expressing WT Bcl-3, ANK mutant or control pcDNA constructs were injected orthotopically into both abdominal mammary fat pads bilaterally (1×10^6 cells in $100 \mu\text{l}$) of 6 week old female Hsd: Athymic Nude-Foxn 1^{nu} mice (Harlan Laboratories). Orthotopic tumour growth was measured by palpation. Graph showing the growth rate of each cell line detailing average tumour volume over the course of 42 days. Error bars represent \pm SEM of 8 tumours in 4 independent mice per cohort.

4.12.2 Ectopic overexpression of WT Bcl-3 increased metastases to distal organs but significantly reduced average tumour size

Histological analysis of H&E stained serial sections of distal organs harvested from mice injected with MDA-MB-231 cells stably expressing control pcDNA, WT Bcl-3 or ANK mutant was carried out. The number of metastases on each section was counted and total area for each metastasis quantified. Overexpression of WT Bcl-3 resulted in a significant increase in the average number of metastases identified in the lungs, however the average size of these metastases were significantly smaller. Overexpression of the ANK mutant resulted in significantly less metastases in the lungs and a near significant

reduction in average metastases size ($p=0.11$) (**Fig. 4.17**). Only a few metastases were found across all liver sections so there was insufficient data to plot anything statistically conclusive. Interestingly within the WT Bcl-3 overexpression cohort, we found distal metastases established in the heart, mammary gland and bone marrow (femur) in addition to the lungs and liver (**Fig. 4.17c**). No tumours at these locations were identified within the control and ANK mutant cohorts.



C

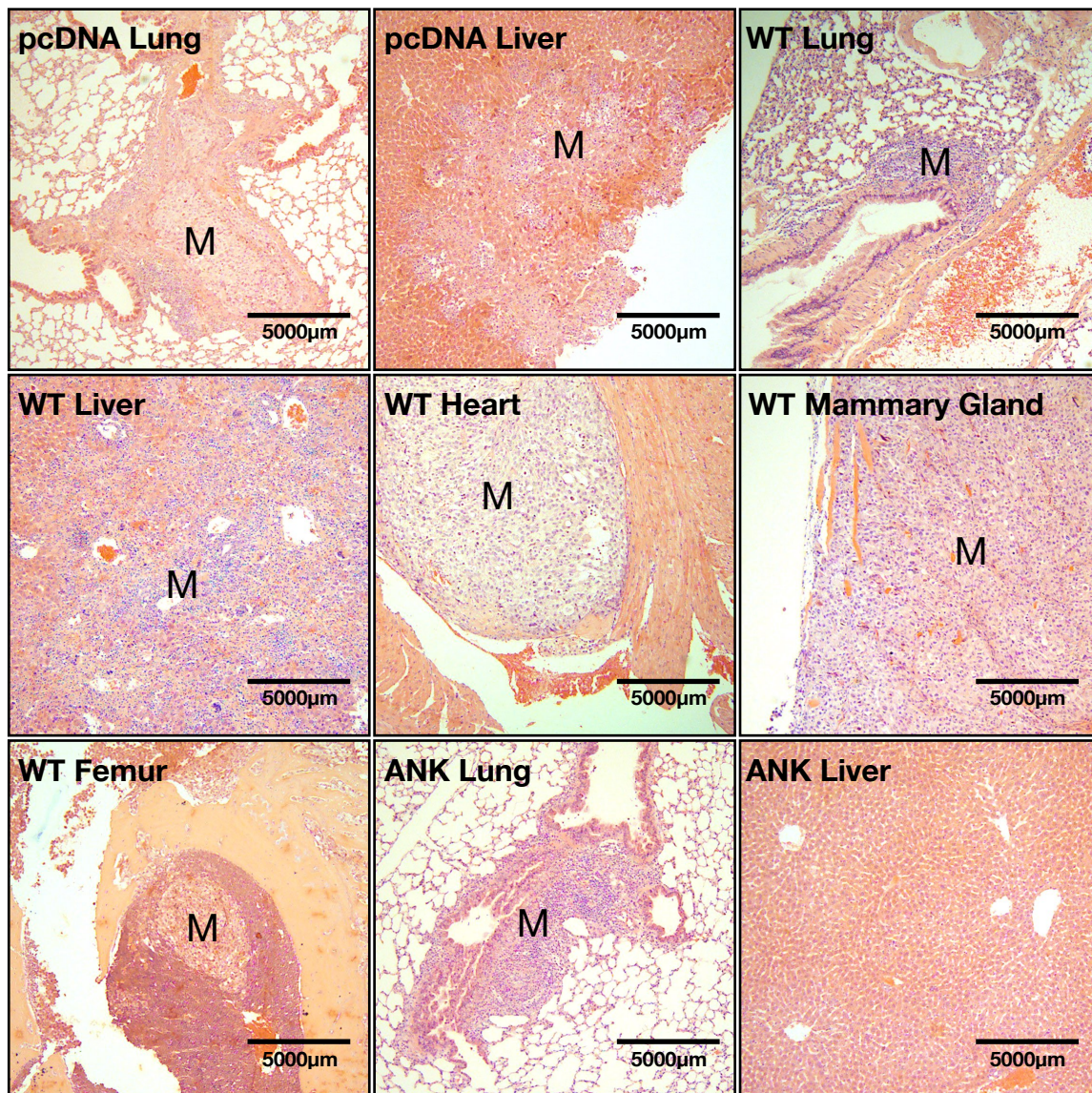


FIG. 4.17 ECTOPIC OVEREXPRESSION OF WT BCL-3 INCREASED METASTASES TO DISTAL ORGANS

MDA-MB-231 cells stably expressing WT Bcl-3, ANK mutant or control pcDNA constructs were injected intravenously via the lateral tail vein (2×10^5 cells in $100 \mu\text{l}$) in 6 week old female Hsd: Athymic Nude-Foxn 1^{nu} mice (Harlan Laboratories). Animals were culled and necropsy performed at 45 days post surgery. Xenograft tissue were fixed, embedded in paraffin blocks, serial sections cut and H&E slides generated for metastases quantification through histological analysis. **a.** Average metastasis count in the lung and liver, **b.** average metastasis size in lung for control pcDNA cohort ($n=5$), WT cohort ($n=5$) and ANK cohort ($n=5$). Error bars represent \pm SEM of 5 independent mice. (T-test, $*=p<0.05$, $**=p<0.01$, $***=p<0.001$) **c.** Representative haematoxylin and eosin (H&E) staining of mouse lung, liver, heart, femur and mammary gland sections with metastatic tumours marked as M.

4.13 Discussion

Bcl-3 is widely regarded as an oncogene and in the previous chapter we were able to demonstrate its knockdown led to a range of tumour suppressive phenotypes. Following those findings, we wanted to investigate the effects of Bcl-3 up-regulation by generating human TNBC cell lines stably overexpressing either WT Bcl-3 or a non-binding ANK mutant Bcl-3. This allowed us to address the hypothesis of whether up-regulated Bcl-3 is associated with increased tumorigenicity in TNBC cell lines, as commonly seen in many solid cancers (Maldonado and Melendez-Zajgla, 2011). Additionally the ANK non-binding mutant gave us a way to validate effects seen with siRNA knockdown because when overexpressed, unpublished studies within our group showed it effectively acted as a dominantly negative Bcl-3 inhibitor.

4.13.1 Overexpression of WT Bcl-3 reduced cell turnover

Contrary to our original expectations, up-regulation of Bcl-3 in both MDA-MB-231-Luc and MDA-MB-436 cell lines amounted to overall reductions in the expansion of cell population as quantified by the metabolism based viability assay (**Fig. 4.3**). Though interestingly when we dissected the different components of cell population growth, Bcl-3 overexpression actually resulted in an increase in cellular proliferation, highlighted by increased Ki67 and pHH3 (**Fig. 4.4 & 4.5**), as well as larger G2/M populations in the cell cycle phases (**Fig. 4.6 & 4.7**). Mechanistically, studies often found elevated Bcl-3 to up-regulate cyclin D1, leading to increased proliferation (Tu et al., 2016). However, both of our TNBC cell lines also featured elevated subG1 populations indicative of increased apoptosis. Up-regulated apoptosis was confirmed by the Caspase-Glo assay and the Bcl-3 overexpressing cell lines had roughly 1.5-fold increased caspase-3/-7 activities (**Fig. 4.8**). Taken together, these results allowed us to calculate the CTI as the ratio of proliferating cells to those undergoing apoptosis and Bcl-3 overexpression in both cell lines resulted in significantly reduced cell turnover (**Fig. 4.6f & 4.7f**).

There are many examples in the literature demonstrating the pro-proliferative natures of up-regulated Bcl-3 (Maldonado and Melendez-Zajgla, 2011), however it is rarer for its overexpression to be associated with increased apoptosis. A recent study showed that Bcl-3 overexpression in hepatocytes attenuated *in vivo* hepatocarcinogenesis. Mice with hepatocytes overexpressing Bcl-3 featured smaller hepatocellular carcinomas,

decreased cell growth, as well as a higher rate of apoptotic cell death. Activation of JNK and ERK signalling was reduced and the number of activated intrahepatic macrophages, CD8⁺ T cells and activated B cells were all reduced in tumours with elevated Bcl-3 (Gehrke et al., 2017). It is formally possible that similar pro-apoptotic mechanisms exist in the TNBC cells we tested.

A study using a dextran sulphate sodium induced mouse colon tumourigenesis model found elevated Bcl-3 to suppress colorectal tumour formation (Tang et al., 2016). Tumour burden was dependent on tumour necrosis factor- α , a NF κ B-mediated pathway dampened by Bcl-3 (Walker et al., 2013). These findings suggest that depending on the cellular and environmental context, Bcl-3 can function either as a tumour promoter or have tumour-suppressive roles. It is likely for this atypical NF κ B family member to have varied mechanisms of action, perhaps acting as a fine-tuned permissive regulator in some cancers, while acting as a classical proto-oncogene in others.

4.13.2 Overexpression of WT Bcl-3 did not affect mammosphere numbers but impaired clonogenicity

There were no observable differences in anoikis-resistant cancer mammosphere population following Bcl-3 up-regulation, though the average mammosphere sizes were smaller (**Fig. 4.9**). Taking into consideration that Bcl-3 overexpression reduced cell growth, it made sense for sphere sizes to be smaller as a subsequent carried forward effect. Although continued serial passage of mammospheres were not carried out, hence we cannot conclude on the self-renewal population. Though Bcl-3 is most likely not specifically implicated in promoting the selective survival of a stem-like population in TNBC based on previous findings with siRNA. When testing clonogenicity, the overexpressing cell lines exhibited reduced colony numbers as well as size (**Fig. 4.10**) and this could also be explained by the downstream result of reduced cell turnover.

A recent study showed that ectopic Bcl-3 overexpression was able to significantly reduce both proliferation and self-renewal in mouse embryonic stem cells. Interestingly knockdown of Bcl-3 also resulted in similarly reduced proliferation and loss of self-renewal. In this case Bcl-3 was found to be a transcriptional repressor of Nanog expression and a sufficiently optimal concentration of Bcl-3 was critical for the maintenance of normal functions (Kang et al., 2018). In our TNBC cell lines, both

overexpression and suppression of Bcl-3 resulted in up-regulated apoptosis. It is perhaps possible for different cancers to have different optimal Bcl-3 concentrations where its oncogenic properties are best balanced to promote tumourigenicity without triggering transcriptional imbalances that might promote apoptosis. This is reminiscent of the Goldilocks or 'just right' model of WNT signalling in cancer, where not the highest levels of activation, but rather a specific increase in WNT was able to support tumour formation (Albuquerque et al., 2002).

4.13.3 Overexpression of WT Bcl-3 enhanced metastatic capacity

When assessing the effects of Bcl-3 overexpression on cellular migration, we saw significant reductions in collective migration (**Fig. 4.11 & 4.12**). Although it is worth considering the characteristics of the wound healing assay as it is sensitive to changes in the rate of cell growth and to better represent this data, perhaps it would have been wise to normalise for apoptosis. We saw significantly increased amoeboid-like single cell migratory capabilities (**Fig. 4.13**). It is also worth considering that a higher proportion of cells overexpressing Bcl-3 plated into the Fluroblok assay would have been apoptotic, meaning these results may in fact be under-representative of the true effect. Time-lapse tracking of single cells, which is by definition independent of cell growth or death in the cell population, highlighted an increase in mesenchymal-like migration in the MDA-MB-231-Luc Bcl-3 overexpressing cell line which further supported the role of Bcl-3 in contributing to increased single cell motility (**Fig. 4.14c&d**). In the light of gene expression analysis following Bcl-3 knockdown in the previous chapter, it is possible that overexpression of Bcl3 acted through similar migration pathways, potentially also through Rho GTPase signalling (**Fig. 3.24**).

4.13.4 Overexpression of WT Bcl-3 increased NFkB activity

In line with the role of Bcl-3 as a transactivator of p50/p52-mediated transcription, we saw a significant increase in NFkB activity following overexpression (**Fig. 4.15**). This supports the notion that Bcl-3 is transcriptionally active as ectopic up-regulation was able to drive NFkB signalling. It may be informative to perform global gene expression analysis in the future, contrasting the differences between the overexpression cell lines with controls. This will also give us a chance to integrate results from the prior Bcl-3

knockdown affymetrix experiment, allowing further refinement of our knowledge regarding the signalling pathways involved.

4.13.5 Overexpression of WT Bcl-3 increased *in vivo* metastatic seeding but tumours had reduced growth rates

When we transplanted MDA-MB-231 cells overexpressing Bcl-3 into an orthotopic xenograft mouse model, the tumours grew significantly slower (**Fig. 4.16**). By the end of the experiment at day 42 these tumours were only around half the size of the controls. This confirmed our *in vitro* cell growth reduction observations following Bcl-3 overexpression also held true for the *in vivo* setting. The complementary normal mouse stromal microenvironment was not able to rescue or promote any increased tumour growth commonly associated with Bcl-3 up-regulation. Interestingly, following necropsy of animals injected with cells through the tail vein, it was found that Bcl-3 overexpression greatly increased the number of distinct metastases in the lungs, even if each individual metastasis was smaller in size (**Fig. 4.17a&b**). Increased Bcl-3 also drove tumours to seed at additional sites such as the heart, mammary gland and bone marrow (femur) (**Fig. 4.17c**). This finding appeared to support our *in vitro* migration observations as despite the slowdown in cell growth, Bcl-3 up-regulation seemed to enhance metastatic capabilities allowing cells to seed more effectively and also in varying microenvironments.

A recent study showed that Bcl-3 promoted pulmonary metastasis of breast cancer cells through transforming growth factor beta (TGF β) signalling. Bcl-3 was found to bind to Smad3, preventing its ubiquitination and subsequent protein degradation (Chen et al., 2016). This mechanism could help explain the increased *in vivo* metastatic potential seen in our xenograft model, as overexpressing Bcl-3 could have resulted increased Smad3 stability and promotion of metastasis through TGF β signalling. It might prove informative to investigate the binding status of Bcl-3 and Smad3, as well as other downstream TGF β activated genes, in our overexpression lines through co-immunoprecipitation experiments.

4.13.6 Overexpression of Bcl-3 ANK mutant in TNBC cell lines mimicked Bcl-3 suppression with siRNA

The Bcl-3 ANK mutant construct was designed to serve as a non-binding control vector. It featured three mutations within the second ankyrin (ANK) repeat domain (**Fig. 4.1**) and this structure is important in facilitating binding interactions with p50 and p52. We hypothesised that overexpressing this Bcl-3 binding mutant would lead to dominant negative inhibition of Bcl-3 signalling as the ANK mutant would dimerise with endogenous Bcl-3, preventing the normal formation of p50-/p52-Bcl-3 complexes.

We ran MDA-MB-231-Luc and MDA-MB-436 TNBC cell lines stably expressing the Bcl-3 ANK mutant along side all of the assays investigating WT Bcl-3 overexpression. The Bcl-3 ANK cell lines exhibited slowdowns in cell population growth, reduced proliferative marker expression, increased apoptosis, reduced clonogenicity, impaired migration, reduced NFkB signalling, and decreased tumour growth and metastatic burden in xenograft models. These results entirely mimicked those seen with siRNA knockdown of Bcl-3 in the previous chapter, demonstrating the ANK mutant construct was able to act as an effective way of suppressing Bcl-3. These findings suggest that the protein-protein interactions between Bcl-3 and p50/p52 could be a viable target for inhibition and may serve as an attractive therapeutic option in TNBC.

4.13.7 Concluding remarks

We showed in this chapter that although ectopic Bcl-3 overexpression in two TNBC cell lines increased cellular proliferation it also promoted apoptosis, resulting in lower overall cell turnover. Despite reduced tumour growth, elevated Bcl-3 also promoted an enhanced single-cell migratory phenotype, allowing for improved *in vivo* metastatic seeding in xenograft mouse models. Though it worth considering the limitations of drawing conclusions from overexpression in only two TNBC cell lines. This may not be a true representation of the effects of Bcl-3 up-regulation within TNBC. Within the scopes of this chapter, we attempted overexpression in the other cell lines previous investigated in our panel, however these attempts failed to produce stable clones as cells rapidly died following transfection. Further elucidation of the cause of this lethality following ectopic overexpression could prove interesting. But considering the results within the two tested cell lines, it suggested that although Bcl-3 has many dominant oncogenic properties, depending on the cellular context its up-regulation can be tumour suppressive.

Chapter 5: Results

Investigating Small Molecule
Inhibition of Bcl-3 in TNBC Cell
Lines

5.1 Introduction

We know Bcl-3 is able to regulate NF κ B signalling through interactions with both p50 and p52 proteins (Bours et al., 1993). In the previous chapters we showed that suppression of Bcl-3 through both siRNA and overexpression of a dominantly negative Bcl-3 ANK mutant resulted in tumour suppressive phenotypes. This highlighted the therapeutic potential of inhibiting Bcl-3 and in collaboration with the Cardiff School of Pharmacy, spurred the development of small molecule inhibitors targeting the Bcl-3-p50 and Bcl-3-p52 protein-protein interactions.

The Bcl-3 inhibitor design process began with generation of computational models of Bcl-3-p50 and Bcl-3-p52 protein complexes. This allowed for a structure based virtual screening approach for commercial available pharmacophores from a large database, resulting in the compilation of a ranked list of suitable known compounds that best matched specific chemical features pertaining to the interacting residues in the protein binding sites. Ultimately a small number of compounds were selected following further stringent visual inspection. These compounds were subsequently biologically evaluated and a lead molecule, JS6, was selected based its effectiveness at disrupting Bcl-3 protein-protein binding, suppressing NF κ B signalling and inhibiting cellular migration. Working off the known chemical structure of this selected lead compound, structural analogues were synthesised to determine structure-activity relationships and investigate the importance of individual functional groups. With this information, we were able to design and synthesise completely novel Bcl-3 inhibitor analogues with the ultimate goal of establishing a new lead that is more efficacious at lower drug concentrations. This led to the subsequent synthesis of CB1, a structurally novel Bcl-3 inhibitor analogue compound (Clarkson, Unpublished).

The main aims of this chapter were to evaluate the biological effects of JS6 and CB1 in context of TNBC and determine whether small molecule inhibition of Bcl-3 could be clinically viable. We investigated the ability of the inhibitors to disrupt Bcl-3 protein-protein binding, as well as their effects on cell viability, stemness, clonogenicity, NF κ B signalling and the global gene expression profile. Following on from our *in vitro* findings, we set up a number of *in vivo* xenograft models designed to assess the effectiveness of our inhibitors at treating different aspects of metastatic disease. These experiments will be effective at assessing a range of potential cellular outputs in response to our drugs.

We hoped to generate promising preclinical data to showcase our novel Bcl-3 inhibitors as effective therapeutics and pave the way for future clinical trials.

5.2 JS6 and CB1 disrupted Bcl-3-p50 protein-protein binding

In order to test whether both Bcl-3 inhibitors had the ability to disrupt Bcl-3-p50 protein-protein binding and evaluate their effectiveness, we carried out some coimmunoprecipitation (coIP) experiments. Immunoprecipitation is a commonly used method used for antigen purification, whereby an antibody against a specific protein is allowed to form an immune complex with that target in a sample. This immune complex is then captured by an antibody binding protein, such as sepharose protein A or G immobilised on a beaded support, and any proteins not precipitated on the beads are washed away. CoIP builds upon the potential of IP reactions to capture and purify a primary target as well as any other interacting proteins that are bound by native interactions. Once captured, both the primary and secondary proteins can be eluted from the support beads and analysed through western blotting (Phizicky and Fields, 1995).

Total cellular protein from MDA-MB-231-Luc cells overexpressing WT Bcl-3 was extracted following treatment with either 30 minutes or 2 hours of JS6, CB1 or control DMSO at a concentration of 50 μ M. We also extracted protein from the pcDNA control MDA-MB-231-Luc cells, as well as MDA-MB-231-Luc cells overexpressing the non-binding ANK Bcl-3 mutant. Bcl-3 and p50 protein complexes were then immunoprecipitated by centrifugation using the respective antibodies immobilised to sepharose protein A beads. Unbound proteins were washed away from these beads and the target Bcl-3 and p50 protein complexes were denatured and eluted through boiling. The secondary complexed component for each coimmunoprecipitant was quantified by western blotting and normalised to the total content of the primary protein immunoprecipitant (**Fig. 5.1a&b**).

Both JS6 and CB1 compounds were able to inhibit the protein-protein binding of Bcl-3 with p50. Following 30 minutes treatment with JS6, we saw a roughly 30% decrease in binding and after 2 hours treatment, this inhibition increase to roughly 45%. CB1 was found to be more effective inhibitor, with 30 minutes treatment resulting in 55-75% binding inhibition and 2 hours treatment resulting in 80-95% inhibition (**Fig. 5.1c&d**). The MDA-MB-231-Luc cell line expressing the empty control pcDNA vector

featured 30-40% reduced protein binding and the MDA-MB-231-Luc cell line overexpressing the ANK Bcl-3 mutant featured around 75% reduced complex binding.

5.3 48h JS6 and CB1 treatment reduced cell viability at higher drug concentrations

Our results from previous chapters have demonstrated Bcl-3 suppression to have suppressive effects upon overall cell turnover in TNBC cell lines. Therefore we wanted to test our Bcl-3 inhibitor compounds and assess whether they have any potential cell cytotoxic effects. We used the CellTiter-Blue cell viability assay (Promega), a homogenous, fluorescence based method for assessing cell viability. This reagent assayed the ability of living cells to convert a redox dye, resazurin, into the fluorescent end product resorufin. Nonviable cells rapidly lose metabolic capacity and thus do not generate a fluorescent signal. The assay involved adding a single nontoxic reagent directly to the medium of cultured cells and after an incubation step of 1 hour, viability data is recorded using a plate reader based on the intensity of fluorescence.

Three TNBC cell lines and the non-tumourigenic MCF10a cell line were plated into 96-well assay plates and treated with three different concentrations of JS6, CB1 or DMSO control. Cells were incubated for 48 hours before CellTiter-Blue reagent was added and viability assessed. JS6 significantly reduced cell viabilities by about 15% only at the highest 100 μ M concentration in the MDA-MB-436 and MDA-MB-231-Luc cell lines (**Fig. 5.2a&b**). CB1 significantly reduced cell viabilities by around 20% at the highest 100 μ M concentration in all TNBC cell lines and about 15% at 10 μ M in MDA-MB-436 and MDA-MB-231-Luc cells (**Fig. 5.2a-c**). MCF10a cells were not significantly affected by the Bcl-3 inhibitors (**Fig. 5.2d**).

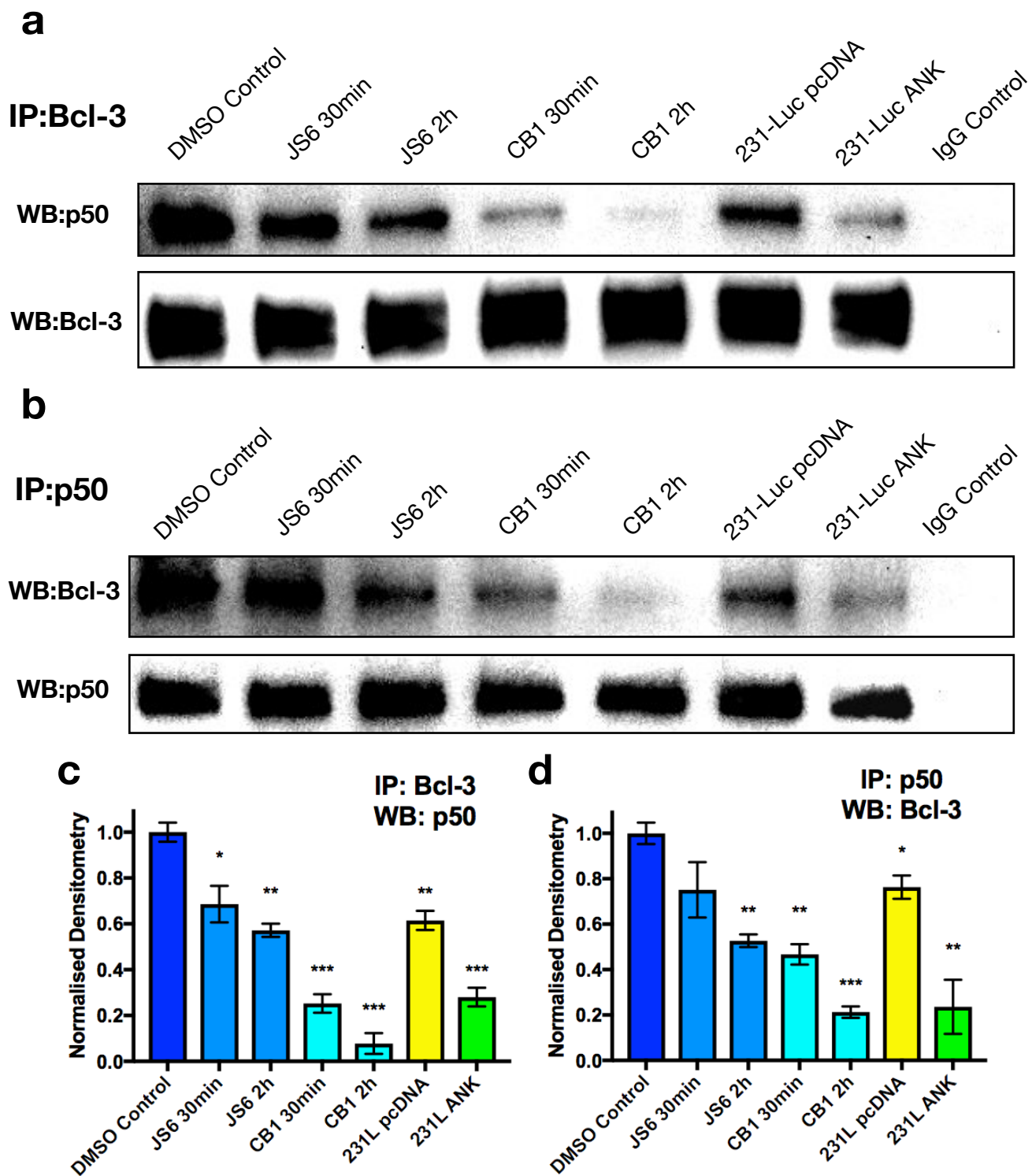


FIG. 5.1 JS6 AND CB1 DISRUPTED BCL-3-P50 PROTEIN-PROTEIN BINDING

The abilities of both compounds to disrupt Bcl-3-p50 protein-protein binding was tested using coimmunoprecipitation (coIP) assays. Protein from MDA-MB-231-Luc cells overexpressing WT Bcl-3 was extracted following treatment with either 30min or 2h of JS6, CB1 or control DMSO at a concentration of 50 μ M. Protein from the pcDNA control MDA-MB-231-Luc cell line, as well as one overexpressing the ANK Bcl-3 mutant was also extracted. Bcl-3 and p50 protein complexes were then immunoprecipitated by centrifugation using antibodies bound to sepharose A beads. Representative western blots for Bcl-3 or p50 protein following coIP of **a**. Bcl-3 complexes or **b**. p50 complexes. Bar charts depicting the quantification and normalisation of protein band intensities using ImageJ following coIP of **c**. Bcl-3 complexes or **d**. p50 complexes. Error bars represent \pm SEM of 3 independent experiments. (T-test, *= p <0.05, **= p <0.01, ***= p <0.001)

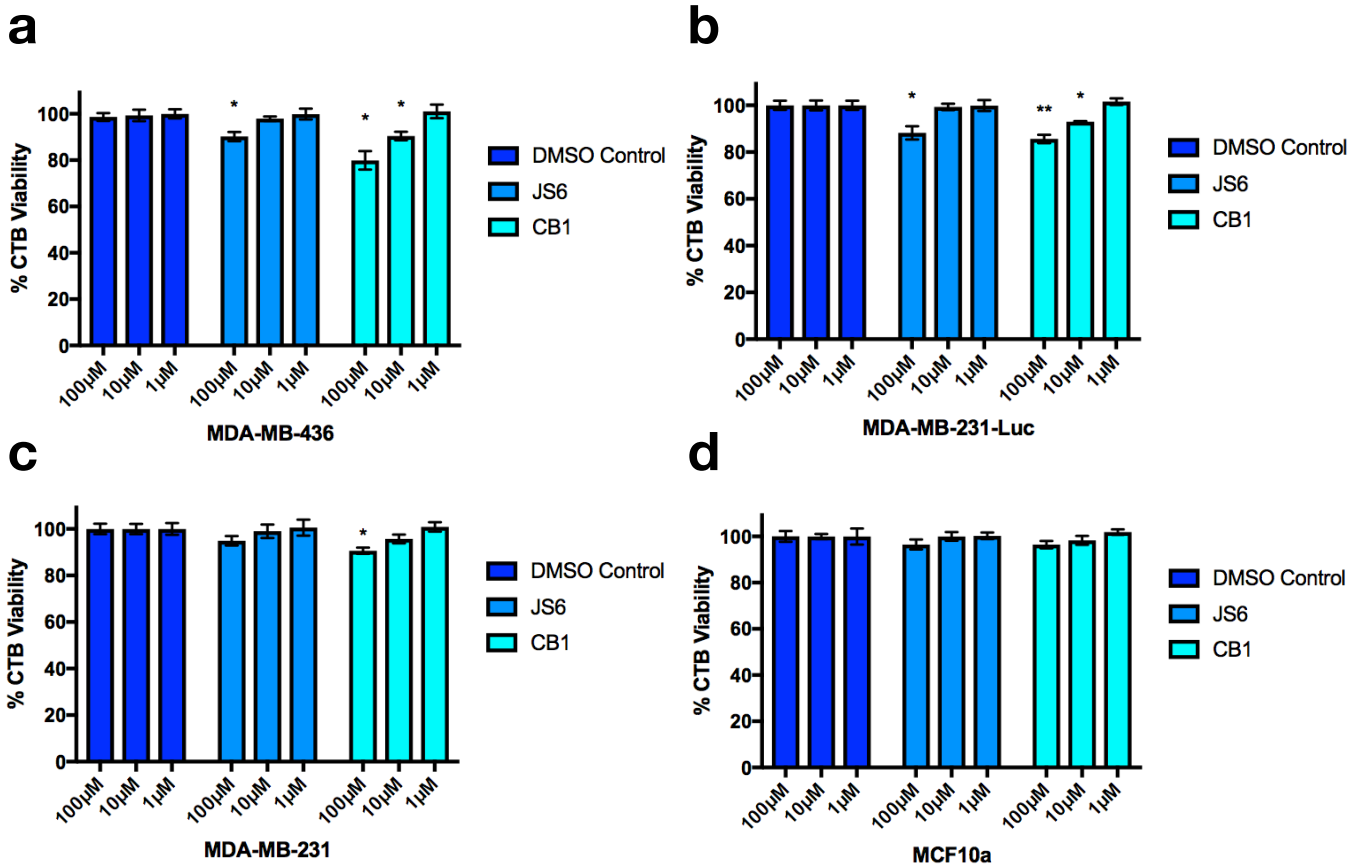
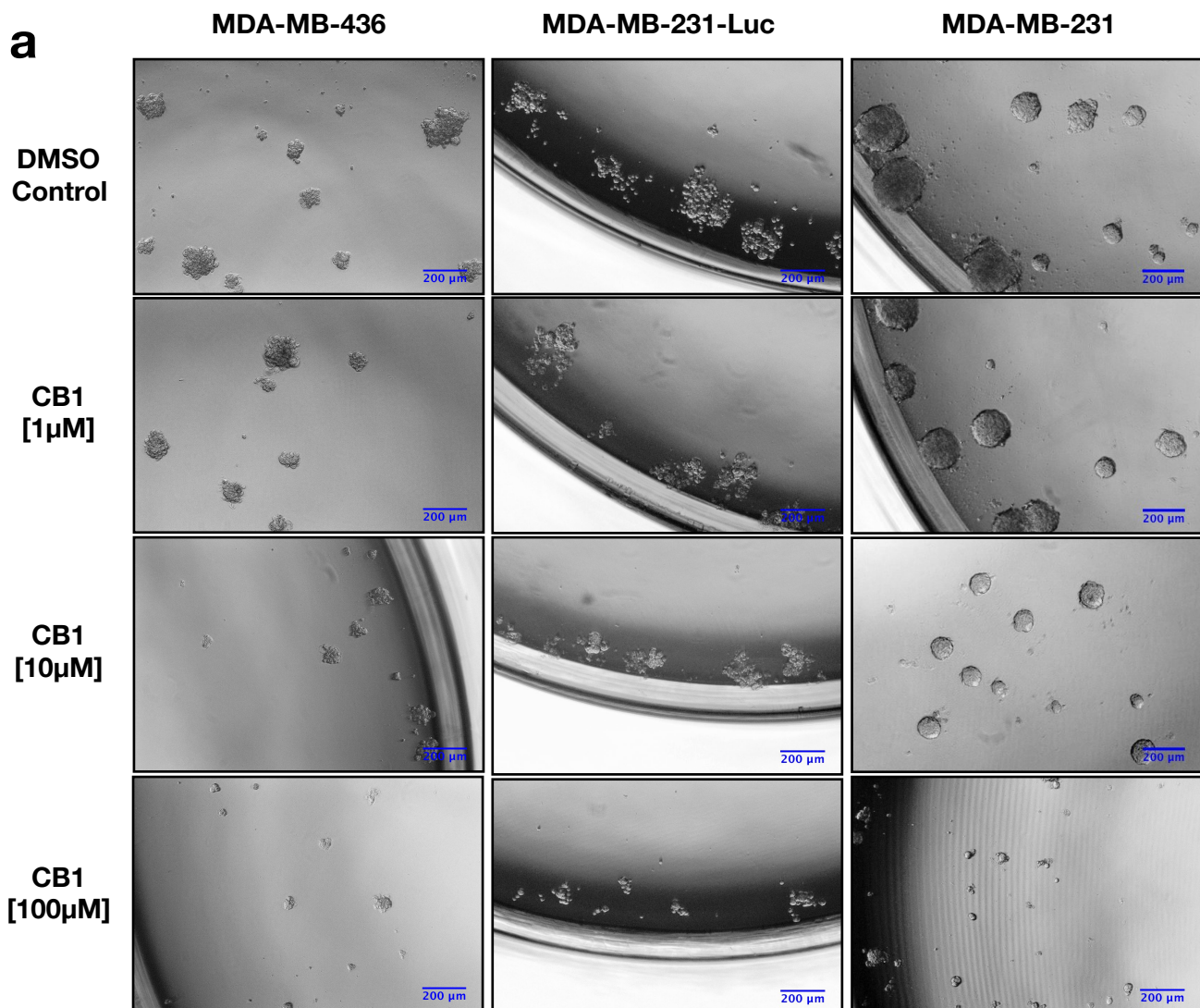


FIG. 5.2 48H JS6 AND CB1 TREATMENT REDUCED CELL VIABILITY AT HIGHER DRUG CONCENTRATIONS

The toxicity of both inhibitors were assessed using the CellTiter-Blue viability assay. Three TNBC cell lines and the non-tumourigenic MCF10a cell line were plated into assay plates and treated with three different concentrations of JS6, CB1 or DMSO control. Cells were incubated for 48h before CellTiter-Blue reagent was added and viability assessed. Percentage of viable cells for each treatment condition was normalised to the relevant controls for **a.** MDA-MB-436 **b.** MDA-MB-231-Luc **c.** MDA-MB-231 **d.** MCF10a cell line. Error bars represent \pm SEM of 3 independent experiments. (T-test, * = $p < 0.05$, ** = $p < 0.01$, *** = $p < 0.001$)

5.4 48h CB1 treatment did not affect mammosphere numbers but significantly reduced mammosphere size

The mammosphere assay was performed to assess the effect of the Bcl-3 inhibitors on the stem-like anoikis resistant cell population. TNBC cell lines were treated with CB1 at concentrations of 1 μ M, 10 μ M, 100 μ M or DMSO control for 48h before being disaggregated into single cells and plated into non-adherent mammosphere plates and cultured for 10 days. CB1 treatment did not affect the total number of mammospheres formed but at 10 μ M and 100 μ M concentrations, we saw a respective 30% and 60% significant reduction in average mammosphere sizes (**Fig. 5.3**).



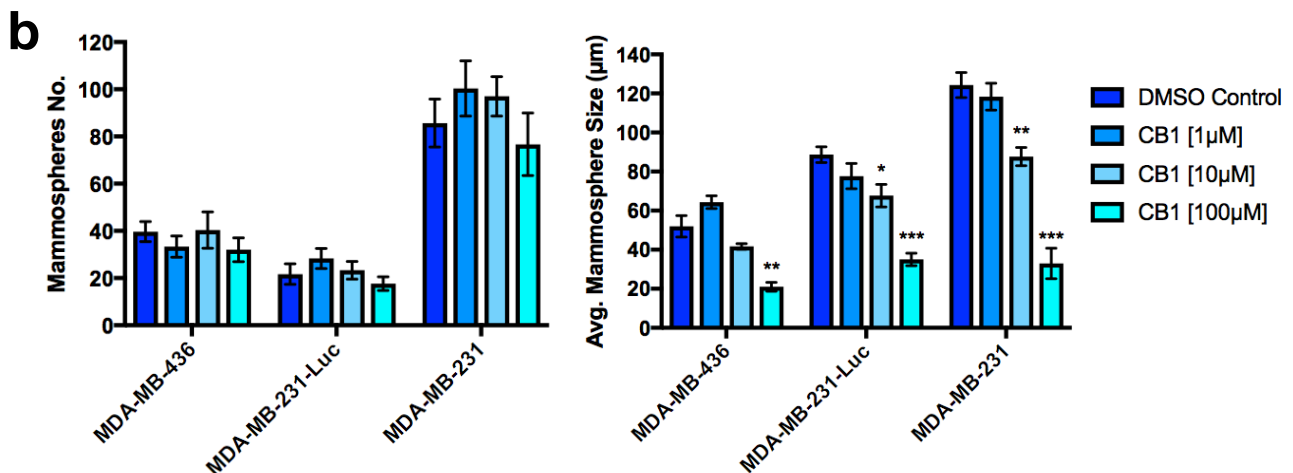


FIG. 5.3 48h CB1 TREATMENT DID NOT AFFECT MAMMOSPHERE NUMBERS BUT SIGNIFICANTLY REDUCED MAMMOSPHERE SIZE

TNBC cell lines were treated with CB1 at a range of concentrations for 48h before being disaggregated into single cells and plated into non-adherent mammosphere plates and cultured for 10 days. Representative bright-field microscopy images for **a.** MDA-MB-436, MDA-MB-231-Luc, and MDA-MB-231 cell lines. **b.** Total mammosphere numbers and average mammosphere sizes for each cell line. Error bars represent \pm SEM of 3 independent experiments. (T-test, *= $p < 0.05$, **= $p < 0.01$, ***= $p < 0.001$)

5.3 48h JS6 and CB1 impaired clonogenic survival at 100μM concentration

Clonogenic potential was tested by treating MDA-MB-231-Luc cells with either JS6, CB1 or DMSO control at concentrations of 1μM, 10μM, or 100μM for 48 hours before plating the cells at low density in a colony formation assay and cultured for 10 days before being fixed and stained with crystal violet. Treatment with JS6 and CB1 at 100μM resulted in significantly reduced colony numbers as well as their average sizes (**Fig. 5.4**). The other drug concentrations did not significantly affect this cell line in this assay.

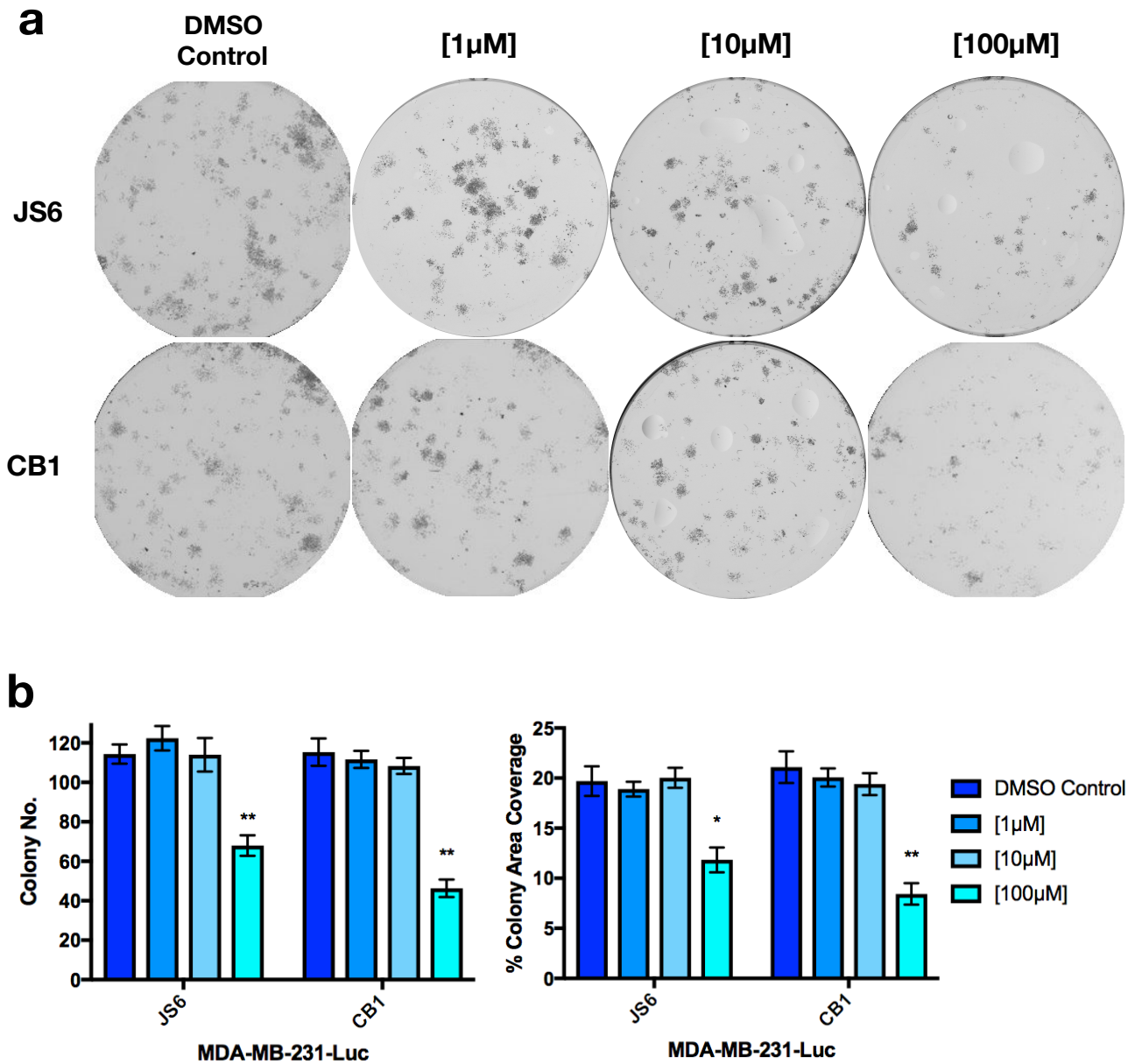


FIG. 5.4 48H JS6 AND CB1 TREATMENT IMPAIRED CLONOGENIC SURVIVAL AT 100 μ M CONCENTRATION

Clonogenic potential was tested by treating MDA-MB-231-Luc cells with either JS6, CB1 or DMSO control at a range of concentrations for 48h before plating the cells at low density in a colony formation assay and cultured for 10 days before being fixed and stained with crystal violet. **a.** Representative bright-field images and **b.** total colony number and average colony coverage for MDA-MB-231-Luc cells. Error bars represent \pm SEM of 3 independent experiments. (T-test, *= p <0.05, **= p <0.01, ***= p <0.001)

5.4 48h JS6 and CB1 treatment did not affect NFkB activity

Since previous Bcl-3 suppression experiments resulted in down regulation of NFkB activity, we wanted to test the effects of our Bcl-3 inhibitors to see if they acted in a similar manner. A luciferase NFkB reporter plasmid was used to quantify NFkB levels in MDA-MB-231-Luc cells following 48h treatment with either JS6, CB1 or DMSO control at 10 μ M or 100 μ M concentrations. Cells were transfected with the luciferase NFkB reporter plasmid, LacZ control plasmid 24h after initial drug treatment and incubated for 24h. Cells were then lysed and NFkB activity measured as luminescence readout using a plate reader. NFkB activity was then normalised to LacZ luminescence to control for transfection efficiency. Surprisingly following 48 hours of JS6 or CB1 treatment at either 10 μ M or 100 μ M concentrations, there were no significant changes to NFkB activity in the MDA-MB-231-Luc cell line (**Fig. 5.5**).

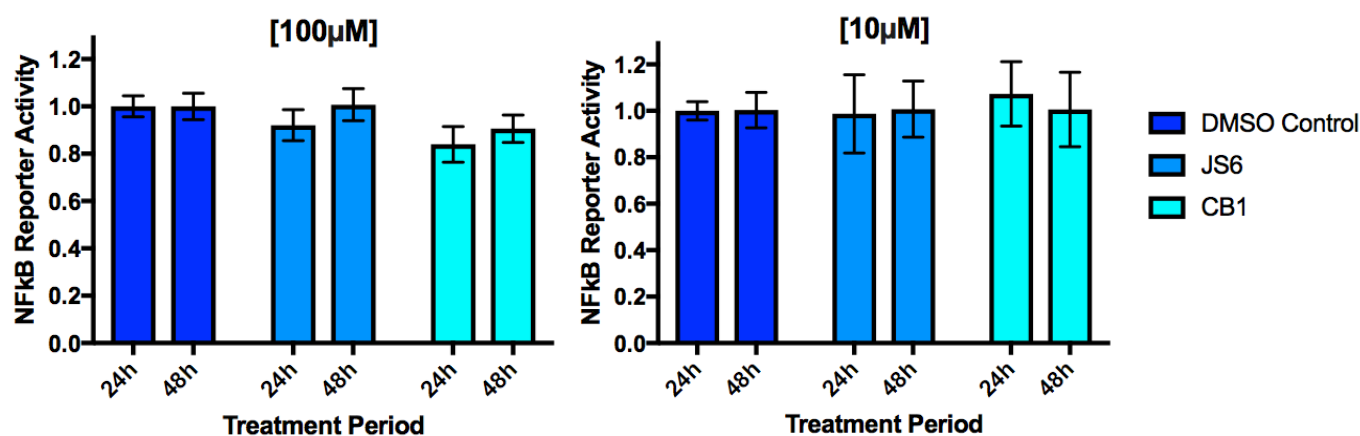


FIG. 5.5 48H JS6 AND CB1 TREATMENT DID NOT AFFECT NFkB ACTIVITY

A luciferase NFkB reporter plasmid was used to quantify NFkB levels in MDA-MB-231-Luc cells following 48h treatment with either JS6, CB1 or DMSO control at 10 μ M or 100 μ M concentrations. Cells were transfected with the luciferase NFkB reporter plasmid, LacZ control plasmid 24h after initial drug treatment and incubated for 24h. Cells were then lysed and NFkB activity measured as luminescence readout using a plate reader. NFkB activity was then normalised to LacZ luminescence to control for transfection efficiency. Error bars represent \pm SEM of 3 independent experiments.

5.5 Affymetrix DNA microarray analysis following 48h CB1 treatment

To further investigate the transcriptional effects of Bcl-3 inhibition using our novel inhibitor, we carried out a global gene expression profiling experiment using the Affymetrix DNA GeneChip microarray platform. mRNA was extracted from MDA-MD-231-Luc cells treated for 48 hours with CB1 at 100 μ M concentration or DMSO control. Experimental data were normalised and analysed using GeneSpring GX Pathway Architect software. Genes were filtered based on their corrected p-values and a statistical cut off of 0.05 was chosen. In stark contrast to the changes seen following Bcl-3 siRNA knockdown, only 110 out of 43590 genes satisfied this cut off following 48h CB1 treatment.

PANTHER functional classification, statistical overrepresentation and statistical enrichment analyses were carried out on the 110 significant gene hits and stratified by biological process, pathways, molecular function and cellular components.

5.5.1 PANTHER functional classification analysis

For biological processes (**Fig 5.6a**) the genes changes primarily fell into:

Cellular processes (28.6%), these are processes carried out at the cellular level such as cellular communication.

Metabolic processes (20.4%), these are chemical reactions including anabolism and catabolism by which living organisms transform chemical substances.

Biological regulation (9.2%), these are processes that modulate measurable attributes of any biological process, quality or function.

Cellular component organisation or biogenesis (8.7%), these are processes that biosynthesise constituent macromolecules, assembly, arrangement or disassembly of cellular components.

Developmental processes (7.7%), processes resulting in the progression from an initial condition to a later condition.

Response to stimuli (7.1%), processes that results in a change in state of a cell as a result of a stimulus.

Multicellular organismal process (7.1%), processes occurring at the level of a multicellular organism.

Localisation (5.6%), these are processes in which a cell, substance or cellular entity is transported, tethered or otherwise maintained in a specific location.

For molecular functions (**Fig 5.6b**) the genes changes primarily fell into:

Catalytic activity (42.5%), catalysis of biochemical reactions at physiological temperatures.

Binding (39.7%), selective, non-covalent, interactions of a molecule with one or more specific sites on a another molecule.

Structural molecule activity (6.8%), contributing to the structural integrity of a complex or its assembly within or outside a cell.

Transporter activity (5.5%), the direct movement of substances into, out of, or between cells.

Signal transducer activity (4.1%), conveying a signal across a cell to trigger a change in cell function or state.

For cellular components (**Fig 5.6c**) the genes changes primarily fell into:

Cell part (38.3%), any constituent part of a cell.

Organelle (29.9%), organised structure of distinctive morphology and function.

Macromolecular complex (9.3%), stable assembly of two or more macromolecules functioning together.

Membrane (9.3%), lipid bilayer along with all proteins and complexes embedded in or attached to it.

Extracellular region (8.4%), space external to the outermost structure of a cell.

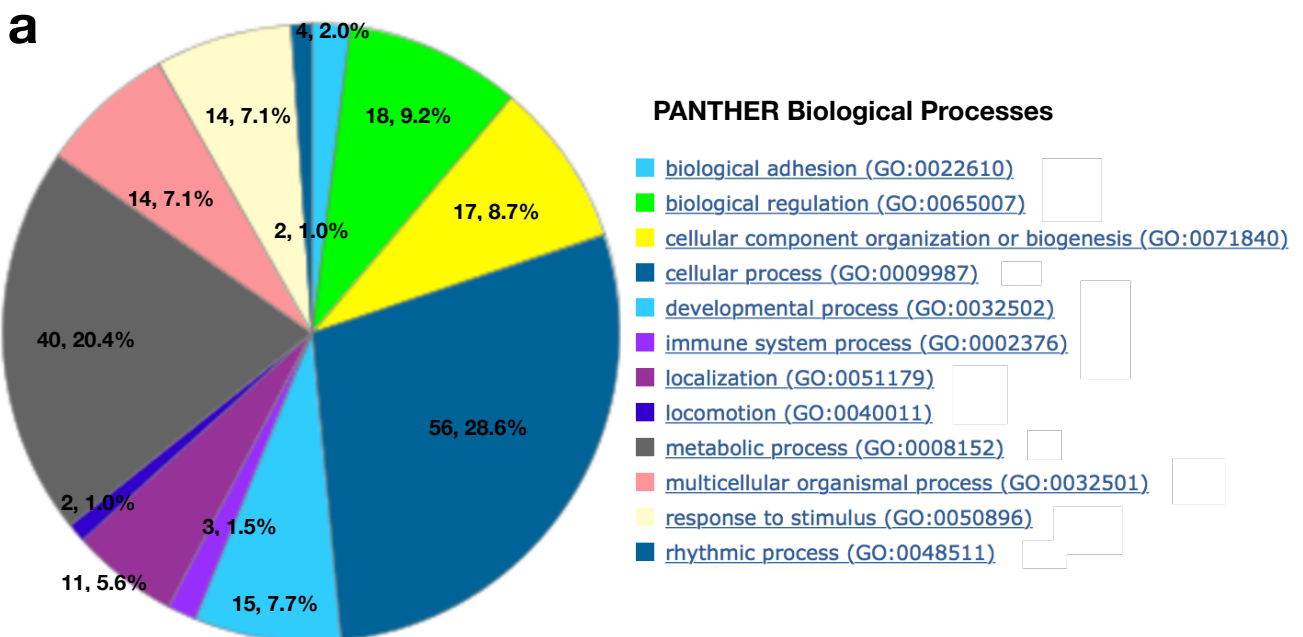
5.5.2 PANTHER statistical overrepresentation analysis

Following PANTHER statistical overrepresentation analysis, only genes associated with nitrogen compound metabolism was found to be significantly overrepresented. No other specific PANTHER molecular functions or PANTHER signalling pathways were found to be significantly overrepresented through this analysis.

5.5.3 PANTHER statistical enrichment analysis

Following PANTHER statistical enrichment analysis only genes associated with biological processes pertaining to cellular component organisation or biogenesis was

found to be down-regulated ($p=0.003$). Genes associated with molecular functions pertaining to DNA binding transcription factor activity was also found to be up-regulated ($p=0.006$). Finally genes associated with pathways linked to interleukin signalling ($p=0.03$) and gonadotropin-releasing hormone receptors ($p=0.017$) were found to be up-regulated.



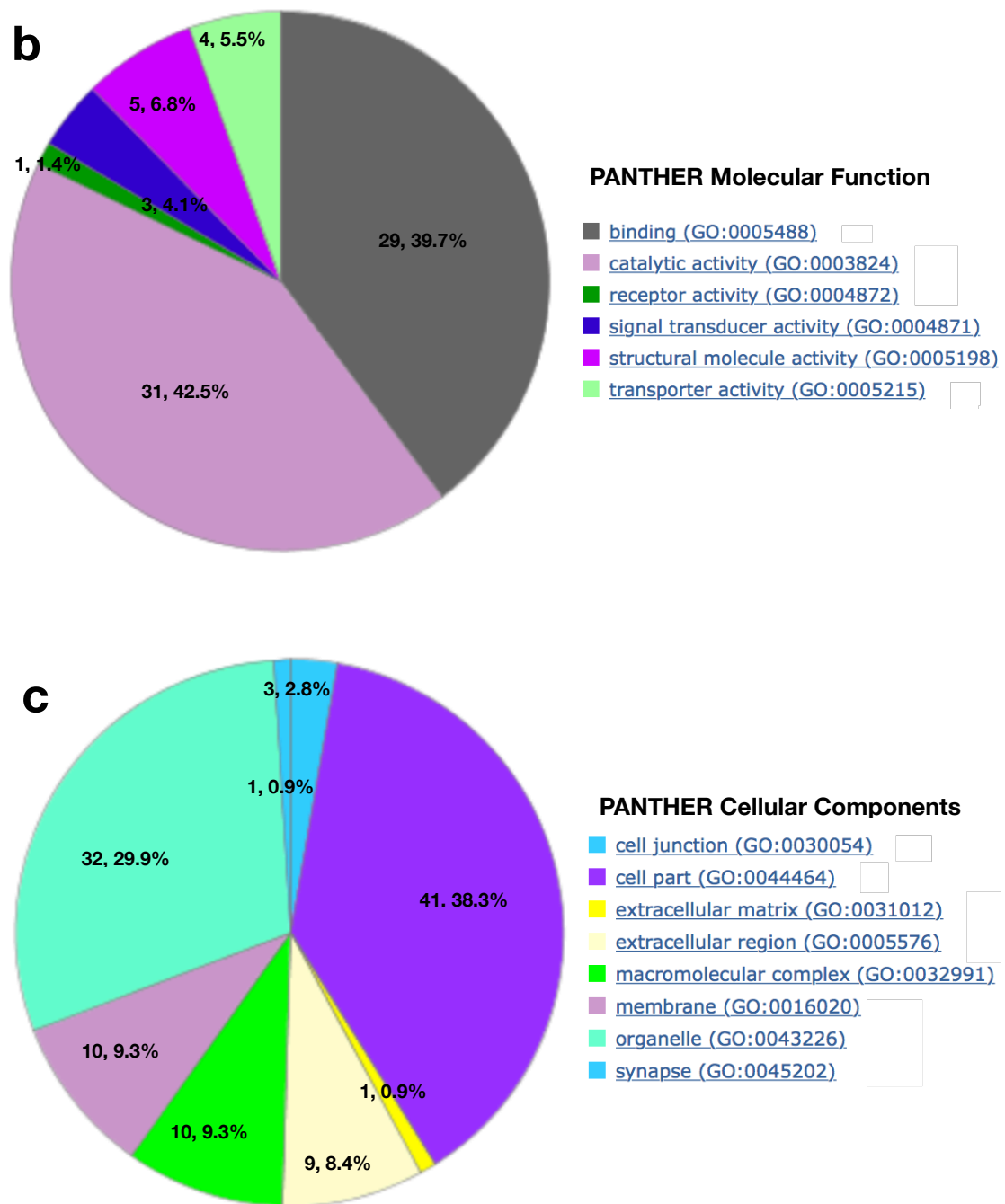


FIG. 5.6 PANTHER FUNCTIONAL CLASSIFICATION TOOL FOR 48H 100MM CB1 TREATMENT

Genes found to be significantly up/down-regulated (p -value<0.05) in the MDA-MB-231-Luc 48h 100 μ M CB1 treatment Affymetrix microarray experiment were used to perform PANTHER functional classification. Result of analyses are visualised as pie charts with information within each wedge detailing the number of genes and percent of genes against total hits for **a.** PANTHER biological processes **b.** PANTHER Molecular Function **c.** PANTHER Cellular Components.

5.5.4 Overlapping gene changes between CB1 treatment and Bcl-3 siRNA knockdown

Within the 110 significant gene changes gene changes following CB1 treatment, there were 63 overlaps with significant changes also seen following Bcl-3 siRNA knockdown. These overlapping genes along with the corresponding Log Fold Change value associated with each condition are listed in the table below.

Gene Symbol	CB1 Treatment (FC)	Bcl-3 siRNA (FC)
FOS	1.669	1.364
HES1	1.582	1.216
CSF2	1.553	-1.179
CSF3	1.453	1.825
IL1B	1.451	1.843
ST6GALNAC2	1.388	-1.133
FHDC1	1.384	-1.861
RNASE1	1.377	-1.429
CYP1B1	1.354	1.083
KLF2	1.341	1.586
HTRA1	1.336	1.806
DUSP5	1.331	1.281
PTGES	1.320	1.466
GDF15	1.300	-1.671
IL24	1.289	1.376
COL6A3	1.266	1.416
PIM1	1.242	-1.486
EPAS1	1.238	-1.124
ITGA3	1.209	-1.077
SIK1	1.197	-1.515
TAGLN2	1.186	1.105
TNS4	1.184	-2.928
L1CAM	1.174	1.099
NTN4	1.164	1.170
TGFB1	1.149	1.136
PLAU	1.127	1.903
DHX32	1.112	1.138
GRN	1.102	1.257

Gene Symbol	CB1 Treatment (FC)	Bcl-3 siRNA (FC)
SLX1A	1.096	1.155
MARK4	1.086	1.144
EPN2	1.080	-1.144
CDCP1	1.077	-1.125
LOX	1.054	-1.283
DARS2	-1.098	1.097
POLR1A	-1.104	-1.083
KIF18A	-1.107	-1.344
GUF1	-1.119	-1.137
FERMT1	-1.121	-1.174
EOGT	-1.127	1.192
INPP4B	-1.129	-1.207
EPB41L2	1.133	1.118
BMP5	-1.134	2.189
POLR3B	-1.144	1.229
RIF1	-1.147	-1.138
CHD1	-1.147	1.086
RIMS1	-1.149	-1.294
LINC01123	-1.164	-1.305
PARD6B	-1.168	-1.162
LMNB1	-1.173	1.120
ANK3	-1.187	-1.127
SEMA3D	-1.192	-1.316
TNFRSF10D	-1.197	1.602
HAS2	-1.201	-1.947
ATP8B1	-1.224	-1.462
HHIP	-1.228	-2.071
FRAS1	-1.236	-1.448
DCLK1	-1.240	-1.418
SDPR	-1.255	-1.873
CNN1	-1.271	-1.414
RELN	-1.297	1.176
CYP24A1	-1.303	-1.281
GRPR	-1.364	-1.222
NRK	-1.376	-1.617

5.6 Relative expression of a Bcl-3 responsive gene panel following siRNA knockdown, JS6 or CB1 treatment

The surprisingly low number of significantly altered gene hits following 48 hours of CB1 treatment, especially when compared to the changes seen after Bcl-3 siRNA knockdown in the same cell line, prompted us to investigate and validate the effect of the Bcl-3 inhibitors in a time course experiment. We drafted a panel comprised of both significantly altered genes from the 48 hour CB1 Affymetric experiment (IL1B, ESM1, FOS, EGR1, IL6), as well as some genes that have been shown in the literature to be direct transcriptional targets of Bcl-3 complexes (TNF α , CDH2, MDM2, IL10).

Bcl-3 was shown to bind the TNF α promoter in RAW cells and inhibit its LPS-induced activation (Kuwata et al., 2003). The N-cadherin (CDH2) promoter region has been shown to contain NF κ B binding sites and DNA-bound Bcl-3 complexes were found within these regions in melanoma cells (Kuphal and Bosserhoff, 2005). Bcl-3 overexpression in MCF-7 cells has been shown increase MDM2 expression. The activation of tumour suppressor p53 is controlled by modifications and interactions with its inhibitor MDM2 (Vousden and Prives 2005). ChIP analysis revealed that Bcl-3 complexes bound the P2 promoter region of MDM2 leading to its stabilisation and resulting in lower levels of p53 (Kashatus et al., 2006). It has been shown that Bcl-3 is negatively implicated in the initiation of IL10 transcription in macrophages (Kuwata et al., 2003).

The relative gene expression of the selected panel was quantified using TaqMan qRT-PCR probes in MDA-MB-231-Luc cells for the conditions of 48 hour knockdown with Bcl-3 siRNA, control siRNA or treatment with 100 μ M of JS6, CB1 or DMSO control for either 3 hours, 8 hours, 24 hours or 48 hours. We want to compare the transcriptional changes seen following Bcl-3 knockdown with siRNA versus treatment with our Bcl-3 inhibitor compounds. The rationale is that if drug inhibition of Bcl-3 acted in a similar way as siRNA suppression, then we ought to observe a similar transcriptional signature.

Following 48 hour Bcl-3 siRNA knockdown, expression of TNF α (3.11-fold), IL1B (2.24-fold), FOS (1.84-fold) and EGR1 (1.79-fold) were all significantly up-regulated, ESM1 and IL6 expression did not significantly change and expression of CDH2 (0.56-fold), MDM2 (0.51-fold) and IL10 (0.38-fold) were significantly down-regulated (**Fig. 5.7a**).

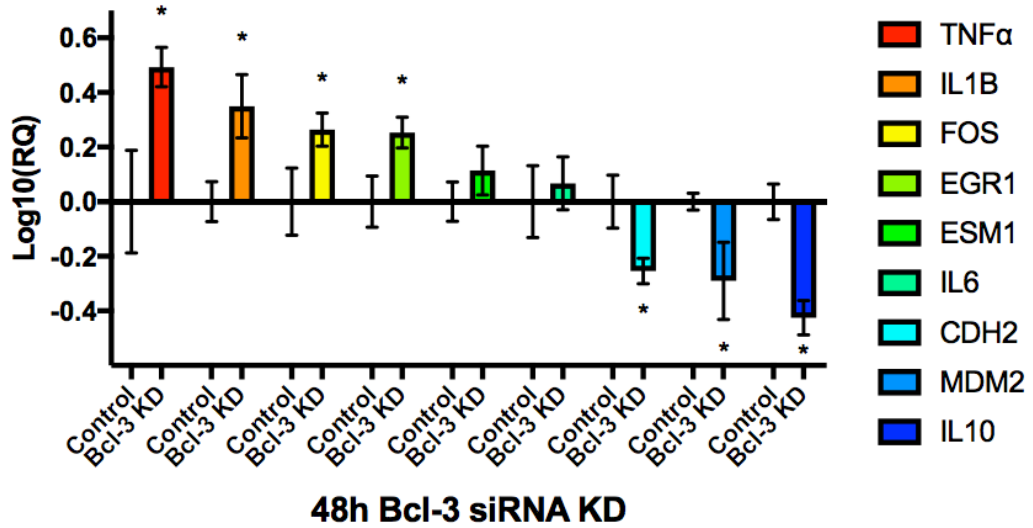
Following 3 hour JS6 treatment, IL1B (2.2-fold), FOS (2.2-fold) and IL6 (2.6-fold) were significantly up-regulated; CB1 treatment resulted in TNF α (2.4-fold), FOS (2.6-fold), EGR1 (2.1-fold) and IL6 (1.5-fold) to be significantly up-regulated (**Fig. 5.7b**).

Following 8 hour JS6 treatment, TNF α (3.3-fold), IL1B (2.9-fold), FOS (2.3-fold) and EGR1 (3.1-fold) were significantly up-regulated and ESM1 (0.52-fold) and MDM2 (0.64-fold) was significantly down-regulated; CB1 treatment resulted in TNF α (2.5-fold), IL1B (2.5-fold), FOS (2.5-fold), EGR1 (1.8-fold) and IL6 (2.2-fold) to be significantly up-regulated and ESM1 (0.45-fold), MDM2 (0.47-fold) and IL10 (0.46-fold) were significantly down-regulated (**Fig. 5.7c**).

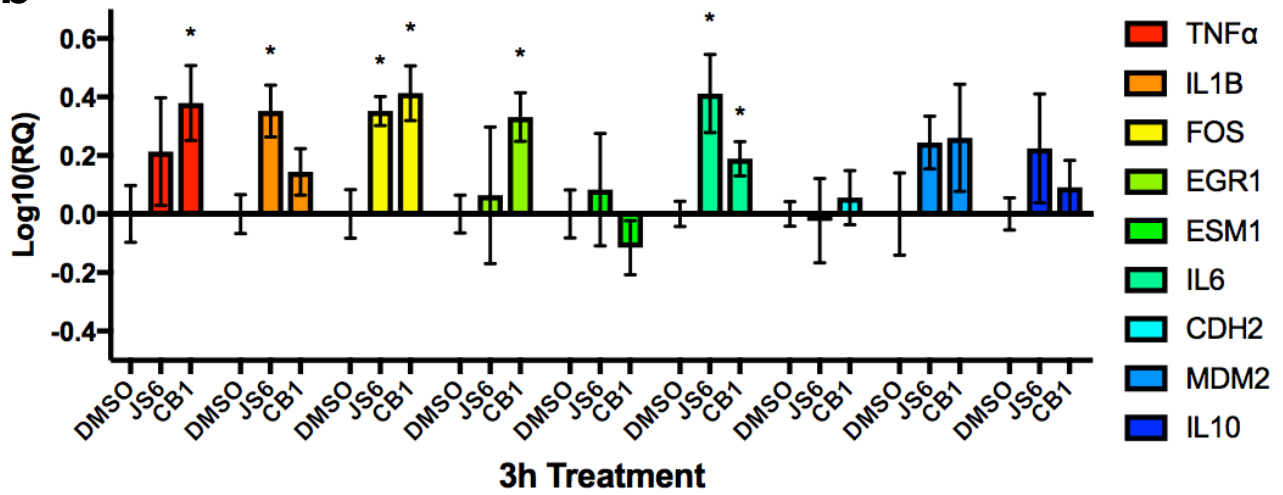
Following 24 hour JS6 treatment, no significant changes were observed; CB1 treatment resulted in TNF α (1.7-fold), IL1B (3.3-fold), FOS (2.5-fold), EGR1 (3.3-fold) and IL6 (2.5-fold) to be significantly up-regulated and ESM1 (0.53-fold), CDH2 (0.63-fold) and MDM2 (0.59-fold) were significantly down-regulated (**Fig. 5.7d**).

Following 48 hour JS6 treatment, no significant changes were observed; CB1 treatment resulted in IL1B (1.5-fold), FOS (1.5-fold), EGR1 (1.7-fold) and IL6 (1.8-fold) to be significantly up-regulated and ESM1 (0.62-fold) to be down-regulated (**Fig. 5.7e**).

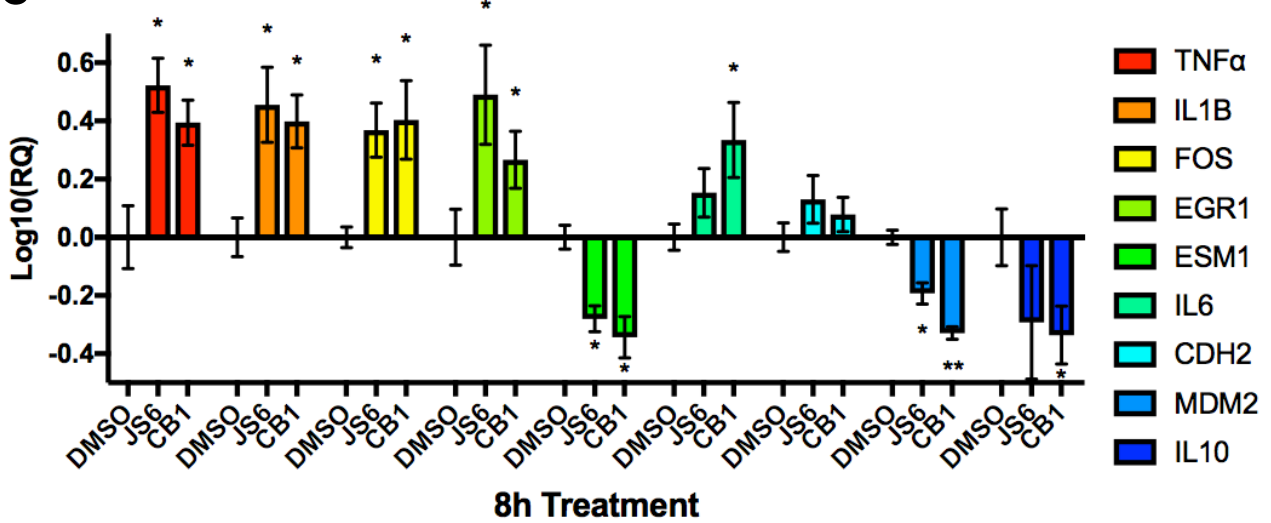
a



b



c



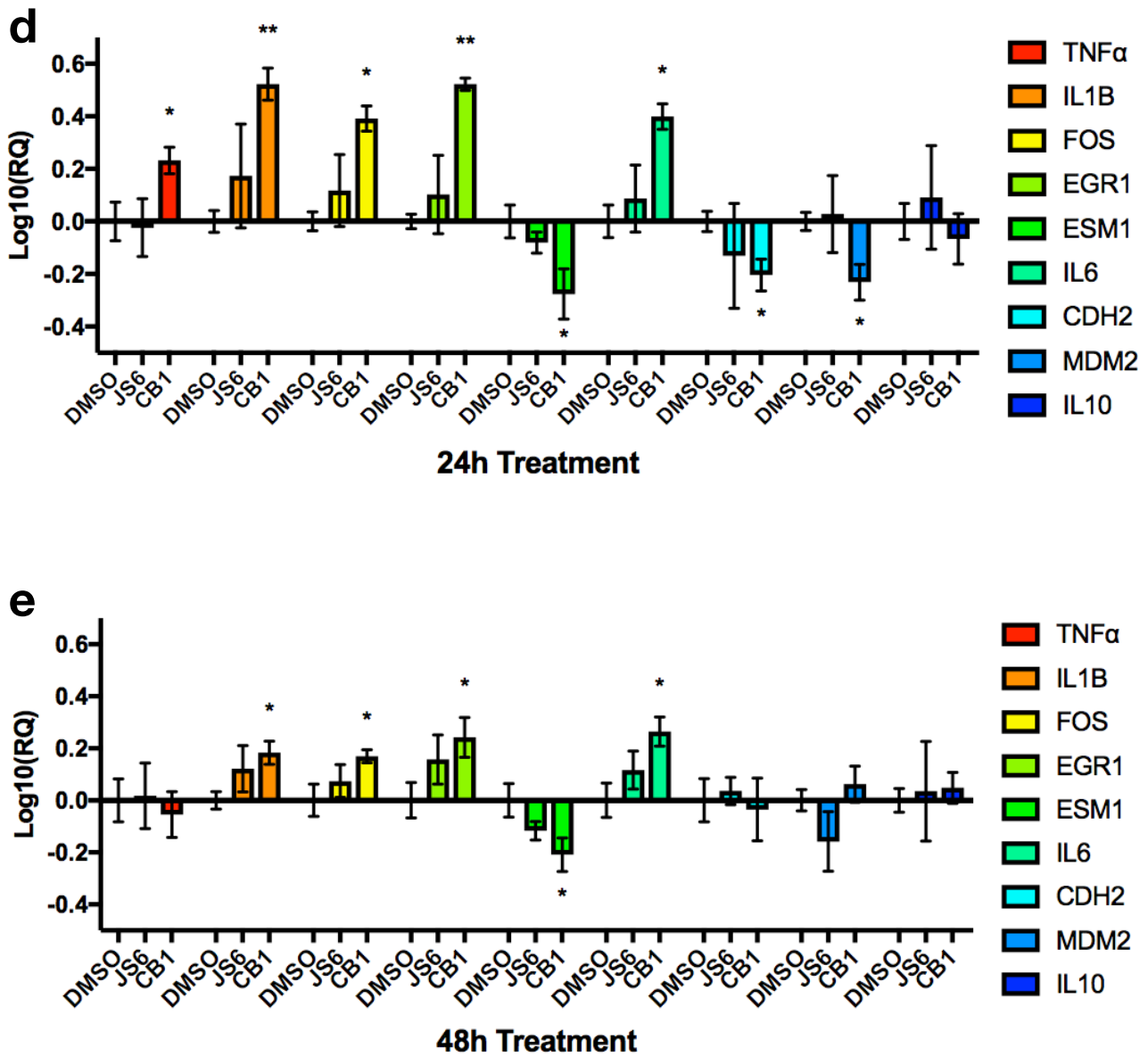


FIG. 5.7 RELATIVE EXPRESSION A BCL-3 RESPONSIVE GENE PANEL FOLLOWING SIRNA KNOCKDOWN, JS6 OR CB1 TREATMENT.

The relative gene expression of a selected panel was quantified using TaqMan qRT-PCR probes in MDA-MB-231-Luc cells with the conditions of 48 hour knockdown with **a.** Bcl-3 siRNA, control siRNA or treatment with 100 μ M of JS6, CB1 or DMSO control for either **b.** 3 hours, **c.** 8 hours, **d.** 24 hours or **e.** 48 hours. Error bars represent \pm SEM of 3 independent experiments. (T-test, *= $p < 0.05$, **= $p < 0.01$, ***= $p < 0.001$)

5.7 Daily refresh of JS6 and CB1 more effectively impaired clonogenic survival

It was evident from the qRT-PCR time course gene panel experiments that both Bcl-3 inhibitors most effectively imparted transcriptional signatures similar to that of siRNA knockdown within the 24 hour time point. By 48 hours many of the remaining significant gene changes had become much less pronounced and none of the changes to the genes that were direct transcriptional targets for Bcl-3 remained. This suggests that perhaps in order to maintain a comparable effect to siRNA knockdown, the drug treatment ought to be refreshed every 24 hours. The colony formation assay was used to test the effects of daily drug treatment.

MDA-MB-436 and MDA-MB-231-Luc cells were treated with either JS6, CB1 or DMSO control at a range of concentrations for 24 hours before plating the cells at low density in a colony formation assay. Medium containing either JS6, CB1 or DMSO control was replaced every 24 hours and cells were cultured for 10 days. Daily treatment with JS6 or CB1 significantly reduced colony numbers as well as average sizes at all concentrations in the MDA-MB-436 cell line (**Fig. 5.8**). For the MDA-MB-231-Luc cell line, JS6 was able to significantly reduce colony numbers and average sizes at 10 μ M and 100 μ M concentrations, while CB1 reduced colony numbers and sizes at all concentrations (**Fig. 5.9**).

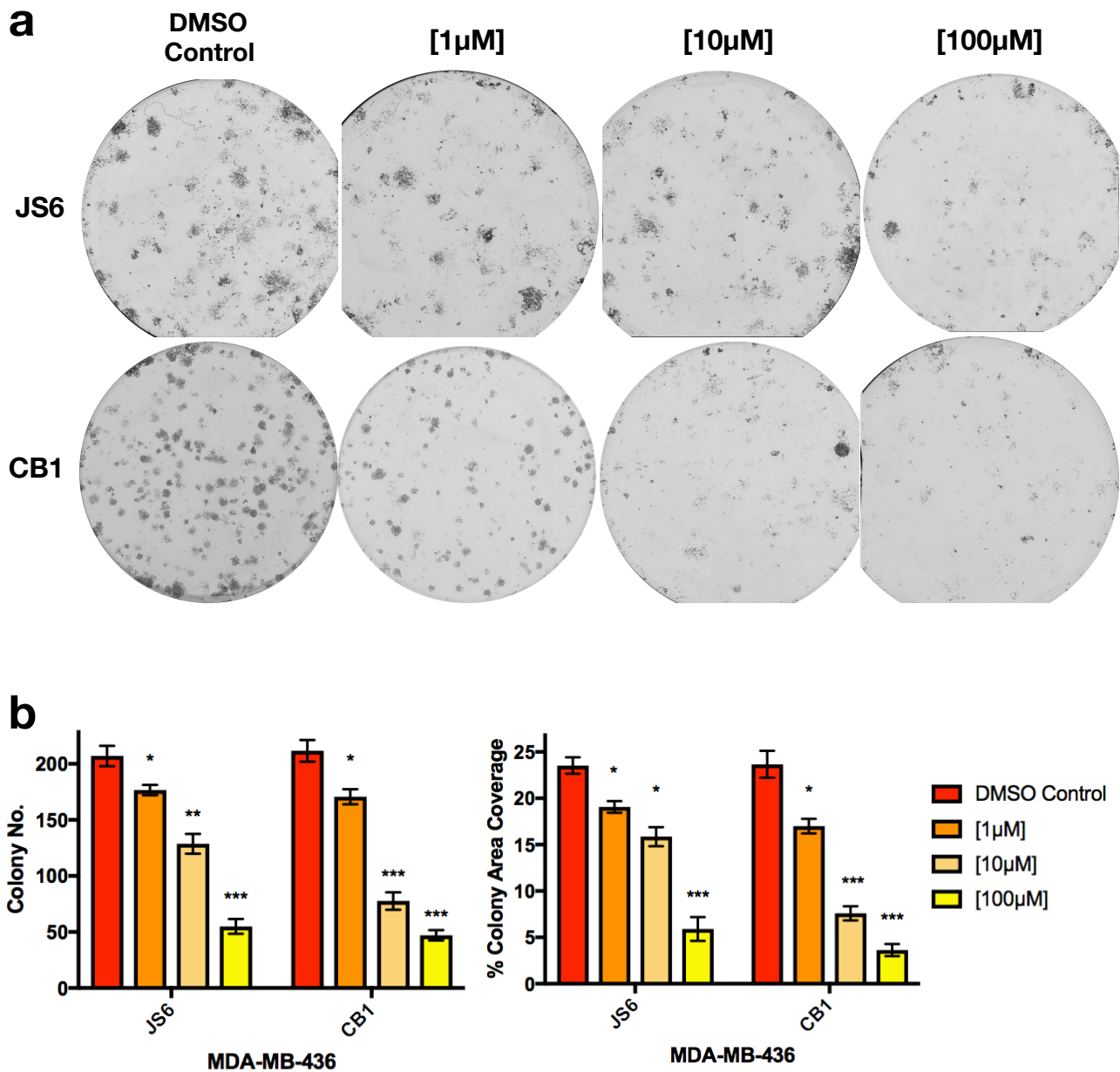


FIG. 5.8 DAILY REFRESH OF JS6 AND CB1 MORE EFFECTIVELY IMPAIRED CLONOGENIC SURVIVAL

Clonogenic potential was tested by treating MDA-MB-436 cells with either JS6, CB1 or DMSO control at a range of concentrations for 24h before plating the cells at low density in a colony formation assay. Medium containing either JS6, CB1 or DMSO control was replaced every 24 hours and cells cultured for 10 days before being fixed and stained with crystal violet. **a.**

Representative bright-field images and **b.** total colony number and average colony coverage for MDA-MB-436 cells. Error bars represent \pm SEM of 3 independent experiments. (T-test, *= $p < 0.05$, **= $p < 0.01$, ***= $p < 0.001$)

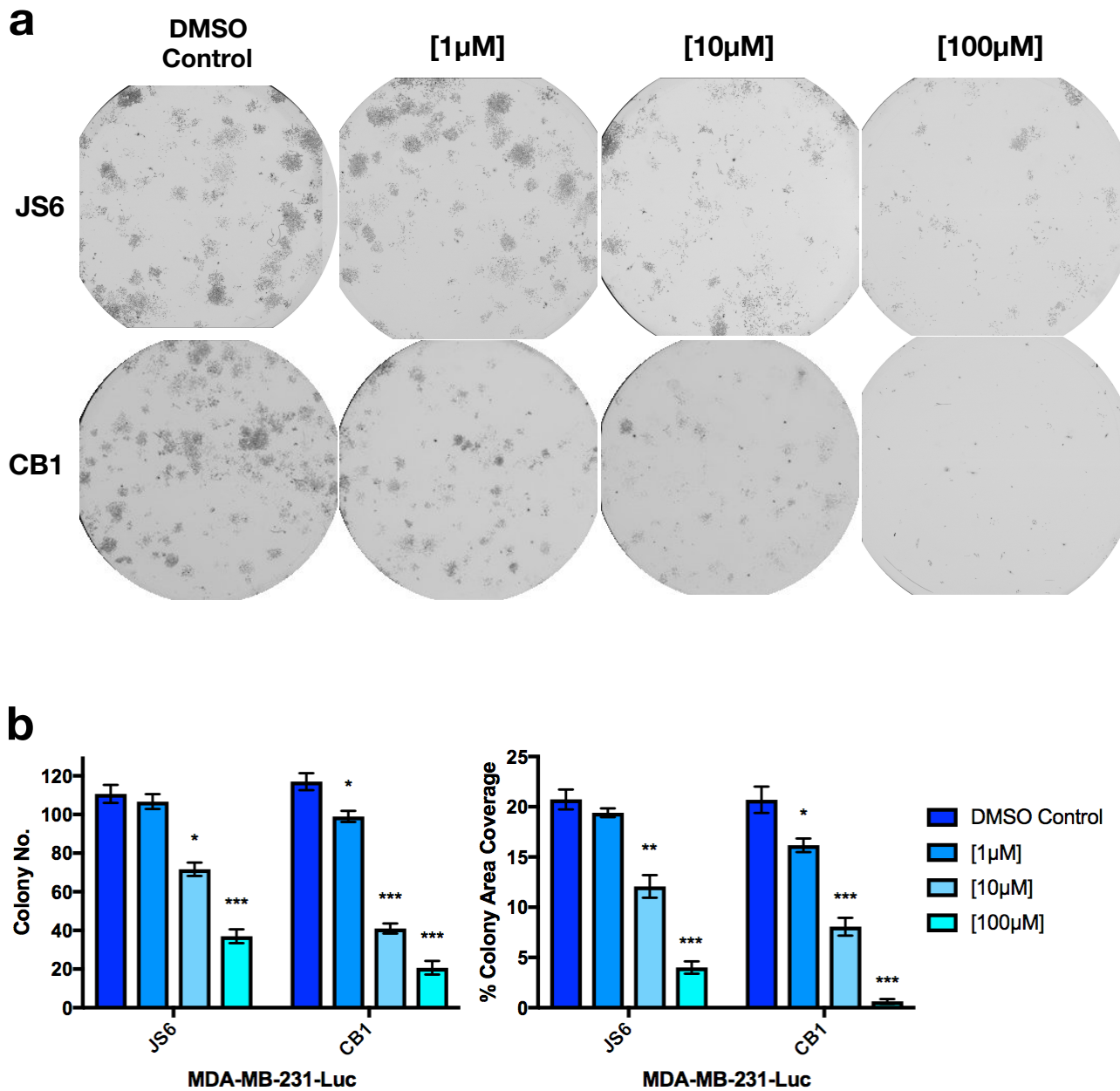


FIG. 5.9 DAILY REFRESH OF JS6 AND CB1 MORE EFFECTIVELY IMPAIRED CLONOGENIC SURVIVAL

Clonogenic potential was tested by treating MDA-MB-231-Luc cells with either JS6, CB1 or DMSO control at a range of concentrations for 24h before plating the cells at low density in a colony formation assay. Medium containing either JS6, CB1 or DMSO control was replaced every 24 hours and cells cultured for 10 days before being fixed and stained with crystal violet. **a.** Representative bright-field images and **b.** total colony number and average colony coverage for MDA-MB-231-Luc cells. Error bars represent \pm SEM of 3 independent experiments. (T-test, *= $p < 0.05$, **= $p < 0.01$, ***= $p < 0.001$)

5.8 *In vivo* xenograft modelling

Xenograft models have been extensively used as predictive models for cancer therapeutic efficacy. Before we can consider moving into human clinical trials, it is essential to evaluate drug efficacy and any potential toxicities *in vivo*. Though it is worth noting that although *in vivo* studies are valuable, the results has not consistently translated to the clinic and the significance of these studies can be hotly debated (Sausville and Burger, 2006). Nonetheless if we are to push forward with the ultimate goal of small molecule inhibition of Bcl-3 in human TNBC patients, it would be extremely beneficial to first demonstrate *in vivo* efficacy. Based on the results from *in vitro* assays, we decided a daily drug treatment regime was optimal provided it was well tolerated by the animals.

5.8.1 Xenograft model one: The effects of Bcl-3 inhibitors on metastatic seeding capabilities of MDA-MB-231-Luc cells

We wanted to model the later stages of the metastatic seeding process using the luciferase expressing MDA-MB-231-Luc cell line we thoroughly characterised in previous chapters. This is an aggressive line that proliferated rapidly, meaning it would not have allowed for sufficient time for cells transplanted at the orthotopic site to metastasise before reaching a size impeding normal animal function. Therefore experimental metastases were established by intravenous injection of 2×10^5 MDA-MD-231-Luc cells. Cells were suspended in 100 μ L of RPMI media and injected via the tail vein of 8-week old female Hsd: Athymic Nude-Foxn 1^{nu} mice (Harlan Laboratories). It had been shown that tail vein tumours exhibited no gene profile differences when compared to metastases generated by orthotopic tumours (Rashid et al., 2013).

Metastatic progression to distal organs was assessed through bioluminescence imaging with the IVIS Spectrum In Vivo Imaging System (Perkin Elmer). Prior to imaging, an intraperitoneal injection of 100 μ L D-luciferin was administered to each animal. The mice were then anaesthetised with 2.5% isoflurane, oxygen mix and imaged with the charge-coupled IVIS camera device selecting an exposure time of 2 minutes. Luminescence signal was measured through region of interest selection and quantified as total flux (photon count) overlaying corresponding grayscale photographs (**Fig. 5.10**) and composite images were analysed using the Living Image software (Xenogen Bioscience Corp).

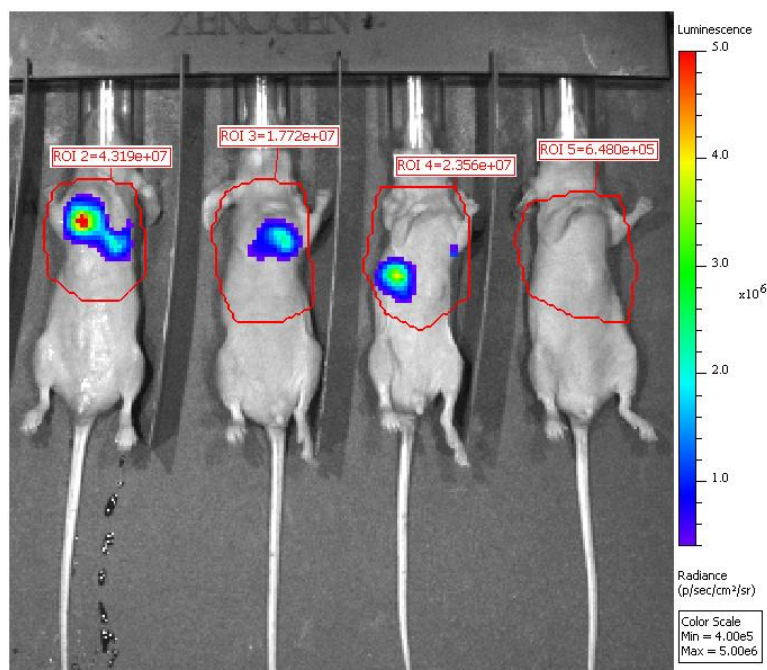


FIG. 5.10 QUANTIFICATION OF METASTATIC PROGRESSION THROUGH *IN VIVO* LUMINESCENCE IMAGING

Experimental metastases were established by intravenous injection of 2×10^5 MDA-MD-231-Luc cells. Cells were suspended in 100 μL of RPMI media and injected via the tail vein of 8-week old female Hsd: Athymic Nude-Foxn 1^{nu} mice (Harlan Laboratories). Metastatic progression to distal organs was assessed through bioluminescence imaging with the IVIS Spectrum In Vivo Imaging System. Prior to imaging, an intraperitoneal injection of 100 μL D-luciferin was administered to each animal. The mice were then anaesthetised with 2.5% isoflurane, oxygen mix and imaged with an exposure time of 2 minutes. Luminescence signal was measured through region of interest selection and quantified as total flux (photon count) overlaying corresponding grayscale photographs and composite images were analysed using the Living Image software.

5.8.1.1 Anti-metastatic efficacy of JS6 and 15F in xenograft model one

The first experiment using xenograft model one tested the anti-metastatic efficacies of JS6 and another Bcl-3 inhibitor analogue, 15F. The mice were pretreated 24 hours and 10 minutes prior to injection of cells with either 1% DMSO vehicle control (n=5), 3.5mg/kg of 15F (n=4) or 3.5mg/kg of JS6 (n=5); subsequent daily intraperitoneal injections were carried out for 9 days following first injection of cells. Imaging of animals was carried out on day 11, day 24, day 28, day 41 and day 47. Animals were sacrificed on day 47 and at this experimental endpoint, 5/5 mice in the DMSO control cohort, 2/4 mice in the 15F cohort and 0/5 mice in the JS6 cohort developed detectable tumours (**Fig. 5.11a**). When compared to DMSO controls, the mean metastatic burden was significantly reduced in the JS6 cohort ($p < 0.0001$).

Two additional model one xenograft experiments both focusing on the efficacy of JS6 were carried out. In the second experiment, 3/5 mice in the DMSO control cohort and 1/3 mice in the JS6 treated cohort developed detectable tumours (**Fig. 5.11b**). Animals were last imaged at day 30. In the third experiment, 2/3 mice in the DMSO control cohort and 3/4 animals in the JS6 cohort developed detectable tumours (**Fig. 5.11c**). Animals were last imaged at day 56. Although there were no statistically significant differences between JS6 and DMSO control cohorts in these experiments, there was a noticeable trend of increased individual tumour burden within the control cohorts. When we consider results from all experiments, we can observe 3/13 (23%) of DMSO control mice were tumour free, contrasted to the much higher tumour free proportion of 2/4 (50%) for 15F treated mice and 8/12 (67%) of JS6 treated mice.

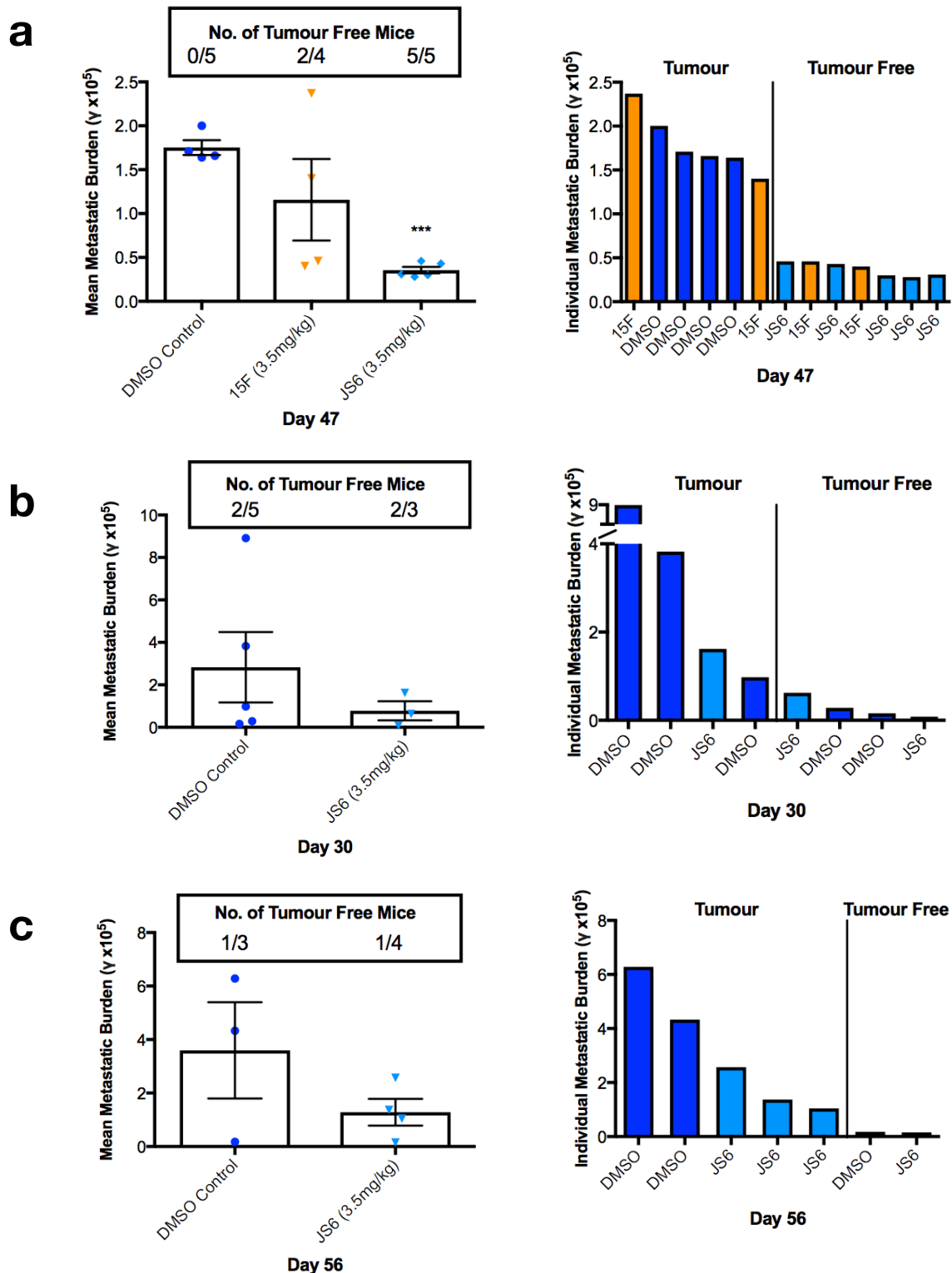


FIG. 5.11 ANTI-METASTATIC EFFICACY OF JS6 AND 15F IN XENOGRRAFT MODEL ONE

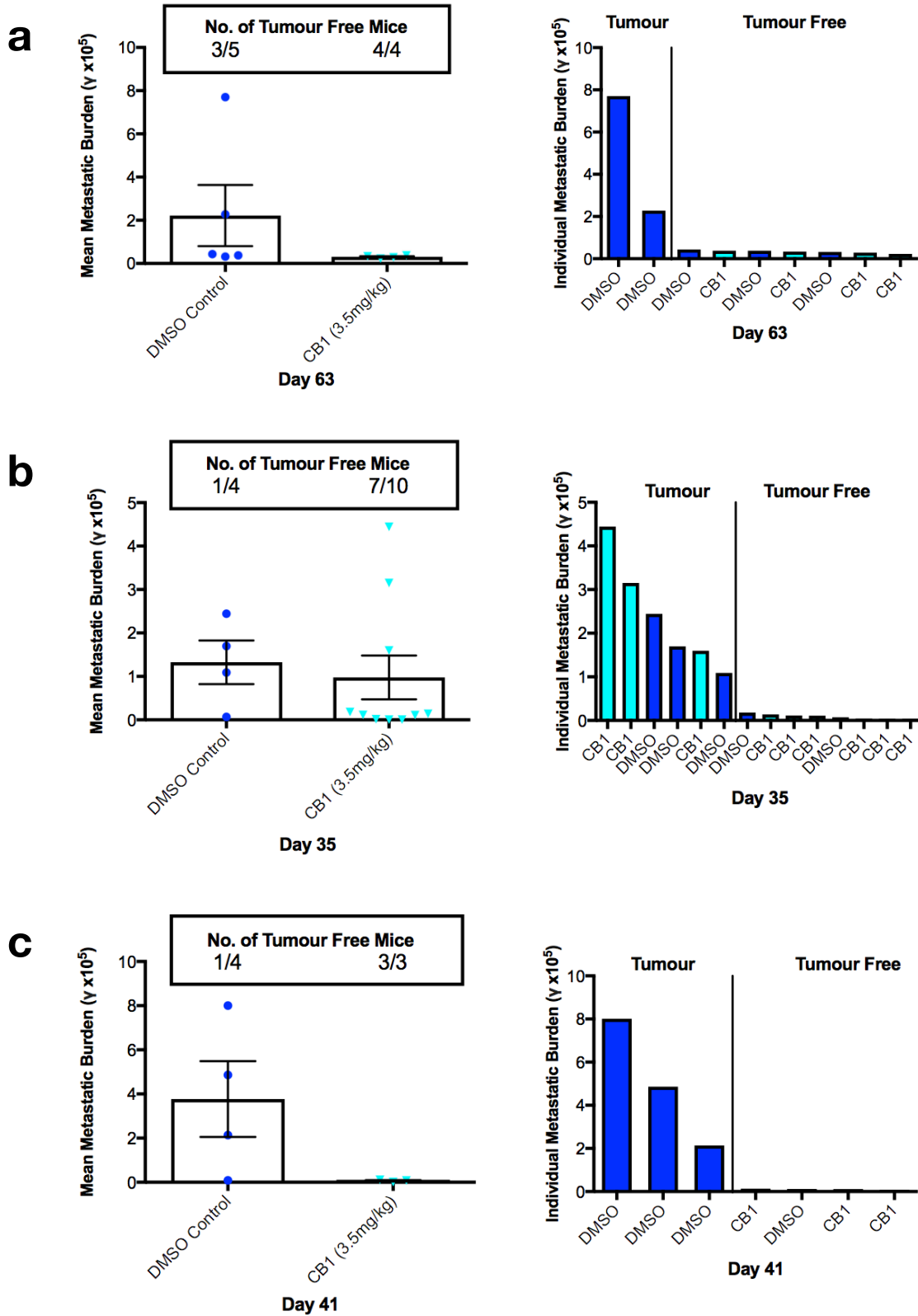
The anti-metastatic efficacies of JS6 and 15F were investigated in MDA-MB-231-Luc cells using xenograft model one. Mice were pretreated 24 hours and 10 minutes prior to injection of cells with either 1% DMSO vehicle control, 3.5mg/kg of 15F or 3.5mg/kg of JS6; subsequent daily intraperitoneal injections were carried out for 9 days following first injection of cells. Imaging of animals was carried out periodically until experimental endpoint. **a. b. c.** Scatter plots with bars detailing average metastatic burden for each cohort and waterfall plots detailing the individual metastatic burden of each mouse in three independent model one xenograft experiments. Error bars represent \pm SEM. (T-test, ***= $p < 0.001$)

5.8.1.2 Anti-metastatic efficacy of CB1 in xenograft model one

The anti-metastatic efficacy of CB1 was tested in four independent model one xenograft experiments. Once again, mice were pretreated 24 hours and 10 minutes prior to injection of cells with either 1% DMSO vehicle control or 3.5mg/kg of CB1; subsequent daily intraperitoneal injections were carried out for 9 days. Imaging of animals was carried periodically until experimental endpoint.

In the first experiment, 2/5 mice in the DMSO control cohort and 0/4 mice in the CB1 cohort developed detectable tumours by experimental endpoint of day 63 (**Fig. 5.12a**). In the second experiment, 3/4 mice in the DMSO control cohort and 3/10 mice in the CB1 cohort developed detectable tumours by experimental endpoint of day 35 (**Fig. 5.12b**). In the third experiment, 3/4 mice in the DMSO control cohort and 0/3 mice in the CB1 cohort developed detectable tumours by experimental endpoint of day 41 (**Fig. 5.12c**). In the fourth experiment, 3/6 mice in the DMSO control cohort and 6/10 mice in the CB1 cohort developed detectable tumours by experimental endpoint of day 41 (**Fig. 5.12d**). For this experiment we closely monitored the health status of the mice past the final imaging date and did not cull them until signs of morbidity from tumour burden was observed. The CB1 treated cohort exhibited delayed time until morbidity when compared with DMSO controls as illustrated by the Kaplan-Meier curve detailing disease free survival (**Fig. 5.12e**).

Although there were no statistically significant differences between the average metastatic burden following CB1 treatment within each individual experiment, from the waterfall plots, we can observe a trend of DMSO control mice developing greater individual metastatic burdens. When we aggregate the results from all experiments, 8/19 (42%) of DMSO control mice were tumour free, contrasted to the much high proportion of 18/27 (67%) of tumour free CB1 treated mice.



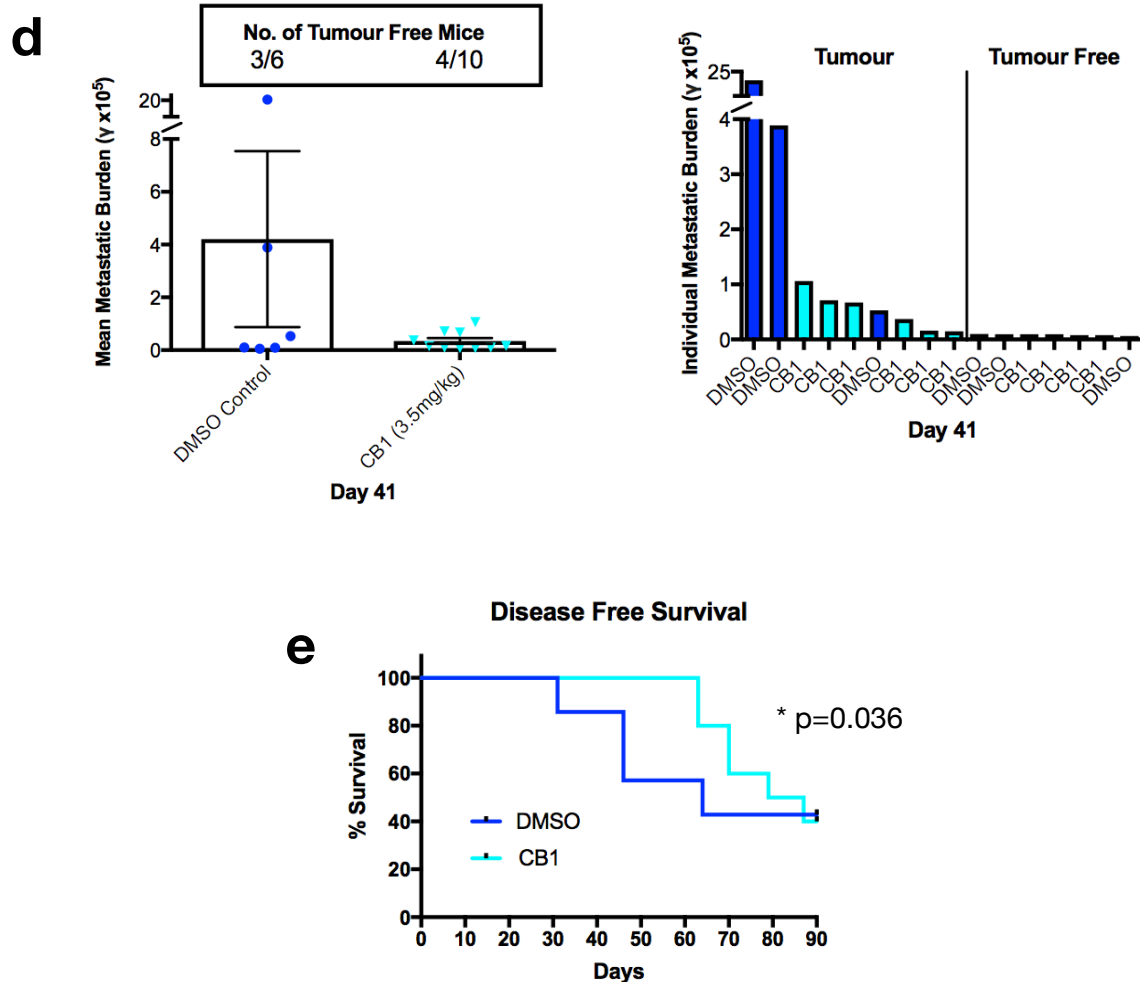


FIG. 5.12 ANTI-METASTATIC EFFICACY OF CB1 IN XENOGRRAFT MODEL ONE

The anti-metastatic efficacy of CB1 was investigated in MDA-MB-231-Luc cells using xenograft model one. Mice were pretreated 24 hours and 10 minutes prior to injection of cells with either 1% DMSO vehicle control or 3.5mg/kg of CB1; subsequent daily intraperitoneal injections were carried out for 9 days following first injection of cells. Imaging of animals was carried out periodically until experimental endpoint. **a. b. c. d.** Scatter plots with bars detailing average metastatic burden for each cohort and waterfall plots detailing the individual metastatic burden of each mouse in four independent model one xenograft experiments. **e.** Kaplan-Meier curve detailing disease free survival for DMSO control and CB1 cohorts from experiment four. Error bars represent \pm SEM

5.8.1.3 JS6 and CB1 significantly reduced metastatic burden in xenograft model one

Individual metastatic burden data from all xenograft model one experiments were aggregated and nonlinear regression analysis carried out in GraphPad Prism. Exponential growth curves were fitted to each experimental cohort (R-squared for DMSO=0.29, CB1=0.014, JS6=0.23, 15F=0.19) and paired t-tests were performed between DMSO and each drug treated cohort (**Fig. 5.13**). CB1 ($p=0.035$) and JS6 ($p=0.024$) treated cohorts were found to significantly reduce metastatic burden when compared to DMSO control animals.

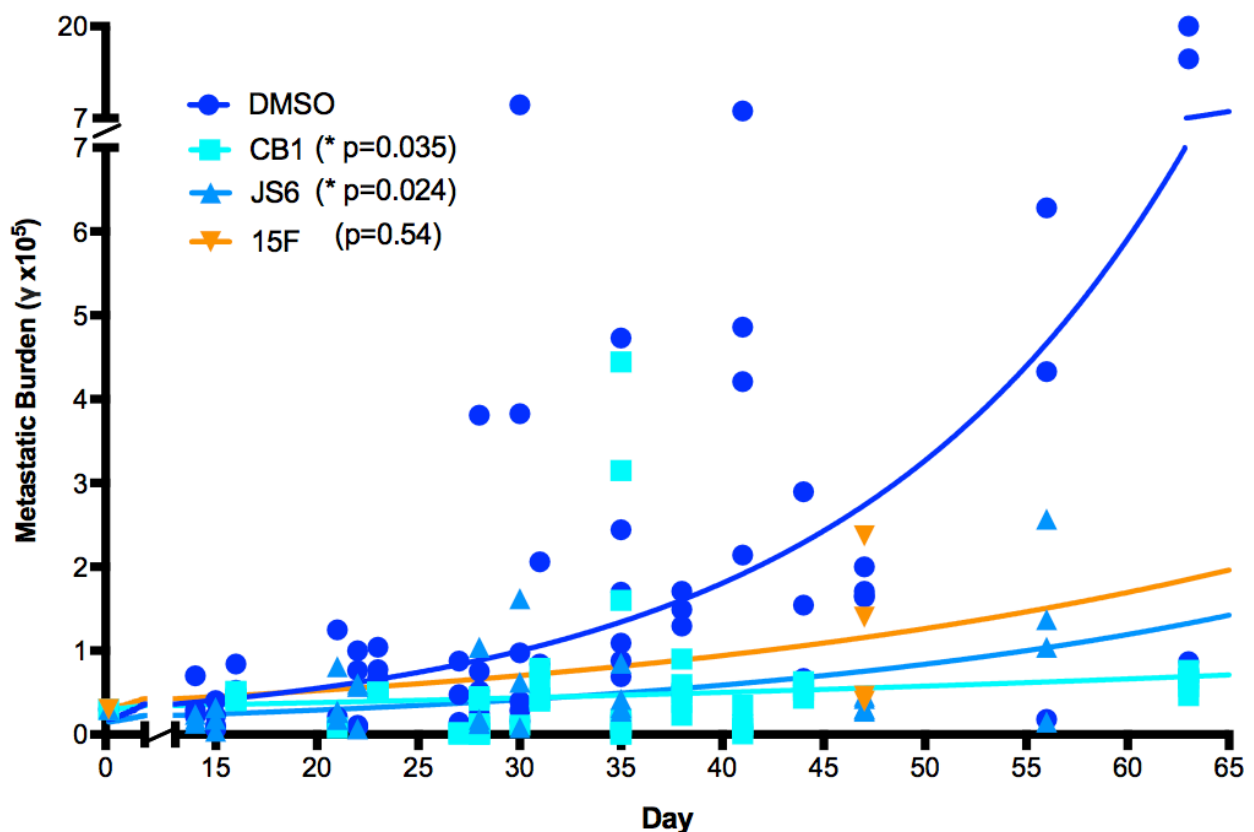


FIG. 5.13 CB1 AND JS6 SIGNIFICANTLY REDUCED METASTATIC BURDEN IN XENOGRRAFT MODEL ONE

Individual metastatic burden results from all xenograft model one experiments were aggregated and plotted as a scatter chart. Nonlinear regression analysis was carried out in GraphPad Prism and exponential growth curves were fitted to each experimental cohort (R-squared for DMSO=0.29, CB1=0.014, JS6=0.23, 15F=0.19). Paired t-tests were performed between DMSO and each drug treated cohort; CB1 ($p=0.035$) and JS6 ($p=0.024$) treatments were found to significantly reduce metastatic burden.

5.8.2 Anti-metastatic efficacy of CB1 was maintained in xenograft model one when administered via oral gavage

An important factor to consider when developing a drug is the different ways it can be administered. We wanted to test the oral availability and efficacy of CB1 when it is administered via oral gavage in an xenograft model one experiment. Mice were treated with either 3.5mg/kg (n=5), 20mg/kg (n=5) of CB1 or DMSO vehicle control (n=5) and tumour burden quantified periodically until the experimental endpoint at day 28. The lower CB1 concentration of 3.5mg/kg, did not significantly reduce tumour burden ($p=0.173$) with a small cohort size of 5 animals, but the higher concentration of 20mg/kg did profoundly reduce tumour burden ($p=0.038$) (**Fig. 5.14**). 1/5 (20%) of DMSO control mice, 2/5 (40%) 3.5mg/kg CB1 treated mice and 3/5 (60%) of 20mg/kg CB1 treated mice were tumour free at the experimental endpoint.

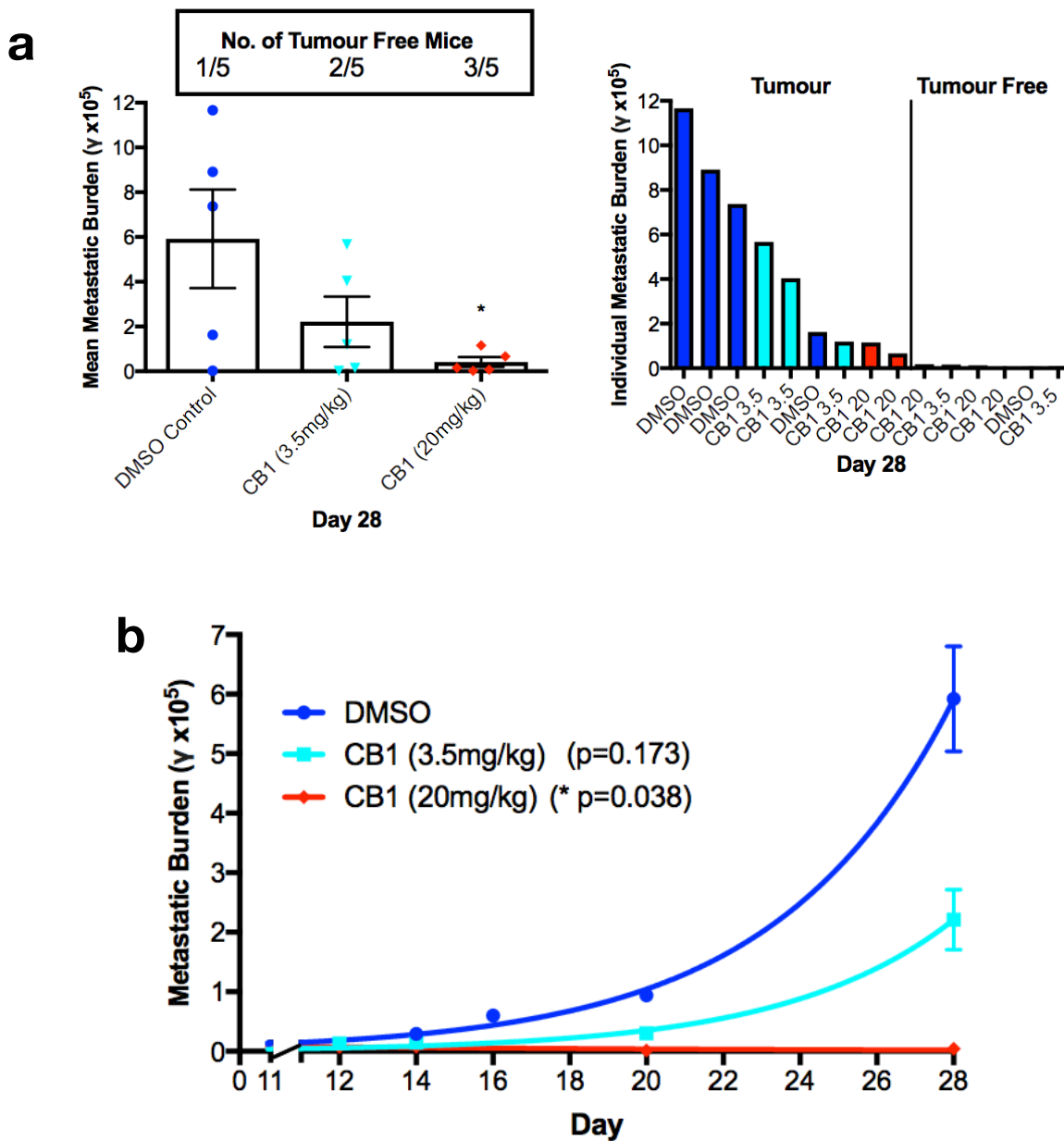


FIG. 5.14 ANTI-METASTATIC EFFICACY OF CB1 WAS MAINTAINED IN XENOGRAFT MODEL ONE WHEN ADMINISTERED VIA ORAL GAVAGE

The anti-metastatic efficacy CB1 was investigated in MDA-MB-231-Luc cells using xenograft model one. Mice were pretreated 24 hours and 10 minutes prior to injection of cells with either 5% DMSO vehicle control, 3.5mg/kg or 20mg/kg of CB1; subsequent daily oral gavages were carried out for 9 days following first injection of cells. Imaging of animals was carried out periodically until experimental endpoint at day 28. **a.** Scatter plot with bars detailing average metastatic burden for each cohort and waterfall plot detailing the individual metastatic burden of each mouse. **b.** Exponential growth regression for each cohort. Error bars represent \pm SEM. (T-test, * $p < 0.05$, ** $p < 0.01$, *** $p < 0.001$)

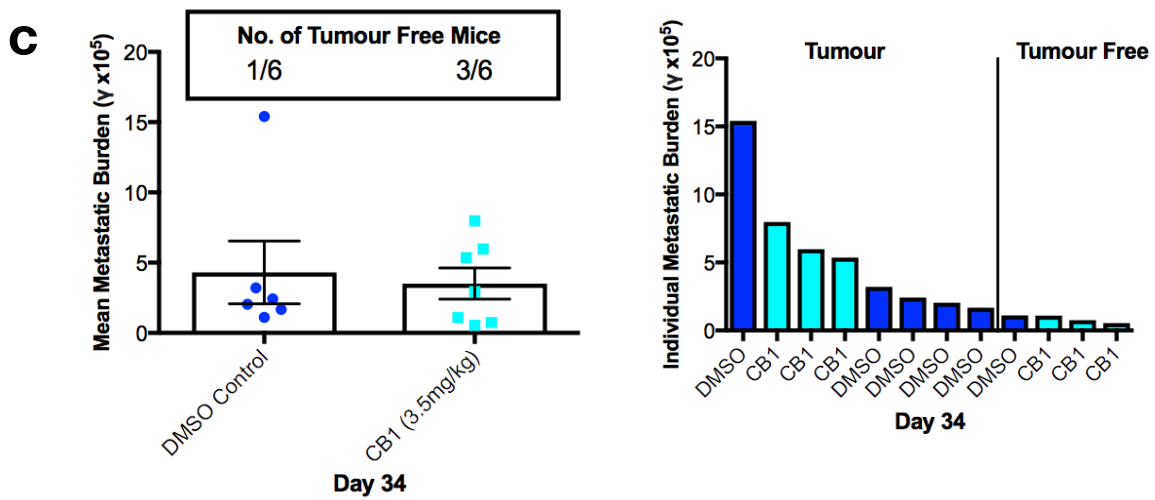
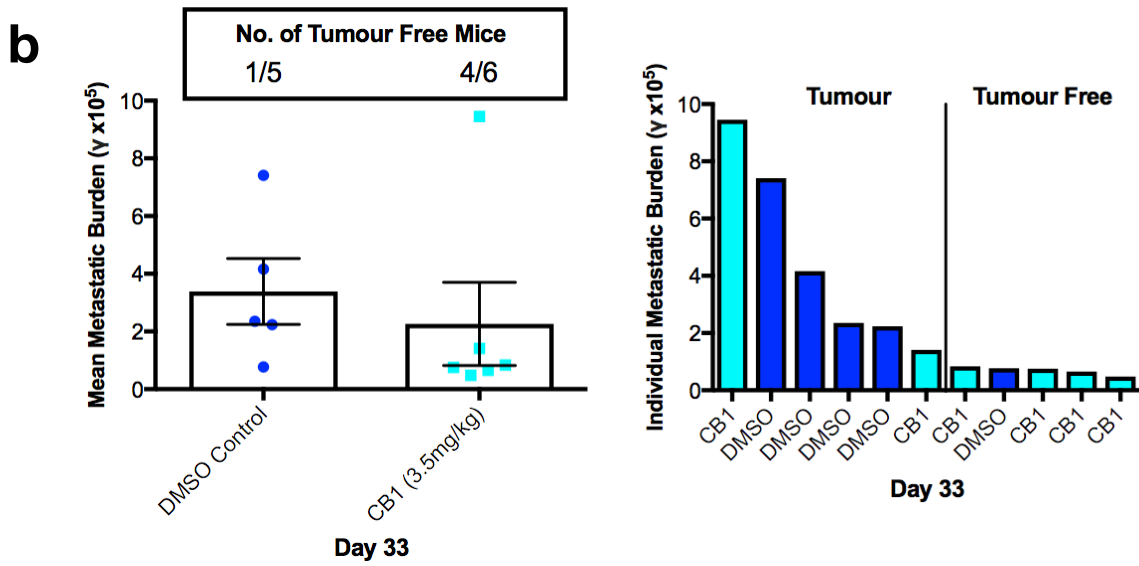
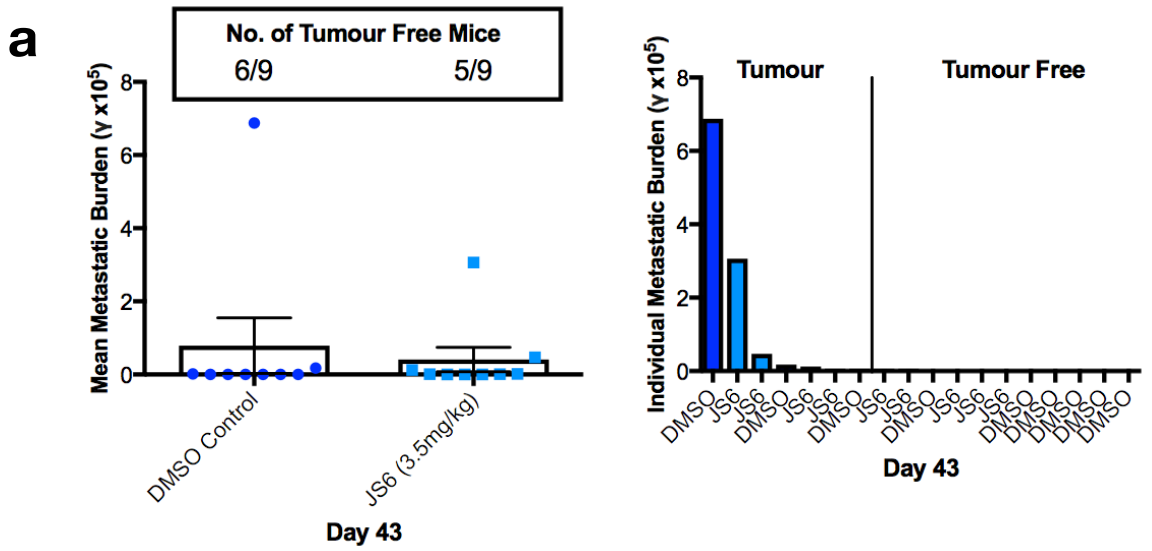
5.8.3 Xenograft model two: The effects of Bcl-3 inhibitors on metastatic colonisation and expansion capabilities of MDA-MB-231-Luc cells

We were able to demonstrate with our first xenograft model that the Bcl-3 inhibitors significantly reduced metastatic burden. This was especially evident in the context of reducing initial tumour seeding as a smaller proportion of animals in the drug treated cohorts developed detectable tumours compared to the controls. In the second xenograft model, we wanted to assess the efficacy of the inhibitors on subsequent colonisation and expansion of cells that have successfully seeded in their preferred distal sites.

5.8.3.1 JS6 and CB1 did not significantly inhibit metastatic colonisation and expansion

Experimental metastases were once again established by intravenous injection of 2×10^5 MDA-MD-231-Luc cells. Cells were suspended in 100 μ L of RPMI media and injected via the tail vein of 8-week old female Hsd: Athymic Nude-Foxn 1^{nu} mice (Harlan Laboratories). Cells were allowed to seed for 3 days and animals were treated from day 4 with daily intraperitoneal injections of either 1% DMSO vehicle control, 3.5mg/kg of JS6 or CB1 until experimental endpoint. In vivo bioluminescence imaging was carried out periodically and metastatic burden quantified.

When we aggregate the metastatic burden data from all experiments, neither JS6 (**Fig. 5.15a**) nor CB1 (**Fig. 5.15b&c**) was found to significantly inhibit metastatic colonisation and expansion in this experimental model. However 8/19 (42.1%) animals in the DMSO control cohorts developed no detectable tumours by the end of the experiments, while 5/9 (55.6%) animals in the JS6 cohort and 7/12 (58.3%) animals in the CB1 cohorts remained tumour free.



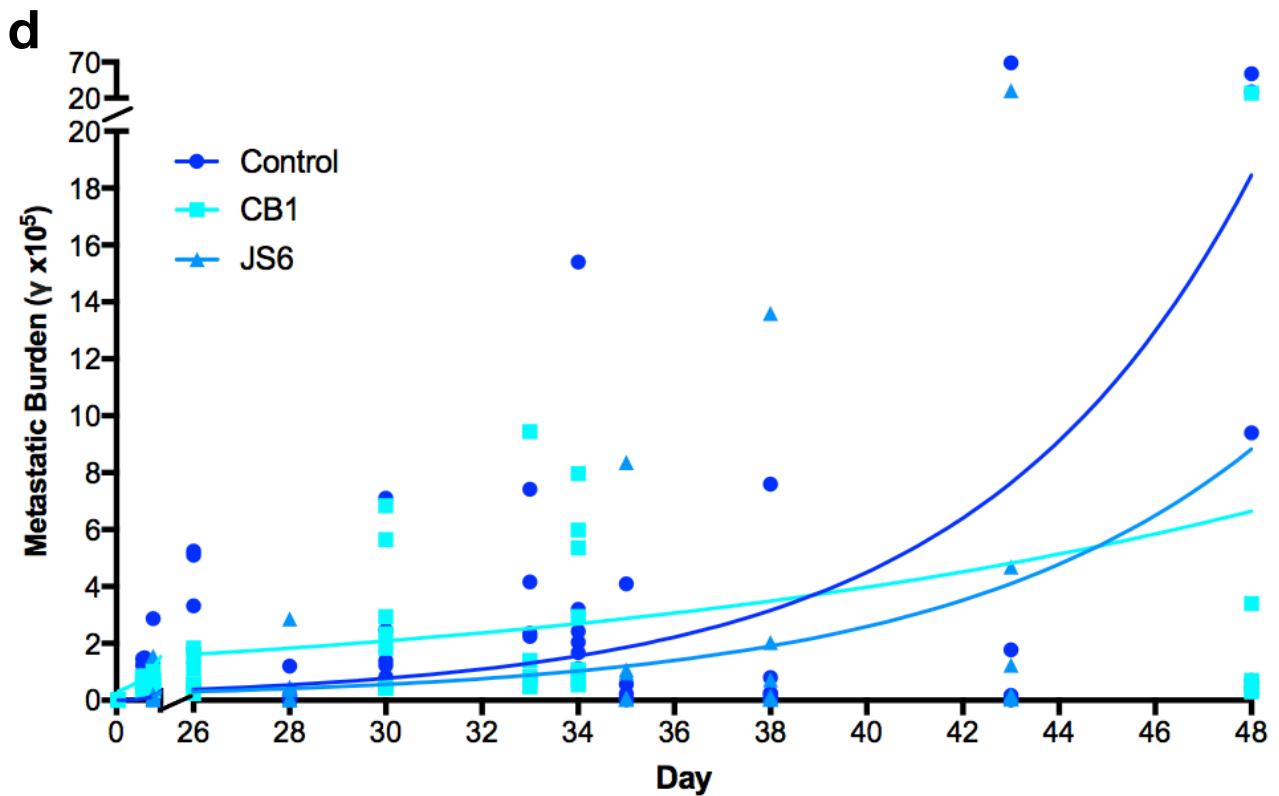


FIG. 5.15 JS6 AND CB1 DID NOT SIGNIFICANTLY INHIBIT METASTATIC COLONISATION AND EXPANSION

The anti-metastatic efficacy of JS6 and CB1 was tested in MDA-MB-231-Luc cells using xenograft model two. Cells were allowed to seed for 3 days and animals were treated from day 4 with daily intraperitoneal injections of either 1% DMSO vehicle control, 3.5mg/kg of JS6 or CB1 until experimental endpoint. In vivo bioluminescence imaging was carried out periodically and metastatic burden quantified. Scatter plots with bars detailing average metastatic burden for each cohort and waterfall plots detailing the individual metastatic burden of each mouse for **a.** JS6 treated cohort and **b&c.** CB1 treated cohorts. Error bars represent \pm SEM. **d.** Exponential growth regression for each cohort.

5.8.3.2 Daily JS6 and CB1 treatment did not significantly cause adverse toxicity

An important factor to consider when administering daily drug treatments was whether the regime caused adverse side effects. We closely monitored the health status of each animal on a daily basis and recorded their weights as this is often a good indicator of toxicity even if the animals did not show signs of morbidity. We found no significant differences between the growth rates of animals treated with daily 1% DMSO vehicle control, or 3.5mg/kg of JS6 or CB1 (**Fig. 5.16**).

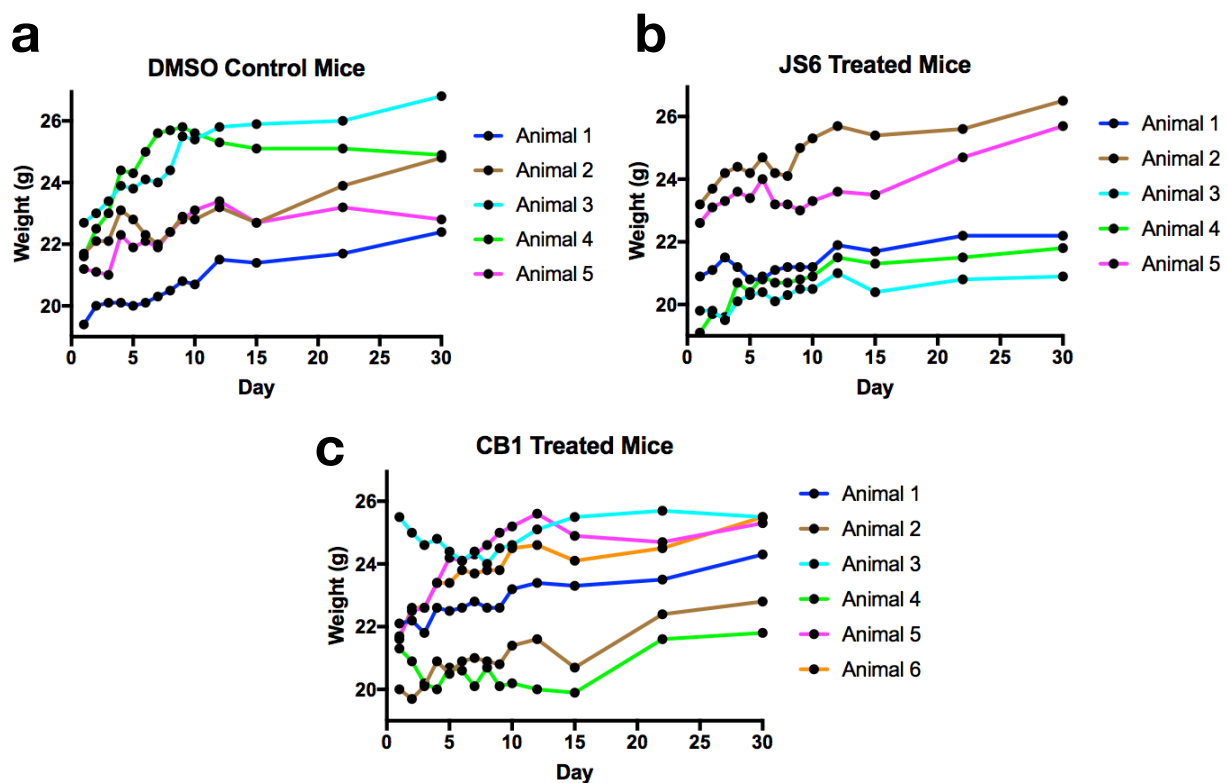


FIG. 5.16 DAILY JS6 AND CB1 TREATMENT DID NOT SIGNIFICANTLY CAUSE ADVERSE TOXICITY

Any possible toxicities associated with daily JS6 or CB1 i.p. injections was investigated using MDA-MB-231-Luc cells in xenograft model two. The health status of each animal was closely monitored on a daily basis and weights for animals treated with **a.** 1% DMSO vehicle control, **b.** 3.5mg/kg JS6 or **c.** 3.5mg/kg CB1 was recorded over a period of 30 days.

5.8.4 Xenograft model three: The effects of CB1 on TNBC orthotopic tumour growth

Although the Bcl-3 inhibitors did not significantly inhibit tumour expansion once seeding had taken place in xenograft model two, there was a trend of decreased tumour sizes in the drug treated cohorts. In xenograft model three we wanted to investigate the effects of CB1 on TNBC tumour growth at the orthotopic site and see if we could recapitulate the reduced cell turnover seen with Bcl-3 suppression in the previous chapters.

5.8.4.1 CB1 significantly reduced orthotopic tumour growth

Primary orthotopic metastases were established by subcutaneous injection of 1×10^6 MDA-MD-231-Luc or MDA-MB-436 cells. Cells were suspended in 100 μ L of RPMI/Matrigel solution and injected into bilateral mammary fat pads of 8-week old female Hsd: Athymic Nude-Foxn 1^{nu} mice (Harlan Laboratories). Cells were allowed to seed for 4 days and animals were treated from day 5 with daily intraperitoneal injections of either 1% DMSO vehicle control or 3.5mg/kg CB1 until experimental endpoint. Tumour sizes were measured and recorded periodically and animals were sacrificed when tumour diameter exceeded 20mm in any one dimension. Daily treatment of CB1 at a dosage of 3.5mg/kg was found to significantly reduce average orthotopic tumour sizes of both MDA-MB-231-Luc and MDA-MB-436 cell lines from day 38 onwards (**Fig. 5.17**).

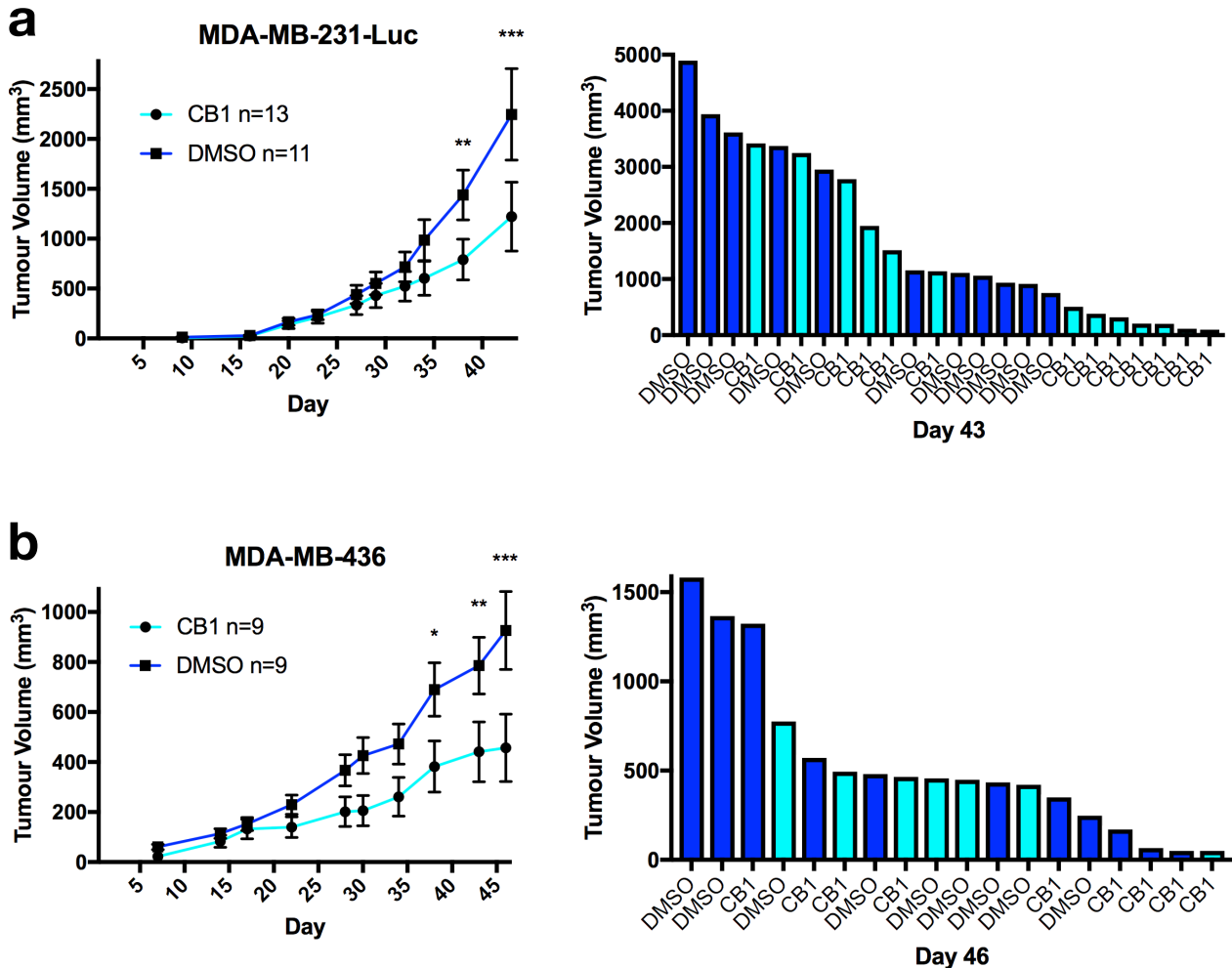


FIG. 5.17 CB1 SIGNIFICANTLY REDUCED ORTHOTOPIC TUMOUR GROWTH IN XENOGRAFT MODEL THREE

Primary orthotopic metastases were established by subcutaneous injection of 1×10^6 MDA-MB-231-Luc or MDA-MB-436 cells. Cells were suspended in 100 μ L of RPMI/Matrigel solution and injected into bilateral mammary fat pads of 8-week old female Hsd: Athymic Nude-Foxn1^{nu} mice. Cells were allowed to seed for 4 days and animals were treated from day 5 with daily intraperitoneal injections of either 1% DMSO vehicle control or 3.5mg/kg CB1 until experimental endpoint. Tumour sizes were measured and recorded periodically and animals were sacrificed when tumour diameter exceeded 20mm in any one dimension. Average tumour volume and waterfall plot detailing individual tumour volume of each mouse on the final day for **a.** MDA-MB-231-Luc and **b.** MDA-MB-436. Error bars represent \pm SEM. (T-test, *= $p < 0.05$, **= $p < 0.01$, ***= $p < 0.001$)

5.9 Discussion

In the previous chapters we highlighted proto-oncogenic properties of Bcl-3 within TNBC cell lines and especially its associations with promoting an increased metastatic phenotype. Bcl-3 suppression was found to reduce overall cell turnover, decrease migration and generally promoted tumour suppressive phenotypes. Using structure based computational modelling, small molecule inhibitor compounds targeting the Bcl-3-p50/Bcl-3-p52 protein interactions were designed and synthesised. In this final chapter, we focused on evaluating the efficacy of two lead compounds in TNBC cell lines, JS6 and a structurally novel analogue, CB1.

5.9.1 JS6 and CB1 disrupted Bcl-3-p50 protein-protein binding

In order to confirm mechanism of action, we tested the capabilities of the inhibitor compounds to disrupt protein-protein binding of Bcl-3 and p50 using a coimmunoprecipitation setup. We chose the MDA-MB-231-Luc cell line stably overexpressing WT Bcl-3 for this experiment as it ensured a high concentration of Bcl-3 in the lysate used for protein pulldown. In line with expectations, both JS6 and CB1 treatments at 50 μ M concentrations resulted in significant reductions of secondary p50 or Bcl-3 complexes depending on the primary protein pulldown when compared to DMSO controls. Two hour drug treatment duration proved to be more efficacious than thirty minutes and CB1 was found to be more effective than JS6 in both durations (**Fig.5.1c&d**). Despite there being similar quantities of p50 and p52 proteins in MDA-MD-231 cell lines (Eckhardt et al., 2013), we failed to find a suitably robust p52 antibody to carry out colP pulldown and western blotting.

It was evident from the western blots that we were able to consistently pulldown similar amounts of Bcl-3 protein (**Fig. 5.1a**) despite the pcDNA control cell line having significantly less Bcl-3 than the overexpression mutant line. This suggested that we were able to saturate the sepharose protein beads with either Bcl-3 or p50 protein to achieve a consistent pulldown quantity each time. Interestingly, despite this constant Bcl-3 protein pulldown quantity, we found significantly less complexed p50 in the pcDNA control cell lysates, implying Bcl-3 in these cells bound less p50 compared to the WT Bcl-3 overexpression line. When we pulled-down p50 (**Fig. 5.1b**), there were also significantly less complexed Bcl-3 in the pcDNA control cells. These results indirectly suggested that

overexpression of Bcl-3 led to increased p50 complexing dynamics. Lysates from cells overexpressing the Bcl-3 ANK mutant also resulted in significantly reduced quantities of bound p50 and Bcl-3 secondary complexes. This is due to the Bcl-3 ANK mutant being unable to bind p50.

5.9.2 JS6 and CB1 demonstrated *in vitro* efficacy

We treated three TNBC cell lines with either JS6 or CB1 at a range of drug concentrations for 48 hours and observed their effects on cell viability (**Fig. 5.2**). JS6 significantly reduced viability of two of the cell lines at the highest 100 μ M concentration, while CB1 had slightly better potency at the same concentration and was also significantly efficacious at 10 μ M. Neither inhibitors reduced cell viability in the non-tumourigenic MCF10a cell line, similar to the effects seen following Bcl-3 siRNA knockdown in chapter 3, supporting the idea that the drug effect was Bcl-3 specific.

In line with our previous Bcl-3 suppression findings, 48 hour CB1 treatment did not affect the number of mammospheres formed but instead reduced their average sizes (**Fig. 5.3**). This meant CB1 did not preferentially target the anoikis resistant cell populations in this assay. Subsequently resulting mammospheres were not serially passaged, so we cannot conclude on the effects of CB1 on self-renewal and the stem-like cell population in TNBC cells. 48 hour JS6 and CB1 treatment at 100 μ M was also able to significantly impair clonogenic survival of MDA-MB-231-Luc cells (**Fig. 5.4**). Interestingly, unlike the previous Bcl-3 suppression experiments, 48 hour period of CB1 treatment did not have any effects on NF κ B activity when assayed with a reporter construct (**Fig. 5.5**).

5.9.3 Global gene expression profiling following 48 hour CB1 treatment

In order to investigate the transcriptional effects of CB1, we carried out an Affymetrix DNA GeneChip microarray experiment on RNA harvested from MDA-MB-231-Luc cells treated with 100 μ M CB1 for 48 hours. We chose these treatment conditions as at this concentration we saw comparable effects to those seen in previous *in vitro* Bcl-3 suppression assays. We hypothesised that if small molecule inhibition of Bcl-3 acted upon similar transcriptional pathways as Bcl-3 siRNA knockdown, then we should see a degree of overlap between the subsequent gene changes. Surprisingly, we only saw 110

significantly altered genes out of a possible 43590 following CB1 treatment. This is in stark contrast to the >4000 significant changes following Bcl-3 siRNA knockdown, however there were many interesting biologically significant overlaps.

5.9.3.1 Overlapping genes in similar directions following CB1 and siRNA

A large number of the significantly overlapping gene changes following both CB1 treatment and Bcl-3 siRNA knockdown supported biological relevant rationales for the tumour suppressive functional outcomes we observed. In the next section we will list and explore some of the most relevant overlaps and their transcriptional roles.

HtrA Serine Peptidase 1 (HTRA1) was up 1.34-fold (1.81-fold with siRNA) and encodes a highly conserved member of the trypsin family of serine proteases. It has been recently implicated in suppression of EMT and cell motility in breast cancer by inhibiting TGF-beta signalling and its down-regulation is also associated with shorter patient survival (Lehner et al., 2013). Kindlin-1 (FERMT1) was down 0.83-fold (0.85-fold with siRNA) and encodes an integrin-interacting protein implicated in the activation of TGF-beta/Smad3 signalling. Functionally, Kindlin-1 promoted proliferation and was required for EMT in colorectal cancer (Kong et al., 2016). Transforming growth factor beta 1 (TGFB1) was up 1.15-fold (1.14-fold with siRNA) and encodes a secreted ligand of TGF-beta superfamily of proteins. It is a multifunctional regulatory cytokine that controls proliferation, differentiation and many other cellular functions, with both tumour suppressor and promoting effects in breast cancer depending on cancer stage (Zarzynska, 2014). These findings support a recent publication detailing the involvements of Bcl-3 with the stabilisation of Smad3 within TGF-beta signalling (Chen et al., 2016).

Kinesin family member 18A (KIF18A) was down 0.91-fold (0.74-fold with siRNA) and encodes a plus-end directed microtubule depolymerase kinesin. It has been found to be overexpressed in human breast cancer and is associated with higher grade, metastasis and poor survival. Its inhibition was shown to critically affect mitotic function as well as reducing migration by stabilising microtubules at the leading edges and induction of anoikis following inactivation of PI3K-Akt signalling (Zhang et al., 2010). Inositol polyphosphate-4-phosphatase type II B (INPP4B) was down 0.88-fold (0.83-fold with siRNA) and encodes one of the enzymes involved in phosphatidylinositol signalling

pathways. INPP4B has been shown to mediate PI3K signalling in breast cancer, enhancing SGK3 activation and suppressing Akt phosphorylation, all processes required for 3D proliferation, invasive migration and tumourigenesis *in vivo* (Gasser et al., 2014).

Hyaluronan Acid Synthase 2 (HAS2) was down 0.83-fold (0.51-fold with siRNA) and it encodes a protein that catalyses the synthesis of hyaluronan acid (HA), a high molecular weight unbranched polysaccharide that is one of the main components of the extracellular matrix. HA been shown to actively regulate cell adhesion, migration and proliferation by interacting with surface receptors such as CD44. HAS2 has been observed to be overexpressed in breast cancer cell lines and its high expression has been correlated with lymph node metastasis. Functional assays showed that knockdown of HAS2 inhibited proliferation both *in vivo* and *in vitro*, through the induction of apoptosis or cell cycle arrest (Li et al., 2015). Dual specificity phosphatase 5 (DUSP5) was up 1.33-fold (1.28-fold with siRNA) and it encodes a negative regulator of mitogen-activated protein kinase pathways. In basal-like breast cancers low DUSP5 expression was significantly correlated with poor survival, paclitaxel resistance and tumour progression (T. Liu et al., 2018).

Par-6 family cell polarity regulator beta (PARD6B) was down 0.85-fold (0.86-fold with siRNA), it encodes a PAR6 family member, an essential component in epithelial cell tight junction formation and maintenance of polarity in breast cancer cell lines. Its imbalance radically alters epithelial cell architecture and was found to contribute to tumour progression (Cunliffe et al., 2012). Netrin 4 (NTN4) was up 1.16-fold (1.17-fold with siRNA), it encodes a laminin-related protein and its decreased expression in TNBC has recently been associated with EMT-related biomarkers. NTN4 overexpression attenuated cell migration and invasion, and induced N-cadherin and vimentin downregulation, while NTN4 siRNA knockdown significantly increased migration and invasion (Xu et al., 2017). Semaphorin 3D (SEMA3D) was down 0.84-fold (0.76-fold with siRNA), it encodes a protein typically associated with migration of blood vessels during angiogenesis and neuronal axons during development. SEMA3D up-regulation has been implicated in the promoting metastasis in pancreatic ductal adenocarcinomas (Foley et al., 2015). Together these gene changes further highlight the links between Bcl-3 and transcriptional changes affecting the EMT process and tumour interactions with the microenvironment.

Interleukin 1 beta (IL1B) was up 1.45-fold (1.84-fold with siRNA) and encodes a member of the IL1 cytokine family. A recent study showed that up-regulation and secretion of IL1B production by TNBC cells induced a significant infiltration of anti-tumour neutrophils into the metastatic niche by chemotaxis (Zhao et al., 2018). Prostaglandin E synthase (PTGES) was up 1.32-fold (1.47-fold with siRNA) and encodes a glutathione-dependent prostaglandin E synthase. Its expression has been shown to be induced by IL1B, as well as TP53, and may be implicated in p53-mediated apoptosis (Lee et al., 2010). Colony stimulating factor 3 (CSF3) was up 1.45-fold (1.83-fold with siRNA) and encodes another cytokine associated with the recruitment of tumour associated macrophages (Hollmén et al., 2016). Interleukin 24 (IL24) was up 1.29-fold (1.37-fold with siRNA) and has been shown to be a tumour suppressor cytokine capable of reducing *in vivo* breast cancer growth by promoting the up-regulation of pro-apoptotic BAX as well as notable inhibition of tumour angiogenesis (Wei et al., 2015). A different animal study showed that IL-24 transformed the tumour microenvironment in colorectal cancer and promoted local CD4(+) and CD8(+) T cells to secrete interferon gamma, which enhanced the cytotoxicity of CD8(+) T cells (Ma et al., 2016). These overlapping gene changes proposed a very interesting alternative mechanism of drug action centred around immune signalling, as pharmacological activation of inflammatory cytokines could potentially augment the host innate immunity and promote suppression of metastatic colonisation.

Kruppel-like factor 2 (KLF2) was up 1.34-fold (1.59-fold with siRNA) and encodes a transcription factor that displays anti-carcinogenic properties. It is often found to be down-regulated in breast cancers and its expression positively correlates with patient survival. A recent study showed that KLF2 acted upon the retinoic acid pathway and induced the expression of tumour suppressive cellular retinoic acid-binding protein 2 (CRABP2) and inhibited the expression pro-tumourigenic fatty acid-binding protein 5 (FABP5) (Zhang et al., 2015). Vitamin D 24-hydroxylase (CYP24A1) was down 0.77-fold (0.78-fold with siRNA) and encodes a member of the cytochrome P450 superfamily of enzymes. Dysregulated CYP24A1 acts like a putative oncogene and its suppression conferred breast cancer cells with increased susceptibility to apoptosis and inhibited anchorage-independent growth (Osanai and Lee, 2016). Rap1-interacting protein 1 (RIF1) was down 0.87-fold (0.88-fold with siRNA) and encodes a protein involved in homologous recombination-mediated DNA double-strand break repair. It was found to be highly expressed in breast cancers and correlated positively with invasion

(Wang et al., 2009). These gene changes suggest that Bcl-3 signalling could be further implicated in cellular metabolism as well as DNA repair pathways.

Although most of the overlapping changes supported a tumour suppressive function for Bcl-3 inhibition, there were a few gene changes that argued against this notion. Proto-oncogene *c-fos* (FOS) was up 1.67-fold (1.36-fold with siRNA), this encodes the early gene product part of the activator protein-1 (AP-1) transcription factor and has been associated with mechanisms of cell proliferations, differentiation, apoptosis and transformation. Although the mainstream opinion on FOS considers it an oncogene some reports describe a tumour suppressive function (Durchdewald et al., 2009). Hairy and enhance of split homolog-1 (HES1) was up 1.58-fold (1.21-fold with siRNA) and encodes a transcription factor regulated by NOTCH, Hedgehog and Wnt signalling pathways. It has been associated with invasiveness, induction of EMT and tumour survival (Rani et al., 2016). Serum deprivation response (SDPR) was down 0.8-fold (0.53-fold with siRNA) and encodes a calcium-independent phospholipid-binding protein whose overexpression in metastatic breast cancer models promoted apoptosis and suppressed the formation of metastatic lesions in mice (Ozturk et al., 2016). Ultimately any given cellular phenotype will be the result and summation of a myriad of different signalling pathways, nonetheless it is important to pay attention to this balance.

5.9.3.2 Overlapping genes in opposing directions following CB1 and siRNA

There were a number of biologically interesting gene changes that overlapped between the two conditions but in opposing manners. It would be interesting to further investigate these targets to try and better understand the differences between small molecule Bcl-3 inhibition and siRNA knockdown.

Growth differentiation factor 15 (GDF15) was up 1.3-fold (down 0.60-fold with siRNA). It encodes a secreted ligand of the TGF-beta superfamily and expression of this inflammatory cytokine is associated with EMT, drug resistance and disease progression. A recent study demonstrated the association of GDF15 with high tumour grade, ER-negativity, and HER2 overexpression in breast cancer patients. Stable overexpression of GDF15 up-regulated expression of mesenchymal markers, and increases cellular invasion (Peake et al., 2017). PIM1 was up 1.24-fold following CB1 treatment, (down 0.67-

fold with siRNA). PIM has recently been associated with MYC and its inhibition in TNBCs has been shown to promote apoptosis and enhance sensitivity to chemotherapy (Zhao et al., 2017). Tensin 4 (TNS4) was up 1.18-fold (down 0.34-fold with siRNA) and it is involved in MET tyrosine kinase receptor signalling. TNS4 has been shown to directly interact with phosphorylated MET to positively regulate cell survival, proliferation, and migration, through increased MET protein stability (Muharram et al., 2014). Bcl-3 suppression with siRNA in these cases appeared to have been associated with beneficial therapeutic outcomes, while CB1 treatment signalled in the opposite direction.

There were also a number of gene changes where CB1 treatment correlated with beneficial outputs, while siRNA had the opposite effect. ST6GalNAc2 was up 1.39-fold (down 0.88-fold with siRNA) and this sialyltransferase has been identified as a novel *in vivo* breast cancer metastasis suppressor by altering the profile of O-glycans on the tumour cell surface, preventing the binding of soluble lectin galectin-3 (Murugaesu et al., 2014). TRAIL receptor 4 (TNFRSF10D) was down 0.83-fold (up 1.60 fold with siRNA) and encodes a member of the TNF-receptor superfamily. Tumour necrosis factor (TNF)-related apoptosis inducing ligand (TRAIL) selectively induced apoptosis in cancer cell and not normal cell, but expression of TRAIL-R4 in breast cancer cells is well correlated with TRAIL resistance (Sanlioglu et al., 2005). RNA Polymerase III subunit B (POLR3B) was down 0.88-fold (up 1.22-fold with siRNA) and it encodes the second largest subunit of RNA polymerase III. It has been shown to be down-regulated following chemotherapy in ER negative breast cancer (Einbond et al., 2010).

5.9.3.3 Gene changes seen only following CB1 treatment

There were a number of gene changes that did not overlap with Bcl-3 siRNA knockdown, but may still reflect biologically important drug responses. Pharmacological inhibition of Bcl-3 targeting its protein-protein interactions will fundamentally operate differently on a mechanistic level from knockdown of a particular gene. It is possible for the Bcl-3 protein to have novel involvements within cellular signalling pathways beyond simply their interactions with p50 and p52.

Early growth response 1 (EGR1) was up 1.74-fold and it encodes a stress response Cys2-His2-type zinc-finger transcription factor. It plays an important role in the regulation of cell survival, proliferation and cell death. It has been shown to regulate and activate the

expression of multiple tumour suppressors such as TP53 and TGFB1, thereby helping in the prevention of tumour formation (Baron et al., 2006). Interleukin 6 (IL6) was up 1.44-fold, this pleiotropic cytokine plays an important role in regulating systemic inflammation and studies have linked intra-tumour IL6 signalling with inhibited proliferation in breast cancer (Dethlefsen et al., 2013). Endocan (ESM1) was down-regulated 0.63-fold, it encodes a secreted protein and its high expression in MDA-MB-231 cells is associated with aggressive disease and worse *in vivo* relapse-free survival (Sagara et al., 2017).

There were a few changes that did not seem to align with our therapeutic goals and it may be important to monitor them in future studies. Inhibitor of DNA binding 1 (ID1) and inhibitor of DNA binding 3 (ID3) were both up 1.24-fold, these encode TGF-beta target genes shown to be stabilised by Bcl-3 and their expression was associated with breast cancer metastatic progression (Chen et al., 2016). miR-222, a microRNA implicated in the development of many cancers, including breast was up 2.1-fold, though high miR-222 expression is typically associated with poor overall survival (Wei et al., 2016). ATP binding cassette subfamily C member 3 (ABCC3) was up 1.59-fold and encodes a transporter protein majorly implicated with multi-drug resistance in breast cancer (Balaji et al., 2016).

5.9.4 CB1 found to most effectively confer transcriptional changes between the 8 and 24 hour time points

Leading on from the CB1 microarray experiment, we were curious to further explore why following 48h drug treatment we saw only a fraction of the transcriptional changes seen after 48h Bcl-3 siRNA knockdown. A gene panel consisting of five significantly altered genes following CB1 treatment (IL1B, ESM1, FOS, EGR1, IL6), and four known transcriptional targets of Bcl-3 (TNF α , CDH2, MDM2, IL10) were chosen.

First, Bcl-3 siRNA was used to characterise and valid the targets in the panel. All genes other than ESM1 and IL6 were found to significantly change in the correct, biologically accurate direction following 48h Bcl-3 knockdown (**Fig. 5.7a**). Next, we treated MDA-MB-231-Luc cells with either 100 μ M of JS6, CB1 or DMSO control for 3h, 8h, 24h or 48h and compared the gene expression profiles with that of siRNA. At 3h, we saw modest increases in TNF α , IL1B, FOS, EGR1 and IL6 expression, mostly with CB1 treatment (**Fig. 5.7b**). At 8h, the expression profiles began to more closely match that of

siRNA for both JS6 and CB1 treated cells (**Fig. 5.7c**). By 24h, all significant changes associated with JS6 treatment was lost, but CB1 treated cells retained most of the transcriptional responses previously seen (**Fig. 5.7d**). By 48h, no significant changes were seen with JS6 treatment and only dampened responses for IL1B, FOS, EGR1, ESM1 and IL6 remained following CB1 treatment (**Fig. 5.7e**). The results from these qRT-PCR experiments suggested that CB1 was able to accurately replicate transcriptional changes seen with siRNA knockdown, but only within a 8 to 24 hour timeframe. JS6 was also able to impart similar effects, but its efficacy was entirely lost by 24 hours. These findings also implied, there may have been substantially more gene changes if we carried out a microarray experiment using samples from cells treated with a shorter timeframe as by 48h, all expression of Bcl-3 specific targets within our panel had returned back to basal levels.

5.9.5 Daily JS6 and CB1 treatment improved drug efficacy

Based on the observation that transcriptional changes following drug treatment faded beyond 24 hours, it was possible our small molecule inhibitors were unstable within standard cell culture conditions, or perhaps the cells metabolised the compounds within this timeframe. Therefore we wanted to investigate the effects of refreshing inhibitor treatments in one of the longer functional assays. We chose the colony forming assay as this assessed clonogenic survival over the course of 10 days. In both MDA-MB-231-Luc (**Fig. 5.9**) and MDA-MB-436 cells (**Fig. 5.8**), daily treatment with JS6 or CB1, by replacing culture media preventing drug accumulation, drastically improved the efficacy and lowered the concentration required to achieve significant growth inhibition when compared with previous single 48h treatment.

5.9.6 Bcl-3 inhibitors demonstrated *in vivo* efficacy

We designed a number of xenograft models to assess the *in vivo* efficacy of Bcl-3 inhibitors in several different aspects of metastatic disease. We generated experimental TNBC metastases in athymic nude mice through tail vein injections of MDA-MB-231-Luc cells and used this model to test the anti-metastatic capabilities of our inhibitor compounds. The first model pre-treated animals with inhibitors before injection of cancer cells and daily intraperitoneal drug treatments were subsequently carried out for 9 consecutive days. Both JS6 and CB1 were found to inhibit the initial metastatic seeding

process and significantly reduced average tumour burden, as well increasing the proportion of disease free animals by experimental endpoints (**Fig. 5.13**). When we tracked the health status of one experiment past the final imaging date, it was found that CB1 treatment also significantly delayed time until morbidity and extended the survival time of treated cohort (**Fig. 5.12e**).

Due to the high variance nature of biological systems and *in vivo* experimentation, not all animals in the DMSO control cohorts developed detectable tumour burdens within the designated experimental timeframe. This was problematic as it made it difficult to derive statistical significance between cohorts within individual experiments. It was hard to explain whether the lack of detectable tumour load was due to natural variance or drug efficacy. Therefore it was especially important to increase overall sample sizes by carrying out biological repeats for each experimental cohort in order to obtain biologically representative results. When we integrated the results from all individual model one experiments, it allowed us to derive statistical significance for drug treated cohorts compared to DMSO controls.

The oral efficacy of CB1 was also tested using this first metastasis model and mice were treated with the intraperitoneal dose (3.5mg/kg) as well as a higher dose (20mg/kg) via oral gavage. In this experiment the higher oral dose was found to significantly reduce metastatic burden ($p=0.038$) when compared to the DMSO vehicle controls. Although the lower CB1 dose only exhibited a trend of reduced metastatic burden ($p=0.173$), this was most likely due to the low experimental animal numbers per cohort ($n=5$) and biological repeats should be carried out (**Fig. 5.14**). But based on the results from this experiment alone, we cannot rule out the possibility that treatment via oral gavage is less effective than intraperitoneal injections at the same concentrations.

Our first xenograft model was able to significantly demonstrate the efficacy of both JS6 and CB1, especially in the context of disrupting the earliest seeding processes of metastatic disease. In our second xenograft model we tweaked the drug treatment timings to determine whether the Bcl-3 inhibitors also disrupted the subsequent colonisation and expansion of established tumour cells. Experimental metastases were established using the same intravenous injection of MDA-MD-231-Luc cells, but this time the cells were allowed to seed for 3 days before animals were treated with either JS6, CB1 or DMSO

control. Drug treatments were continuously administered daily and animals imaged periodically until experimental endpoint. We closely monitored the weights and health status the animals following daily drug treatment in case there were accumulated toxicities associated with long term drug treatments. We observed no significant differences between JS6, CB1 and DMSO control animal cohorts over the course of 30 days (**Fig. 5.16**).

When the results from all individual experiments were aggregated, we saw no significant reductions in average metastatic burden between JS6, CB1 or DMSO control treated cohorts (**Fig. 5.15**). Although similar to model one, there was an increased proportion of animals within the drug treated cohorts that remained completely tumour free by the experimental endpoint compared to the controls. This suggested that the Bcl-3 inhibitors most likely acted by completely disrupting the ability of a subset of circulating tumour to seed and establish during the earliest stages of metastasis. Once tumour cells have successfully colonised, the inhibitors cannot effectively suppress their expansion, as we have only been able to observe modest effects upon proliferation *in vitro*. Therefore it is likely neither JS6 nor CB1 can be considered as effective mono-therapies in the clinical setting and their primary effects *in vivo* appeared to be suppression of metastatic seeding.

Although in model two there were no significant effects on tumour expansion once seeding had taken place, there was a trend of reduced tumour size in the drug treated cohorts. In our final xenograft model we wanted to test the effects of CB1 on primary orthotopic tumour growth. We established primary orthotopic tumours via subcutaneous injection of either MDA-MD-231-Luc or MDA-MB-436 cells into the bilateral mammary fat pads of mice. Cells were allowed to seed for 4 days before animals were treated with daily intraperitoneal injections of CB1 (3.5mg/kg) until experimental endpoint. Tumour volumes were recorded and CB1 was found to significantly reduce average tumour sizes of both cell lines from the 38th day onwards (**Fig. 5.17**). This finding supported our *in vitro* observations of growth suppression and although CB1 was not able to cause tumour regression, it was nonetheless able to impart a modest growth suppression within TNBC cells.

In recently years there has been significant advances in the development of patient-derived tumour xenografts (PDX). PDX models have the advantage of maintaining the molecular and histological heterogeneity of the original tumour. Breast cancer PDX

models have been shown to effectively recapitulate the molecular, stromal, and phenotypic heterogeneities seen within breast cancer (DeRose et al., 2013). Additionally they have been shown to be superior at predicting drug responses compared to standard cell cultured xenograft models (Hait, 2010). It would be interesting to investigate the efficacy of CB1 within these tumour models for future studies.

5.9.7 Concluding remarks

In this chapter we demonstrated that our two lead Bcl-3 inhibitor compounds were able to recapitulate *in vitro* biological phenotypes seen previously with Bcl-3 suppression in TNBC cell lines. CB1 was consistently found to have a greater efficacy than JS6. We also found a large number of biologically relevant overlapping transcriptional signalling changes following Bcl-3 inhibition with CB1 and siRNA. There were also a number of interesting non-overlapping changes, as well as opposing overlapping changes, highlighting the mechanistic differences between pharmacological disruption of Bcl-3 protein-protein interactions and siRNA gene expression knockdown. It would be very interesting to further investigate and validate the overlapping downstream signalling pathways following drug treatment and siRNA in regards to the tumour suppressive phenotypes observed to elucidate a more exact mechanism of action for Bcl-3. CB1 was also demonstrated have potent *in vivo* anti-metastatic efficacies, as well as a lack of non-specific toxicities, it could present as an effective combination treatment option in TNBCs. When paired with a more traditional chemotherapeutic designed to regress the tumour bulk, Bcl-3 inhibition could more effectively contain the disease and impair the ability of any subsequently circulating metastatic cells from seeding in distal organs.

Chapter 6:

General Discussion

6.1 General Discussion

We began this project by carrying out ectopic Bcl-3 suppression in four different TNBC cell lines using siRNA. We wanted to characterise the effects of knocking down this widely accepted proto-oncogene in a range of functional assays. Following Bcl-3 knockdown, we saw significant reductions in overall cell turnover in all TNBC lines. This phenotype was comprised of a reduction in proliferation, seen by decreased Ki67 and phospho-histone H3 expression, a shift away from the S and G2/M cell cycle phases towards the G0/G1 resting phase, as well as increased apoptosis, seen by increased caspase-3/-7 activities, along with the identification of an atypical subG1 cell cycle phase indicative of apoptotic bodies. By transfecting the cell lines with a NFkB reporter plasmid, we were able to show that Bcl-3 knockdown resulted in an overall reduction in transcriptional activity specifically targeting NFkB DNA binding elements. Since NFkB signalling is generally associated with promoting cancer cell proliferation, this could be an explanation for the observed reduction in cell growth. Following Bcl-3 knockdown in the non-tumourigenic MCF10a cell line, we didn't observe any of similar changes, which helps support the idea that the oncogenic roles of Bcl-3 were specific to our TNBC cell lines. However we could further test this specificity by knocking down Bcl-3 in a range of different non-tumourigenic tissue types, such as HMECs, a human dermal microvascular endothelium cell line.

Leading on from siRNA suppression of Bcl-3 we wanted to investigate the effects of ectopic overexpression. Two TNBC cell lines stably overexpressing wild type Bcl-3 protein were generated. Surprisingly, not only did we not see oncogene-driven increased cell growth, both overexpression cell lines exhibited reductions in overall cell turnovers. When we stained for proliferative markers, Bcl-3 overexpression indeed resulted in increased Ki67, pHH3, as well as larger G2/M dividing cell cycle phases. However both cell lines also featured increased subG1 cell cycle populations, along with increased caspase-3/-7 activities. The resulting cell turnover indexes demonstrated a greater ratio of cell undergoing apoptosis than those proliferating, explaining the overall reductions in cell growth. The NFkB reporter assay demonstrated overall increases in NFkB activity following ectopic overexpression, correlating with the increased proliferative phenotype. While most reports in the literature demonstrated pro-proliferative outcomes following Bcl-3 up-regulation, there were a few cases of Bcl-3 overexpression resulting in higher rates of apoptosis (Gehrke et al., 2017) and reduced tumourigenesis (Tang et al., 2016).

Gene expression profiling was carried out for MDA-MB-231-Luc cells comparing Bcl-3 siRNA knockdown with control. Bcl-3 suppression resulted in a significant up-regulation of genes positively associated with apoptosis signalling. Within this group, we saw many gene changes associated with promotion of the intrinsic mitochondria-mediated apoptosis pathway, such as down-regulated BCL2, up-regulated BAK1, BAX, MCL1 and TP53 expressions. These findings suggesting that Bcl-3 potentially plays an important role in protecting TNBCs against the activation of the intrinsic apoptosis pathway. There were also significant changes to a number of genes associated with the extrinsic receptor-mediated apoptosis pathways, as well as pathways linked to stress induced apoptosis. However the mixed expression change for these genes indicate a more complex regulatory involvement requiring further investigation.

Bcl-3 siRNA knock was also found to significantly impair three different modes of cellular migration in TNBC cell lines. We saw reduced collective migration, in the wound healing assay, reduced amoeboid-like single cell migration when cells were tasked to move across narrow pores, and also reduced mesenchymal-like single cell migration, when single cell motility was tracked with time-lapse microscopy. Gene expression profiling highlighted significantly down-regulated cytoskeletal regulation by Rho GTPase signalling pathways following Bcl-3 suppression. We saw changes in many important motility associated genes such as up-regulated RHOB, CFL2 and down-regulated ROCK1, CDC42, PAK1 and PFN2 expressions, encompassing diverse downstream metastasis related pathways such as Ras, RAF, MEK, ERK, PI3K, Akt, mTOR, MAPK, TGFB, VEGF and Wnt signalling. These findings fit our existing understanding of Bcl-3 and suggest that in TNBCs, its expression could potentially be extensively correlated with metastatic progression.

When WT Bcl-3 was ectopically overexpressed, we saw reductions in collective migration, conversely both amoeboid-like and mesenchymal-like single cell migratory outputs were increased. It is important to consider the natures of the assays, the wound healing assay featured collective cell monolayers and was sensitive the effects of cell turnover and apoptosis, the single cell assays only assessed viable cells and were therefore independent of cell growth and death. These results supported the role of Bcl-3 in contributing towards an increased single cell associated motility phenotype.

Tail vein injection of MDA-MB-231 cells treated with Bcl-3 siRNA resulted in a significantly lower total number of individual metastatic lesions in an *in vivo* murine tail vein xenograft model of metastasis. However there were no significant differences between average size most likely due to the transient nature of siRNA suppression. Tail vein injection of cells ectopically overexpressing WT Bcl-3 resulted in greatly increased numbers of metastatic lesions in the lungs, although each individual tumour was much smaller in size compared to the controls. Overexpressing Bcl-3 also drove cells to seed and colonise at novel distal organs such as the heart, mammary gland and bone marrow, sites previously unseen with control cells. Orthotopic tumours generated with Bcl-3 overexpression cells results in tumours significantly smaller than controls at the experimental endpoint. These *in vivo* findings are in line with the phenotypes observed in our *in vitro* functional assays.

A recent study in mouse embryonic stem cells reported that Bcl-3 overexpression resulted in significantly reduced proliferation, as well as self-renewal; interestingly, siRNA knockdown also produced comparable results. Bcl-3 was found to be a transcriptional repressor of Nanog gene expression and a cell-type specific optimal concentration of Bcl-3 was critical for the maintenance of normal functions (Kang et al., 2018). In light of similar observations in our TNBC cell lines, it is perhaps feasible for different cancers to have different optimal Bcl-3 concentrations where its oncogenic properties are best balanced to promote tumourigenicity without triggering transcriptional imbalances that might promote apoptosis. In order to take further investigate these hypotheses, it would be imperative to investigate ectopic Bcl-3 overexpression in other cancer cell line models and determine cell line specific effects.

Up to this point in the project we were able to successfully demonstrate Bcl-3 as a potential therapeutic target following tumour suppressive phenotypes seen after knockdown of the Bcl-3 gene with either siRNA knockdown, or disruption of the Bcl-3 protein-protein interactions through overexpression of a dominantly negative, non-binding Bcl-3 ANK mutant protein in TNBC cell lines. The effects were also likely to be TNBC specific as the anti-tumour phenotypes were not replicated in the non-tumourigenic MFC10a breast cancer cell line. This allowed us to use computational modelling to design and synthesise small molecule inhibitors that targeted Bcl-3 protein interactions. We screened two lead compounds (termed JS6 and CB1) in a number of *in vitro* functional assays and showed that they were both able to recapitulate previously reported

phenotypes associated with Bcl-3 inhibition. CB1 was found to be consistently more efficacious and was ultimately selected as the primary drug lead. The Bcl-3 small molecule inhibitors were tested in a number of *in vivo* xenograft TNBC models and was found to significantly inhibit the initial tumour seeding process in a tail vein metastasis model, as well as displaying modest growth suppression capabilities in an orthotopic mouse model. Together with no observable long term non-specific toxicities and significant oral uptake availability, our Bcl-3 inhibitor appears to be a promising anti-metastatic agent. Also due to its non-cytotoxic nature, we propose it could be an excellent candidate for both combination therapy with existing standard of care chemotherapy, as well as perhaps an effective long term prophylactic for metastasis suppression following early cancer identification.

We performed gene expression profiling comparing CB1 treatment with siRNA knockdown and found a large number of biologically relevant overlapping gene changes. This supports the target specificity of our inhibitor and provides some interesting mechanistic explanations for the therapeutic outcomes we observed. The results showed both CB1 and Bcl-3 siRNA significantly imparted gene changes associated with TGF-beta signalling, PI3K-Akt signalling, extracellular matrix remodelling, EMT, DNA damage repair, and immune-surveillance related cytokines. The later is of particular interest as the field of immunotherapy has become very prominent in recent years. It is possible for Bcl-3 in TNBC to have roles in regulating the secretion of cytokines responsible for transforming the tumour microenvironment. This will potentially affect the recruitment and functions of the host immunity and can provide interested alternative mechanisms of drug action for our small molecule inhibitor in regards to the suppression of metastatic progression.

It might also be interesting to query Bcl-3 expression in different TNBC cell lines and patient tissues already published in publicly available databases to try and compare whether changes seen in our microarray experiment could be correlated. This meta-analysis approach allows us to either bolster or disprove the findings in this study as it bypasses the need for repeated experimentation within additional TNBC cell lines, provided different groups has previously published on the relevant data. These findings provided a general overview into the complex signalling pathways associated with the Bcl-3 protein in TNBCs and perhaps offers insight into new therapeutic targets. It is also possible to further investigate some of the significantly altered targets and ask the question of whether one of them could serve as a biomarker for clinical response.

Ascertaining a robust biomarker will also be especially important in order to push our small molecule inhibitor into clinical trials. Also it is important to remember Bcl-3 has been shown to be dysregulated and oncogenic in a wide range of different cancers and diseases. Our novel small molecule inhibitor paves the ways for an easy method to further study the effects of Bcl-3 suppression in a range of different biological models.

Chapter 7:

References

7 References

- Aas, T., Børresen, A.L., Geisler, S., Smith-Sørensen, B., Johnsen, H., Varhaug, J.E., Akslen, L.A., Lønning, P.E., 1996. Specific P53 mutations are associated with de novo resistance to doxorubicin in breast cancer patients. *Nat. Med.* 2, 811–814.
- Abella, J.V.G., Galloni, C., Pernier, J., Barry, D.J., Kjær, S., Carlier, M.-F., Way, M., 2016. Isoform diversity in the Arp2/3 complex determines actin filament dynamics. *Nat. Cell Biol.* 18, 76–86. <https://doi.org/10.1038/ncb3286>
- Adorno, M., Cordenonsi, M., Montagner, M., Dupont, S., Wong, C., Hann, B., Solari, A., Bobisse, S., Rondina, M.B., Guzzardo, V., Parenti, A.R., Rosato, A., Bicciato, S., Balmain, A., Piccolo, S., 2009. A Mutant-p53/Smad complex opposes p63 to empower TGFbeta-induced metastasis. *Cell* 137, 87–98. <https://doi.org/10.1016/j.cell.2009.01.039>
- Ajay, A., Radhakrishnan, P., 2017. Clinical pathological and epidemiological study of triple negative breast cancer. *International Journal of Research in Medical Sciences* 5, 2657–2661. <https://doi.org/10.18203/2320-6012.ijrms20172465>
- Albuquerque, C., Breukel, C., van der Luijt, R., Fidalgo, P., Lage, P., Slors, F.J.M., Leitão, C.N., Fodde, R., Smits, R., 2002. The “just-right” signaling model: APC somatic mutations are selected based on a specific level of activation of the beta-catenin signaling cascade. *Hum. Mol. Genet.* 11, 1549–1560.
- Al-Zoubi, A.M., Efimova, E.V., Kaithamana, S., Martinez, O., El-Idrissi, M.E.-A., Dogan, R.E., Prabhakar, B.S., 2001. Contrasting Effects of IG20 and Its Splice Isoforms, MADD and DENN-SV, on Tumor Necrosis Factor α -induced Apoptosis and Activation of Caspase-8 and -3. *J. Biol. Chem.* 276, 47202–47211. <https://doi.org/10.1074/jbc.M104835200>
- Ashkenazi, A., 2002. Targeting death and decoy receptors of the tumour-necrosis factor superfamily. *Nat. Rev. Cancer* 2, 420–430. <https://doi.org/10.1038/nrc821>
- Au, W.Y., Horsman, D.E., Ohno, H., Klasa, R.J., Gascoyne, R.D., 2002. Bcl-3/IgH translocation (14;19)(q32;q13) in non-Hodgkin's lymphomas. *Leuk. Lymphoma* 43, 813–816. <https://doi.org/10.1080/10428190290016935>
- Baig, S., Seevasant, I., Mohamad, J., Mukheem, A., Huri, H.Z., Kamarul, T., 2016. Potential of apoptotic pathway-targeted cancer therapeutic research: Where do we stand? *Cell Death Dis.* 7, e2058. <https://doi.org/10.1038/cddis.2015.275>
- Balaji, S.A., Udupa, N., Chamallamudi, M.R., Gupta, V., Rangarajan, A., 2016. Role of the Drug Transporter ABCC3 in Breast Cancer Chemoresistance. *PloS One* 11, e0155013. <https://doi.org/10.1371/journal.pone.0155013>
- Balko, J.M., Giltneane, J.M., Wang, K., Schwarz, L.J., Young, C.D., Cook, R.S., Owens, P., Sanders, M.E., Kuba, M.G., Sánchez, V., Kurupi, R., Moore, P.D., Pinto, J.A., Doimi, F.D., Gómez, H., Horiuchi, D., Goga, A., Lehmann, B.D., Bauer, J.A., Pietenpol, J.A., Ross, J.S., Palmer, G.A., Yelensky, R., Cronin, M., Miller, V.A., Stephens, P.J., Arteaga, C.L., 2014. Molecular profiling of the residual disease of triple-negative breast cancers after neoadjuvant chemotherapy identifies actionable therapeutic targets. *Cancer Discov.* 4, 232–245. <https://doi.org/10.1158/2159-8290.CD-13-0286>
- Baron, V., Adamson, E.D., Calogero, A., Ragona, G., Mercola, D., 2006. The transcription factor Egr1 is a direct regulator of multiple tumor suppressors including TGFbeta1, PTEN, p53, and fibronectin. *Cancer Gene Ther.* 13, 115–124. <https://doi.org/10.1038/sj.cgt.7700896>
- Barton, V.N., D'Amato, N.C., Gordon, M.A., Christenson, J.L., Elias, A., Richer, J.K., 2015. Androgen Receptor Biology in Triple Negative Breast Cancer: a Case for Classification as AR+ or

- Quadruple Negative Disease. *Horm. Cancer* 6, 206–213. <https://doi.org/10.1007/s12672-015-0232-3>
- Baselga, J., Gómez, P., Greil, R., Braga, S., Climent, M.A., Wardley, A.M., Kaufman, B., Stemmer, S.M., Pêgo, A., Chan, A., Goeminne, J.-C., Graas, M.-P., Kennedy, M.J., Ciruelos Gil, E.M., Schneeweiss, A., Zubeł, A., Groos, J., Melezínková, H., Awada, A., 2013. Randomized phase II study of the anti-epidermal growth factor receptor monoclonal antibody cetuximab with cisplatin versus cisplatin alone in patients with metastatic triple-negative breast cancer. *J. Clin. Oncol.* 31, 2586–2592. <https://doi.org/10.1200/JCO.2012.46.2408>
- Beg, S., Siraj, A.K., Prabhakaran, S., Jehan, Z., Ajarim, D., Al-Dayel, F., Tulbah, A., Al-Kuraya, K.S., 2015. Loss of PTEN expression is associated with aggressive behavior and poor prognosis in Middle Eastern triple-negative breast cancer. *Breast Cancer Res. Treat.* 151, 541–553. <https://doi.org/10.1007/s10549-015-3430-3>
- Berrada, N., Delaloge, S., André, F., 2010. Treatment of triple-negative metastatic breast cancer: toward individualized targeted treatments or chemosensitization? *Ann. Oncol.* 21 Suppl 7, vii30–35. <https://doi.org/10.1093/annonc/mdq279>
- Bertucci, F., Finetti, P., Cervera, N., Charafe-Jauffret, E., Mamessier, E., Adélaïde, J., Debono, S., Houvenaeghel, G., Maraninchi, D., Viens, P., Charpin, C., Jacquemier, J., Birnbaum, D., 2006. Gene expression profiling shows medullary breast cancer is a subgroup of basal breast cancers. *Cancer Res.* 66, 4636–4644. <https://doi.org/10.1158/0008-5472.CAN-06-0031>
- Bishop, A.L., Hall, A., 2000. Rho GTPases and their effector proteins. *Biochem. J.* 348, 241–255.
- Bosma, M.J., Carroll, A.M., 1991. The SCID mouse mutant: definition, characterization, and potential uses. *Annu. Rev. Immunol.* 9, 323–350. <https://doi.org/10.1146/annurev.iy.09.040191.001543>
- Bouchalova, K., Svoboda, M., Kharraishvili, G., Vrbkova, J., Bouchal, J., Trojanec, R., Koudelakova, V., Radova, L., Cwiertka, K., Hajdúch, M., Kolar, Z., 2015. BCL2 is an independent predictor of outcome in basal-like triple-negative breast cancers treated with adjuvant anthracycline-based chemotherapy. *Tumour Biol. J. Int. Soc. Oncodevelopmental Biol. Med.* 36, 4243–4252. <https://doi.org/10.1007/s13277-015-3061-7>
- Bourne, H.R., Sanders, D.A., McCormick, F., 1991. The GTPase superfamily: conserved structure and molecular mechanism. *Nature* 349, 117–127. <https://doi.org/10.1038/349117a0>
- Bours, V., Franzoso, G., Azarenko, V., Park, S., Kanno, T., Brown, K., Siebenlist, U., 1993. The oncoprotein Bcl-3 directly transactivates through kappa B motifs via association with DNA-binding p50B homodimers. *Cell* 72, 729–739.
- Brasier, A.R., Lu, M., Hai, T., Lu, Y., Boldogh, I., 2001. NF- κ B-inducible BCL-3 Expression Is an Autoregulatory Loop Controlling Nuclear p50/NF- κ B1 Residence. *J. Biol. Chem.* 276, 32080–32093. <https://doi.org/10.1074/jbc.M102949200>
- Brocke-Heidrich, K., Ge, B., Cvijic, H., Pfeifer, G., Löffler, D., Henze, C., McKeithan, T.W., Horn, F., 2006. BCL3 is induced by IL-6 via Stat3 binding to intronic enhancer HS4 and represses its own transcription. *Oncogene* 25, 7297–7304. <https://doi.org/10.1038/sj.onc.1209711>
- Bruno, S., Darzynkiewicz, Z., 1992. Cell cycle dependent expression and stability of the nuclear protein detected by Ki-67 antibody in HL-60 cells. *Cell Prolif.* 25, 31–40.
- Bryant, C., Rawlinson, R., Massey, A.J., 2014. Chk1 inhibition as a novel therapeutic strategy for treating triple-negative breast and ovarian cancers. *BMC Cancer* 14, 570. <https://doi.org/10.1186/1471-2407-14-570>
- Bulut, N., Kilickap, S., Sari, E., Altundag, K., 2008. Response to taxanes in triple negative breast cancer. *Cancer Chemother. Pharmacol.* 63, 189. <https://doi.org/10.1007/s00280-008-0717-7>

- Caiazza, F., Murray, A., Madden, S.F., Synnott, N.C., Ryan, E.J., O'Donovan, N., Crown, J., Duffy, M.J., 2016. Preclinical evaluation of the AR inhibitor enzalutamide in triple-negative breast cancer cells. *Endocr. Relat. Cancer* 23, 323–334. <https://doi.org/10.1530/ERC-16-0068>
- Cancer Genome Atlas Network, 2012. Comprehensive molecular portraits of human breast tumours. *Nature* 490, 61–70. <https://doi.org/10.1038/nature11412>
- Cardoso, F., Senkus-Konefka, E., Fallowfield, L., Costa, A., Castiglione, M., ESMO Guidelines Working Group, 2010. Locally recurrent or metastatic breast cancer: ESMO Clinical Practice Guidelines for diagnosis, treatment and follow-up. *Ann. Oncol.* 21 Suppl 5, v15-19. <https://doi.org/10.1093/annonc/mdq160>
- Chan, K.-K., Shen, L., Au, W.-Y., Yuen, H.-F., Wong, K.-Y., Guo, T., Wong, M.L., Shimizu, N., Tsuchiyama, J., Kwong, Y.-L., Liang, R.H., Srivastava, G., 2010. Interleukin-2 induces NF-kappaB activation through BCL10 and affects its subcellular localization in natural killer lymphoma cells. *J. Pathol.* 221, 164–174. <https://doi.org/10.1002/path.2699>
- Chen, X., Cao, X., Sun, X., Lei, R., Chen, P., Zhao, Y., Jiang, Y., Yin, J., Chen, R., Ye, D., Wang, Q., Liu, Z., Liu, S., Cheng, C., Mao, J., Hou, Y., Wang, M., Siebenlist, U., Eugene Chin, Y., Wang, Y., Cao, L., Hu, G., Zhang, X., 2016. Bcl-3 regulates TGF β signaling by stabilizing Smad3 during breast cancer pulmonary metastasis. *Cell Death Dis.* 7, e2508. <https://doi.org/10.1038/cddis.2016.405>
- Cheng, C.L., Thike, A.A., Tan, S.Y.J., Chua, P.J., Bay, B.H., Tan, P.H., 2015. Expression of FGFR1 is an independent prognostic factor in triple-negative breast cancer. *Breast Cancer Res. Treat.* 151, 99–111. <https://doi.org/10.1007/s10549-015-3371-x>
- Choi, H.J., Lee, J.M., Kim, H., Nam, H.J., Shin, H.-J.R., Kim, D., Ko, E., Noh, D.-Y., Kim, K.I., Kim, J.H., Baek, S.H., 2010. Bcl3-dependent stabilization of CtBP1 is crucial for the inhibition of apoptosis and tumor progression in breast cancer. *Biochem. Biophys. Res. Commun.* 400, 396–402. <https://doi.org/10.1016/j.bbrc.2010.08.084>
- Choi, S.K., Kim, H.S., Jin, T., Moon, W.K., 2017. LOXL4 knockdown enhances tumor growth and lung metastasis through collagen-dependent extracellular matrix changes in triple-negative breast cancer. *Oncotarget* 8, 11977–11989. <https://doi.org/10.18632/oncotarget.14450>
- Coates, A.S., Winer, E.P., Goldhirsch, A., Gelber, R.D., Gnant, M., Piccart-Gebhart, M., Thürlimann, B., Senn, H.-J., Panel Members, 2015. Tailoring therapies--improving the management of early breast cancer: St Gallen International Expert Consensus on the Primary Therapy of Early Breast Cancer 2015. *Ann. Oncol. Off. J. Eur. Soc. Med. Oncol.* 26, 1533–1546. <https://doi.org/10.1093/annonc/mdv221>
- Cogswell, P.C., Guttridge, D.C., Funkhouser, W.K., Baldwin, A.S., 2000. Selective activation of NF-kappa B subunits in human breast cancer: potential roles for NF-kappa B2/p52 and for Bcl-3. *Oncogene* 19, 1123–1131. <https://doi.org/10.1038/sj.onc.1203412>
- Cunliffe, H.E., Jiang, Y., Fornace, K.M., Yang, F., Meltzer, P.S., 2012. PAR6B is required for tight junction formation and activated PKC ζ localization in breast cancer. *Am. J. Cancer Res.* 2, 478–491.
- Czabotar, P.E., Lessene, G., Strasser, A., Adams, J.M., 2014. Control of apoptosis by the BCL-2 protein family: implications for physiology and therapy. *Nat. Rev. Mol. Cell Biol.* 15, 49–63. <https://doi.org/10.1038/nrm3722>
- Dai, J., Sultan, S., Taylor, S.S., Higgins, J.M.G., 2005. The kinase haspin is required for mitotic histone H3 Thr 3 phosphorylation and normal metaphase chromosome alignment. *Genes Dev.* 19, 472–488. <https://doi.org/10.1101/gad.1267105>
- Danial, N.N., Korsmeyer, S.J., 2004. Cell death: critical control points. *Cell* 116, 205–219.

- Darzynkiewicz, Z., Juan, G., Bedner, E., 2001. Determining cell cycle stages by flow cytometry. *Curr. Protoc. Cell Biol.* Chapter 8, Unit 8.4. <https://doi.org/10.1002/0471143030.cb0804s01>
- Darzynkiewicz, Z., Zhao, H., Zhang, S., Lee, M.Y.W.T., Lee, E.Y.C., Zhang, Z., 2015. Initiation and termination of DNA replication during S phase in relation to cyclins D1, E and A, p21WAF1, Cdt1 and the p12 subunit of DNA polymerase δ revealed in individual cells by cytometry. *Oncotarget* 6, 11735–11750. <https://doi.org/10.18632/oncotarget.4149>
- Daugaard, M., Rohde, M., Jäättelä, M., 2007. The heat shock protein 70 family: Highly homologous proteins with overlapping and distinct functions. *FEBS Lett., Cellular Stress* 581, 3702–3710. <https://doi.org/10.1016/j.febslet.2007.05.039>
- Dawood, S., 2010. Triple-negative breast cancer: epidemiology and management options. *Drugs* 70, 2247–2258. <https://doi.org/10.2165/11538150-000000000-00000>
- De Craene, B., Berx, G., 2013. Regulatory networks defining EMT during cancer initiation and progression. *Nat. Rev. Cancer* 13, 97–110. <https://doi.org/10.1038/nrc3447>
- Delbridge, A.R.D., Grabow, S., Strasser, A., Vaux, D.L., 2016. Thirty years of BCL-2: translating cell death discoveries into novel cancer therapies. *Nat. Rev. Cancer* 16, 99–109. <https://doi.org/10.1038/nrc.2015.17>
- DerMardirossian, C., Bokoch, G.M., 2005. GDIs: central regulatory molecules in Rho GTPase activation. *Trends Cell Biol.* 15, 356–363. <https://doi.org/10.1016/j.tcb.2005.05.001>
- DeRose, Y.S., Gligorich, K.M., Wang, G., Georgelas, A., Bowman, P., Courdy, S.J., Welm, A.L., Welm, B.E., 2013. Patient-derived models of human breast cancer: protocols for in vitro and in vivo applications in tumor biology and translational medicine. *Curr. Protoc. Pharmacol.* Chapter 14, Unit14.23. <https://doi.org/10.1002/0471141755.ph1423s60>
- DesMarais, V., Ghosh, M., Eddy, R., Condeelis, J., 2005. Cofilin takes the lead. *J Cell Sci* 118, 19–26. <https://doi.org/10.1242/jcs.01631>
- Dethlefsen, C., Højfeldt, G., Hojman, P., 2013. The role of intratumoral and systemic IL-6 in breast cancer. *Breast Cancer Res. Treat.* 138, 657–664. <https://doi.org/10.1007/s10549-013-2488-z>
- Dongre, A., Rashidian, M., Reinhardt, F., Bagnato, A., Keckesova, Z., Ploegh, H.L., Weinberg, R.A., 2017. Epithelial-to-mesenchymal Transition contributes to Immunosuppression in Breast Carcinomas. *Cancer Res.* 77, 3982–3989. <https://doi.org/10.1158/0008-5472.CAN-16-3292>
- Douma, S., Van Laar, T., Zevenhoven, J., Meuwissen, R., Van Garderen, E., Peeper, D.S., 2004. Suppression of anoikis and induction of metastasis by the neurotrophic receptor TrkB. *Nature* 430, 1034–1039. <https://doi.org/10.1038/nature02765>
- Downward, J., 2003. Targeting RAS signalling pathways in cancer therapy. *Nat. Rev. Cancer* 3, 11–22. <https://doi.org/10.1038/nrc969>
- Durchdewald, M., Angel, P., Hess, J., 2009. The transcription factor Fos: a Janus-type regulator in health and disease. *Histol. Histopathol.* 24, 1451–1461. <https://doi.org/10.14670/HH-24.1451>
- Eckhardt, I., Roesler, S., Fulda, S., 2013. Identification of DR5 as a critical, NF- κ B-regulated mediator of Smac-induced apoptosis. *Cell Death Dis.* 4, e936. <https://doi.org/10.1038/cddis.2013.457>
- Edfeldt, K., Hellman, P., Westin, G., Stalberg, P., 2016. A plausible role for actin gamma smooth muscle 2 (ACTG2) in small intestinal neuroendocrine tumorigenesis. *BMC Endocr. Disord.* 16, 19. <https://doi.org/10.1186/s12902-016-0100-3>

- Einbond, L.S., Wu, H.-A., Su, T., Chang, T., Panjikaran, M., Wang, X., Goldsberry, S., 2010. Digitoxin activates EGR1 and synergizes with paclitaxel on human breast cancer cells. *J. Carcinog.* 9, 10. <https://doi.org/10.4103/1477-3163.72578>
- Elliott, S.F., Coon, C.I., Hays, E., Stadheim, T.A., Vincenti, M.P., 2002. Bcl-3 is an interleukin-1-responsive gene in chondrocytes and synovial fibroblasts that activates transcription of the matrix metalloproteinase 1 gene. *Arthritis Rheum.* 46, 3230–3239. <https://doi.org/10.1002/art.10675>
- Elstrodt, F., Hollestelle, A., Nagel, J.H.A., Gorin, M., Wasielewski, M., van den Ouweland, A., Merajver, S.D., Ethier, S.P., Schutte, M., 2006. BRCA1 mutation analysis of 41 human breast cancer cell lines reveals three new deleterious mutants. *Cancer Res.* 66, 41–45. <https://doi.org/10.1158/0008-5472.CAN-05-2853>
- Engel, M.E., Datta, P.K., Moses, H.L., 1998. RhoB is stabilized by transforming growth factor beta and antagonizes transcriptional activation. *J. Biol. Chem.* 273, 9921–9926.
- Farmer, P., Bonnefoi, H., Becette, V., Tubiana-Hulin, M., Fumoleau, P., Larsimont, D., Macgrogan, G., Bergh, J., Cameron, D., Goldstein, D., Duss, S., Nicoulaz, A.-L., Brisken, C., Fiche, M., Delorenzi, M., Iggo, R., 2005. Identification of molecular apocrine breast tumours by microarray analysis. *Oncogene* 24, 4660–4671. <https://doi.org/10.1038/sj.onc.1208561>
- Fedele, C.G., Ooms, L.M., Ho, M., Vieusseux, J., O’Toole, S.A., Millar, E.K., Lopez-Knowles, E., Sriratana, A., Gurung, R., Baglietto, L., Giles, G.G., Bailey, C.G., Rasko, J.E.J., Shields, B.J., Price, J.T., Majerus, P.W., Sutherland, R.L., Tiganis, T., McLean, C.A., Mitchell, C.A., 2010. Inositol polyphosphate 4-phosphatase II regulates PI3K/Akt signaling and is lost in human basal-like breast cancers. *Proc. Natl. Acad. Sci. U. S. A.* 107, 22231–22236. <https://doi.org/10.1073/pnas.1015245107>
- Flanagan, S.P., 1966. ‘Nude’, a new hairless gene with pleiotropic effects in the mouse. *Genet. Res.* 8, 295–309. <https://doi.org/10.1017/S0016672300010168>
- Folco, E.J., Rocha, V.Z., López-Illasaca, M., Libby, P., 2009. Adiponectin inhibits pro-inflammatory signaling in human macrophages independent of interleukin-10. *J. Biol. Chem.* 284, 25569–25575. <https://doi.org/10.1074/jbc.M109.019786>
- Foley, K., Rucki, A.A., Xiao, Q., Zhou, D., Leubner, A., Mo, G., Kleponis, J., Wu, A.A., Sharma, R., Jiang, Q., Anders, R.A., Iacobuzio-Donahue, C.A., Hajar, K.A., Maitra, A., Jaffee, E.M., Zheng, L., 2015. Semaphorin 3D autocrine signaling mediates the metastatic role of annexin A2 in pancreatic cancer. *Sci. Signal.* 8, ra77. <https://doi.org/10.1126/scisignal.aaa5823>
- Foulkes, W.D., Smith, I.E., Reis-Filho, J.S., 2010. Triple-negative breast cancer. *N. Engl. J. Med.* 363, 1938–1948. <https://doi.org/10.1056/NEJMra1001389>
- Franken, N.A.P., Rodermond, H.M., Stap, J., Haveman, J., van Bree, C., 2006. Clonogenic assay of cells in vitro. *Nat. Protoc.* 1, 2315–2319. <https://doi.org/10.1038/nprot.2006.339>
- Freedman, G.M., Anderson, P.R., Li, T., Nicolaou, N., 2009. Local-Regional Recurrence of Triple Negative Breast Cancer after Breast-Conserving Surgery and Radiation. *Cancer* 115, 946–951. <https://doi.org/10.1002/cncr.24094>
- Fritz, G., Kaina, B., 2000. Ras-related GTPase RhoB forces alkylation-induced apoptotic cell death. *Biochem. Biophys. Res. Commun.* 268, 784–789. <https://doi.org/10.1006/bbrc.2000.2211>
- Fujita, T., Nolan, G.P., Liou, H.C., Scott, M.L., Baltimore, D., 1993. The candidate proto-oncogene bcl-3 encodes a transcriptional coactivator that activates through NF-kappa B p50 homodimers. *Genes Dev.* 7, 1354–1363. <https://doi.org/10.1101/gad.7.7b.1354>
- Fulda, S., 2013. Targeting c-FLICE-like inhibitory protein (CFLAR) in cancer. *Expert Opin. Ther. Targets* 17, 195–201. <https://doi.org/10.1517/14728222.2013.736499>

- Gampel, A., Parker, P.J., Mellor, H., 1999. Regulation of epidermal growth factor receptor traffic by the small GTPase rhoB. *Curr. Biol. CB* 9, 955–958.
- Gandalovicova, A., et al., Migrastatics-Anti-metastatic and Anti-invasion Drugs: Promises and Challenges. *Trends Cancer*, 2017. **3**(6): p. 391-406.
- Gasser, J.A., Inuzuka, H., Lau, A.W., Wei, W., Beroukhim, R., Toker, A., 2014. SGK3 mediates INPP4B-dependent PI3K signaling in breast cancer. *Mol. Cell* 56, 595–607. <https://doi.org/10.1016/j.molcel.2014.09.023>
- Gehrke, N., Wörns, M.A., Huber, Y., Hess, M., Straub, B.K., Hövelmeyer, N., Waisman, A., Kim, Y.O., Schuppan, D., Galle, P.R., Schattenberg, J.M., 2016. Hepatic B cell leukemia-3 promotes hepatic steatosis and inflammation through insulin-sensitive metabolic transcription factors. *J. Hepatol.* 65, 1188–1197. <https://doi.org/10.1016/j.jhep.2016.06.026>
- Gehrke, N., Wörns, M.A., Mann, A., Huber, Y., Hoevelmeyer, N., Longerich, T., Waisman, A., Galle, P.R., Schattenberg, J.M., 2017. Hepatic B cell leukemia-3 suppresses chemically-induced hepatocarcinogenesis in mice through altered MAPK and NF- κ B activation. *Oncotarget* 8, 56095–56109. <https://doi.org/10.18632/oncotarget.10893>
- Gertler, F., Condeelis, J., 2011. Metastasis: tumor cells becoming MENAcing. *Trends Cell Biol.* 21, 81–90. <https://doi.org/10.1016/j.tcb.2010.10.001>
- Ghazanfar, S., Fatima, I., Aslam, M., Musharraf, S.G., Sherman, N.E., Moskaluk, C., Fox, J.W., Akhtar, M.W., Sadaf, S., 2017. Identification of actin beta-like 2 (ACTBL2) as novel, upregulated protein in colorectal cancer. *J. Proteomics* 152, 33–40. <https://doi.org/10.1016/j.jprot.2016.10.011>
- Giancotti, F.G., 2013. Mechanisms governing metastatic dormancy and reactivation. *Cell* 155, 750–764. <https://doi.org/10.1016/j.cell.2013.10.029>
- Giancotti, F.G., Ruoslahti, E., 1999. Integrin Signaling. *Science* 285, 1028–1033. <https://doi.org/10.1126/science.285.5430.1028>
- Gonzalez-Angulo, A.M., Stemke-Hale, K., Palla, S.L., Carey, M., Agarwal, R., Meric-Berstam, F., Traina, T.A., Hudis, C., Hortobagyi, G.N., Gerald, W.L., Mills, G.B., Hennessy, B.T., 2009. Androgen receptor levels and association with PIK3CA mutations and prognosis in breast cancer. *Clin. Cancer Res. Off. J. Am. Assoc. Cancer Res.* 15, 2472–2478. <https://doi.org/10.1158/1078-0432.CCR-08-1763>
- Goode, B.L., Eck, M.J., 2007. Mechanism and Function of Formins in the Control of Actin Assembly. *Annu. Rev. Biochem.* 76, 593–627. <https://doi.org/10.1146/annurev.biochem.75.103004.142647>
- Gorovoy, M., Niu, J., Bernard, O., Profirovic, J., Minshall, R., Neamu, R., Voyno-Yasenetskaya, T., 2005. LIM Kinase 1 Coordinates Microtubule Stability and Actin Polymerization in Human Endothelial Cells. *J. Biol. Chem.* 280, 26533–26542. <https://doi.org/10.1074/jbc.M502921200>
- Gregory, P.A., Bert, A.G., Paterson, E.L., Barry, S.C., Tsykin, A., Farshid, G., Vadas, M.A., Khew-Goodall, Y., Goodall, G.J., 2008. The miR-200 family and miR-205 regulate epithelial to mesenchymal transition by targeting ZEB1 and SIP1. *Nat. Cell Biol.* 10, 593–601. <https://doi.org/10.1038/ncb1722>
- Greten, F.R., Eckmann, L., Greten, T.F., Park, J.M., Li, Z.-W., Egan, L.J., Kagnoff, M.F., Karin, M., 2004. IKKbeta links inflammation and tumorigenesis in a mouse model of colitis-associated cancer. *Cell* 118, 285–296. <https://doi.org/10.1016/j.cell.2004.07.013>
- Grivennikov, S.I., Greten, F.R., Karin, M., 2010. Immunity, inflammation, and cancer. *Cell* 140, 883–899. <https://doi.org/10.1016/j.cell.2010.01.025>

- Gucalp, A., Tolaney, S., Isakoff, S.J., Ingle, J.N., Liu, M.C., Carey, L.A., Blackwell, K., Rugo, H., Nabell, L., Forero, A., Stearns, V., Doane, A.S., Danso, M., Moynahan, M.E., Momen, L.F., Gonzalez, J.M., Akhtar, A., Giri, D.D., Patil, S., Feigin, K.N., Hudis, C.A., Traina, T.A., Translational Breast Cancer Research Consortium (TBCRC 011), 2013. Phase II trial of bicalutamide in patients with androgen receptor-positive, estrogen receptor-negative metastatic Breast Cancer. *Clin. Cancer Res. Off. J. Am. Assoc. Cancer Res.* 19, 5505–5512. <https://doi.org/10.1158/1078-0432.CCR-12-3327>
- Gunasinghe, N.P.A.D., Wells, A., Thompson, E.W., Hugo, H.J., 2012. Mesenchymal-epithelial transition (MET) as a mechanism for metastatic colonisation in breast cancer. *Cancer Metastasis Rev.* 31, 469–478. <https://doi.org/10.1007/s10555-012-9377-5>
- Guttridge, D.C., Albanese, C., Reuther, J.Y., Pestell, R.G., Baldwin, A.S., 1999. NF-kappaB controls cell growth and differentiation through transcriptional regulation of cyclin D1. *Mol. Cell Biol.* 19, 5785–5799.
- Hait, W.N., 2010. Anticancer drug development: the grand challenges. *Nat. Rev. Drug Discov.* 9, 253–254. <https://doi.org/10.1038/nrd3144>
- Hanahan, D., Weinberg, R.A., 2011. Hallmarks of cancer: the next generation. *Cell* 144, 646–674. <https://doi.org/10.1016/j.cell.2011.02.013>
- Hans, F., Dimitrov, S., 2001. Histone H3 phosphorylation and cell division. *Oncogene* 20, 3021–3027. <https://doi.org/10.1038/sj.onc.1204326>
- Hayden, M.S., Ghosh, S., 2012. NF-κB, the first quarter-century: remarkable progress and outstanding questions. *Genes Dev.* 26, 203–234. <https://doi.org/10.1101/gad.183434.111>
- Hayden, M.S., Ghosh, S., 2008. Shared principles in NF-kappaB signaling. *Cell* 132, 344–362. <https://doi.org/10.1016/j.cell.2008.01.020>
- Heissmeyer, V., Krappmann, D., Wulczyn, F.G., Scheidereit, C., 1999. NF-kappaB p105 is a target of IkkappaB kinases and controls signal induction of Bcl-3-p50 complexes. *EMBO J.* 18, 4766–4778. <https://doi.org/10.1093/emboj/18.17.4766>
- Heitz, F., Harter, P., Lueck, H.-J., Fissler-Eckhoff, A., Lorenz-Salehi, F., Scheil-Bertram, S., Traut, A., du Bois, A., 2009. Triple-negative and HER2-overexpressing breast cancers exhibit an elevated risk and an earlier occurrence of cerebral metastases. *Eur. J. Cancer Oxf. Engl.* 1990 45, 2792–2798. <https://doi.org/10.1016/j.ejca.2009.06.027>
- Hendzel, M.J., Wei, Y., Mancini, M.A., Van Hooser, A., Ranalli, T., Brinkley, B.R., Bazett-Jones, D.P., Allis, C.D., 1997. Mitosis-specific phosphorylation of histone H3 initiates primarily within pericentromeric heterochromatin during G2 and spreads in an ordered fashion coincident with mitotic chromosome condensation. *Chromosoma* 106, 348–360.
- Hoesel, B., Schmid, J.A., 2013. The complexity of NF-κB signaling in inflammation and cancer. *Mol. Cancer* 12, 86. <https://doi.org/10.1186/1476-4598-12-86>
- Hollmén, M., Karaman, S., Schwager, S., Lisibach, A., Christiansen, A.J., Maksimow, M., Varga, Z., Jalkanen, S., Detmar, M., 2016. G-CSF regulates macrophage phenotype and associates with poor overall survival in human triple-negative breast cancer. *Oncoimmunology* 5, e1115177. <https://doi.org/10.1080/2162402X.2015.1115177>
- Hotchkiss, R.S., Strasser, A., McDunn, J.E., Swanson, P.E., 2009. Cell Death in Disease: Mechanisms and Emerging Therapeutic Concepts. *N. Engl. J. Med.* 361, 1570–1583. <https://doi.org/10.1056/NEJMra0901217>
- Huber, M.A., Azoitei, N., Baumann, B., Grünert, S., Sommer, A., Pehamberger, H., Kraut, N., Beug, H., Wirth, T., 2004. NF-kappaB is essential for epithelial-mesenchymal transition and metastasis in

- a model of breast cancer progression. *J. Clin. Invest.* 114, 569–581. <https://doi.org/10.1172/JCI21358>
- Hussain, S.P., Harris, C.C., 2006. p53 biological network: at the crossroads of the cellular-stress response pathway and molecular carcinogenesis. *J. Nippon Med. Sch. Nippon Ika Daigaku Zasshi* 73, 54–64.
- Ibrahim, Y.H., García-García, C., Serra, V., He, L., Torres-Lockhart, K., Prat, A., Anton, P., Cozar, P., Guzmán, M., Grueso, J., Rodríguez, O., Calvo, M.T., Aura, C., Díez, O., Rubio, I.T., Pérez, J., Rodón, J., Cortés, J., Ellisen, L.W., Scaltriti, M., Baselga, J., 2012. PI3K inhibition impairs BRCA1/2 expression and sensitizes BRCA-proficient triple-negative breast cancer to PARP inhibition. *Cancer Discov.* 2, 1036–1047. <https://doi.org/10.1158/2159-8290.CD-11-0348>
- Jiang, K., Sun, J., Cheng, J., Djeu, J.Y., Wei, S., Sebt, S., 2004. Akt mediates Ras downregulation of RhoB, a suppressor of transformation, invasion, and metastasis. *Mol. Cell. Biol.* 24, 5565–5576. <https://doi.org/10.1128/MCB.24.12.5565-5576.2004>
- Ju, J.A., Gilkes, D.M., 2018. RhoB: Team Oncogene or Team Tumor Suppressor? *Genes* 9, 67. <https://doi.org/10.3390/genes9020067>
- Julian, L., Olson, M.F., 2014. Rho-associated coiled-coil containing kinases (ROCK). *Small GTPases* 5. <https://doi.org/10.4161/sgtp.29846>
- Kabuta, T., Hakuno, F., Cho, Y., Yamanaka, D., Chida, K., Asano, T., Wada, K., Takahashi, S.-I., 2010. Insulin receptor substrate-3, interacting with Bcl-3, enhances p50 NF-kappaB activity. *Biochem. Biophys. Res. Commun.* 394, 697–702. <https://doi.org/10.1016/j.bbrc.2010.03.054>
- Kajstura, M., Halicka, H.D., Pryjma, J., Darzynkiewicz, Z., 2007. Discontinuous fragmentation of nuclear DNA during apoptosis revealed by discrete “sub-G1” peaks on DNA content histograms. *Cytom. Part J. Int. Soc. Anal. Cytol.* 71, 125–131. <https://doi.org/10.1002/cyto.a.20357>
- Kanda, T., Yokosuka, O., Nagao, K., Saisho, H., 2006. State of hepatitis C viral replication enhances activation of NF-kB- and AP-1-signaling induced by hepatitis B virus X. *Cancer Lett.* 234, 143–148. <https://doi.org/10.1016/j.canlet.2005.03.030>
- Kanellos, G., Frame, M.C., 2016. Cellular functions of the ADF/cofilin family at a glance. *J. Cell Sci.* 129, 3211–3218. <https://doi.org/10.1242/jcs.187849>
- Kang, S., Yun, J., Kim, D.Y., Jung, S.Y., Kim, Y.J., Park, J.H., Ji, S.T., Jang, W.B., Ha, J., Kim, J.H., Baek, S.H., Kwon, S.-M., 2018. Adequate concentration of B cell leukemia/lymphoma 3 (Bcl3) is required for pluripotency and self-renewal of mouse embryonic stem cells via downregulation of Nanog transcription. *BMB Rep.* 51, 92–97.
- Karin, M., Cao, Y., Greten, F.R., Li, Z.-W., 2002. NF-kappaB in cancer: from innocent bystander to major culprit. *Nat. Rev. Cancer* 2, 301–310. <https://doi.org/10.1038/nrc780>
- Kashatus, D., Cogswell, P., Baldwin, A.S., 2006. Expression of the Bcl-3 proto-oncogene suppresses p53 activation. *Genes Dev.* 20, 225–235. <https://doi.org/10.1101/gad.1352206>
- Kastenhuber, E.R., Lowe, S.W., 2017. Putting p53 in Context. *Cell* 170, 1062–1078. <https://doi.org/10.1016/j.cell.2017.08.028>
- Kazerounian, S., Gerald, D., Huang, M., Chin, Y.R., Udayakumar, D., Zheng, N., O'Donnell, R.K., Perruzzi, C., Mangiante, L., Pourat, J., Phung, T.L., Bravo-Nuevo, A., Shechter, S., McNamara, S., DuHadaway, J.B., Kocher, O.N., Brown, L.F., Toker, A., Prendergast, G.C., Benjamin, L.E., 2013. RhoB Differentially Controls Akt Function in Tumor Cells and Stromal Endothelial Cells during Breast Tumorigenesis. *Cancer Res.* 73, 50–61. <https://doi.org/10.1158/0008-5472.CAN-11-3055>
- Keutgens, A., Zhang, X., Shostak, K., Robert, I., Olivier, S., Vanderplasschen, A., Chapelle, J.-P., Viatour, P., Merville, M.-P., Bex, F., Gothot, A., Chariot, A., 2010. BCL-3 Degradation Involves Its

- Polyubiquitination through a FBW7-independent Pathway and Its Binding to the Proteasome Subunit PSMB1. *J. Biol. Chem.* 285, 25831–25840. <https://doi.org/10.1074/jbc.M110.112128>
- Kim, C., Yang, H., Fukushima, Y., Saw, P.E., Lee, J., Park, J.-S., Park, I., Jung, J., Kataoka, H., Lee, D., Heo, W.D., Kim, I., Jon, S., Adams, R.H., Nishikawa, S.-I., Uemura, A., Koh, G.Y., 2014. Vascular RhoJ is an effective and selective target for tumor angiogenesis and vascular disruption. *Cancer Cell* 25, 102–117. <https://doi.org/10.1016/j.ccr.2013.12.010>
- Kim, M.-J., Lee, Y.-S., Han, G.-Y., Lee, H.-N., Ahn, C., Kim, C.-W., 2015. Profilin 2 promotes migration, invasion, and stemness of HT29 human colorectal cancer stem cells. *Biosci. Biotechnol. Biochem.* 79, 1438–1446. <https://doi.org/10.1080/09168451.2015.1043118>
- Kong, J., Du, J., Wang, Y., Yang, M., Gao, J., Wei, X., Fang, W., Zhan, J., Zhang, H., 2016. Focal adhesion molecule Kindlin-1 mediates activation of TGF- β signaling by interacting with TGF- β RI, SARA and Smad3 in colorectal cancer cells. *Oncotarget* 7, 76224–76237. <https://doi.org/10.18632/oncotarget.12779>
- Körner, C., Keklikoglou, I., Bender, C., Wörner, A., Münstermann, E., Wiemann, S., 2013. MicroRNA-31 sensitizes human breast cells to apoptosis by direct targeting of protein kinase C epsilon (PKCepsilon). *J. Biol. Chem.* 288, 8750–8761. <https://doi.org/10.1074/jbc.M112.414128>
- Kuwata, H., Watanabe, Y., Miyoshi, H., Yamamoto, M., Kaisho, T., Takeda, K., Akira, S., 2003. IL-10-inducible Bcl-3 negatively regulates LPS-induced TNF- α production in macrophages. *Blood* 102, 4123–4129. <https://doi.org/10.1182/blood-2003-04-1228>
- Layman, R.M., Ruppert, A.S., Lynn, M., Mrozek, E., Ramaswamy, B., Lustberg, M.B., Wesolowski, R., Ottman, S., Carothers, S., Bingman, A., Reinbolt, R., Kraut, E.H., Shapiro, C.L., 2013. Severe and prolonged lymphopenia observed in patients treated with bendamustine and erlotinib for metastatic triple negative breast cancer. *Cancer Chemother. Pharmacol.* 71, 1183–1190. <https://doi.org/10.1007/s00280-013-2112-2>
- LeClaire, L.L., Baumgartner, M., Iwasa, J.H., Mullins, R.D., Barber, D.L., 2008. Phosphorylation of the Arp2/3 complex is necessary to nucleate actin filaments. *J. Cell Biol.* 182, 647–654. <https://doi.org/10.1083/jcb.200802145>
- Lee, J.J., Natsuizaka, M., Ohashi, S., Wong, G.S., Takaoka, M., Michaylira, C.Z., Budo, D., Tobias, J.W., Kanai, M., Shirakawa, Y., Naomoto, Y., Klein-Szanto, A.J.P., Haase, V.H., Nakagawa, H., 2010. Hypoxia activates the cyclooxygenase-2-prostaglandin E synthase axis. *Carcinogenesis* 31, 427–434. <https://doi.org/10.1093/carcin/bgp326>
- Legge, D.N., et al., BCL-3 promotes a cancer stem cell phenotype by enhancing β -catenin signalling in colorectal tumour cells. *Disease Models & Mechanisms*, 2019: p. dmm.037697.
- Lehmann, B.D., Bauer, J.A., Chen, X., Sanders, M.E., Chakravarthy, A.B., Shyr, Y., Pietenpol, J.A., 2011. Identification of human triple-negative breast cancer subtypes and preclinical models for selection of targeted therapies. *J. Clin. Invest.* 121, 2750–2767. <https://doi.org/10.1172/JCI45014>
- Lehmann, B.D., Bauer, J.A., Schafer, J.M., Pendleton, C.S., Tang, L., Johnson, K.C., Chen, X., Balko, J.M., Gómez, H., Arteaga, C.L., Mills, G.B., Sanders, M.E., Pietenpol, J.A., 2014. PIK3CA mutations in androgen receptor-positive triple negative breast cancer confer sensitivity to the combination of PI3K and androgen receptor inhibitors. *Breast Cancer Res. BCR* 16, 406. <https://doi.org/10.1186/s13058-014-0406-x>
- Lehmann, B.D., Pietenpol, J.A., 2014. Identification and use of biomarkers in treatment strategies for triple-negative breast cancer subtypes. *J. Pathol.* 232, 142–150. <https://doi.org/10.1002/path.4280>
- Lehner, A., Magdolen, V., Schuster, T., Kotsch, M., Kiechle, M., Meindl, A., Sweep, F.C.G.J., Span, P.N., Gross, E., 2013. Downregulation of serine protease HTRA1 is associated with poor survival in breast cancer. *PloS One* 8, e60359. <https://doi.org/10.1371/journal.pone.0060359>

- Lemke, J., Karstedt, S. von, Zinngrebe, J., Walczak, H., 2014. Getting TRAIL back on track for cancer therapy. *Cell Death Differ.* 21, 1350–1364. <https://doi.org/10.1038/cdd.2014.81>
- Li, J., Liu, Y., Yin, Y., 2017. ARHGAP1 overexpression inhibits proliferation, migration and invasion of C-33A and SiHa cell lines. *OncoTargets Ther.* 10, 691–701. <https://doi.org/10.2147/OTT.S112223>
- Li, P., Xiang, T., Li, H., Li, Q., Yang, B., Huang, J., Zhang, X., Shi, Y., Tan, J., Ren, G., 2015. Hyaluronan synthase 2 overexpression is correlated with the tumorigenesis and metastasis of human breast cancer. *Int. J. Clin. Exp. Pathol.* 8, 12101–12114.
- Li, P., Zhou, L., Zhao, T., Liu, X., Zhang, P., Liu, Y., Zheng, X., Li, Q., 2017. Caspase-9: structure, mechanisms and clinical application. *Oncotarget* 8, 23996. <https://doi.org/10.18632/oncotarget.15098>
- Lin, N.U., Vanderplas, A., Hughes, M.E., Theriault, R.L., Edge, S.B., Wong, Y.-N., Blayney, D.W., Niland, J.C., Winer, E.P., Weeks, J.C., 2012. Clinicopathologic features, patterns of recurrence, and survival among women with triple-negative breast cancer in the National Comprehensive Cancer Network. *Cancer* 118, 5463–5472. <https://doi.org/10.1002/cncr.27581>
- Liou, G.-Y., Storz, P., 2010. Reactive oxygen species in cancer. *Free Radic. Res.* 44, 479–496. <https://doi.org/10.3109/10715761003667554>
- Lips, E.H., Mulder, L., Oonk, A., van der Kolk, L.E., Hogervorst, F.B.L., Imholz, A.L.T., Wesseling, J., Rodenhuis, S., Nederlof, P.M., 2013. Triple-negative breast cancer: BRCAness and concordance of clinical features with BRCA1-mutation carriers. *Br. J. Cancer* 108, 2172–2177. <https://doi.org/10.1038/bjc.2013.144>
- Liu, A.X., Rane, N., Liu, J.P., Prendergast, G.C., 2001. RhoB is dispensable for mouse development, but it modifies susceptibility to tumor formation as well as cell adhesion and growth factor signaling in transformed cells. *Mol. Cell. Biol.* 21, 6906–6912. <https://doi.org/10.1128/MCB.21.20.6906-6912.2001>
- Liu, L., Chen, J., Sun, L., Xu, Y., 2018. RhoJ promotes hypoxia induced endothelial-to-mesenchymal transition by activating WDR5 expression. *J. Cell. Biochem.* 119, 3384–3393. <https://doi.org/10.1002/jcb.26505>
- Liu, T., Sun, H., Liu, S., Yang, Z., Li, L., Yao, N., Cheng, S., Dong, X., Liang, X., Chen, C., Wang, Y., Zhao, X., 2018. The suppression of DUSP5 expression correlates with paclitaxel resistance and poor prognosis in basal-like breast cancer. *Int. J. Med. Sci.* 15, 738–747. <https://doi.org/10.7150/ijms.24981>
- Liu, Z., Jiang, Y., Hou, Y., Hu, Y., Cao, X., Tao, Y., Xu, C., Liu, S., Wang, S., Wang, L., Shi, Y., Siebenlist, U., Zhang, X., 2013. The I κ B family member Bcl-3 stabilizes c-Myc in colorectal cancer. *J. Mol. Cell Biol.* 5, 280–282. <https://doi.org/10.1093/jmcb/mjt020>
- Loi, S., Sirtaine, N., Piette, F., Salgado, R., Viale, G., Van Eenoo, F., Rouas, G., Francis, P., Crown, J.P.A., Hitre, E., de Azambuja, E., Quinaux, E., Di Leo, A., Michiels, S., Piccart, M.J., Sotiriou, C., 2013. Prognostic and predictive value of tumor-infiltrating lymphocytes in a phase III randomized adjuvant breast cancer trial in node-positive breast cancer comparing the addition of docetaxel to doxorubicin with doxorubicin-based chemotherapy: BIG 02-98. *J. Clin. Oncol. Off. J. Am. Soc. Clin. Oncol.* 31, 860–867. <https://doi.org/10.1200/JCO.2011.41.0902>
- Lu, X., Wang, X., Zhuo, W., Jia, L., Jiang, Y., Fu, Y., Luo, Y., 2014. The regulatory mechanism of a client kinase controlling its own release from Hsp90 chaperone machinery through phosphorylation. *Biochem. J.* 457, 171–183. <https://doi.org/10.1042/BJ20130963>
- Ma, Y.-F., Ren, Y., Wu, C.-J., Zhao, X.-H., Xu, H., Wu, D.-Z., Xu, J., Zhang, X.-L., Ji, Y., 2016. Interleukin (IL)-24 transforms the tumor microenvironment and induces anticancer immunity in a

- murine model of colon cancer. *Mol. Immunol.* 75, 11–20. <https://doi.org/10.1016/j.molimm.2016.05.010>
- Maldonado, V., Espinosa, M., Pruefer, F., Patiño, N., Ceballos-Canciono, G., Urzua, U., Juretic, N., Melendez-Zajgla, J., 2010. Gene regulation by BCL3 in a cervical cancer cell line. *Folia Biol. (Praha)* 56, 183–193.
- Maldonado, V., Melendez-Zajgla, J., 2011. Role of Bcl-3 in solid tumors. *Mol. Cancer* 10, 152. <https://doi.org/10.1186/1476-4598-10-152>
- Malinin, N.L., Boldin, M.P., Kovalenko, A.V., Wallach, D., 1997. MAP3K-related kinase involved in NF-kappaB induction by TNF, CD95 and IL-1. *Nature* 385, 540–544. <https://doi.org/10.1038/385540a0>
- Mao, Y., Qu, Q., Zhang, Y., Liu, J., Chen, X., Shen, K., 2014. The value of tumor infiltrating lymphocytes (TILs) for predicting response to neoadjuvant chemotherapy in breast cancer: a systematic review and meta-analysis. *PLoS One* 9, e115103. <https://doi.org/10.1371/journal.pone.0115103>
- Marienfeld, R., May, M.J., Berberich, I., Serfling, E., Ghosh, S., Neumann, M., 2003. RelB forms transcriptionally inactive complexes with RelA/p65. *J. Biol. Chem.* 278, 19852–19860. <https://doi.org/10.1074/jbc.M301945200>
- May, M.J., Ghosh, S., 1997. Rel/NF-kappa B and I kappa B proteins: an overview. *Semin. Cancer Biol.* 8, 63–73. <https://doi.org/10.1006/scbi.1997.0057>
- Mi, H., Muruganujan, A., Casagrande, J.T., Thomas, P.D., 2013. Large-scale gene function analysis with the PANTHER classification system. *Nat. Protoc.* 8, 1551–1566. <https://doi.org/10.1038/nprot.2013.092>
- Micheau, O., 2018. Regulation of TNF-Related Apoptosis-Inducing Ligand Signaling by Glycosylation. *Int. J. Mol. Sci.* 19. <https://doi.org/10.3390/ijms19030715>
- Mittendorf, E.A., Philips, A.V., Meric-Bernstam, F., Qiao, N., Wu, Y., Harrington, S., Su, X., Wang, Y., Gonzalez-Angulo, A.M., Akcakanat, A., Chawla, A., Curran, M., Hwu, P., Sharma, P., Litton, J.K., Mollndrem, J.J., Alatrash, G., 2014. PD-L1 expression in triple-negative breast cancer. *Cancer Immunol. Res.* 2, 361–370. <https://doi.org/10.1158/2326-6066.CIR-13-0127>
- Montero, J.C., Esparís-Ogando, A., Re-Louhau, M.F., Seoane, S., Abad, M., Calero, R., Ocaña, A., Pandiella, A., 2014. Active kinase profiling, genetic and pharmacological data define mTOR as an important common target in triple-negative breast cancer. *Oncogene* 33, 148–156. <https://doi.org/10.1038/onc.2012.572>
- Moon, S.Y., Zheng, Y., 2003. Rho GTPase-activating proteins in cell regulation. *Trends Cell Biol.* 13, 13–22.
- Morley, S., You, S., Pollan, S., Choi, J., Zhou, B., Hager, M.H., Steadman, K., Spinelli, C., Rajendran, K., Gertych, A., Kim, J., Adam, R.M., Yang, W., Krishnan, R., Knudsen, B.S., Di Vizio, D., Freeman, M.R., 2015. Regulation of microtubule dynamics by DIAPH3 influences amoeboid tumor cell mechanics and sensitivity to taxanes. *Sci. Rep.* 5, 12136. <https://doi.org/10.1038/srep12136>
- Muharram, G., Sahgal, P., Korpela, T., De Franceschi, N., Kaukonen, R., Clark, K., Tulasne, D., Carpén, O., Ivaska, J., 2014. Tensin-4-dependent MET stabilization is essential for survival and proliferation in carcinoma cells. *Dev. Cell* 29, 421–436. <https://doi.org/10.1016/j.devcel.2014.03.024>
- Murugaesu, N., Irvani, M., van Weverwijk, A., Ivetic, A., Johnson, D.A., Antonopoulos, A., Fearn, A., Jamal-Hanjani, M., Sims, D., Fenwick, K., Mitsopoulos, C., Gao, Q., Orr, N., Zvelebil, M., Haslam, S.M., Dell, A., Yarwood, H., Lord, C.J., Ashworth, A., Isacke, C.M., 2014. An in vivo

- functional screen identifies ST6GalNAc2 sialyltransferase as a breast cancer metastasis suppressor. *Cancer Discov.* 4, 304–317. <https://doi.org/10.1158/2159-8290.CD-13-0287>
- Nakai, K., Hung, M.-C., Yamaguchi, H., 2016. A perspective on anti-EGFR therapies targeting triple-negative breast cancer. *Am. J. Cancer Res.* 6, 1609–1623.
- Nami, B., Wang, Z., 2018. Genetics and Expression Profile of the Tubulin Gene Superfamily in Breast Cancer Subtypes and Its Relation to Taxane Resistance. *Cancers* 10. <https://doi.org/10.3390/cancers10080274>
- Narumiya, S., Tanji, M., Ishizaki, T., 2009. Rho signaling, ROCK and mDia1, in transformation, metastasis and invasion. *Cancer Metastasis Rev.* 28, 65–76. <https://doi.org/10.1007/s10555-008-9170-7>
- Neophytou, C., Boutsikos, P., Papageorgis, P., 2018. Molecular Mechanisms and Emerging Therapeutic Targets of Triple-Negative Breast Cancer Metastasis. *Front. Oncol.* 8. <https://doi.org/10.3389/fonc.2018.00031>
- Neri, A., Chang, C.C., Lombardi, L., Salina, M., Corradini, P., Maiolo, A.T., Chaganti, R.S., Dalla-Favera, R., 1991. B cell lymphoma-associated chromosomal translocation involves candidate oncogene *lyt-10*, homologous to NF-kappa B p50. *Cell* 67, 1075–1087.
- Nguyen, D.X., Massagué, J., 2007. Genetic determinants of cancer metastasis. *Nat. Rev. Genet.* 8, 341–352. <https://doi.org/10.1038/nrg2101>
- Oeckinghaus, A., Ghosh, S., 2009. The NF-kappaB family of transcription factors and its regulation. *Cold Spring Harb. Perspect. Biol.* 1, a000034. <https://doi.org/10.1101/cshperspect.a000034>
- Ohno, H., Takimoto, G., McKeithan, T.W., 1990. The candidate proto-oncogene *bcl-3* is related to genes implicated in cell lineage determination and cell cycle control. *Cell* 60, 991–997.
- Osanai, M., Lee, G.-H., 2016. CYP24A1-induced vitamin D insufficiency promotes breast cancer growth. *Oncol. Rep.* 36, 2755–2762. <https://doi.org/10.3892/or.2016.5072>
- Otto, K.B., Acharya, S.S., Robinson, V.L., 2012. Stress-activated kinase pathway alteration is a frequent event in bladder cancer. *Urol. Oncol.* 30, 415–420. <https://doi.org/10.1016/j.urolonc.2010.03.002>
- Ozturk, S., Papageorgis, P., Wong, C.K., Lambert, A.W., Abdolmaleky, H.M., Thiagalingam, A., Cohen, H.T., Thiagalingam, S., 2016. SDPR functions as a metastasis suppressor in breast cancer by promoting apoptosis. *Proc. Natl. Acad. Sci. U. S. A.* 113, 638–643. <https://doi.org/10.1073/pnas.1514663113>
- Padua, D., Zhang, X.H.-F., Wang, Q., Nadal, C., Gerald, W.L., Gomis, R.R., Massagué, J., 2008. TGFbeta primes breast tumors for lung metastasis seeding through angiopoietin-like 4. *Cell* 133, 66–77. <https://doi.org/10.1016/j.cell.2008.01.046>
- Pahl, H.L., 1999. Activators and target genes of Rel/NF-kappaB transcription factors. *Oncogene* 18, 6853–6866. <https://doi.org/10.1038/sj.onc.1203239>
- Palmer, B.F., Clegg, D.J., 2014. Oxygen sensing and metabolic homeostasis. *Mol. Cell. Endocrinol., Cellular energy sensors and endocrine function* 397, 51–58. <https://doi.org/10.1016/j.mce.2014.08.001>
- Papageorgis, P., Lambert, A.W., Ozturk, S., Gao, F., Pan, H., Manne, U., Alekseyev, Y.O., Thiagalingam, A., Abdolmaleky, H.M., Lenburg, M., Thiagalingam, S., 2010. Smad signaling is required to maintain epigenetic silencing during breast cancer progression. *Cancer Res.* 70, 968–978. <https://doi.org/10.1158/0008-5472.CAN-09-1872>

- Peake, B.F., Eze, S.M., Yang, L., Castellino, R.C., Nahta, R., 2017. Growth differentiation factor 15 mediates epithelial mesenchymal transition and invasion of breast cancers through IGF-1R-FoxM1 signaling. *Oncotarget* 8, 94393–94406. <https://doi.org/10.18632/oncotarget.21765>
- Pecci, A., Ma, X., Savoia, A., Adelstein, R.S., 2018. MYH9: Structure, functions and role of non-muscle myosin IIA in human disease. *Gene*. <https://doi.org/10.1016/j.gene.2018.04.048>
- Pérez-Yépez, E.A., Saldívar-Cerón, H.I., Villamar-Cruz, O., Pérez-Plasencia, C., Arias-Romero, L.E., 2018. p21 Activated kinase 1: Nuclear activity and its role during DNA damage repair. *DNA Repair* 65, 42–46. <https://doi.org/10.1016/j.dnarep.2018.03.004>
- Perkins, N.D., Gilmore, T.D., 2006. Good cop, bad cop: the different faces of NF-kappaB. *Cell Death Differ.* 13, 759–772. <https://doi.org/10.1038/sj.cdd.4401838>
- Perou, C.M., Sørlie, T., Eisen, M.B., van de Rijn, M., Jeffrey, S.S., Rees, C.A., Pollack, J.R., Ross, D.T., Johnsen, H., Akslen, L.A., Fluge, O., Pergamenschikov, A., Williams, C., Zhu, S.X., Lønning, P.E., Børresen-Dale, A.L., Brown, P.O., Botstein, D., 2000. Molecular portraits of human breast tumours. *Nature* 406, 747–752. <https://doi.org/10.1038/35021093>
- Pertz, O., Hodgson, L., Klemke, R.L., Hahn, K.M., 2006. Spatiotemporal dynamics of RhoA activity in migrating cells. *Nature* 440, 1069–1072. <https://doi.org/10.1038/nature04665>
- Peters, A.A., Buchanan, G., Ricciardelli, C., Bianco-Miotto, T., Centenera, M.M., Harris, J.M., Jindal, S., Segara, D., Jia, L., Moore, N.L., Henshall, S.M., Birrell, S.N., Coetzee, G.A., Sutherland, R.L., Butler, L.M., Tilley, W.D., 2009. Androgen receptor inhibits estrogen receptor-alpha activity and is prognostic in breast cancer. *Cancer Res.* 69, 6131–6140. <https://doi.org/10.1158/0008-5472.CAN-09-0452>
- Phizicky, E.M., Fields, S., 1995. Protein-protein interactions: methods for detection and analysis. *Microbiol. Rev.* 59, 94–123.
- Powell, E., Shao, J., Yuan, Y., Chen, H.-C., Cai, S., Echeverria, G.V., Mistry, N., Decker, K.F., Schlosberg, C., Do, K.-A., Edwards, J.R., Liang, H., Piwnica-Worms, D., Piwnica-Worms, H., 2016. p53 deficiency linked to B cell translocation gene 2 (BTG2) loss enhances metastatic potential by promoting tumor growth in primary and metastatic sites in patient-derived xenograft (PDX) models of triple-negative breast cancer. *Breast Cancer Res. BCR* 18, 13. <https://doi.org/10.1186/s13058-016-0673-9>
- Prat, A., Parker, J.S., Karginova, O., Fan, C., Livasy, C., Herschkowitz, J.I., He, X., Perou, C.M., 2010. Phenotypic and molecular characterization of the claudin-low intrinsic subtype of breast cancer. *Breast Cancer Res. BCR* 12, R68. <https://doi.org/10.1186/bcr2635>
- Pusztai, L., Krishnamurti, S., Perez Cardona, J., Sneige, N., Esteva, F.J., Volchenok, M., Breitenfelder, P., Kau, S.-W., Takayama, S., Krajewski, S., Reed, J.C., Bast, R.C., Hortobagyi, G.N., 2004. Expression of BAG-1 and Bcl-2 proteins before and after neoadjuvant chemotherapy of locally advanced breast cancer. *Cancer Invest.* 22, 248–256.
- Puvvada, S.D., Funkhouser, W.K., Greene, K., Deal, A., Chu, H., Baldwin, A.S., Tepper, J.E., O’Neil, B.H., 2010. NF-kB and Bcl-3 activation are prognostic in metastatic colorectal cancer. *Oncology* 78, 181–188. <https://doi.org/10.1159/000313697>
- Rana, M.K., Aloisio, F.M., Choi, C., Barber, D.L., 2018. Formin-dependent TGF-β signaling for epithelial to mesenchymal transition. *Mol. Biol. Cell* mbcE17050325. <https://doi.org/10.1091/mbc.E17-05-0325>
- Rani, A., Greenlaw, R., Smith, R.A., Galustian, C., 2016. HES1 in immunity and cancer. *Cytokine Growth Factor Rev.* 30, 113–117. <https://doi.org/10.1016/j.cytogfr.2016.03.010>
- Rashid, O.M., Nagahashi, M., Ramachandran, S., Dumur, C.I., Schaum, J.C., Yamada, A., Aoyagi, T., Milstien, S., Spiegel, S., Takabe, K., 2013. Is tail vein injection a relevant breast cancer lung

- metastasis model? *J. Thorac. Dis.* 5, 385–392. <https://doi.org/10.3978/j.issn.2072-1439.2013.06.17>
- Rayet, B., Gélinas, C., 1999. Aberrant rel/nfkb genes and activity in human cancer. *Oncogene* 18, 6938–6947. <https://doi.org/10.1038/sj.onc.1203221>
- Rebollo, A., Dumoutier, L., Renauld, J.C., Zaballos, A., Ayllón, V., Martínez-A, C., 2000. Bcl-3 expression promotes cell survival following interleukin-4 deprivation and is controlled by AP1 and AP1-like transcription factors. *Mol. Cell. Biol.* 20, 3407–3416.
- Reißig, S., Tang, Y., Nikolaev, A., Gerlach, K., Wolf, C., Davari, K., Gallus, C., Masri, J., Mufazalov, I.A., Neurath, M.F., Wunderlich, F.T., Schattenberg, J.M., Galle, P.R., Weigmann, B., Waisman, A., Glasmacher, E., Hövelmeyer, N., 2017. Elevated levels of Bcl-3 inhibits Treg development and function resulting in spontaneous colitis. *Nat. Commun.* 8, 15069. <https://doi.org/10.1038/ncomms15069>
- Ridley, A.J., 2013. RhoA, RhoB and RhoC have different roles in cancer cell migration. *J. Microsc.* 251, 242–249. <https://doi.org/10.1111/jmi.12025>
- Riggio, M., Perrone, M.C., Polo, M.L., Rodriguez, M.J., May, M., Abba, M., Lanari, C., Novaro, V., 2017. AKT1 and AKT2 isoforms play distinct roles during breast cancer progression through the regulation of specific downstream proteins. *Sci. Rep.* 7, 44244. <https://doi.org/10.1038/srep44244>
- Ring, B.Z., Hout, D.R., Morris, S.W., Lawrence, K., Schweitzer, B.L., Bailey, D.B., Lehmann, B.D., Pietenpol, J.A., Seitz, R.S., 2016. Generation of an algorithm based on minimal gene sets to clinically subtype triple negative breast cancer patients. *BMC Cancer* 16, 143. <https://doi.org/10.1186/s12885-016-2198-0>
- Robson, M., Im, S.-A., Senkus, E., Xu, B., Domchek, S.M., Masuda, N., Delaloge, S., Li, W., Tung, N., Armstrong, A., Wu, W., Goessl, C., Runswick, S., Conte, P., 2017. Olaparib for Metastatic Breast Cancer in Patients with a Germline BRCA Mutation. *N. Engl. J. Med.* 377, 523–533. <https://doi.org/10.1056/NEJMoa1706450>
- Rodriguez, L.G., Wu, X., Guan, J.-L., 2005. Wound-healing assay. *Methods Mol. Biol.* Clifton NJ 294, 23–29.
- Rossman, K.L., Der, C.J., Sondek, J., 2005. GEF means go: turning on RHO GTPases with guanine nucleotide-exchange factors. *Nat. Rev. Mol. Cell Biol.* 6, 167–180. <https://doi.org/10.1038/nrm1587>
- Rottenberg, S., Jaspers, J.E., Kersbergen, A., van der Burg, E., Nygren, A.O.H., Zander, S.A.L., Derksen, P.W.B., de Bruin, M., Zevenhoven, J., Lau, A., Boulter, R., Cranston, A., O'Connor, M.J., Martin, N.M.B., Borst, P., Jonkers, J., 2008. High sensitivity of BRCA1-deficient mammary tumors to the PARP inhibitor AZD2281 alone and in combination with platinum drugs. *Proc. Natl. Acad. Sci. U.S.A.* 105, 17079–17084. <https://doi.org/10.1073/pnas.0806092105>
- Rottner, K., Hall, A., Small, J.V., 1999. Interplay between Rac and Rho in the control of substrate contact dynamics. *Curr. Biol.* CB 9, 640–648.
- Sadok, A., et al., Rho kinase inhibitors block melanoma cell migration and inhibit metastasis. *Cancer Res*, 2015. **75**(11): p. 2272–84.
- Sagara, A., Igarashi, K., Otsuka, M., Kodama, A., Yamashita, M., Sugiura, R., Karasawa, T., Arakawa, K., Narita, Michiko, Kuzumaki, N., Narita, Minoru, Kato, Y., 2017. Endocan as a prognostic biomarker of triple-negative breast cancer. *Breast Cancer Res. Treat.* 161, 269–278. <https://doi.org/10.1007/s10549-016-4057-8>
- Sanlioglu, A.D., Dirice, E., Aydin, C., Erin, N., Koksoy, S., Sanlioglu, S., 2005. Surface TRAIL decoy receptor-4 expression is correlated with TRAIL resistance in MCF7 breast cancer cells. *BMC Cancer* 5, 54. <https://doi.org/10.1186/1471-2407-5-54>

- Sausville, E.A., Burger, A.M., 2006. Contributions of human tumor xenografts to anticancer drug development. *Cancer Res.* 66, 3351–3354, discussion 3354. <https://doi.org/10.1158/0008-5472.CAN-05-3627>
- Schlette, E., Rassidakis, G.Z., Canoz, O., Medeiros, L.J., 2005. Expression of bcl-3 in chronic lymphocytic leukemia correlates with trisomy 12 and abnormalities of chromosome 19. *Am. J. Clin. Pathol.* 123, 465–471. <https://doi.org/10.1309/6Q27-Q3ND-GV8L-W1BU>
- Schmid, J.A., Birbach, A., 2008. I κ B kinase beta (IKK β /IKK2/I κ BK β)--a key molecule in signaling to the transcription factor NF- κ B. *Cytokine Growth Factor Rev.* 19, 157–165. <https://doi.org/10.1016/j.cytogfr.2008.01.006>
- Scholzen, T., Gerdes, J., 2000. The Ki-67 protein: from the known and the unknown. *J. Cell. Physiol.* 182, 311–322. [https://doi.org/10.1002/\(SICI\)1097-4652\(200003\)182:3<311::AID-JCP1>3.0.CO;2-9](https://doi.org/10.1002/(SICI)1097-4652(200003)182:3<311::AID-JCP1>3.0.CO;2-9)
- Schwarz, E.M., et al., Immunological defects in mice with a targeted disruption in Bcl-3. *Genes Dev.* 1997. **11**(2): p. 187-97.
- Shah, S.P., Roth, A., Goya, R., Oloumi, A., Ha, G., Zhao, Y., Turashvili, G., Ding, J., Tse, K., Haffari, G., Bashashati, A., Prentice, L.M., Khattra, J., Burleigh, A., Yap, D., Bernard, V., McPherson, A., Shumansky, K., Crisan, A., Giuliany, R., Heravi-Moussavi, A., Rosner, J., Lai, D., Birol, I., Varhol, R., Tam, A., Dhalla, N., Zeng, T., Ma, K., Chan, S.K., Griffith, M., Moradian, A., Cheng, S.-W.G., Morin, G.B., Watson, P., Gelmon, K., Chia, S., Chin, S.-F., Curtis, C., Rueda, O.M., Pharoah, P.D., Damaraju, S., Mackey, J., Hoon, K., Harkins, T., Tadigotla, V., Sigaroudinia, M., Gascard, P., Tlsty, T., Costello, J.F., Meyer, I.M., Eaves, C.J., Wasserman, W.W., Jones, S., Huntsman, D., Hirst, M., Caldas, C., Marra, M.A., Aparicio, S., 2012. The clonal and mutational evolution spectrum of primary triple-negative breast cancers. *Nature* 486, 395–399. <https://doi.org/10.1038/nature10933>
- Shakeri, R., Kheirollahi, A., Davoodi, J., 2017. Apaf-1: Regulation and function in cell death. *Biochimie* 135, 111–125. <https://doi.org/10.1016/j.biochi.2017.02.001>
- Shan, B., Pan, H., Najafov, A., Yuan, J., 2018. Necroptosis in development and diseases. *Genes Dev.* 32, 327–340. <https://doi.org/10.1101/gad.312561.118>
- Sharpe, R., Pearson, A., Herrera-Abreu, M.T., Johnson, D., Mackay, A., Welti, J.C., Natrajan, R., Reynolds, A.R., Reis-Filho, J.S., Ashworth, A., Turner, N.C., 2011. FGFR signaling promotes the growth of triple-negative and basal-like breast cancer cell lines both in vitro and in vivo. *Clin. Cancer Res.* 17, 5275–5286. <https://doi.org/10.1158/1078-0432.CCR-10-2727>
- Shaw, F.L., Harrison, H., Spence, K., Ablett, M.P., Simões, B.M., Farnie, G., Clarke, R.B., 2012. A detailed mammosphere assay protocol for the quantification of breast stem cell activity. *J. Mammary Gland Biol. Neoplasia* 17, 111–117. <https://doi.org/10.1007/s10911-012-9255-3>
- Shen, K., Ramirez, B., Mapes, B., Shen, G.R., Gokhale, V., Brown, M.E., Santarsiero, B., Ishii, Y., Dudek, S.M., Wang, T., Garcia, J.G.N., 2015. Structure-Function Analysis of the Non-Muscle Myosin Light Chain Kinase (nmMLCK) Isoform by NMR Spectroscopy and Molecular Modeling: Influence of MYLK Variants. *PLoS One* 10, e0130515. <https://doi.org/10.1371/journal.pone.0130515>
- Shiang, C.Y., Qi, Y., Wang, B., Lazar, V., Wang, J., Fraser Symmans, W., Hortobagyi, G.N., Andre, F., Pusztai, L., 2010. Amplification of fibroblast growth factor receptor-1 in breast cancer and the effects of brivanib alaninate. *Breast Cancer Res. Treat.* 123, 747–755. <https://doi.org/10.1007/s10549-009-0677-6>
- Shultz, L.D., Lyons, B.L., Burzenski, L.M., Gott, B., Chen, X., Chaleff, S., Kotb, M., Gillies, S.D., King, M., Mangada, J., Greiner, D.L., Handgretinger, R., 2005. Human lymphoid and myeloid cell development in NOD/LtSz-scid IL2R gamma null mice engrafted with mobilized human hemopoietic stem cells. *J. Immunol. Baltim. Md* 1950 174, 6477–6489.

- Skaland, I., Janssen, E.A.M., Gudlaugsson, E., Klos, J., Kjellevoid, K.H., Søliland, H., Baak, J.P.A., 2007. Phosphohistone H3 expression has much stronger prognostic value than classical prognosticators in invasive lymph node-negative breast cancer patients less than 55 years of age. *Mod. Pathol. Off. J. U. S. Can. Acad. Pathol. Inc* 20, 1307–1315. <https://doi.org/10.1038/modpathol.3800972>
- Sleeman, J. and P.S. Steeg, Cancer metastasis as a therapeutic target. *European Journal of Cancer*, 2010. **46**(7): p. 1177-1180.
- Smyth, M.J., Dunn, G.P., Schreiber, R.D., 2006. Cancer immunosurveillance and immunoediting: the roles of immunity in suppressing tumor development and shaping tumor immunogenicity. *Adv. Immunol.* 90, 1–50. [https://doi.org/10.1016/S0065-2776\(06\)90001-7](https://doi.org/10.1016/S0065-2776(06)90001-7)
- Solt, L.A., May, M.J., 2008. The I κ B kinase complex: master regulator of NF- κ B signaling. *Immunol. Res.* 42, 3–18. <https://doi.org/10.1007/s12026-008-8025-1>
- Spiering, D., Hodgson, L., 2011. Dynamics of the Rho-family small GTPases in actin regulation and motility. *Cell Adhes. Migr.* 5, 170–180. <https://doi.org/10.4161/cam.5.2.14403>
- Sun, S.-C., 2011. Non-canonical NF- κ B signaling pathway. *Cell Res.* 21, 71–85. <https://doi.org/10.1038/cr.2010.177>
- Tang, W., Wang, H., Ha, H.L., Tassi, I., Bhardwaj, R., Claudio, E., Siebenlist, U., 2016. The B-cell tumor promoter Bcl-3 suppresses inflammation-associated colon tumorigenesis in epithelial cells. *Oncogene* 35, 6203–6211. <https://doi.org/10.1038/onc.2016.152>
- Tang, Y.-N., Ding, W.-Q., Guo, X.-J., Yuan, X.-W., Wang, D.-M., Song, J.-G., 2015. Epigenetic regulation of Smad2 and Smad3 by profilin-2 promotes lung cancer growth and metastasis. *Nat. Commun.* 6, 8230. <https://doi.org/10.1038/ncomms9230>
- Tao, Y., Liu, Zhanjie, Hou, Y., Wang, S., Liu, S., Jiang, Y., Tan, D., Ge, Q., Li, C., Hu, Y., Liu, Zhi, Chen, X., Wang, Q., Wang, M., Zhang, X., 2018. Alternative NF- κ B signaling promotes colorectal tumorigenesis through transcriptionally upregulating Bcl-3. *Oncogene*. <https://doi.org/10.1038/s41388-018-0363-4>
- Thornberry, N.A., Lazebnik, Y., 1998. Caspases: enemies within. *Science* 281, 1312–1316.
- Thornburg, N.J., Pathmanathan, R., Raab-Traub, N., 2003. Activation of Nuclear Factor- κ B p50 Homodimer/Bcl-3 Complexes in Nasopharyngeal Carcinoma. *Cancer Res.* 63, 8293–8301.
- Thuerauf, D.J., Marcinko, M., Belmont, P.J., Glembotski, C.C., 2007. Effects of the isoform-specific characteristics of ATF6 alpha and ATF6 beta on endoplasmic reticulum stress response gene expression and cell viability. *J. Biol. Chem.* 282, 22865–22878. <https://doi.org/10.1074/jbc.M701213200>
- Torre, L.A., Siegel, R.L., Ward, E.M., Jemal, A., 2016. Global Cancer Incidence and Mortality Rates and Trends--An Update. *Cancer Epidemiol. Biomark. Prev. Publ. Am. Assoc. Cancer Res. Cosponsored Am. Soc. Prev. Oncol.* 25, 16–27. <https://doi.org/10.1158/1055-9965.EPI-15-0578>
- Tu, K., Liu, Z., Yao, B., Xue, Y., Xu, M., Dou, C., Yin, G., Wang, J., 2016. BCL-3 promotes the tumor growth of hepatocellular carcinoma by regulating cell proliferation and the cell cycle through cyclin D1. *Oncol. Rep.* 35, 2382–2390. <https://doi.org/10.3892/or.2016.4616>
- Tutt, A., Robson, M., Garber, J.E., Domchek, S.M., Audeh, M.W., Weitzel, J.N., Friedlander, M., Arun, B., Loman, N., Schmutzler, R.K., Wardley, A., Mitchell, G., Earl, H., Wickens, M., Carmichael, J., 2010. Oral poly(ADP-ribose) polymerase inhibitor olaparib in patients with BRCA1 or BRCA2 mutations and advanced breast cancer: a proof-of-concept trial. *Lancet* 376, 235–244. [https://doi.org/10.1016/S0140-6736\(10\)60892-6](https://doi.org/10.1016/S0140-6736(10)60892-6)

- Turner, N., Tutt, A., Ashworth, A., 2004. Hallmarks of “BRCAness” in sporadic cancers. *Nat. Rev. Cancer* 4, 814–819. <https://doi.org/10.1038/nrc1457>
- Upadhyaya, D., Ogata, M., Reneker, L.W., 2013. MAPK1 is required for establishing the pattern of cell proliferation and for cell survival during lens development. *Dev. Camb. Engl.* 140, 1573. <https://doi.org/10.1242/dev.081042>
- Urban, B.C., Collard, T.J., Eagle, C.J., Southern, S.L., Greenhough, A., Hamdollah-Zadeh, M., Ghosh, A., Poulsom, R., Paraskeva, C., Silver, A., Williams, A.C., 2016. BCL-3 expression promotes colorectal tumorigenesis through activation of AKT signalling. *Gut* 65, 1151–1164.
- Valenzuela, J.O., Hammerbeck, C.D., Mescher, M.F., 2005. Cutting edge: Bcl-3 up-regulation by signal 3 cytokine (IL-12) prolongs survival of antigen-activated CD8 T cells. *J. Immunol. Baltim. Md* 1950 174, 600–604.
- van Krieken, J.H., McKeithan, T.W., Raghoebier, S., Medeiros, L.J., Kluin, P.M., Raffeld, M., 1990. Chromosomal translocation t(14;19) as indicated by bcl-3 rearrangement is a rare phenomenon in non-Hodgkin’s lymphoma and chronic lymphocytic leukemia: a molecular genetic analysis of 176 cases. *Leukemia* 4, 811–812.
- Viatour, P., Merville, M.-P., Bours, V., Chariot, A., 2004. Protein phosphorylation as a key mechanism for the regulation of BCL-3 activity. *Cell Cycle Georget. Tex* 3, 1498–1501. <https://doi.org/10.4161/cc.3.12.1328>
- von Minckwitz, G., Eidtmann, H., Rezai, M., Fasching, P.A., Tesch, H., Eggemann, H., Schrader, I., Kittel, K., Hanusch, C., Kreienberg, R., Solbach, C., Gerber, B., Jackisch, C., Kunz, G., Blohmer, J.-U., Huober, J., Hauschild, M., Fehm, T., Müller, B.M., Denkert, C., Loibl, S., Nekljudova, V., Untch, M., German Breast Group, Arbeitsgemeinschaft Gynäkologische Onkologie–Breast Study Groups, 2012. Neoadjuvant chemotherapy and bevacizumab for HER2-negative breast cancer. *N. Engl. J. Med.* 366, 299–309. <https://doi.org/10.1056/NEJMoa1111065>
- von Minckwitz, G., Schneeweiss, A., Loibl, S., Salat, C., Denkert, C., Rezai, M., Blohmer, J.U., Jackisch, C., Paepke, S., Gerber, B., Zahm, D.M., Kümmel, S., Eidtmann, H., Klare, P., Huober, J., Costa, S., Tesch, H., Hanusch, C., Hilfrich, J., Khandan, F., Fasching, P.A., Sinn, B.V., Engels, K., Mehta, K., Nekljudova, V., Untch, M., 2014. Neoadjuvant carboplatin in patients with triple-negative and HER2-positive early breast cancer (GeparSixto; GBG 66): a randomised phase 2 trial. *Lancet Oncol.* 15, 747–756. [https://doi.org/10.1016/S1470-2045\(14\)70160-3](https://doi.org/10.1016/S1470-2045(14)70160-3)
- Wakefield, A., Soukupova, J., Montagne, A., Ranger, J., French, R., Muller, W.J., Clarkson, R.W.E., 2013. Bcl3 selectively promotes metastasis of ERBB2-driven mammary tumors. *Cancer Res.* 73, 745–755. <https://doi.org/10.1158/0008-5472.CAN-12-1321>
- Walker, T., Adamson, A., Jackson, D.A., 2013. BCL-3 Attenuation of TNFA Expression Involves an Incoherent Feed-Forward Loop Regulated by Chromatin Structure. *PLoS ONE* 8. <https://doi.org/10.1371/journal.pone.0077015>
- Walsh, C.M., 2014. Grand challenges in cell death and survival: apoptosis vs. necroptosis. *Front. Cell Dev. Biol.* 2. <https://doi.org/10.3389/fcell.2014.00003>
- Wang, H., Zhao, A., Chen, L., Zhong, X., Liao, J., Gao, M., Cai, M., Lee, D.-H., Li, J., Chowdhury, D., Yang, Y., Pfeifer, G.P., Yen, Y., Xu, X., 2009. Human RIF1 encodes an anti-apoptotic factor required for DNA repair. *Carcinogenesis* 30, 1314–1319. <https://doi.org/10.1093/carcin/bgp136>
- Wang, V.Y.-F., Li, Y., Kim, D., Zhong, X., Du, Q., Ghassemian, M., Ghosh, G., 2017. Bcl3 Phosphorylation by Akt, Erk2, and IKK Is Required for Its Transcriptional Activity. *Mol. Cell* 0. <https://doi.org/10.1016/j.molcel.2017.06.011>
- Watanabe, N., Iwamura, T., Shinoda, T., Fujita, T., 1997. Regulation of NFKB1 proteins by the candidate oncoprotein BCL-3: generation of NF-kappaB homodimers from the cytoplasmic pool

- of p50-p105 and nuclear translocation. *EMBO J.* 16, 3609–3620. <https://doi.org/10.1093/emboj/16.12.3609>
- Watanabe, N., Wachi, S., Fujita, T., 2003. Identification and Characterization of BCL-3-binding Protein IMPLICATIONS FOR TRANSCRIPTION AND DNA REPAIR OR RECOMBINATION. *J. Biol. Chem.* 278, 26102–26110. <https://doi.org/10.1074/jbc.M303518200>
- Wei, S., Cao, H., Zhou, X., Wu, H., Yang, J., 2015. Prokaryotically and eukaryotically expressed interleukin-24 induces breast cancer growth suppression via activation of apoptosis and inhibition of tumor angiogenesis. *Mol. Med. Rep.* 11, 3673–3681. <https://doi.org/10.3892/mmr.2014.3136>
- Wei, T., Ye, P., Peng, X., Wu, L.-L., Yu, G.-Y., 2016. Prognostic Value of miR-222 in Various Cancers: a Systematic Review and Meta-Analysis. *Clin. Lab.* 62, 1387–1395.
- Wenzel, J., Zeisig, R., Fichtner, I., 2010. Inhibition of metastasis in a murine 4T1 breast cancer model by liposomes preventing tumor cell-platelet interactions. *Clin. Exp. Metastasis* 27, 25–34. <https://doi.org/10.1007/s10585-009-9299-y>
- Westerheide, S.D., Mayo, M.W., Anest, V., Hanson, J.L., Baldwin, A.S., 2001. The Putative Oncoprotein Bcl-3 Induces Cyclin D1 To Stimulate G1 Transition. *Mol. Cell. Biol.* 21, 8428–8436. <https://doi.org/10.1128/MCB.21.24.8428-8436.2001>
- Wickström, S.A., Masoumi, K.C., Khochbin, S., Fässler, R., Massoumi, R., 2010. CYLD negatively regulates cell-cycle progression by inactivating HDAC6 and increasing the levels of acetylated tubulin. *EMBO J.* 29, 131–144. <https://doi.org/10.1038/emboj.2009.317>
- Wilson, E., Leszczynska, K., Poulter, N.S., Edelmann, F., Salisbury, V.A., Noy, P.J., Bacon, A., Rappoport, J.Z., Heath, J.K., Bicknell, R., Heath, V.L., 2014. RhoJ interacts with the GIT-PIX complex and regulates focal adhesion disassembly. *J. Cell Sci.* 127, 3039–3051. <https://doi.org/10.1242/jcs.140434>
- Wong, C.C.-L., Gilkes, D.M., Zhang, H., Chen, J., Wei, H., Chaturvedi, P., Fraley, S.I., Wong, C.-M., Khoo, U.-S., Ng, I.O.-L., Wirtz, D., Semenza, G.L., 2011. Hypoxia-inducible factor 1 is a master regulator of breast cancer metastatic niche formation. *Proc. Natl. Acad. Sci. U. S. A.* 108, 16369–16374. <https://doi.org/10.1073/pnas.1113483108>
- Wu, J., Li, L., Jiang, G., Zhan, H., Wang, N., 2016. B-cell CLL/lymphoma 3 promotes glioma cell proliferation and inhibits apoptosis through the oncogenic STAT3 pathway. *Int. J. Oncol.* 49, 2471–2479. <https://doi.org/10.3892/ijo.2016.3729>
- Wulczyn, F.G., Naumann, M., Scheidereit, C., 1992. Candidate proto-oncogene bcl-3 encodes a subunit-specific inhibitor of transcription factor NF-kappa B. *Nature* 358, 597–599. <https://doi.org/10.1038/358597a0>
- Xiao, G., Harhaj, E.W., Sun, S.C., 2001. NF-kappaB-inducing kinase regulates the processing of NF-kappaB2 p100. *Mol. Cell* 7, 401–409.
- Xu, X., Yan, Q., Wang, Y., Dong, X., 2017. NTN4 is associated with breast cancer metastasis via regulation of EMT-related biomarkers. *Oncol. Rep.* 37, 449–457. <https://doi.org/10.3892/or.2016.5239>
- Yang, J., Williams, R.S., Kelly, D.P., 2009. Bcl3 interacts cooperatively with peroxisome proliferator-activated receptor gamma (PPARgamma) coactivator 1alpha to coactivate nuclear receptors estrogen-related receptor alpha and PPARalpha. *Mol. Cell. Biol.* 29, 4091–4102. <https://doi.org/10.1128/MCB.01669-08>
- Yang-Yen, H.-F., Yeh, H.-L., Chen, U.-I., 2015. Characterization of Mcl-1 isoforms and their impacts on mammalian cell growth. *Exp. Hematol.* 43, S103. <https://doi.org/10.1016/j.exphem.2015.06.287>

- Yerushalmi, R., Woods, R., Ravdin, P.M., Hayes, M.M., Gelmon, K.A., 2010. Ki67 in breast cancer: prognostic and predictive potential. *Lancet Oncol.* 11, 174–183. [https://doi.org/10.1016/S1470-2045\(09\)70262-1](https://doi.org/10.1016/S1470-2045(09)70262-1)
- Yoshida, A., Yoshida, S., Ishibashi, T., Kuwano, M., Inomata, H., 1999. Suppression of retinal neovascularization by the NF-kappaB inhibitor pyrrolidine dithiocarbamate in mice. *Invest. Ophthalmol. Vis. Sci.* 40, 1624–1629.
- Zamzami, N., Kroemer, G., 2001. The mitochondrion in apoptosis: how Pandora's box opens. *Nat. Rev. Mol. Cell Biol.* 2, 67–71. <https://doi.org/10.1038/35048073>
- Zandvakili, I., Lin, Y., Morris, J.C., Zheng, Y., 2017. Rho GTPases: Anti- or pro-neoplastic targets? *Oncogene* 36, 3213–3222. <https://doi.org/10.1038/onc.2016.473>
- Zarzynska, J.M., 2014. Two faces of TGF-beta1 in breast cancer. *Mediators Inflamm.* 2014, 141747. <https://doi.org/10.1155/2014/141747>
- Zhang, C., Zhu, C., Chen, H., Li, L., Guo, L., Jiang, W., Lu, S.H., 2010. Kif18A is involved in human breast carcinogenesis. *Carcinogenesis* 31, 1676–1684. <https://doi.org/10.1093/carcin/bgq134>
- Zhang, T., et al., Cucurbitacin E inhibits breast tumor metastasis by suppressing cell migration and invasion. *Breast Cancer Res Treat.* 2012. **135**(2): p. 445-58.
- Zhang, W., Levi, L., Banerjee, P., Jain, M., Noy, N., 2015. Kruppel-like factor 2 suppresses mammary carcinoma growth by regulating retinoic acid signaling. *Oncotarget* 6, 35830–35842. <https://doi.org/10.18632/oncotarget.5767>
- Zhang, X., Wang, H., Claudio, E., Brown, K., Siebenlist, U., 2007. A ROLE FOR BCL-3 IN CONTROL OF CENTRAL IMMUNOLOGIC TOLERANCE. *Immunity* 27, 438–452. <https://doi.org/10.1016/j.immuni.2007.07.017>
- Zhao, L., Huang, S., Mei, S., Yang, Z., Xu, L., Zhou, N., Yang, Q., Shen, Q., Wang, W., Le, X., Lau, W.B., Lau, B., Wang, X., Yi, T., Zhao, X., Wei, Y., Warner, M., Gustafsson, J.-Å., Zhou, S., 2018. Pharmacological activation of estrogen receptor beta augments innate immunity to suppress cancer metastasis. *Proc. Natl. Acad. Sci. U. S. A.* 115, E3673–E3681. <https://doi.org/10.1073/pnas.1803291115>
- Zhao, W., Qiu, R., Li, P., Yang, J., 2017. PIM1: a promising target in patients with triple-negative breast cancer. *Med. Oncol. Northwood Lond. Engl.* 34, 142. <https://doi.org/10.1007/s12032-017-0998-y>
- Zhao, Y., Ramakrishnan, A., Kim, K.-E., Rabson, A.B., 2005. Regulation of Bcl-3 through interaction with the Lck tyrosine kinase. *Biochem. Biophys. Res. Commun.* 335, 865–873. <https://doi.org/10.1016/j.bbrc.2005.07.162>
- Zheng, H., Shao, F., Martin, S., Xu, X., Deng, C.-X., 2017. WEE1 inhibition targets cell cycle checkpoints for triple negative breast cancers to overcome cisplatin resistance. *Sci Rep* 7, 43517. <https://doi.org/10.1038/srep43517>